Investigation into the importance of DNA repair gene *Ercc1* in the skin and central nervous system

Nicola Lawrence

Thesis presented for the degree of PhD

The University of Edinburgh

2006

I hereby declare that this thesis has been composed by me and it has not been accepted in any previous applications for a degree at this or at any other university. The work described has been performed by me, except where expressly indicated otherwise. All sources of information have been specifically acknowledged.

Acknowledgements

I am extremely grateful to Professor David Melton and Professor Sarah Howie for support and guidance over the past three years, as well as to the Raven Trust for funding. I would also like to thank the following people for their help: Bob Benson for help with the CBA assay, David Brownstein whose animal pathology knowledge has been invaluable, Linda Clark for help in the mouse house, Jennifer Doig who has helped immensely with too many things to mention, Tom Gillingwater for his neuroscience expertise, Alan Hart for help with the ophthalmoscope, OKR kit and retinal staining, Shonna Johnstone for her expertise with the temperamental FACSArray machine, Oliver Maddocks for tips on Western blotting and immunohistochemistry as well as for providing Welshcakes for the lab, Ian McCall for keeping my mice healthy, for advice and for making visits to the mouse house a bit more fun, Bob Morris for never complaining about how many skin sections I sent him, Pauline McCloone and Mary Norval for help with immunological assays, Frances Rae for Masson-Fontana staining, Anne-Marie Ritchie and Lesley Shaw for help in cell culture, Jim Selfridge for lively discussion and general harassment, Liang Song for how to make a beautiful Western blot and Richard Weller for his dermatology expertise. I'm also grateful to other members of the lab past and present that I haven't already mentioned specifically; including Scott Bader, Ewan Brown, Kate Britton, Kristina Kirschner, Lynn Morrice, Joanne Povey, Annelies Turksma and Alice Walmesley; particularly those in the student office. Finally, I am indebted to Rob and to my family, whose support has been unwavering.

Abstract

Nucleotide excision repair (NER) is responsible for the removal of helix distorting lesions from DNA. These include cyclobutane pyrimidine dimers and 6-4 photoproducts, caused primarily by ultraviolet (UV) radiation. The persistence of these lesions in the genome can lead to the development of skin cancer, and furthermore, exposure to UV radiation has been linked with systemic immunosuppression, which can also increase the risk of tumour development. Patients with xeroderma pigmentosum have defective NER, with around a 1000 fold increased risk of developing skin cancer compared with the rest of the population. In NER, ERCC1 acts in complex with XPF to make an incision 5′ of the lesion and as such is essential for this damage repair process. ERCC1 is also involved in other types of repair including the repair of interstrand crosslinks and double strand breaks. *Ercc1* null mice die at 3 weeks with severe liver abnormalities, so in the laboratory we have created two longer lived *Ercc1* deficient models: firstly a liver corrected *Ercc1* null, and secondly an epidermis specific *Ercc1* knockout. In this study we considered the short and long term effects of UV irradiation on the skin using the epidermis specific *Ercc1* knockout, in particular the consequences of unrepaired DNA damage in keratinocytes on UV induced erythema, immunosuppression, tanning and carcinogenesis. We found the epidermis specific *Ercc1* knockout mice to be extremely sensitive in all these respects. As these mice have NER deficient keratinocytes but NER proficient fibroblasts, immunological cells and melanocytes, we were able to show that DNA damage in keratinocytes is responsible for initiating a cascade of events

that leads to systemic immunosuppression, and we also report that DNA damage in keratinocytes alone leads to UV induced tanning. We went on to use these mice to investigate proposed anti-cancer therapy, the topical application of thymidine dinucleotides. We have also further characterised the liver corrected *Ercc1* null mouse, specifically the neurological features and an unusual hair phenotype that was observed. We report that progressive ataxia in animals with an *Ercc1* deficient nervous system is due to chronic uraemia caused by kidney pathology. Furthermore, we characterised a brittle hair phenotype in these mice, and concluded that it was due to an unidentified background effect rather than a specific trait caused by lack of *Ercc1*.

Table of contents

Abbreviations

A	adenosine
Ab	antibody
ADP	adenosine diphosphate
AK	actinic keratosis
ANOVA	analysis of variance
ATP	adenosine triphosphate
BER	base excision repair
bp(s)	base pair(s)
C	cytosine
CBA	cytometric bead array
CD	cluster of differentiation
cGMP	cyclic guanosine monophosphate
CIS	carcinoma *in situ*
CK	cytokeratin
cM	centimorgan
CNS	central nervous system
CO_2	carbon dioxide
CS	Cockayne's syndrome
D-	dextro
DC(s)	dendritic cell(s)
dH_20	deionised water
DNA	deoxyribonucleic acid
DMEM	Dulbecco's modified Eagle's medium

DMSO	dimethylsulphoxide
DSB	double strand break
EDTA	ethanediaminetetraacetic acid
ERCC	excision repair cross complementing
ESKO(s)	epidermis specific knockout(s)
Fab	antigen binding fragment
FACSArray	fluorescence activated cell array
FACScan	fluorescence activated cell scanning
Fc	crystallisable fragment
FCS	foetal calf serum
FITC	fluorescein isothiocyanate
g	gravitational force
g	gram(s)
G	guanosine
H&E	haematoxylin and eosin
HNPCC	hereditary non polyposis colorectal cancer
HPRT	hypoxanthine phosphoribosyltransferase
HRR	homologous recombination repair
ICL	interstrand crosslinks
IFN	interferon
IHC	immunohistochemistry
IL	interleukin
J	joule(s)
K5	keratin 5
kb	kilobase(s)

KO	knockout
l	litre(s)
L-	laevo
LC(s)	Langerhans cell(s)
m	micro
m	milli
m	metre(s)
M	molar
MHC	major histocompatibility complex
MOM	mouse on mouse
MCP-1	monocyte chemotractant protein-1
MMR	mismatch repair
MSH	melanocyte stimulating hormone
NER	nucleotide excision repair
NHEJ	non-homologous end joining
NMJ	neuromuscular junction
NMSC	non-melanoma skin cancer
NSAIDs	non-steroidal anti-inflammatory drugs
p	pico
PAF	platelet activating factor
PBS	phosphate buffered saline
PCNA	proliferating cell nuclear antigen
PCR	polymerase chain reaction
PG	propylene glycol
PGE_2	prostaglandin E2

pTpT	thymidine dinucleotide
RNA	ribonucleic acid
ROS	reactive oxygen species
SCC	squamous cell carcinoma
SD	standard deviation
SDS	sodium dodecyl sulphate
SE	synapse elimination
SEM	standard error of the mean
T	thymine
TG	transgene
Th1	T helper 1
Th2	T helper 2
TLS	translesion synthesis
TNFα	tumour necrosis factor alpha
t-oligo	telomere homologous oligonucleotide
TTD	trichothiodystrophy
TTR	transthyretin
UV	ultraviolet
V	volts
v/v	volume against volume
WT	wild type
w/v	weight against volume
XP	xeroderma pigmentosum

Chapter 1

Introduction

1.1 Fundamentals of DNA repair

Maintenance of the genetic code is fundamental for species survival, and although Darwinian evolutionary theory requires some degree of genetic variation, cells and organisms must be able to pass on their DNA through generations and generations. DNA must withstand replicative cycles and recombinational processes, as well as insult from environmental factors.

Mutations in germ line cells can result in hereditary syndromes and disease susceptibility being passed through generations. Mutations in somatic cells can also result in disease, with cancer possibly the most severe consequence.

In order to protect the integrity of the genome and maintain the information stored within, several repair mechanisms are in place. Each repair mechanism deals with a particular type of DNA damage, although there is evidence for some overlap occurring between some of the mechanisms. These include direct repair, mismatch repair, base excision repair, nucleotide excision repair, recombinational repair, non-homologous end joining and repair of inter strand cross-links.

Direct repair is a simple repair method where an enzyme catalyses the straightforward removal of a DNA adduct (reviewed by Sancar, 1995 and 1996). Such enzymes include DNA photolyase (found in some prokaryotes

as well as marsupials), 6-4 photoproduct photolyase (found in Drosophila and some other species), spore photoproduct lyase (found in the spores of *Bacillus subtilis*) and O^6-methylguanine DNA methyl transferase (found in all species investigated), which removes alkyl groups from the DNA.

Mismatch repair (MMR) is important for maintaining the replicative fidelity of the genome (reviewed by Jun et al, 2006 and Jiricny, 2006). Mismatches are identified, the DNA is unwound, then an incision is made in the affected single strand and the mismatched base removed by exonuclease activity. The gap is then filled and ligated. The consequences of defective MMR are demonstrated in hereditary non polyposis colorectal cancer (HNPCC), a syndrome where germline mutations in MMR genes predispose the patient to colorectal carcinoma (reviewed by de la Chapelle, 2004).

Base excision repair (BER) is the removal of non-bulky adducts from the DNA (reviewed by Sancar, 1996), often the result of metabolic by-products. Such damage can be caused by reactive oxygen species, methylation and hydroxylation. A glycosylase cleaves the damaged base from the attached deoxyribose, then the abasic sugar is released by apurinic/apyrimidinic lyase and endonucleases, before a nucleotide fills the gap.

Nucleotide excision repair (NER) is a mechanism for removing bulky adducts from the DNA, generally caused by UV light or polycyclic aromatic hydrocarbons (found for example in cigarette smoke). Incisions are made in

the damaged strand of DNA by endonucleases, upstream and downstream of the lesion, before this section is replaced and ligated. In prokaryotes this is a relatively simple process, involving just three proteins. In eukaryotes however the mechanism is more complex, involving many more proteins, and will be considered in more detail in the following section. In mammals, nucleotide excision repair mainly deals with lesions caused by exposure to ultraviolet light.

Homologous recombinational repair (HRR) (reviewed by Thompson and Schild, 2002) is a pathway involved in the repair of DNA double strand breaks (DSBs). DSBs are caused primarily by x rays or by other types of ionising radiation, as well as certain chemicals. In this pathway, the 5' strand of DNA is degraded, resulting in a single strand that can be used to identify homologous sequence on the paired chromosome and therefore repair the damage.

Non homologous end joining (NHEJ) is a second pathway for the repair of DNA DSBs (reviewed by Hefferin and Tomkinson, 2005). This process requires the broken ends to be physically closely aligned, before NHEJ proteins bind the broken ends of the DNA. The Ku complex is crucial for this process and protects the exposed DNA. Bridging then occurs, involving processing followed by ligation by DNA ligase IV.

Inter-strand cross-link (ICL) repair is a complex process involving proteins characteristically part of other repair pathways as well as its own set of enzymes (reviewed by Mirchandani and D'Andrea, 2006). Cross-linking agents include cisplatin, mitomycin c and other alkylating agents, many of which form an important class of chemotherapeutic, anti-cancer drugs. Their effectiveness is derived from the severe cytotoxic effect of these drugs on proliferating cells. The exact details of the pathways involved in ICL repair have yet to be elucidated, although a possible mechanism has been proposed (Niedernhofer et al, 2005). In short, it appears that the *FANC* (Fanconi anaemia) gene products are involved in the initial processing of the lesion, creating a structure that is then repaired either by NER or by HRR. The ERCC1/XPF complex appears to be crucial for the repair of ICLs (de Laat et al, 1998, Chipchase and Melton, 2002, Niedernhofer et al, 2004), and this will be discussed in more detail later in this chapter.

At this point it is also important to note a cellular process known as translesion synthesis (TLS). In this process, the cell uses low fidelity polymerases to bypass a lesion and thus continue replication (reviewed by Lehmann, 2006). One of these polymerases is DNA Polη, which is defective in variant XP syndrome (Masutani et al, 1999). When proliferating cell nuclear antigen (PCNA), a sliding DNA clamp, is stalled by the presence of a lesion, it is ubiquitinated and able to form interactions with TLS polymerases.

1.2 Nucleotide excision repair

This thesis will focus on mammalian nucleotide excision repair, and in particular on the endonuclease ERCC1. NER has been reviewed extensively (de Laat et al, 1999 and Hoeijmakers, 2001, amongst others), and the majority of the proteins involved in the pathway are well characterised.

Nucleotide excision repair (NER) deals with helix distorting lesions, primarily caused by UV radiation. DNA acts as a chromophore for UV, absorbing energy and forming bulky adducts. The majority of these are *cis-syn*-cyclobutane pyrimidine dimers (CPDs), whilst pyrimidine 6-4 pyrimidone photoproducts (6-4PPs) are also produced (de Boer and Hoeijmakers, 2000).

Briefly, helix distorting lesions are identified. The helix is then held open, whilst incisions are made on either side of the lesion. The damaged section is removed, and the gap filled by a DNA polymerase, using the intact strand as a template. The ends are then joined by DNA ligase.

Two variations on the NER pathway exist. The first of these is global genome repair (GGR), where damage throughout the genome is repaired at a constant rate. The alternative is transcription coupled repair (TCR), where damage in transcribed genes is repaired. TCR employs a different recognition system in order to allow lesions in transcribed genes, and specifically those in the transcribed strand, to be repaired at a greater rate

than damage found in other areas of the genome. The availability of this pathway allows a cell to repair damage in genes required for transcription, with priority over damage in parts of the genome not required until the cell undergoes replication. In this way, a lesion that stalls the transcription machinery is repaired prefentially over any other lesion.

Figure 1.1 gives an overview of the NER mechanism, showing how GGR and TCR pathways differ in the first step and subsequently converge.

As mentioned, GGR is a constant process involving inspection of the entire genome. Lesions are recognised by the XPC-hHR23B complex, which has been reported as being dispensable for TCR (Venema et al, 1990a). hHR23B has been identified as a stimulator for XPC activity (Masutani et al, 1997), and together these proteins sense and bind DNA lesions (Volker et al, 2001), recruiting the NER machinery (de Laat et al, 1999). GGR is very efficient at repairing 6-4PPs and less efficient at removing CPDs (de Boer and Hoeijmakers, 2000). This is likely to be due to the differing affinity of XPC for these types of lesions.

The *Xpe* gene product has also been implicated in damage recognition, although its exact function remains unclear. XPE seems to be unnecessary for NER *in vitro*, as determined by complementation analysis, (de Laat et al, 1999), and XPE patients suffer from mild XP symptoms compared with those from other complementation groups. The damaged DNA binding complex

Fig 1.1

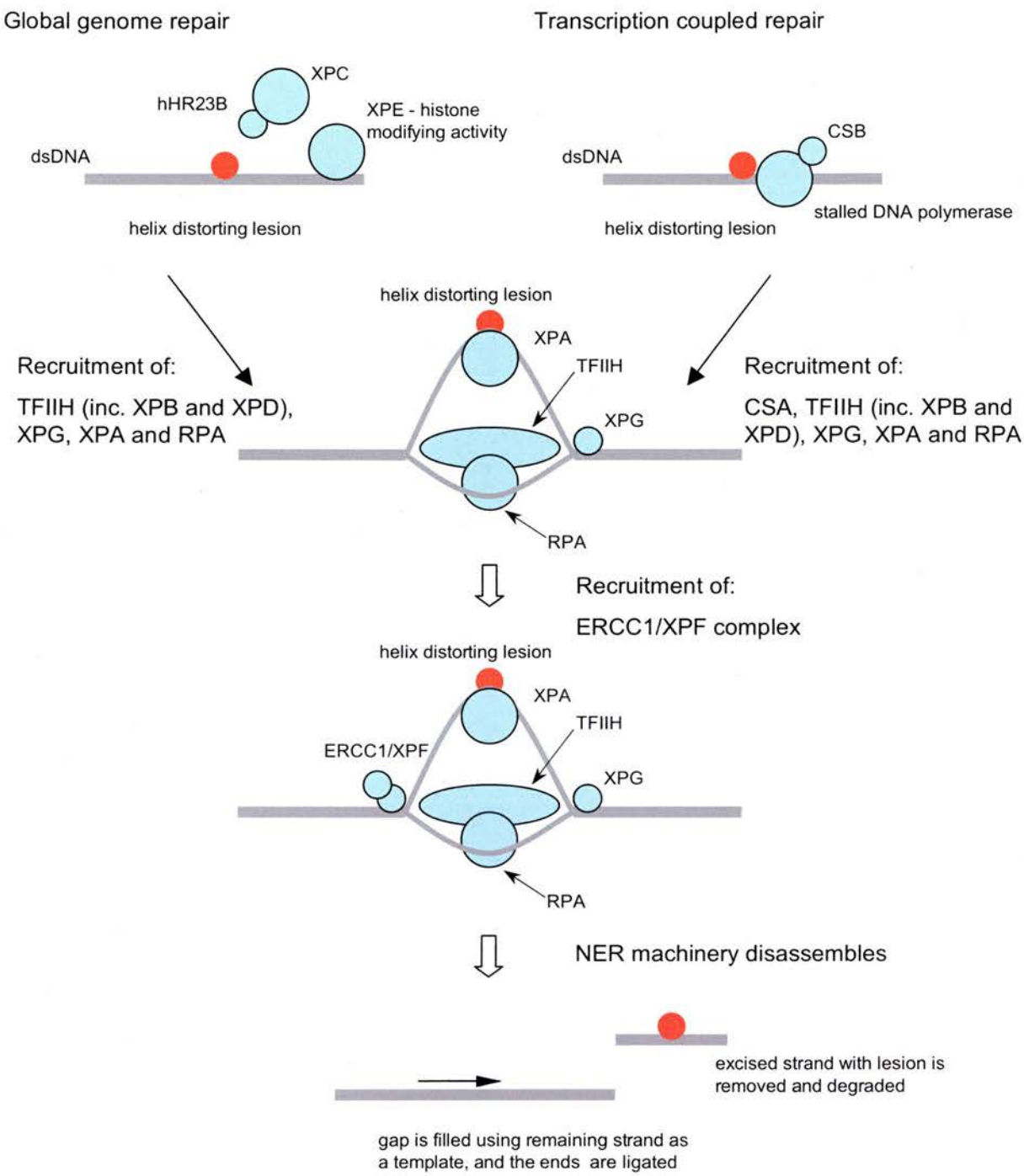

Figure 1.1 Overview of NER mechanism

The recognition steps of GGR and TCR differ but thereafter the NER mechanism is the same. TFIIH opens the dsDNA, RPA binds the template strand, and XPA identifies the lesion. XPG makes the 3′ incision, then ERCC1/XPF makes the 5′ incision. The damaged strand is removed, and the gap filled by DNA polymerase and ligated by DNA ligase.

(DDB) has high affinity for UV induced DNA lesions, and consists of a p48/p127 heterodimer (Nichols et al, 2000). The p48 subunit (also known as DDB2) has been identified as the XPE gene product (Rapic-Otrin et al, 2003) and this appears to be a protein with several roles in cell cycle checkpoints as well as NER (Kulaksiz et al, 2005). Recently, DDB2 has been reported to have a role in the modification of histone H2A by ubiquitination, and it is suggested that this causes a conformational change which may enable the NER machinery to bind the lesion (Kapetanaki et al, 2006).

Recognition in TCR occurs when RNA polymerase II is stalled by a lesion, whilst in the process of transcription (Donahue et al, 1994). Cells from Cockayne Syndrome (CS) patients are defective in TCR (Venema et al, 1990b), and it appears that CS proteins interact with RNA pol II once it has come across a lesion in the DNA (van Gool et al, 1997). However the precise functions of CSA and CSB remain unclear.

After a lesion has been identified by either GGR or TCR proteins, the rest of the NER machinery is recruited to the damaged site. This includes transcription factor TFIIH, RPA, XPA and endonucleases XPG, XPF and ERCC1. These roles of these proteins will subsequently be considered in more detail.

The function of the TFIIH protein complex is to unwind the DNA helix, and it is involved in transcription as well as NER. TFIIH is composed of ten

different proteins, with individual functions. XPB unwinds DNA in a 3' to 5' direction (Ma et al, 1994) and XPD unwinds DNA in a 5' to 3' direction (Sung et al, 1993). The CAK subcomplex is composed of Cdk7, cyclin H and Mat 1, and is essential for transcription but not for NER (Mu et al, 1996). The remaining proteins appear to have structurally important roles. p44 anchors XPD (Seroz et al, 2000 and Tremeau-Bravard et al, 2001) and p52 anchors XPB within the TFIIH complex (Jawhari et al, 2003). p62 has been shown to bind XPG (Gervais et al, 2004), and p34 has DNA binding capacity, although its exact role is unclear. Finally, TTDA is the most recently identified TFIIH subunit (Giglia-Mari et al, 2004). This has been shown to be essential for NER, and associates closely with TFIIH during the repair process (Giglia-Mari et al, 2006).

Replication protein A (RPA) specifically binds to single stranded DNA, and was initially described as a requisite protein for DNA replication (Wold and Kelly, 1988). A role for RPA in excision repair was confirmed by the finding that RPA specific antibodies inhibited DNA repair in vitro (Coverly et al, 1991). This role has been identified as the stabilisation of the unwound DNA, as the protein binds the undamaged strand during the NER process (de Laat et al, 1999).

XPA was identified to be responsible for group A XP disease when cloned XPA cDNA alleviated UV sensitivity in XP group A derived cells (Tanaka et al, 1990). XPA binds other proteins involved in NER, and as such is

considered a crucial factor for the positioning of repair machinery around the lesion (de Laat et al, 1999).

XPG is an endonuclease which cuts one strand of double stranded DNA at the 3' side of a double strand/single strand junction. In NER, XPG makes the 3' incision (O'Donovan et al, 1994). Previously it was reported that it does this before the 5' incision is made (Mu et al, 1996), however it is now debated whether in fact the incisions are made concurrently (Thorel et al, 2004). Some patients with XPG deficiency show features of Cockayne syndrome, and it is postulated therefore that XPG may have a role in transcription. This is corroborated by evidence showing XPG has a region which interacts with TFIIH (Thorel et al, 2004). XPG has also been shown to have a role in base excision repair, as it has been reported to act in the repair of thymine glycol by stimulating endonuclease III activity (Bessho, 1999).

In NER, ERCC1 and XPF act in complex as an endonuclease complementary to XPG, identified by purification of the proteins causing XP group F (Sijbers et al, 1996). It has been reported that ERCC1 interacts with DNA and with XPA, enabling XPF to perform the incision in the correct location (Tripsianes et al, 2005). In addition to its role in NER, ERCC1/XPF is essential for the repair of interstrand cross-links, although its precise function remains unclear (Bessho et al, 1997, Chipchase and Melton, 2002 and Niedernhofer et al, 2004). ERCC1/XPF has also been shown to be necessary for homologous recombination repair (Sargent et al, 2000),

recombination in mouse embryonic stem cells (Niedernhofer et al, 2001) and for normal haematopoiesis (Prasher et al, 2005).

In summary, the NER pathway is fairly well characterised, as are most of the proteins involved – however many of these have roles in other cell functions, that are not always well understood. In future, research in this area will not only further our understanding of the roles of these gene products in NER, but also enable us to piece together the overlapping pathways involved in the maintenance, replication and transcription of the genetic code.

1.3 Human nucleotide excision repair syndromes

Hereditary human NER deficiency results in three syndromes, each with distinct and overlapping features: xeroderma pigmentosum, Cockayne syndrome and trichothiodystrophy.

Xeroderma pigmentosum (XP) is characterised by extreme photosensitivity, excessive pigmentation in response to UV and a heightened susceptibility to UV induced skin cancer. Several complementation groups have been identified, XPA-G as well as variant XP, or XPV. XPV is caused by mutation in Polη (Masutani et al, 1999), however the other XP syndromes are caused by mutations in the NER genes. XP patients have around one thousand fold increased risk of skin cancer, and the mean age for initial development of

skin cancer is 8 years of age, compared with around 50 in the general population (reviewed by Kraemer, 1997). A small number of XP patients have neurological symptoms, and these appear to be those patients with a more severe NER defect (Bootsma et al, 1998). This phenotype is likely to be due to the accumulation of oxidative lesions in neurons, leading to neurodegeneration.

Cockayne's syndrome (CS) is characterised by neurological and developmental abnormalities, such as microcephaly, kyphosis, gait defects and mental retardation, as well as incomplete sexual development and cachectic dwarfism (reviewed by de Boer and Hoeijmakers, 2000). Genetically, the syndrome is attributed to mutation in either CSA or CSB. CS patients are photosensitive, however they do not have increased susceptibility to developing skin cancers compared with the rest of the population. This conveniently underlines the key differences between transcription coupled NER and global genome NER, illustrating the consequences for the organism of the loss of TCR and not GGR. From these patients we are able to conclude that it is GGR that is essential for preventing the skin cancers to which XP patients are so susceptible. However, it is important to note that there are features of CS that cannot be explained by NER deficiency alone, as XPA patients do not show them, and these are caused by defects in transcription resulting from lack of TCR. Cells from CS patients have been reported to be hypersensitive to oxidative damage (Leadon and Cooper, 1993), although it seems unclear that these

results were produced reliably (Cozzarelli, 2003). However, an increased sensitivity to oxidative damage may explain the neurological phenotype of CS patients, as the neurological system is particularly sensitive to oxidative damage (reviewed by Halliwell, 2006).

Trichothiodystrophy (TTD) is a syndrome characterised by brittle hair. In these patients, there is an insufficiency of cysteine rich matrix proteins in the hair, which leads to hair shafts that are extremely fragile and break easily (Gillespie and Marshall, 1983, reviewed by Itin and Pittelkow, 1990). This feature is accompanied by ichthyosis, reduced growth, impaired fertility and mental retardation. Interestingly, some, but not all, TTD patients show sun sensitivity, and there are no reports of skin cancer susceptibility. Genetically, TTD is caused by mutations in one of XPB, XPD or TTDA, all of which are TFIIH subunits. Physiologically, trichothiodystrophic hair lacks sulphur rich matrix proteins (reviewed by Nakamura et al, 2001), and this has been linked with a failure in late stage transcription in the highly differentiated keratinocytes. In this model, a marker of a late differentiation stage has been shown to be reduced, implying that transcription has effectively been exhausted in these cells (de Boer et al, 1998b). Aside from the characteristic brittle hair and ichthyosis, the symptoms of TTD are comparable with those of CS. Although XPB, XPD and TTDA are not linked specifically with TCR, as the CS proteins are, they are linked with transcription itself, which also has implications for the neurological system. As neurons do not divide, as

well as being susceptible to oxidative damage, they have unusually high levels of transcription.

DeSanctis-Cacchione syndrome is an extremely rare disease with features of XP as well as a severe neurological phenotype. This disease has been reported to be due to mutation in XPA, as well as CSB in one case (Colella et al, 2000). Another extremely rare disease is combined XP/CS, showing symptoms of both disorders – patients have been identified with mutations in XPB, XPG and XPD (reviewed by Lehmann, 2001).

Mutations in particular NER genes do not necessarily lead to specific syndromes. For example, mutations in XPD can lead to XP, TTD or XP/CS, and mutations in CSB can lead to CS or deSanctis-Cacchione syndrome. This illustrates the complexity of the NER pathway and the roles of the various proteins involved, as well as the relationship between NER and transcription.

1.4 Nucleotide excision repair deficiency and cancer predisposition

Cancer development is the result of genetic and epigenetic changes causing dysregulation of the cell cycle, which leads to uncontrolled proliferation. NER as well as other types of repair already mentioned in this thesis are required to deal with lesions throughout the genome, but it is lesions specifically in

genes involved with cell cycle control, proliferation and apoptosis that are of extreme importance in cancer development. The link between repair deficiency and cancer susceptibility could not be more clear. There are a variety of human syndromes caused by defective repair of one kind or another, the majority of which have increased cancer risk as their main feature.

The balance between proliferation, replicative senescence and apoptosis is tightly regulated by a vast array of proteins (reviewed in Vogelstein and Kinzler, 1998). A schematic of the cell cycle is shown in figure 1.2. Dysregulation of the cell cycle can be caused by the inactivation of tumour suppressor genes or by the activation of oncogenes. Tumour suppressor genes normally regulate cell cycle checkpoints, and ensure that replication does not go ahead if the cell is not ready, thereby preventing the accumulation of mutations. Oncogenes are mutated forms of normal genes which promote cell growth and proliferation.

The p53 gene product acts as a tumour suppressor and plays a crucial role in cell cycle regulation. Normal p53 protein accumulates in cells after exposure to damaging agents, including UV radiation, and causes cycle arrest in G1 (Kuerbitz et al, 1992). This prevents replication of damaged DNA, and allows time for repair of the damage to take place. p53 is mutated in a wide variety of human cancers, including skin cancers, and the implication of this is that cells are able to divide without this crucial

Fig 1.2

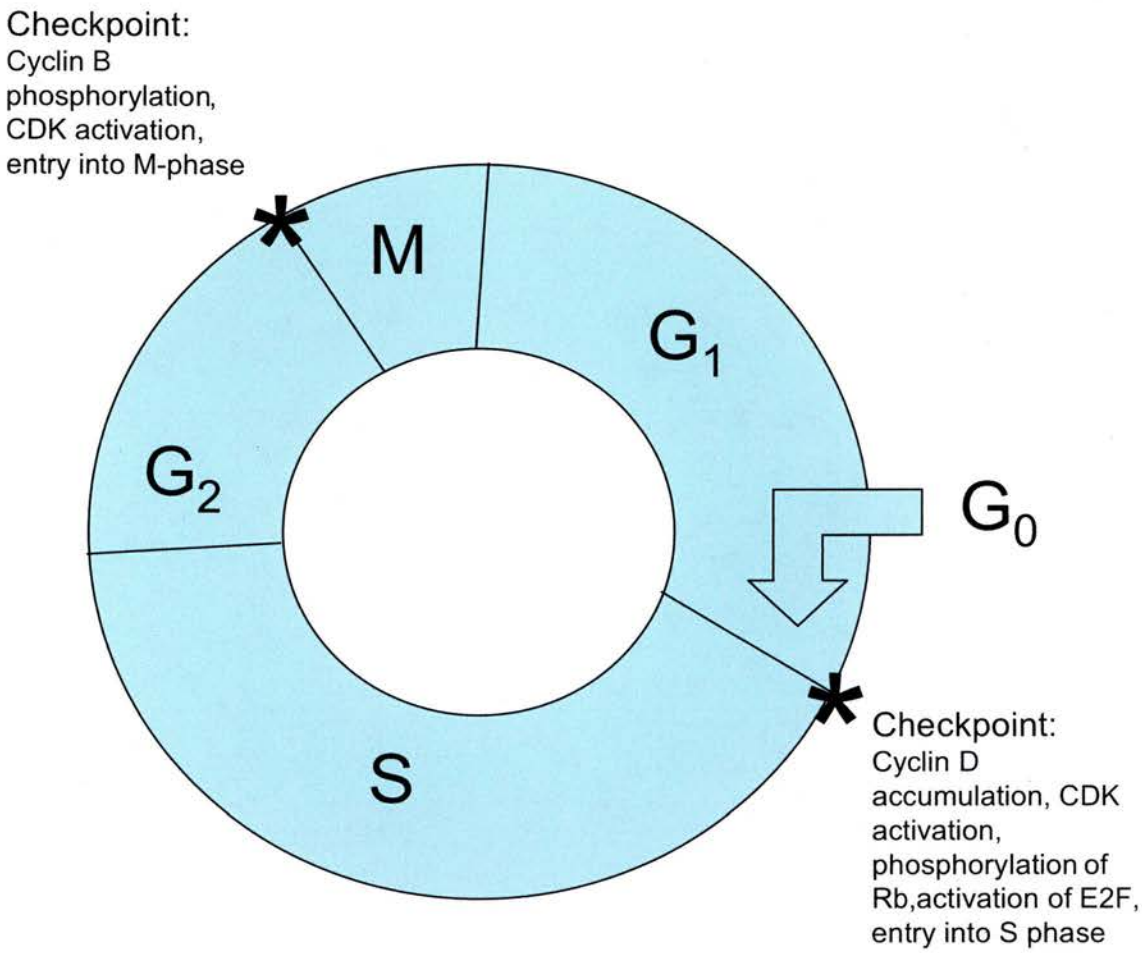

Figure 1.2 Overview of cell cycle

M = mitosis, S = synthesis, G_1 and G_2 = gap stages, G_0 = replicative senescence

The cell cycle is regulated by cyclins, which form complexes with cyclin dependent kinases (CDKs) in specific patterns. The progression of the cell cycle is controlled by CDK inhibitors, including p21 (activated by p53), p16 and p19.

Adapted from Cotran et al, Robbins Pathologic Basis of Disease

checkpoint regulatory activity (Lane, 1992). The p53 gene product is a powerful transcription factor and upregulates the expression of the p21 gene product, which acts in a complex with other factors to inhibit the phosphorylation of the *Rb* gene product, and thereby inhibit cell cycle progression (Harper et al, 1993). p21 also modulates PCNA, inhibiting its role in replication but not repair (Li et al, 1994).

An example of an oncogene is mutated c-*myc*. Proto-oncogenic c-*myc* is involved in the early entrance of a cell to the cycle, and its expression is tightly controlled (reviewed by Chung and Levens, 2005). However in several human tumours c-*myc* is either expressed constitutively or overexpressed, including Burkitt lymphoma (where dysregulation is due specifically to a translocation) as well as some breast, lung and colon cancers (Cotran et al, 1999).

Another important aspect of tumourigenesis is regulation of telomerase. The ends of our chromosomes are protected from exonuclease activity and subsequent degradation by a non-coding repeat sequence, called the telomere. Telomeres vary in length and homogeneity, depending on tissue (de Lange et al, 1990). The telomere repeat sequence is bound by stabilising factors including TRF1 and TRF2, and forms a characteristic loop structure known as a T loop (Griffith et al, 1999). In this structure, the 3' end of the DNA strand loops back on itself and invades the dsDNA. Disruption of the loop lets the cell know that its replicative capacity is exhausted, and

triggers signals which induce replicative senescence or apoptosis, dependent on cell type (reviewed by de Lange, 2002). Telomere length therefore also has implications for organism aging, as telomeres shorten with successive rounds of replication. In germline cells, telomere length has to be maintained to allow infinite reproduction of a species, and therefore these cells express an enzyme called telomerase, which is not normally expressed in other cells. The telomerase complex consists of a reverse transcriptase enzyme, as well as an RNA template and an associated protein (Linger et al, 1997). In the vast majority of cancer cells, the telomerase enzyme has been reactivated (reviewed by Shay and Wright, 2006), leading to the conclusion that the main function of telomeres that are programmed to degrade further with each reproductive cycle is to guard against tumourigenesis. Aberrant telomerase activity is currently an exciting target for many forms of putative cancer therapies.

A further link between telomeres and aging has recently been made by reports that WRN (a protein mutated in the segmental progeroid disorder Werner's syndrome) has a role in the processing of the telomeres and activation of DNA damage responses (Eller et al, 2006).

It should however be noted that differences in telomere damage response pathways between mice and humans have been reported, and this should be considered when interpreting data on telomere damage and maintenance in the mouse model (Smogorzewska and de Lange, 2002).

It is important to consider that cancer does not arise through defects in DNA repair proteins in themselves. The reason that patients and animal models with DNA repair defects are cancer prone is that they experience DNA damage at a normal rate, but are unable to repair it, and crucially, are unable to repair mutations in tumour suppressor genes and protooncogenes. The accumulation of damage and the inevitable disruption of the highly regulated cell cycle process is what leads to tumourigenesis in DNA repair deficient patients.

1.5 Mouse models of nucleotide excision repair defects

A variety of mouse models that are deficient in DNA repair have been generated, and these are listed in a frequently updated database (Friedberg and Meira, 2006). Many mouse models for NER have also been created, and have been reviewed recently (Wijnhoven et al, 2006). For each of the NER proteins, null mice have been created, and these display a range of lifespans and phenotypes. NER null mice are summarised in Table 1.1. For some of the NER proteins, as well as the null mouse models, mice with point mutations, truncations and conditional knockouts have also been made. These have generally alleviated a severe phenotype and allowed researchers to study some of the consequences of NER deficiency that are impossible to consider in mice with an extremely short lifespan. This section

will review the existing NER deficient mouse models, however the Ercc1 models that have been created in our lab will be considered in more detail in the next section.

Independent strains of *Xpa* null mice were created simultaneously (de Vries et al, 1995 and Nakane et al, 1995). These were created by deletion of exons 3 and 4, and by insertion of a *neo* cassette into exon 4, respectively. Around 50% foetal death of *Xpa* nulls was reported by de Vries et al, however normal Mendelian ratios were reported by Nakane et al. However, both groups reported an absence of *Xpa* mRNA and protein product. Both groups also showed a high susceptibility to UV and chemical carcinogen induced carcinogenesis, as expected.

Table 1.1

Mouse model	First report	Lifespan	Spontaneous tumour formation	UV induced tumour formation
Xpa$^{-/-}$	de Vries et al, 1995 and Nakane et al, 1995	Slightly shortened	Yes, liver	Yes
Xpb$^{-/-}$	Weeda et al, 2006	Embryonic lethal?	n/a	n/a
Xpc$^{-/-}$	Sands et al, 1995	Slightly shortened	Yes, lung	Yes
Xpd$^{-/-}$	de Boer et al, 1998	Embryonic lethal	No*	No*
Xpe$^{-/-}$	Yoon et al, 2005	Slightly shortened	Yes, various internal	Yes
Xpf$^{-/-}$	Tian et al, 2004	Around 3 weeks	n/a	n/a
Xpg$^{-/-}$	Harada et al, 1999	Around 3 weeks	n/a	n/a
Ercc1$^{-/-}$	McWhir et al, 1993	Around 3 weeks	No*	Yes*
Polh$^{-/-}$	Lin et al, 2006	Normal	Not at one year	Yes
Csa$^{-/-}$	van der Horst et al, 2002	Normal	No	Yes
Csb$^{-/-}$	van der Horst et al, 1997	Normal	No	Yes

* reported in more recently developed mouse models with a less severe mutation and therefore longer lifespan

An *Xpb* model has been listed in the DNA repair model database (Friedberg and Meira, 2006), however the paper remains unpublished at this date. It is reported that a mouse has been created with a mutation mimicking that found in a human XPB patient, and that the mice are viable although there are disrupted Mendelian inheritance patterns, suggesting impaired prenatal development (Weeda et al, currently unpublished).

Xpc mice were generated using an *Hprt* minigene to disrupt the *Xpc* sequence (Sands et al, 1995). These mice are highly susceptible to UV induced skin cancer, and also show UV induced skin changes reminiscent of XP, such as hyperkeratosis. More recently, these mice have also been shown to suffer from spontaneous lung tumours (Hollander et al, 2005)

Xpd null mice are embryonic lethals (de Boer et al, 1998a). A viable mouse model was created by mimicking a point mutation from a patient, XPD^{R772W}, with a photosensitive form of TTD, and this mouse appeared to show all the features of the TTD patient (de Boer et al, 1998b). This mutation confers a partial NER defect. However on further examination, this mouse model also showed increased susceptibility to UV and chemical carcinogen induced carcinogenesis, (albeit not as much as *Xpa* mice), (de Boer et al, 1999), which has not been reported in TTD patients. This in itself is interesting, as it seems a fair assumption that a defect in NER (as opposed to TCR) should predispose to UV induced carcinogenesis in human patients. However, the rate of GGR is lower in mice than in humans, perhaps due to the difference

in life expectancy between these species, which may account for the increased cancer susceptibility in mice. Furthermore, XPE expression is low in mice, contributing to low GGR (Alan Lehmann, personal communication). It is proposed by the authors that TTD patients are in fact somewhat cancer prone, although not as much as other XP patients, and that the characteristic scaling of TTD skin itself provides protection from UV damage in the basal epithelium (de Boer et al, 1999). Furthermore, the TTD mouse has been shown to display features of premature aging, a phenotype which is exaggerated further when these mice are crossed with *Xpa* null mice (de Boer et al, 2002). This is postulated to be a result of endogenous, oxidative lesions building up and leading to increased levels of cell death, as well as defects in transcription (de Boer et al, 2002). Recently, the TTD mouse model has been determined to have a segmental progeroid, or premature ageing, phenotype, which is also evident in human TTD patients (Wijnhoven et al, 2005). These mice display aging features such as osteoporosis, kyphosis and aortic sarcopaenia. Interestingly, the TTD mouse shows a reduced level of certain aging-related features, including demyelination of peripheral nerves, cataract development and pituitary adenoma formation. This phenotype is similar to that reported for mice on a restricted calorie diet, shown to prolong lifespan. It is hypothesised that the TTD model in some way protects itself from potentially harmful metabolic by-products by energy efficient uptake, explaining the low body weight of these animals (Wijnhoven et al, 2005). If this is the case, this is a finding that raises many questions

about the regulation of metabolic efficiency and the regulation of production of metabolic by-products.

DDB2 mice, postulated to represent *Xpe* deficiency, have been generated by deletion of exons 4 and 5 (Yoon et al, 2005). These appear to be highly susceptible to internal tumours, particularly of the lymphoid tissue, as well as UV induced skin cancers (Yoon et al, 2005).

An *Xpf* model mouse has been created recently, modelling a point mutation from an XPF patient (Tian et al, 2004). This introduced a stop codon into exon 8 of the *Xpf* gene. Despite the fact that the patient did not suffer extremely severe symptoms, all $Xpf^{-/-}$ mice generated died at three weeks, similar to $Ercc1^{-/-}$ mice (McWhir et al, 1993). This implies that the mutation introduced has in fact created a null *Xpf* allele, which is backed up by the lack of evidence for *Xpf* mRNA in cells created (Tian et al, 2004).

Xpg has been knocked out in the mouse using a neo insertion into exon 3 of the gene (Harada et al, 1999). The mice created produce no *Xpg* mRNA and have features reminiscent of *Xpf* or *Ercc1* deficiency, with impaired growth followed by a dramatically reduced lifespan (Harada et al, 1999) and cerebellar abnormalities (Sun et al, 2001).

Since the first *Ercc1* knockout mouse was created (McWhir et al, 1993), a number of different *Ercc1* models have been created in our laboratory.

These will be addressed in more detail in section 1.6 of this introduction. There are also a number of *Ercc1* mouse models that have been created elsewhere. A knockout model has been reported, using a *neo* insertion to disrupt exon 7 of the gene (Weeda et al, 1997). This mouse showed a very similar phenotype to that reported previously, however there was also an indication that sex affected survival of the mice to some extent. Female mice appeared to live somewhat longer and were slightly less runted than male littermates (Weeda et al, 1997). In this publication a second *Ercc1* model was also reported. These mice carry an engineered stop codon at position 292, which results in the production of a truncated Ercc1 protein. These mice are referred to as $Ercc1^{\Delta 7/-}$ and have a life expectancy of around four to six months. $Ercc1^{\Delta 7/-}$ mice are runted, have liver abnormalities and signs of liver dysfunction (Weeda et al, 1997), indicating that this is a useful model with characteristics of Ercc1 absence, but with a longer lifespan.

It should be noted that the consequences of loss of *Xpf*, *Xpg* and *Ercc1* have very similar, severe, consequences for the animals. This reflects the important roles of these endonucleases in other pathways, as well as NER.

Recently a mouse was generated modelling DNA Polη deficiency, with exon 4 of the Polη gene deleted (Lin et al, 2006). These mice have normal life expectancy and do not appear to develop spontaneous tumours, although currently data is not available on these mice after one year of age. Polη

mice do show increased susceptibility to UV induced skin cancer (Lin et al, 2006).

Mouse models have also been created that mimic Cockayne syndrome. The *Csb* model mouse was generated by mimicking a gene truncation found in a CSB patient (van der Horst et al, 1997) and the *Csa* model was created by interrupting exon 2 of the *Csa* gene with a hygromycin insert (van der Horst et al, 2002). These mice are photosensitive, show slightly retarded growth, but have normal sexual function and life expectancy, although the older mice do show some signs of neurodegeneration. Despite these mild CS-like features, these mice are prone to UV induced skin tumours. This highlights a difference between mice and humans: whereas in human CS patients, GGR alone is capable of removing UV induced lesions and preventing tumour formation, in mice TCR must play a greater role (van der Horst et al, 1997 and 2002).

Finally, a mouse model of hHR23B deficiency has been generated, known as *mHR23B*$^{-/-}$. The phenotype reported is much more severe than that of *Xpc*$^{-/-}$ mice, with the majority of mice suffering perinatal death, and although survivors display severely abnormal development, many survive 6 months to one year (Ng et al, 2002). This phenotype confirms that this protein has roles outwith NER, possibly involving protein stability and degradation (Ng et al, 2003).

1.6 Melton group Ercc1 mouse models

Our laboratory was the first to produce an *Ercc1* null mouse model (McWhir et al, 1993), using a previously reported targeted *Ercc1* allele where exon 5 is disrupted by insertion of a *neo* cassette (Selfridge et al, 1992). These animals were severely runted, weighing around 20% that of control littermates, and had an extremely compromised life expectancy of around twenty days. They were found to have a severe liver phenotype which almost certainly was the cause of the premature mortality. Liver polyploidy is a characterised feature of aging, and is likely to be a mechanism by which the liver maintains its complex structure and high function whilst still replicating nuclei (Biesterfeld et al, 1994, reviewed by Gupta, 2000). However, *Ercc1* null mice showed ploidy levels at three weeks of age that were reminiscent of two year old mice. p53 levels were also found to be elevated in the *Ercc1* null mice. Whilst the liver phenotype was extremely interesting, this model of nucleotide repair deficiency did not provide a model comparable with any human diseases and did not allow the study of the consequences of loss of NER on other tissues, simply due to the lifespan of these mice being so short.

As the liver had been identified as the prime focus of pathology in the complete *Ercc1* knockout mice, the next aim was to create a model that was *Ercc1* deficient but had an *Ercc1* proficient liver. This was achieved using an *Ercc1* transgene under the control of the transthyretin promoter (reported in

Selfridge et al, 2001). The use of the transthyretin regulatory sequence provided liver specific expression of the *Ercc1* transgene.

Ercc1 null animals expressing the liver transgene had an alleviated phenotype. Runting was reduced, with animals weighing around 60% of their wild type littermates, and lifespan was extended to 9-12 weeks. Liver pathology was absent in these mice, and hepatic function was normal. However, these animals displayed some kidney abnormalities. These included slightly increased plasma creatinine levels, a four fold increase in kidney 8-oxo-guanine DNA adducts as well as some histopathology and an increase in ploidy levels.

It appeared that having corrected the liver phenotype, these animals were dying with kidney abnormalities. Although these mice have a somewhat extended lifespan, this was still insufficient to carry out any long term studies into the effects of *Ercc1* loss on sensitivity to UV radiation. Some preliminary short term studies were carried out and did show an high sensitivity to UV irradiation in these mice (Selfridge, 1999).

Consequently, work in the laboratory was focused on creating a conditional *Ercc1* knockout with which to study the long term effects of *Ercc1* deficiency in the skin. This was achieved using the *Cre-lox* system of targeted recombination (reviewed by Nagy, 2000). In this system, bacterial recombinase *Cre* is controlled by a tissue specific or development specific

promoter sequence. When or where expressed, *Cre* recombinase recognises two *loxP* sites that have been inserted into the gene of interest, and catalyses a recombination event between these two sites. This effectively excises a portion of the gene, and in our case, renders it inactive. As we wished to create an epidermal specific knockout, we used a transgenic mouse line expressing *Cre* recombinase under the control of the keratin *K5* promoter (Ramirez et al, 2004).

K5::*Cre* has been shown to be expressed in the basal epithelial layer and in hair follicles, but in no other tissue (Ramirez et al, 2004). However, when females carrying the transgene are used for mating, the progeny show recombination activity in all tissue, regardless of whether these mice have themselves inherited the transgene. This is indicative of K5::*Cre* expression in the oocyte (Ramirez et al, 2004). For this reason, our breeding scheme used the K5::*Cre* transgene derived solely through the paternal line.

To create a floxed *Ercc1* allele, exons 3, 4 and 5 of *Ercc1* were replaced with an *Hprt* minigene (Doig et al, 2006, supplementary information figure 1), which in itself created a second *Ercc1* null allele. Subsequently the *Hprt* minigene was replaced by *Ercc1* exons 3 through 5, flanked by *loxP* sites (Doig et al, 2006). A schematic diagram of epidermal specific *Ercc1* inactivation is shown in figure 1.3.

Fig 1.3

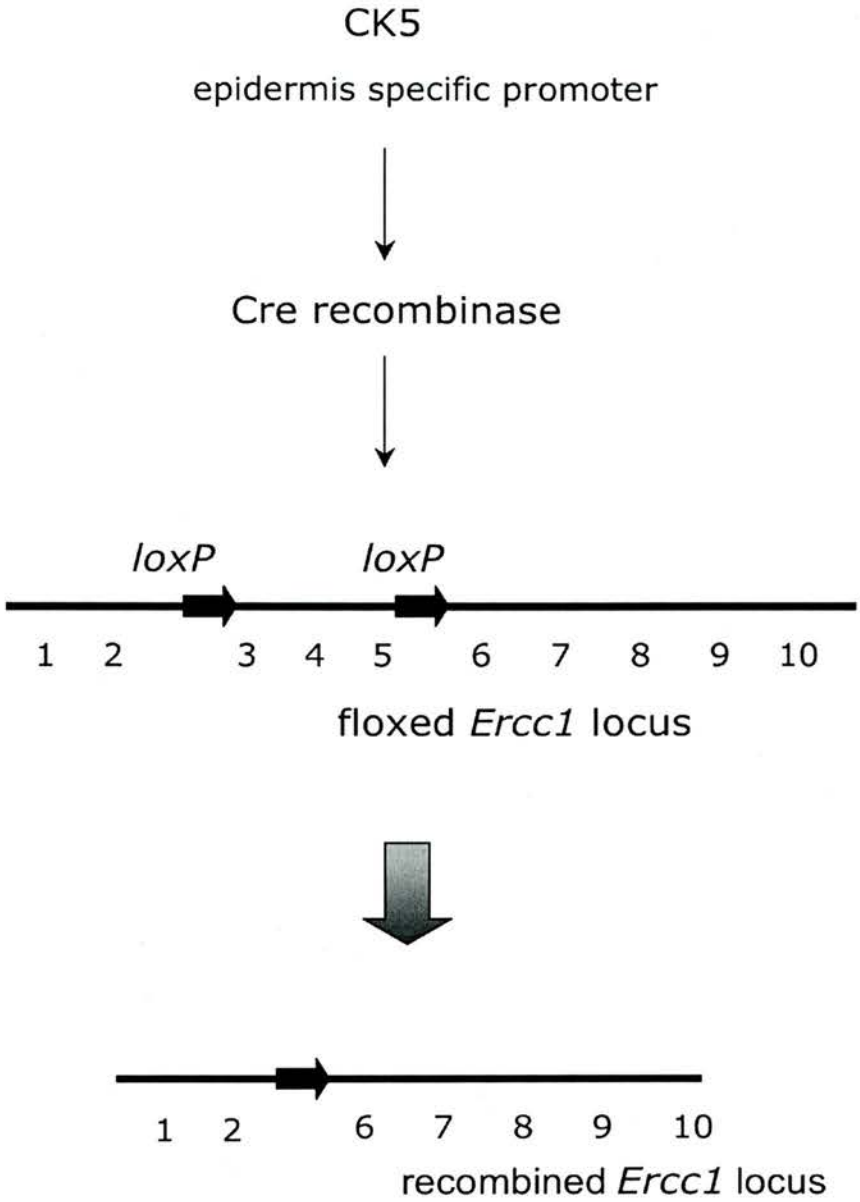

Figure 1.3 Epidermal specific inactivation of *Ercc1*

Cre recombinase expression is controlled by epidermal specific K5 promoter. *Cre* recognises *loxP* sites inserted into the *Ercc1* floxed allele and catalyses a recombination event. This produces the recombined *Ercc1* locus, from which no functional protein is generated.

Using this system we are able to generate mice that have an inactivated *Ercc1* gene in the epidermis. By Southern blot analysis we found 100% recombination levels in the epidermis, whereas recombination levels of less than 5% were found in other internal tissues (Doig et al, 2006).

For all experiments carried out using these animals, *Ercc1*$^{flox/null}$ with K5::*Cre* were used as *Ercc1* epidermal specific knockout (ESKO) mice, and *Ercc1*$^{flox/wild\ type}$ with K5::*Cre* mice were used as controls. As the main reason for developing these mice was to investigate the effects of *Ercc1* deficiency on UV sensitivity, we used these mice on an albino and hairless (*hr*) background.

Using these mice, we were able to study a range of responses to UV radiation. We planned to investigate UV induced carcinogenesis, the importance of which has already been considered, as well as several short term responses to UV irradiation including erythema, photoimmunosuppression and tanning. These aspects will be introduced in some detail below.

1.7 UV induced erythema

Erythema is defined as reddening of the skin and can be caused by a range of factors including infection and inflammation. UV induced erythema is the

result of dilation and congestion of cutaneous blood vessels, and the degree of erythema is proportional to dose until at least 15 MED (Farr and Diffey, 1984). In humans, erythema has been shown to follow a biphasic pattern, with an immediate erythemic peak, followed by a second phase starting around an hour after UV exposure and peaking after 24-48 hours. This pattern is similar in other species apart from the hairless mouse, where only the delayed response is seen (reviewed by Clydesdale et al, 2001).

It is not yet fully clear which substances are responsible for triggering the inflammatory response to UV, as there are contradictory data available. Experiments on rats showed that the addition of BOL-148 inhibited early erythema, implicating 5-hydroxytryptamine (5-HT or serotonin) as having a major role, as BOL-148 is a 5-HT antagonist. In guinea pigs, antagonists of H_1 and H_2 histamine receptors have also been shown to block early erythema. However, unexpectedly, the addition of antihistamines did not block erythema (reviewed by Clydesdale et al, 2001).

Greaves and Sondergaard showed in 1970 that ultraviolet induced erythema in humans is linked with a smooth muscle contracting agent. It is now known that an increase in prostaglandins, in particular PGE_2 and PGF2a, and the prostaglandin precursor arachidonic acid, can be seen at around twenty-four hours after exposure to UVB. PGE_2 is known to be an inflammatory mediator. Tests where inhibitors of prostaglandin synthesis were given, such as indomethacin and aspirin, have shown that these substances decrease

UV-induced erythema but do not prevent it entirely (Clydesdale et al, 2001), suggesting that prostaglandins have a role in the erythemal response but that other substances are also involved.

As well as direct biological damage, UV radiation causes indirect damage by the production of free radicals. Whilst it is mainly UVA that produces reactive oxygen species, UVB does induce the synthesis of nitric oxide from L-arginine. Nitric oxide acts as a vasodilatory agent by increasing levels of cGMP in vascular smooth muscle, causing the blood vessels to relax. Nitric oxide is released by keratinocytes after UVB irradiation, and nitric oxide synthase inhibitor, NG-monomethyl-L-arginine (L-NMMA) has been shown to have a protective effect against UVB *in vivo* in guinea pigs (Deliconstantinos et al, 1995), as well as hairless mice (Russo and Halliday, 2006). This implies a role for nitric oxide in the erythemal response.

The role of DNA damage as an early modulator in the cascade of events leading to UV induced erythema is confirmed by other NER deficient mouse models, which have been shown to be hypersensitive to UV induced erythema. In particular, TCR deficient models are hypersensitive. *Xpa* and *Csb* knockouts have MEDs of 135-270 Jm^{-2} compared with *Xpc* knockouts and controls which have MEDs of 1080-2160 Jm^{-2} (Berg et al, 2000). *Xpa* knockouts have also been reported to have an MED of 62.5 Jm^{-2}, although the controls for this group have MEDs of 500 Jm^{-2} (van Schanke et al, 2005).

1.8 Photoimmunosuppression

Photoimmunosuppression has multiple consequences, including the increased susceptibility of the organism to infections (reviewed by Norval, 2001, 2002 and 2006). However, the importance of photoimmunosuppression in cancer relates primarily to the inability of the organism to recognise antigenic transformed cells which may become malignant tumours.

Langerhans cells (LCs) are a subset of antigen presenting cells found in the epidermis. Their role is to scavenge for antigen, which they trap and internalise using dendritic processes. The LCs then migrate to the draining lymph node and process the antigen using the MHC class II pathway. An LC then presents the antigen to the appropriate naive T cell in the lymph node using MHC class II. In order to activate the T cell fully, the LC must also express other, co-stimulatory molecules on its surface.

Stimulated CD4+ T cells differentiate into either T helper 1 (Th1) or T helper 2 (Th2) cells. Th1 cells release cytokines that promote the cellular immune response (also termed pro-inflammatory). Th2 cells release cytokines that promote the humoral immune response and suppress the cellular immune response (also termed anti-inflammatory). Th2 cytokines are involved in the control of extracellular pathogens, while Th1 cytokines are important in the

control of intracellular pathogens, and, critically, the control of tumour cells. LCs and other DCs can also present antigen to CD8+ T cells, T regulatory (T_{reg}) cells and natural killer T (NK-T) cells.

UV radiation induces the migration of LCs to the lymph nodes in the absence of antigen (Moodycliffe et al, 1992). The function of these LCs is also compromised. LCs visible in the skin after UV irradiation have a drastically altered morphology when viewed using electron microscopy (Dandie et al, 1998). The extensive dendritic processes normally visible are almost completely withdrawn into the cell body. LCs with damaged DNA are found at their highest level in the lymph nodes twenty four hours after exposure to UV (Vink et al, 1996). Enriched populations of dendritic cells from the lymph nodes of UV irradiated sheep have been shown to have impaired antigen presenting capabilities for up to two weeks after a UV dose of a single MED (Dandie et al, 1998). The slow recovery rate of LCs is likely to be due to the repopulation originating in bone marrow (Obata and Tagami, 1985).

LCs from UV exposed skin stimulate the activation of Th2 cells rather than Th1 cells (Simon et al, 1990). T_{reg} cells and NK-T cells are also stimulated by UV exposed LCs and release anti-inflammatory cytokines (Schwarz et al, 2004 and Moodycliffe et al, 2000). This is shown schematically in figure 1.4.

In addition to the loss of normal antigen presenting capacity, there is evidence that UV irradiated LCs are actually inducing tolerance by presenting

Fig 1.4

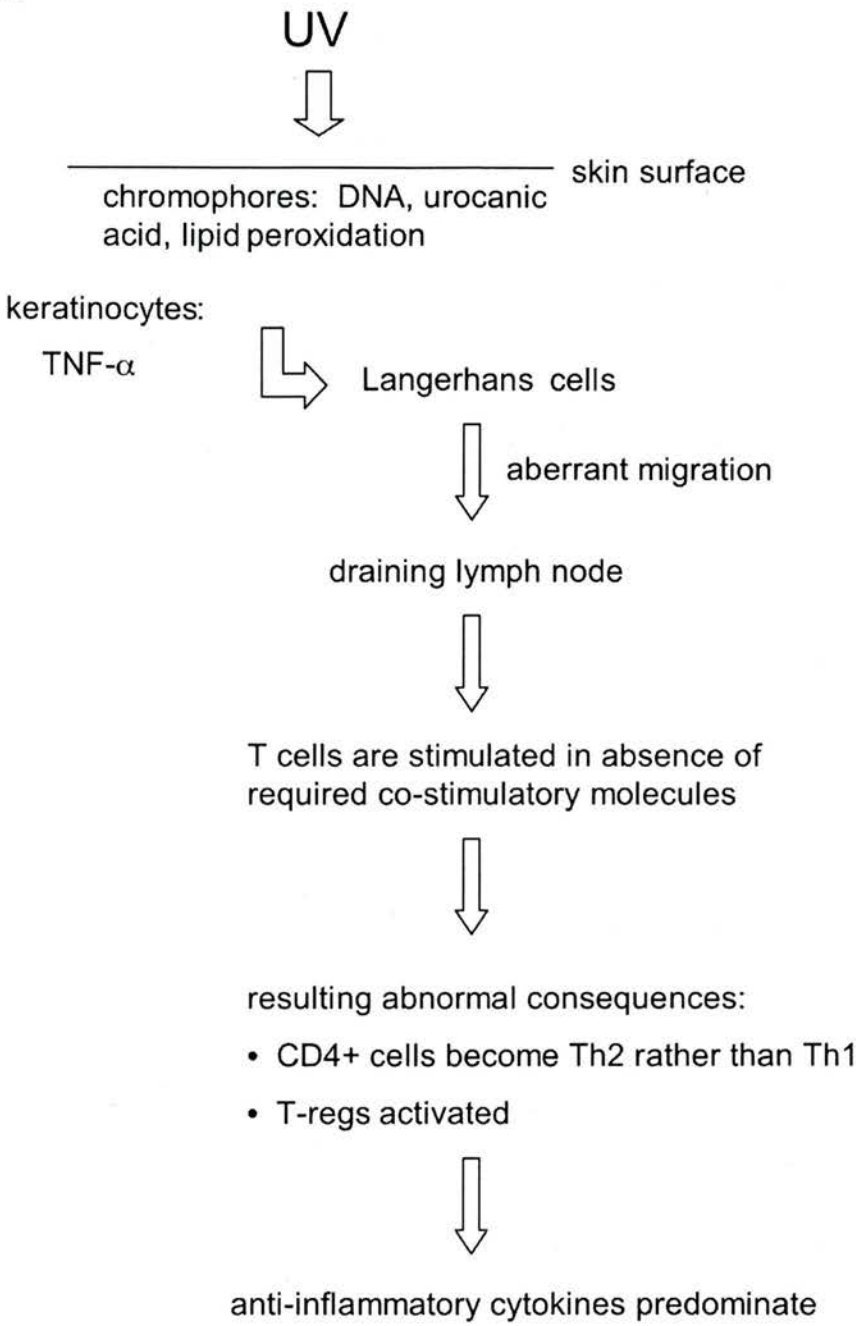

Figure 1.4 Overview of photoimmunosuppression

Photoimmunosuppression is triggered by the release of inflammatory mediators by keratinocytes which induce aberrant Langerhans cell migration. These accumulate in the draining lymph node where they stimulate T cells in the absence of co-stimulatory molecules. This causes a Th2 bias in the immune response, and crucially, activates regulatory T cells (T-regs) which results in the induction of immune tolerance to the antigen in question.

antigen in the absence of the required co-stimulatory molecules. UV exposure has been shown to inhibit the expression of co-stimulatory molecules on the surface of LCs, including intercellular adhesion molecule-1 (ICAM-1) and CD80/CD86 (Komura et al, 2003). Human monocyte derived LC-like dendritic cells have been shown to have reduced endocytic activity and lowered CD32 expression after exposure to UV (Mizuno et al, 2004).

Several factors are implicated in the induction of LC migration. Nitric oxide synthase inhibitor, NG-monomethyl-L-arginine (L-NMMA) has been shown to prevent suppression of the allergic response to nickel as well as preventing the migration of LCs after UV (Yuen et al, 2002 and Kuchel et al, 2003). L-NMMA has also been shown to improve the protective effect of sunscreen on the contact hypersensitivity response (Russo and Halliday, 2006), suggesting a role for nitric oxide. However the main factor is likely to be the bias of the immune system towards a Th2 environment after UV exposure.

DNA is accepted to be an important chromophore for UV radiation. Studies on human XP patients have shown UVB induced depletion of LCs (Jimbo et al, 1992).

In other NER mouse models, epidermal LCs have been shown to be depleted after UV exposure. Previous studies have shown that *Xpa* mice exhibit 59% depletion compared with 33% depletion in controls after a single 250 Jm^{-2} UVB dose (Miyauchi-Hashimoto et al, 1996). In another study, LC

depletion after UV exposure was shown to be greater than control mice in *Xpa* and *Csb* mice but not *Xpc* mice (Kolgen et al, 2003). These findings underline the importance of TCR rather than GGR in the process of photoimmunosuppression.

None of these models studied previously were conditional knockouts, and therefore the cells in the skin and throughout the immune system were repair deficient. Our *Ercc1* knockouts have repair deficient epidermis, but the LCs and other immune system cells are repair proficient. If UV induced migration of LCs is caused solely by DNA damage in the LCs themselves, then our mice might not show increased LC migration after UV exposure compared with repair proficient controls. However if UV induced migration of LCs is caused by factors secreted by DNA damaged keratinocytes, our mice would show increased LC migration after UV.

The contact hypersensitivity (CHS) response is another means with which to assay immune system function, and suppression of the CHS response by UVB radiation is well documented. Previous studies have shown *Xpa* and *Csb* mice to be more susceptible to UV induced suppression of the CHS response than controls, and *Xpc* mice to have a similar sensitivity to controls (Kolgen et al, 2003). This again confirms this importance of TCR over GGR in the immediate response to UV.

Erythema and photoimmunosuppression are provoked at a cellular level by the release of a wide range of cytokines and chemokines. In chapter 3 of this thesis, we will consider the induction of six such factors from repair proficient and deficient keratinocytes after UV irradiation, and consequently a brief introduction to each of these is found below.

Tumour necrosis factor-alpha (TNF-α) promotes local inflammation and endothelial activation, as well as the formation of sunburn cells. Studies have shown that TNF-α is released by keratinocytes after UV exposure (Kock et al, 1990, reviewed by Schade et al, 2005). Levels of TNF-α protein have also been shown to be upregulated in the ears of *Xpa* deficient mice following treatment with systemic immunosuppressive agent dimethylbenz(*a*)anthracene (DMBA) compared with wild type mice (Miyauchi-Hashimoto et al, 2001).

Interleukin-6 (IL-6) is involved in acute phase immune system reaction and fever. Human normal and transformed keratinocytes have been reported to show increased IL-6 mRNA and protein in response to UVB radiation (Kirnbauer et al, 1991). The release of IL-6 by keratinocytes has been linked with DNA damage by the assertion that the UV wavelength spectrum that causes peak IL-6 release coincides with the wavelength spectrum that causes CPD formation (Petit-Frere et al, 1998).

Interleukin-12 (IL-12) is primarily a pro-inflammatory cytokine, its main function being to promote Th1 type differentiation of CD4+ T cells. IL-12 has been shown to prevent photoimmunosuppression as well as restore normal immune function after UV exposure (Schwarz et al, 1996). Furthermore, intra-cutaneous injection of IL-12 has been shown to reduce UV induced apoptosis in wild type mice but not in *Xpa* knockout mice (Schwarz et al, 2002). This may imply a role for IL-12 in the induction of NER. The effects of IL-12 on keratinocytes are well documented (Schwarz et al, 2002 and Molenda et al, 2006). However there is only one published paper documenting UVB induced IL-12 transcription in human keratinocytes (Enk et al, 1996).

Interferon-gamma (IFN-γ) is closely linked to IL-12. IFN-γ activates macrophages and suppresses the Th2 response, and its expression is thought to be induced by IL-12. IL-12 production by spleen cells has been shown to be inhibited by UVB exposure (Garssen et al, 1999). There is no evidence for IFN-γ being released by keratinocytes in response to UV.

Interleukin-10 (IL-10) is a Th2 cytokine and an active suppressor of cellular immune responses. It is released by a range of cells and suppresses macrophage function as well as IFN-γ production (Fiorentino et al, 1991). IL-10 undoubtedly plays an important role in the development of photoimmunosuppression, although its exact role appears to differ between mice and humans. In humans, macrophages and neutrophils appear to be

the main source of IL-10 (Piskin et al, 2005); whilst in mice, keratinocytes produce the majority. In mice, the addition of anti- IL-10 antibodies to supernatants from UVB irradiated keratinocytes has been reported to reverse the immunosuppressive effects of the supernatants on the delayed type hypersensitivity response (Rivas and Ullrich, 1992). Since then, DNA damage has been linked to the production of IL-10 by UVB irradiated keratinocytes, in a paper which showed that liposomes containing a DNA repair enzyme were able to reduce IL-10 secretion by keratinocytes in vitro as well as in vivo (Nishigori et al, 1996). IL-10 has also been shown to be increased in cells of the draining lymph nodes of UV irradiated NER deficient mice (Boonstra et al, 2001).

Macrophage chemoattractant protein-1 (MCP-1) is a chemokine which targets monocytes, T cells and basophils; its main functions being to induce monocytes into a tissue to become active macrophages, to promote histamine release from basophils, and crucially for photoimmunosuppression, to encourage a Th2 type immune response (Janeway et al, 2001). Members of the MCP family have been shown to inhibit the production of IL-12 in tissues rather than in the lymphatic system, and are able to do this specifically without inhibiting IL-10 or TNF-α (Braun et al, 2000). However the effects of UVB radiation on keratinocyte MCP-1 expression have not been studied. With the knowledge that this chemokine suppressed the cellular immune response, we expect MCP-1 levels might be raised in

response to UV, however it is unclear whether studying the effects on keratinocytes alone will provide this result.

1.9 The tanning response

Tanning is an adaptive response that the skin uses to protect itself from UV radiation. Melanin is produced by melanocytes in vesicles called melanosomes and passed to keratinocytes. This is accomplished by a process involving melanocyte exocytosis and keratinocyte phagocytosis (Virador et al, 2002). UV radiation causes melanocytes to increase pigment synthesis (Friedmann and Gilchrest, 1987), although it is clear that keratinocytes play a major role in the regulation of melanin synthesis by paracrine control. Melanocyte stimulating hormone was first defined by Fitzpatrick in the 1950s. There is now known to be a family of hormones which are synthesised by differential processing of pro-opiomelanocortin (POMC) in the pituitary. This family includes α-MSH and adrenocorticotrophic hormone (ACTH). Upon UV exposure, POMC is expressed in the skin, enabling the synthesis of these hormones (Inoue et al, 2003). α-MSH binds melanocortin-1 receptor (MC1-R), a G-protein coupled membrane spanning receptor. When α-MSH binds MC1-R a cascade of events results in expression of tyrosinase and related proteins, which are involved in melanin biosynthesis (reviewed by Yaar and Gilchrest, 2004).

DNA damage was first suggested as a trigger for melanogenesis when T4 endonuclease V, a DNA repair enzyme, was shown to stimulate melanin production by melanocytes in culture (Eller et al, 1994). This hypothesis was strengthened when various DNA damaging agents were shown to increase melanin production by melanocytes in culture (Eller et al, 1996).

Recently, this issue was addressed using *Xpa* knockout mice. These mice showed increased melanogenesis compared with wild type controls after UVB exposure (van Schanke et al, 2005). However the mice used in this study were not conditional knockouts, so all the tissues in the mice were *Xpa* deficient. Consequently, the authors were unable to conclude whether the increased melanocyte proliferation was due to DNA damage in melanocytes themselves or in keratinocytes or fibroblasts.

We plan to approach this issue using our *Ercc1* skin specific knockout mice, although for these experiments we will use mice crossed on to a hairless pigmented background, rather than a hairless albino background. These mice have repair deficient keratinocytes, with wild type melanocytes and fibroblasts. We expect our mice to tan more readily than controls, implicating keratinocytes as major effectors in the tanning response.

1.10 Topically applied thymidine dinucleotides – a possible role in cancer prevention?

The use of topical thymidine dinucleotides was first reported in the mid nineties by Barbara Gilchrest's group in Boston (Eller et al, 1994). Initial reports concerned the application of thymidine dinucleotides (pTpT) to guinea pig and human skin and the subsequent pigment response. These showed that skin 'tanned' in a manner similar to UV-induced increased pigmentation. S91 cells, a murine melanoma line, also responded to pTpT by producing more melanin (Eller et al, 1994; Eller et al, 1996). It was postulated that this response was due to the thymidine dinucleotides mimicking the sequence of DNA excised during the repair of cyclobutane pyrimidine dimers. A year later the same group concluded that pTpT was activating p53 and increasing the rate of DNA repair, using reporter systems as well as measuring damage directly (Eller et al, 1997). This was corroborated when pTpT was shown to upregulate p53, p21 and PCNA in human fibroblasts in a similar manner to UV, and furthermore, pTpT enhanced the UV induced expression of these same factors (Goukassian et al, 1999). pTpT treatment also seems to enhance DNA repair capacity in fibroblasts from older donors, bringing levels of repair proteins in line with those seen in cells derived from newborns (Goukassian et al, 2002).

pTpT appears to mimic the effects of UV radiation in yet another way: levels of tumour necrosis factor-α and interleukin-10 are increased, and in mice, the

contact hypersensitivity response is suppressed (Cruz Jnr et al, 2000 and Curiel-Lewandrowski et al, 2003).

The first paper reporting the long term effect of pTpT application on mouse skin showed that topical treatment alongside a chronic UV irradiation protocol protected against skin cancer development (Goukassian et al, 2004). Interestingly, the published data showed this effect on wild type and *Xpc* heterozygous mice, but did not report the effect on *Xpc* homozygous null mice. As the authors attributed the protective effect of pTpT to an upregulation of DNA repair mechanisms, we would expect to see no protective effect in $Xpc^{-/-}$ mice.

As well as being similar to the by-product of NER, pTpT also shares homology with part of the telomere repeat sequence. As mentioned previously, the ends of our chromosomes are protected from exonuclease activity by a non-coding repeat sequence, TTAGGG (reviewed by de Lange, 2002). The telomere repeat sequence is bound by stabilising factors including TRF1 and TRF2, and forms a characteristic loop structure known as a T loop (Griffith et al, 1999). In this structure, the 3' end of the DNA strand loops back on itself and invades the dsDNA. It is likely that disruption of the loop triggers DNA damage responses within the cell. Oligonucleotides with telomere sequence homology have been shown to induce apoptosis in human lymphocyte cells (Eller et al, 2002) and S phase arrest in human fibroblasts (Eller et al, 2003).

Despite the amount of data published on the activity of topical pTpT treatment and its promising anti-cancer properties, there seems to be a lack of understanding of the mechanisms involved. We believe that our NER deficient model will help further the understanding of how this potentially exciting anti-cancer agent exerts its effects.

1.11 Aims of this thesis

This thesis will further consider the implications of *Ercc1* deficiency by continuing the characterisation of the *Ercc1* mouse models in the lab.

The *Ercc1* epidermal specific knockout (ESKO) mouse will be used to consider the effects of *Ercc1* deficiency on the short and the long term responses to UV, in chapters 3 and 4 respectively, and our hypothesis is that, due to the additional repair functions of *Ercc1* outside the NER pathway, the *Ercc1* ESKO model will prove more sensitive to UV than simple NER knockouts. The short term response refers to UV induced erythema, photoimmunosuppression and tanning. Within this the role of the keratinocyte will be considered, specifically the effect of DNA damage in the keratinocyte on the rest of the skin and indeed the rest of the organism, something we are able to consider thanks to the epidermis specificity of our knockout model. The long term response refers to UV induced

carcinogenicity, which will also be addressed with the *Ercc1* ESKO mouse. The effects of *Ercc1* defiency on UV induced cancer susceptibility is something which has been unable to be considered in the past, due to the absence of a sufficiently long lived mouse model.

The work in chapter 5 follows on from chapter 4, where using the *Ercc1* ESKO mice, we will consider the protective effect of topical thymidine dinucleotide application. This is a treatment that has been shown to protect against UV induced skin cancer in mice, however its mechanism of action remains unclear and is something we are well placed to investigate with our model that is especially susceptible to UV induced cancer.

Chapters 6 and 7 of this thesis characterise further novel aspects of the phenotype seen in the liver corrected *Ercc1* null model, considering additional features of the fur and neurological system respectively.

Chapter 2

Materials and Methods

Materials

2.1 Reagents and suppliers

Abcam: β-tubulin rabbit polyclonal

Aldrich Chemical Company Inc.: sodium maleate hydrate

Amersham: ECL fluorescence kit, Hyperfilm™ MP high performance autoradiography film, Storm 860 PhosphoImager

BD Biosciences: CBA Assay – mouse inflammation kit, FACSArray flow cytometry machine

BDH Ltd.: acetic acid, DePex, hydrochloric acid, 1% aqueous eosin

Becton Dickinson: FACScan flow cytometry machine

Bioline: DNA Hyperladder I

Biometra: thermocycler

BioRad: Gel Doc 2000 System with Quantity One 4.6 software

Calbiochem: anti-neurofilament proteins

Chance Propper Ltd.: micro slides

Dako: monoclonal mouse anti-human Melan-A/Mart 1, goat serum, sheep anti-mouse::FITC

Developmental Studies Hybridoma Bank: anti-SV2

Dia-Stron Ltd.: erythema meter 220

Fisher Scientific: boric acid, chloroform, EDTA, haematoxylin, isoamyl alcohol, isopropanol (propan-2-ol), magnesium sulphate, methanol, 10% SDS, sodium citrate, sodium hydroxide, tri-sodium citrate, xylene

Fluka: glycerol gelatine

Greiner: petri dishes, 96-well plates

Hayman: absolute alcohol

Hettich: Mikro 20 microfuge

Hybaid: gel electrophoresis tank system

Invitrogen: agarose, Benchmark™ prestained protein ladder, NuPAGE™ 4-12% Bis-Tris gel

Menzel-Gläser: Superfrost® plus slides

Midland Oligos: thymidine dinucleotides (pTpT)

Millipore Corp: Immobilon-P transfer membrane

Mitutoyo: micrometer 7309

Molecular Probes: TRITC::α-bungarotoxin

Pfizer: halothane, ramasole

Philips: 20W T12 UVB lamp

Pierce Biotechnology: Bicinchoninic acid (BCA) protein assay kit

Premier International Foods UK Ltd.: Original Marvel dried skimmed milk

Promega: FITC-VAD-FMK (FITC-conjugated active caspase-3 marker), 25mM magnesium chloride, 10x PCR buffer, Taq DNA polymerase

Roche: Protease Inhibitor cocktail tablets

Roche Diagnostics: anti-fluorescein-AP Fab fragments, Combur3 test strips

Sakura: Tissue-Tek O.C.T.™ compound

Santa Cruz Biotechnology: bovine anti-goat::HRP, ERCC1 (D-16) goat polyclonal IgG, goat anti-rabbit::HRP

Scientific Laboratory Supplies Ltd.: 45mm filters, coverslips

Serotec: goat anti-mouse IgG (Fc)::FITC

Sigma: ADP, ammonia, ammonium polysulphide, D-glucose, DMSO, EDTA, fast blue BB diazonium salt, 40% formalin, gold chloride, Hoechst 33258, Igepal CA-630 (previously Nonidet P40), lead(II) nitrate, levamidasole, magnesium sulphate, naphthol-AS-BI-phosphate, neutral red, oxazolone (ethoxymethylene-2-phenyloxazol-5-one), PBS tablets, propidium iodide, ribonuclease inhibitor, silver nitrate, sodium cacodylate, sodium chloride, sodium deoxycholate, sodium hydroxide, sodium maleate dibasic, sodium thiosulphate, spermine tetrahydrochloride, sucrose, trypsin, trypsin inhibitor, Triton X-100, Trizma® hydrochloride, Tween20

Sigma-Genosys: PCR primers

Starstedt: 48- and 96-well PCR plates

Vector: mouse on mouse kit

VWR International: microscope slides

2.2 Cell culture reagents

Beckman-Coulter: Isoton®II diluent

BioRad: Chelex® 100 resin

Cellstar®: tissue culture flasks

Coulter: coulter counter, FACScan machine

Gibco™: DMEM

Greiner Bio-one: cell culture dishes, pipettes

Sigma: DMSO, epidermal growth factor, L-glutaminic acid, penicillin G, streptomycin

2.3 Cell culture media

Keratinocytes were maintained in media with a low calcium concentration to prevent the cells from becoming differentiated.

The following Dulbecco's Modified Eagle's Medium (DMEM) was used:

1x 0.1mm filtered

high glucose

with pyridoxine hydrochloride

without L-glutamine

without sodium pyruvate

without calcium chloride

This medium was supplemented as follows:

8% chelex treated FCS (to minimise $[Ca^{2+}]$)

1% epidermal growth factor

1% L-glutamine

25U/ml penicillin

25μg/ml streptomycin

For long term storage, cells were frozen in liquid nitrogen using the culture medium above supplemented with 10% DMSO and 20% chelex treated FCS.

2.4 Solutions and buffers

Ammoniacal silver solution: concentrated ammonia was added drop by drop to 40ml 5% aqueous silver nitrate until a faint opalescence remained after shaking

CA: 24 parts chloroform, 1 part isoamyl alcohol

Cacodylate formaldehyde fixative: 0.8M sodium cacodylate, 0.2M sucrose, 4% formaldehyde

Davidson's solution: 115ml glacial acetic acid, 330ml 95% ethanol, 220ml neutral buffered formaldehyde and 335ml ultrapure water

FACS citrate buffer: 8.55% sucrose, 5% DMSO, 40mM tri-sodium citrate, pH7.6

FACS stock solution: 3.4M tri-sodium citrate, 0.5M Tris-HCl, 1% NP40, 0.52mg/ml spermine tetrahydrochloride, pH7.6

FACS solution A: 30mg/ml trypsin in stock solution

FACS solution B: 0.5mg/ml trypsin inhibitor, 0.1mg/ml ribonuclease inhibitor in stock solution

FACS solution C: 0.42mg/ml propidium iodide, 1mg/ml spermine tetrahydrochloride in stock solution

Fast blue BB solution: 1mM levamisole, 0.88mM naphthol-AS-BI-phosphate, 0.24mM fast blue BB diazonium salt in 100mM Tris HCl, pH9.2; passed through a 45mm filter

Formalin fixative: 4% formaldehyde in phosphate buffered saline

IHC citrate buffer: 10mM sodium citrate dihydrate

Loading dye: 20% glycerol, 100mM EDTA, 0.1% bromophenol blue

Mixed buffer: 16.6mM $MgSO_4$, 66.7mM D-glucose

Modified RIPA buffer: 50mM Tris-HCl, 1% Triton X-100 v/v, 0.2% sodium deoxycholate w/v, 0.2% sodium dodecyl sulphate v/v, 1x protease inhibitor mix

PCA: 25 parts redistilled phenol, 24 parts chloroform, 1 part isoamyl alcohol

Proteinase K: 2% proteinase K v/v in sterile distilled water

TBE: 90mM Tris-HCl, 90mM boric acid, 2mM EDTA, pH 8.3

TBS: 0.005M Tris-HCl, 0.075M NaCl

TBS-T: 0.005M Tris-HCl, 0.075M NaCl, 0.05% Tween-20 v/v; pH 7.4

Tissue lysis buffer: 400mM NaCl, 10mM Tris-HCl, 3mM EDTA, 1% SDS v/v

Tris/mal buffer: 0.19M Tris-HCl, 0.18M sodium maleate, 0.25M sodium hydroxide

Tris/mal rinsing buffer: Tris/mal buffer diluted 2:3 in water

2.5 Cell culture lines

The cell lines used are described in table 2.1.

Table 2.1 Cell lines

Line	Description	Source
Ercc1 +/+ keratinocytes	Immortalised mouse keratinocytes	Melton, unpublished data
Ercc1 -/- keratinocytes	Immortalised *Ercc1* deficient mouse keratinocytes	Melton, unpublished data
PAM212 keratinocytes	Immortalised mouse keratinocytes	Kindly provided by John Mee, King's College London

2.6 Oligonucleotides

All oligonucleotides were synthesised by Sigma-Genosys.

Table 2.2 PCR primers

Code	Sequence (5'→3')	Location	PCR reaction
432E	TGCAGAGCCTGGGGAAGAACTTCGC	*Ercc1* exon 5	Floxed/WT *Ercc1*
F25732	TCAAAGTATGGTAGCCAAGGCAGC	*Ercc1* exon 5-3'	Floxed/WT *Ercc1*
262W	AGCCTACCCTCTGGTAGATTGTCG	HPRT cassette	KanTai KO
G22234	GCTGTCTCCCTGGCTCTGGATCTG	*Ercc1* exon 1-3'	KanTai KO
SkCre>	ACCTGCCATGAAGACAGCGTTTGCAC	K5::*Cre*	CK5 transgene
SkCre<	TGCACGTTCACCGGCATCAACG	K5::*Cre*	CK5 transgene
F25731	TGTCTCCCTGGCTCTGGATCTGAC	*Ercc1* exon 2-3'	Recombined *Ercc1*
F25732	TCAAAGTATGGTAGCCAAGGCAGC	*Ercc1* exon 5-3'	Recombined *Ercc1*
033M	CCCGTGTTGAAGTTTGTGCG	*Ercc1* exon 4	Original KO/WT
M4956	GGTTCGAAATGACCGACCAAG	Neo cassette	Original KO/WT
Intron5.1	CATTCTGCACTGAGGTCCTGA	*Ercc1* exon 5-3'	Original KO/WT
033M	CCCGTGTTGAAGTTTGTGCG	*Ercc1* exon 4	TTR transgene
035M	CGAAGGGCGAAGTTCTTCCC	*Ercc1* exon 5	TTR transgene
Gen9-3'	GCTCAGTGATGATCAAAGGAGGTGG	*Ercc1* exon 1-5'	Origin of WT *Ercc1*
Gen6	CCCTTCCCGACCCTGCCCGCTCTGG	*Ercc1* exon 1-5'	Origin of WT *Ercc1*
D6Mit357a	TACAATGGCTCTCCTCCCTG	Chromosome 6	α-synuclein
D6Mit357b	CCTCAGGATTTAAATAAATTCAAGC	Chromosome 6	α-synuclein
D6Mit122a	GACACCCAGCATCCATCTTT	Chromosome 6	α-synuclein
D6Mit122b	TTGTAATTTTTAAAAGATAGGTGTGTG	Chromosome 6	α-synuclein
V0727	GTCAGATTCAGAACCAACAAAG	*Ligase* exon 27	Lig1 WT
V2014	AGTGTTCCCATGGCACAAGTGGCTGGAAGC	*Ligase* exon 27-3'	Lig1 WT

2.7 Animal husbandry

Mice were maintained in a specialised facility and all procedures were covered by a Home Office project licence. I am holder of a current Home Office personal licence which also covers all procedures carried out.

Mice were kept under a twelve hour light/dark cycle, with standard mouse feed and tap water. All mice had cages lined with wood shavings apart from the hairless mice, which had a softer paper based bedding, to avoid problems occurring with their sensitive skin.

Pups were weaned into single sex cages, with a maximum of six animals per cage, at twenty one days. Identification of individual animals was by ear marking. The notches removed from the ears for marking was used for DNA preparation and genotyping assays.

Culling was carried out by schedule one method whenever possible. If necessary animals were culled by CO_2 asphyxiation.

Whenever possible, breeding pairs were set up using animals from the fourth litter of the previous cross.

2.8 Breeding schemes

The breeding schemes for animals in the *Ercc1* skin specific knockout stock are shown in figures 2.1, 2.2 and 2.3. All the animals involved in creating this stock were albino and hairless. In order to generate the pigmented hairless animals used for the tanning experiments, the stock was crossed onto a C57BL/6J background. The scheme for the *Ercc1* liver corrected knockout stock is shown in figure 2.4.

Fig. 2.1

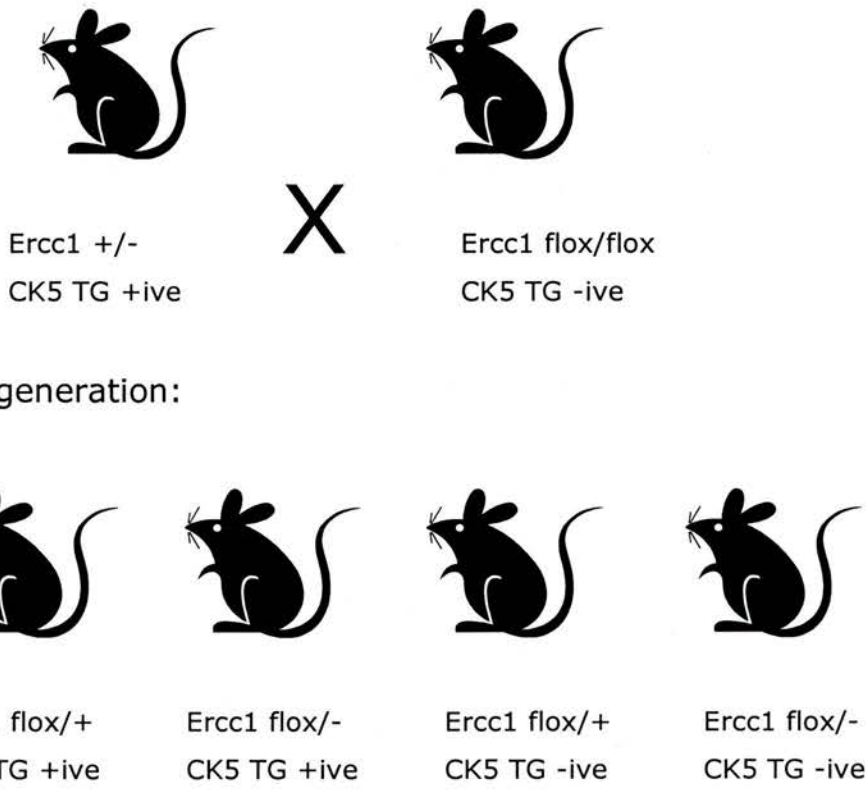

Figure 2.1 Breeding scheme for CK5 transgene stock

This stock is maintained on a hairless, albino background. Ercc1 heterozygous males with the CK5 transgene are crossed with females from a separately maintained floxed Ercc1 homozygous stock. This is because whilst in the adult mouse the CK5 transgene is expressed specifically in the basal layer of the epidermis, it is also expressed transiently in the ova. This causes pups from CK5 TG +ive females to express CK5 throughout their system.

Ercc1 flox/- CK5 TG +ive animals are used in experiments as skin specific knockouts, and Ercc1 flox/+ CK5 TG +ive animals are used as controls.

Fig. 2.2

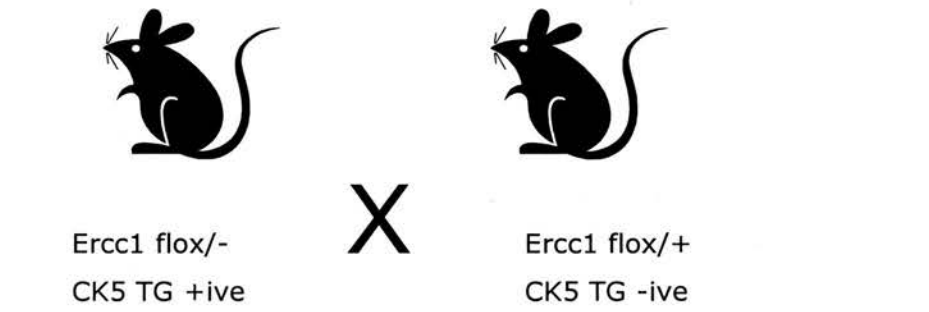

F1 generation:

Of these pups, half will be CK5 TG +ive and half will be TG -ive

Figure 2.2 Breeding scheme for CK5 transgene stock

This alternative cross produces a lower ratio of useful animals, but allows more of the animals from the main cross to be used as breeding animals. The CK5 transgene has to come from the male parent and the ratios given for the pups assume that the male is heterozygous for the transgene.

Fig. 2.3

Ercc1 flox/+
CK5 TG +ive

X

Ercc1 flox/-
CK5 TG -ive

F1 generation:

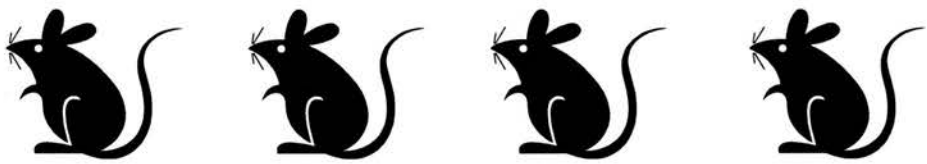

Ercc1 flox/flox | Ercc1 flox/+ | Ercc1 flox/- | Ercc1 +/-

Of these pups, half will be CK5 TG +ive and half will be TG -ive

Figure 2.3 Breeding scheme for CK5 transgene stock

This alternative cross is effectively the same as the one shown in figure 2.2. It is another variation which includes all the necessary alleles, allowing more of the stock animals to be used for breeding. Again, the CK5 transgene has to come from the male parent and the ratios given for the pups assume that the male is heterozygous for the transgene.

Fig. 2.4

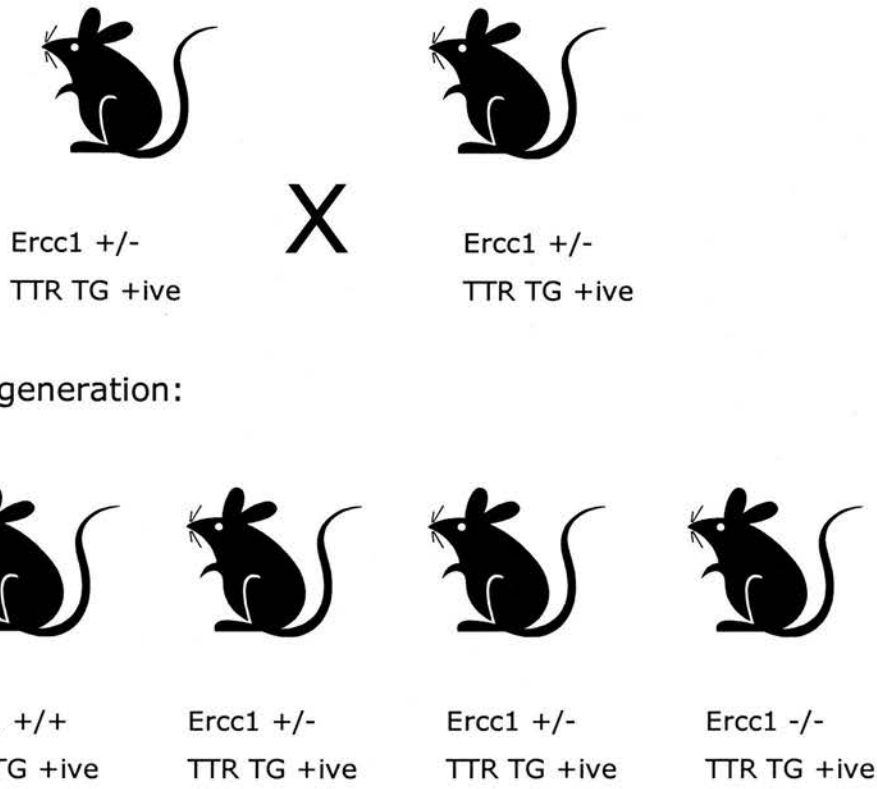

Figure 2.4 Breeding scheme for TTR transgene stock

This stock is maintained by crossing two Ercc1 heterozygotes with the TTR transgene, as Ercc1 nulls (with transgene) are infertile. If both parents are homozygous for the transgene, or even if one is homozygous and one is hemizygous, all the pups will be transgene positive. This is what we have tried to achieve. If both parents are hemizygous then some transgene negative pups will be produced, and will be culled upon identification.

2.9 Preparation of genomic DNA from mouse tissue biopsies

An ear section was taken from the mice using a standard ear punch. The section was then placed in 500μl tissue lysis buffer with 15μl 2% proteinase K solution overnight, on a shaker at 37°C.

Phenol-chloroform extraction: 500μl PCA was added to the suspension and mixed thoroughly. This was then micro-centrifuged at 13000*g* for five minutes. The aqueous phase was removed and transferred to a new eppendorf. The phenol phase was discarded. 500μl CA was added to the new eppendorf and mixed thoroughly, before being micro-centrifuged again at 13000*g* for five minutes. The aqueous phase was removed and transferred to a new eppendorf, and the lower phase was discarded. 500μl propan-2-ol (isopropanol) was added to the new eppendorf and inverted several times. The DNA was allowed to precipitate for ten minutes before micro-centrifugation at 13000*g* for three minutes. The supernatant was the discarded and the pellet washed using 70% ethanol. The pellet was then left to dry for an hour before resuspending in sterile, deionised water. The DNA was then stored at -20°C.

2.10 Genotyping of mouse stocks by Polymerase Chain Reaction (PCR)

PCR was used to determine the genotypes of newly weaned mice in the transgenic stocks. Each reaction tube contained 5μl PCR buffer (Promega),

2μl PCR Mg^{2+} ions (Promega), 1μl Taq polymerase (Promega), 1μl 5mM mixed dNTPs, 1μl of each primer and was made up to 50μl using sterile, double distilled water.

Table 2.3 shows the primers used for each of the genotyping PCR reactions and the conditions that were used.

Table 2.3 PCR asay conditions

PCR	Primers	Products	Conditions
Floxed/WT *Ercc1*	432E F25732	Floxed: 500bp WT: 1100bp	94°C 5 mins, (94°C 1min, 65°C 1min, 72°C 2mins)x30, 72°C 5 mins
KanTai KO	262W G22234	KO: 500bp	94°C 5 mins, (94°C 1min, 65°C 1min, 72°C 1.5mins)x30, 72°C 5 mins
CK5 transgene	Skin Cre> Skin Cre<	TG: 1400bp	94°C 5 mins, (94°C 1min, 65°C 1min, 72°C 1.5mins)x30, 72°C 5 mins
Recombined *Ercc1*	F25731 F25732	R: 200bp	94°C 5 mins, (94°C 1min, 67°C 1min, 72°C 30secs)x30, 72°C 5 mins
Original KO/WT	033M M4956 Intron5.1	KO: 900bp WT: 700bp	94°C 5 mins, (94°C 1min, 68°C 1min, 72°C 1min)x30, 72°C 5 mins
TTR transgene	033M 035M	TG: 170bp	94°C 5 mins, (94°C 1min, 68°C 1min, 72°C 1min)x30, 72°C 5 mins

Figure 2.5 shows the locations of the primers on the alleles in the CK5 TG stock and figure 2.6 shows the locations of the primers on the alleles in the TTR TG stock.

Fig. 2.5

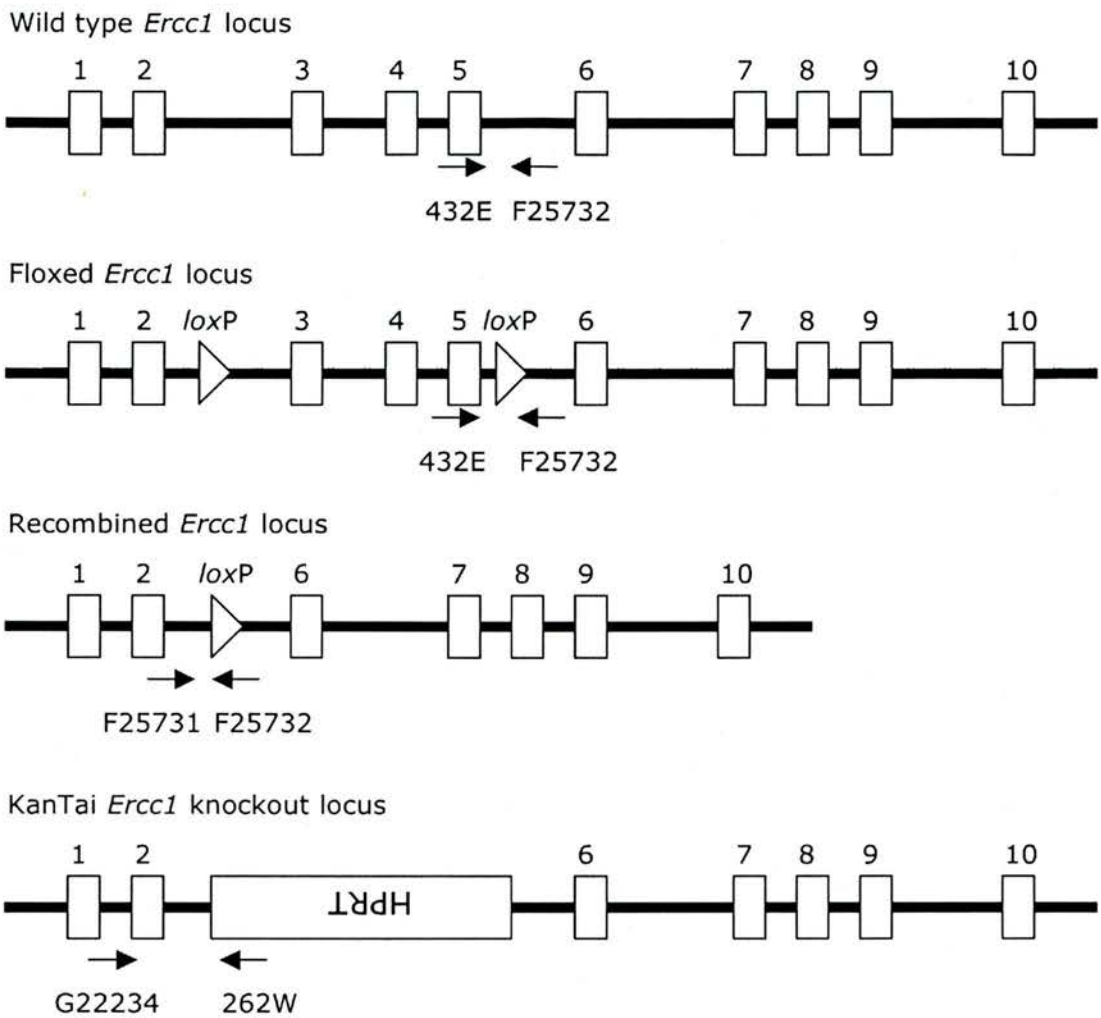

Figure 2.5 Ercc1 loci and primer positions in Ercc1 skin specific knockout animals

One PCR reaction distinguishes between the wild type and floxed allele as these result in slightly different sized products. The recombination PCR will only yield a product when the recombination event has taken place, otherwise the primers are too far apart. A third PCR identifies the KT KO allele, with one of the primer sequences located in the HPRT insert.

Fig 2.5b

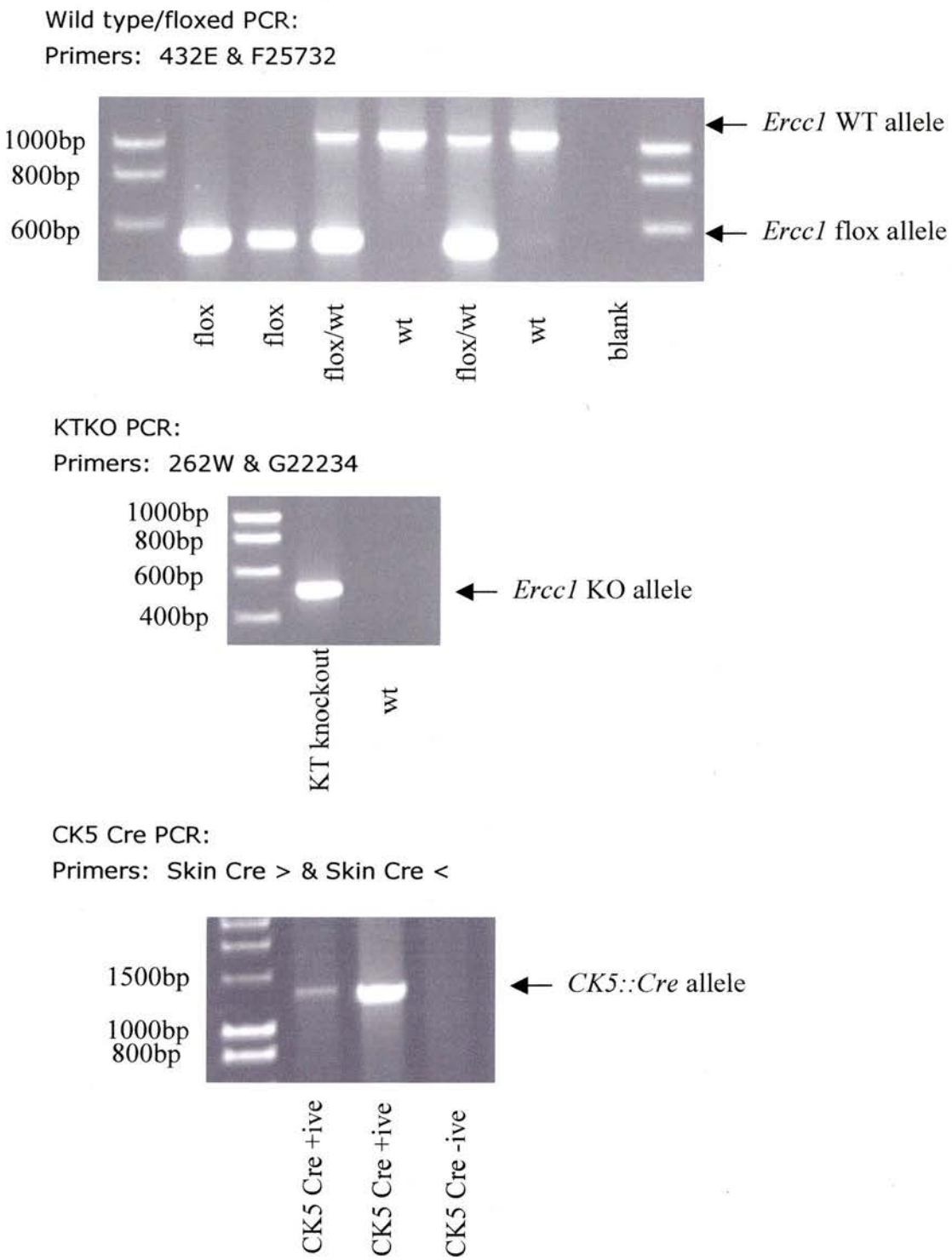

Figure 2.5b Genotyping PCRs used to identify animals in the *Ercc1* ESKO stock

PCRs were run according to conditions shown in table 2.3

Fig. 2.6

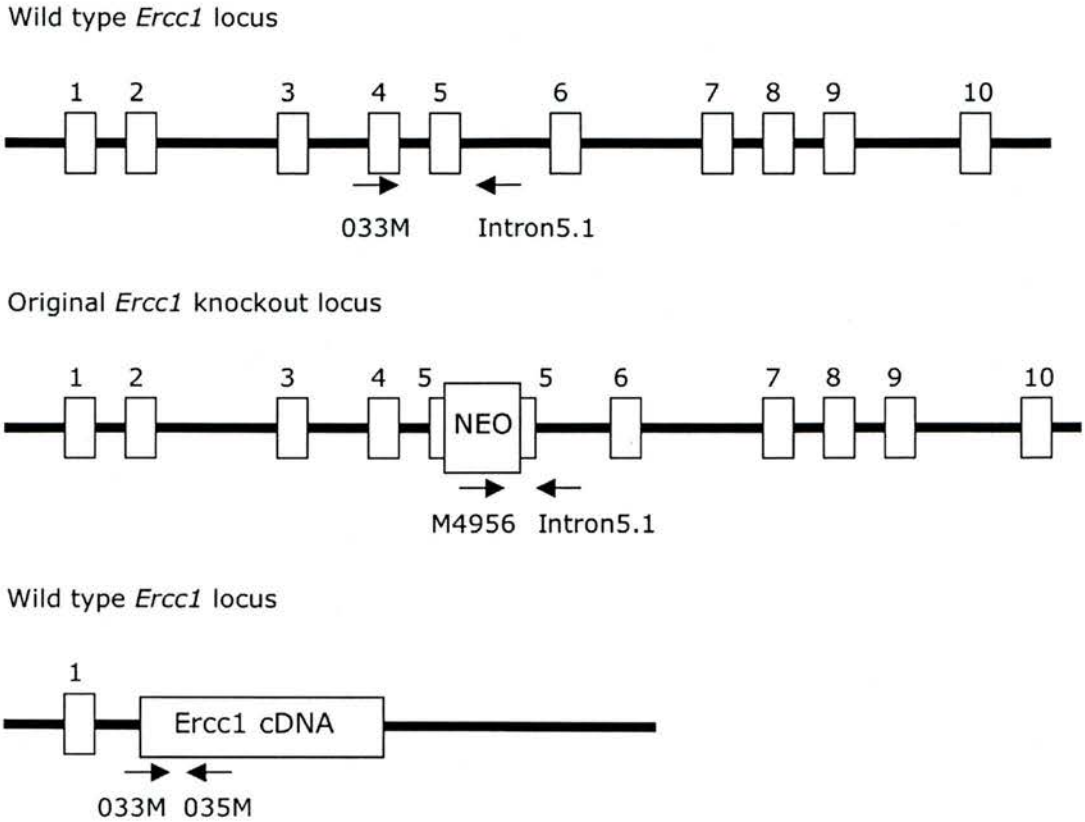

Figure 2.6 Ercc1 loci and primer positions in Ercc1 liver corrected null animals

A single, three primer PCR identifies the wild type and null alleles. Primer M4956 in the NEO insert identifies the original knockout allele. Primers 033M and Intron5.1 identify the wild type allele, and are too far apart to yield a product in the knockout locus. 033M and 035M identify the liver replacement transgene by yielding a small product due to 035M's location in the cDNA.

Fig 2.6b

Wild type/knockout PCR:
Primers: 033M, Intron5.1 & M4956

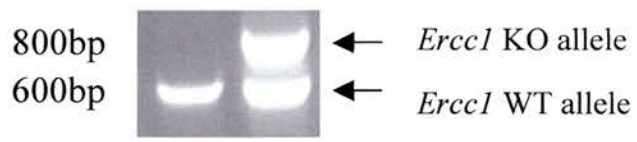

Transgene PCR:
Primers: 033M & 035M

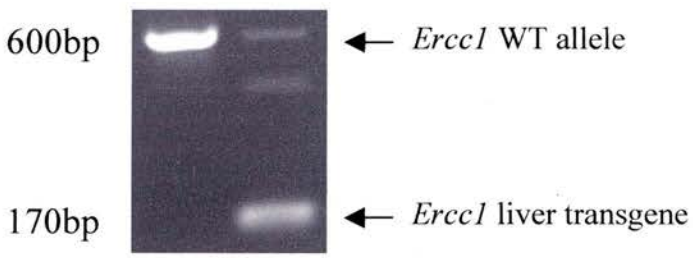

Figure 2.6b Genotyping PCRs used to identify animals in the *Ercc1* liver corrected null stock

PCRs were run according to conditions shown in table 2.3

2.11 Separation of DNA fragments by electrophoresis

DNA fragments were separated by gel electrophoresis using 1-2% (w/v) agarose in TBE with 0.5mg/ml ethidium bromide for visualisation. Loading dye was added to the DNA samples to a final concentration of 20%. DNA Hyperladder I was used to provide size markers with which to compare the band sizes. Electrophoresis was carried out in a horizontal tank, with a TBE buffered system, with a voltage of 75-150V run through the system. UV light was used to visualise the DNA fragments and the gel image captured using Gel Doc EQ software.

2.12 Cell culture

The keratinocytes used in experiments were maintained in low calcium medium as stated previously, in an incubator at 37°C with 5% CO_2. Flasks were split twice a week and medium changed at least every second day, using aseptic technique inside a category II biological safety hood. When required, medium was aspirated (along with dead, floating cells), cells were passaged using trypsin solution and counted using a Coulter cell counter.

2.13 Cell culture irradiation

Keratinocytes were plated out at a density of 10^6 in 35mm Petri dishes in 2ml of medium, the day before UV irradiation. For irradiation, the medium was aspirated from the dishes and replaced with 0.2ml phosphate buffered saline (PBS). Cells were irradiated for a length of time determined exactly by the removal and subsequent replacement of the lids on the Petri dishes. After irradiation, the PBS was aspirated and replaced with 1ml medium. Medium was removed from the cultures and stored at -20°C for future use.

2.14 Ultraviolet light irradiation

Ultraviolet B irradiation was carried out using a Philips TL20W/12RS tube, emitting $2.4 Jm^{-2}s^{-1}$ from a fixed position. The lamp was held in position in the lid of a glass sided aquarium tank, the outer dimensions of which were 76cm x 30.5cm x 38cm. The glass walls of the tank were 5mm thick. The lamp was calibrated to national standards in this position. This lamp emits predominantly UVB, with some UVA as well as small amounts of UVC (Snellman et al, 2003).

2.15 Measurement of erythema and melanin

Erythema and melanin in the mice was measured using an erythema meter (Dia-Stron Ltd, model 220). The erythema meter contains a tungsten-halogen lamp which shines white light into a fibre optic probe. The probe is held in contact with the skin, and collects any light scattered back from the skin. The collected light is analysed at the following three wavelengths:

546nm (green)

632nm (orange/red)

905nm (near infra-red)

Haemoglobin absorbs light at around 546nm, so the strength of the signal at this wavelength is inversely proportional to the amount of haemoglobin present. The signal at 632nm acts as a reference as it corrects for skin tone.

Erythema index is calculated as follows and is based on work published in the British Journal of Dermatology in 1984 (Diffey and Farr):

Erythema index = log10 (632nm/546nm) x 1000

Melanin absorbs light at around 632nm, and the 905nm signal is used as a reference for this index:

Melanin index = log10 (905nm/632nm) x 1000

2.16 Topical application of thymidine dinucleotides

Thymidine dinucleotides were obtained from Midland, TX and maintained as a 2mM stock solution in dH_20 at -20°C. For use, stock solution was diluted 1:20 in 3 parts PG and 1 part DMSO to give a 100μM solution. 60μl of this solution was applied to each animal.

Control animals were treated with PG/DMSO diluent alone.

2.17 Contact hypersensitivity assay

Protocol adapted from El-Ghorr and Norval, 1999: Mice were sensitised using 1% oxazolone (ethoxymethylene-2-phenyloxazol-5-one) dissolved in 4:1 acetone:olive oil. Using a pipette, 50μl of the sensitiser (for negative controls, acetone/olive oil mix alone) was dropped on to the dorsal or ventral skin of the animal and left to absorb. 5 days later, ear thickness was measured using a micrometer (Mitutoyo, Japan). 20μl 0.25% oxazolone was then pipetted on to each ear of the animals. After a further 24 hours, the ear thickness was re-measured using the micrometer. The increase in ear thickness was then calculated, and the values obtained for each ear were averaged to provide a reading for each group.

2.18 ATPase staining of Langerhans cells

Protocol adapted from Chaker et al, 1984: Mouse ears were collected and split, before floating in 20mM EDTA, pH7.2 at 37°C for two hours. Epidermal sheets were peeled off and fixed in cacodylate formaldehyde fixative for one hour, then rinsed three times in PBS. The sheets were then stained in a 3:2 solution of mixed buffer and tris/mal buffer containing 1.4mM ADP and 3.6mM lead (II) nitrate for seventy minutes. The sheets were then rinsed three times in tris/mal rinsing buffer and incubated in 2% ammonium polysulphide for five minutes at room temperature. The epidermal sheets were then transferred to dH_20 and placed on slides, mounted with 90% glycerol in PBS and covered with a coverslip. Sections were stored at 4°C and ATPase positive cells were counted under the microscope. Cells were counted per field view, multiplied up to a value per mm^2. Ten field views were counted per ear and the twenty values averaged to give an average per mouse.

2.19 Cytometric bead array (CBA) test

Cytokine concentrations were assayed using the CBA mouse inflammation kit from BD Biosciences, on supernatants collected from cell culture dishes and stored at -20°C for later use. Briefly, assay standards were prepared using the lyophilised standard provided in the kit. The six bead reagents

were pooled in the appropriate quantities – using 5μl of each capture bead for each assay rather than 10μl as described – and vortexed. 25μl mixed capture beads (rather than 50μl as recommended) was placed in wells of a 96-well plate, followed by 50μl standard or sample. 25μl PE detection reagent from the kit was then added to each well and the plate incubated for two hours at room temperature, protected from the light. 100μl wash buffer from the kit was added to each well, and the plate centrifuged at 200*g* for five minutes. The supernatant was discarded, and 120μl wash buffer added to each well, to resuspend the bead. The plate was then analysed using the FACSArray machine (BD Biosciences) and FACSArray/CBA software.

2.20 Preparation of epidermal samples for FACScanning

A section of dorsal skin was dissected from the mouse. The skin was then floated, inner side down, on 20mM EDTA in PBS for two hours at 37°C. The epidermis was peeled off the rest of the skin section, which was discarded, and placed in 100μl citrate buffer in an eppendorf tube. 450μl FACS solution A (trypsin solution) was added and the tube incubated for 30 minutes on a rotating wheel at room temperature, and vortexed at intervals. 325μl FACS solution B (trypsin inhibitor) was added, before a further 10 minutes on the rotating wheel at room temperature. 250μl FACS solution C (propidium iodide) was added, mixed by inversion, and the mixture incubated on ice for 10 minutes. The sample was then filtered through sterile gauze, before

running through the Becton Dickinson FACScan machine. Data was analysed using Lysis II software to assess the proportions of cells in G1/G0, S-phase or G2. Sub-G1/G0 cells were considered apoptotic.

2.21 Protein extraction

Tissue was collected into eppendorf tubes and snap frozen in liquid nitrogen. Samples were shattered before homogenisation in modified RIPA buffer. Lysates were then kept on ice for 20 minutes before centrifugation at 2000*g* for 15 minutes, then aliquoted and stored at -80°C.

2.22 Protein concentration assay

Protein concentration was determined using the BCA assay kit. 5μl sample was incubated with 200μl mixed A and B solution as per kit instructions for 30 minutes. Absorbance at 562nm was measured and protein concentration calculated using a standard curve.

2.23 Western blotting

Western blotting was used to determine ERCC1 levels in skin samples. Equivalent amounts of total protein lysate were loaded onto a pre-cast SDS-

PAGE gel and run at 100V, then transferred onto a membrane at 4°C for one hour. The membrane was then washed in TBS-T and blocked using 5% powdered skimmed milk in TBS w/v, for one hour, before incubating with primary antibody in 5% powdered skimmed milk in TBS w/v overnight, at 4°C. The membrane was washed three times in TBS-T for 5 minutes each time before incubating with secondary antibody in 5% dried skimmed milk in TBS w/v for one hour. The membrane was washed three times in TBS-T for 5 minutes each time and finally for 5 minutes in TBS. Fluorescence was visualised using enhanced chemiluminescence (ECL) and signals were detected by conventional photographic film, or by the Storm PhosphoImager system. β-TUBULIN was used as a loading control for ERCC1.

2.24 Fixation of tissue

Excised tissue was fixed in 4% formaldehyde in PBS overnight before being transferred into 70% ethanol. Skin sections were laid out onto blotting paper before immersion in fixative to keep them flat and prevent folding of the samples.

2.25 Fixation of eye orbits

Eye orbits were enucleated from the mice using fine forceps. The eye orbits were then fixed in Davidson's solution at room temperature for 24 hours. The orbits were then gently dehydrated at room temperature. Firstly they were immersed in 30% ethanol for 2 hours, then 50% ethanol for a further 2 hours. They were then stored in 70% ethanol at 4°C.

2.26 Haematoxylin and eosin stain

It should be noted that all H&E stains apart from the retinal sections were carried out by the Department of Pathology, University of Edinburgh using their own version of the protocol.

Slides were de-paraffinised using three washes in xylene for five minutes followed by two washes in 100% ethanol for five minutes.

Slides were then hydrated by immersion in 90% ethanol for three minutes, then 70% ethanol for three minutes, then 50% ethanol for three minutes, then 30% ethanol for three minutes and lastly by immersion in running water for three minutes.

Slides were then stained for three minutes in haematoxylin, then rinsed well in running water. They were then immersed in acid/alcohol (1%HCl in 70% ethanol) for ten seconds and rinsed in water, before being immersed in saturated lithium chloride solution for ten seconds and rinsed in water again.

Slides were stained in eosin (three parts 1% aqueous eosin: one part 1% ethanol: two parts glacial acetic acid) for two minutes, rinsed briefly in water then in absolute ethanol. They were then immersed in absolute ethanol for one minute.

Slides were dehydrated by immersing in 100% ethanol for five minutes, three times, then xylene for five minutes, twice.

The slides were left to drip dry before coverslips were mounted using DePex and left to set overnight.

2.27 Masson-Fontana stain

The Masson-Fontana staining was carried out by Frances Rae in the NHS Royal Infirmary of Edinburgh Pathology department. Skin sections were fixed and embedded as for H&E staining. Sections were deparaffinised by two, five minute washes in xylene and then hydrated by three, five minute washes in decreasing concentrations of ethanol before washing in running water. Sections were then stained with ammoniacal silver solution at 56°C for 20 minutes, and checked periodically in this time. They were then washed in copious distilled water, toned in 5% gold chloride w/v for 5 minutes and washed again in distilled water before fixing in 5% sodium thiosulphate w/v. Sections were then washed in distilled water and counterstained with 0.1% neutral red for 1 minute before dehydration by immersing in 100% ethanol for five minutes, three times, then xylene for five minutes, twice. The

slides were left to drip dry before coverslips were mounted using DePex and left to set overnight.

2.28 Melan-A/Mart 1 immunohistochemical stain

Skin samples were fixed in 4% formalin, embedded in paraffin, sectioned and mounted on Superfrost® slides. Sections were deparaffinised by two, five minute washes in xylene and then hydrated by three, five minute washes in decreasing concentrations of ethanol before washing in running water. The slides were then boiled in citrate buffer for five minutes to retrieve antigen, cooled in tap water, then blocked in 0.3% hydrogen peroxide in methanol for five minutes. Sections were then blocked using the mouse on mouse (MOM) kit mouse IgG blocking reagent, diluted 1:25 in PBS, for one hour. Sections were washed in PBS then incubated in MOM kit antibody diluent 1:50 in PBS for five minutes, before blotting and incubating for one hour with the primary antibody, mouse anti-human Mart 1, diluted 1:500 in the MOM kit antibody diluent as used above. The slides were washed in PBS and incubated for one hour with the secondary antibody, goat anti-mouse IgG (Fc)::FITC, diluted 1:200 in PBS. The slides were washed again in PBS and incubated for one hour with the tertiary antibody, anti-fluorescein-AP Fab fragments, diluted 1:2000 in 100mM Tris HCl, 150mM NaCl, pH7.5. The slides were washed in the Tris HCl/NaCl solution before staining with fast blue BB

solution for 3 minutes. Slides were washed in tap water, fixed in 4% formalin overnight and mounted using warmed glycerol gelatine.

2.29 Immunocytochemistry of neuromuscular junctions (NMJs)

For analysis of neuromuscular junctions (NMJs) we used two muscles from each animal, the transverses abdominis and the deep lumbrical muscle (found in the hind paw). Muscles were dissected and fixed in 4% paraformaldehyde in PBS for 1 to 2 hours before labelling with 5μg/ml α-bungarotoxin conjugated to tetramethylrhodamine isothiocyanate (TRITC-α-bungarotoxin). Muscles were then incubated overnight in primary antibodies against 165 kDa neurofilament proteins and synaptic vesicle protein SV2, both at a 1:200 dilution. These were visualised using sheep anti-mouse FITC-conjugated secondary antibodies, also used at 1:200. (Protocol described by Newbery et al, 2005). The NMJs were the imaged using a laser scanning confocal microscope. Axon bundles were checked for fragmentation and NMJs checked for innervation. In each animal around 100 synapses were counted and innervation status recorded.

2.30 Gross classification of skin tumours

Animals in carcinogenesis protocols were monitored weekly for skin tumours. Any tumours were measured using callipers and recorded so that their size

and appearance could be tracked weekly. Skin tumours were classified according to their gross size and appearance as described in table 2.5. Average epidermal thickness was calculated by measuring a length of skin, measuring epidermal area over that length and dividing area by length to give an average thickness. Where possible, ten readings were taken per animal, however sometimes the extent of dysplasia prevented this.

Table 2.5 Gross classification of skin tumours

Tumour	**Size**	**Appearance**
Papule	< 2mm	Raised epidermal mass
Exophytic mass	≥ 2mm	'Stalk-like' appearance; projecting from skin
Endophytic mass	≥ 2mm	Inward growing mass

2.31 Histological classification of tumours

UV induced skin tumours were classified histologically by Dr David Brownstein according to the parameters described in table 2.6.

Table 2.6 Histological classification of skin tumours

Classification	**Appearance**
Acanthosis	Epidermal hyperplasia without dysplasia
Actinic keratosis	Epidermal hyperplasia with dysplasia of basal cell layer, but retention of external granular cell layer
Carcinoma in situ	Full thickness dysplasia, absent stratum granulosum, intact basement membrane
SCC	Penetration of basement membrane and dermal invasion
- Grade 1	Prominent keratin pearls with obvious granular cell layer
- Grade 2	Fewer keratin pearls, few or absent granular cells often associated with parakeratosis
- Grade 3	No keratin pearls, keratinised cells or groups of cells
- Grade not specified (GNS)	Cells or nests of cells judged to have penetrated the basement membrane

2.32 Opto-Kinetic Response (OKR) test

The OKR test was performed to assess the visual ability of the mice. This test was first described by Thuang et al, 2002. A variation on this protocol was used – briefly, mice were placed on a pedestal inside a large, vertical cylinder, approximately 30cm in diameter and 60cm in height. The cylinder could be lined with vertically, black and white striped paper. These stripes were either 2°, 4 °, or 8 ° wide, and the cylinder could be rotated slowly in either direction. Each mouse was recorded using a fixed video-camera for one minute in each direction, with each stripe width – a total of six minutes per mouse.

2.33 Assessment of motor function using Roto-Rod

Accelerating Roto-Rod was used to assess motor function and coordination in the mice. The Roto-Rod is a horizontal, rotating cylinder of around 4cm in diameter, covered with ridged rubber to facilitate grip. The mouse is required to walk forward to remain on top of the cylinder. The mouse was placed on the Roto-Rod, which would rotate at a slow speed for thirty seconds. This was to allow to mouse to become accustomed to the movement required. After thirty seconds, the speed of rotation was slowly increased at a constant rate until the mouse was unable to remain on top of the cylinder. The amount of time the mouse was able to remain on the Roto-Rod before falling

off was recorded. For each mouse, readings were taken on three consecutive days and averaged.

2.34 Proteinurea test

The amount of protein in the urine of the mice was quantified using Combur3 test strips. The strips are dipped in a drop of urine and the colour of the strip compared with a range of colours provided in the kit. These colours then translate to a concentration of protein in the urine.

Chapter 3

Ercc1 epidermis specific knockout mice and the short term effects of UV irradiation

3.1 Introduction

This chapter addresses the consequences of loss of nucleotide excision repair on the short term effects of ultraviolet irradiation in the skin.

Nucleotide excision repair (NER) is of prime importance in the skin due to its role in the removal of UV induced DNA lesions, particularly cyclobutane pyrimidine dimers and 6-4 photoproducts. This is demonstrated by the severe skin related symptoms in the majority of NER deficiency syndromes (reviewed by de Boer and Hoeijmakers, 2000). The issue of carcinogenicity is addressed in chapter 4 of this thesis, while this chapter focuses on the immediate effects of UV on the skin.

Exposure of the skin to UV radiation results in local inflammatory events as well as systemic immunological events. Erythema is triggered by local inflammation as a result of excessive UV exposure. Photoimmunosuppression was first observed in 1977 when modulation of the immune response was described after UV exposure. As well as the immediate consequences of photoimmunosuppression, in the long term this phenomenon contributes to UV induced carcinogenicity by reducing the host's ability to recognise and destroy tumour cells. When UV induced skin tumours were transplanted into non-irradiated syngenic mice, the tumours were destroyed by the immune response. However when UV induced tumours were transplanted into irradiated syngenic mice, the tumours were

not destroyed and continued to grow (Fisher and Kripke, 1977). Kidney transplant patients receiving immunosuppressive drugs have been shown to be especially susceptible to skin cancer (Moloney et al, 2006), as well as other malignancies.

Melanogenesis and melanocyte proliferation are also caused by UV exposure, and result in tanning. *Xpa* null mice have shown increased melanocyte proliferation in response to UV (van Schanke et al, 2005), implying a role for DNA damage in stimulation of melanocyte proliferation.

Transcription coupled repair, rather than global genome repair, is implicated as a factor in the short term effects of UV. Erythema has been linked with deficient TCR, whereas development of squamous cell carcinoma has been linked with deficient GGR (Berg et al, 2000). Mice with deficiencies in GGR alone, for example those lacking *Xpc*, have been shown to have similar immune and erythemic responses to UV as wild type mice (Berg et al, 2000, Garssen et al, 2000). Deficient TCR has also been linked with enhanced photoimmunosuppression (Boonstra et al, 2001). This is likely to be due to the fact that cyclobutane pyrimidine dimers (CPDs) are repaired rapidly by TCR in actively transcribed genes, but CPDs in the rest of the genome are repaired at a much slower rate by GGR. *Xpa* null mice lack TCR and GGR, and are sensitive to both the short and long term effects of UV (de Vries et al, 1995).

Ercc1 is involved in TCR and GGR and as such we expect our *Ercc1* knockout animals to show heightened sensitivity to the short term effects of UV. As *Ercc1* is also involved in the repair of inter-strand crosslinks and homologous recombination (Niedernhofer et al, 2004 and Chipchase and Melton, 2002), we predict that *Ercc1* knockout animals could be even more sensitive than *Xpa* knockout mice.

We investigated the consequences of Ercc1 deficiency using our conditional *Ercc1* knockout mouse, in which *Ercc1* deficiency is restricted to the basal layer of the epidermis. This allowed us to work with mice that have a normal life expectancy. We also used mice on a hairless, albino background, which allowed us to investigate the skin phenotype without the complication of fur or pigment.

3.2 *Ercc1* epidermis specific knockout mice are more sensitive to UV induced erythema than wild type controls

For reasons already discussed, we hypothesised that *Ercc1* epidermal specific knockout (ESKO) knockout mice would show increased sensitivity to UV induced erythema compared with controls, and potentially compared with other NER knockout mice.

Fig 3.1

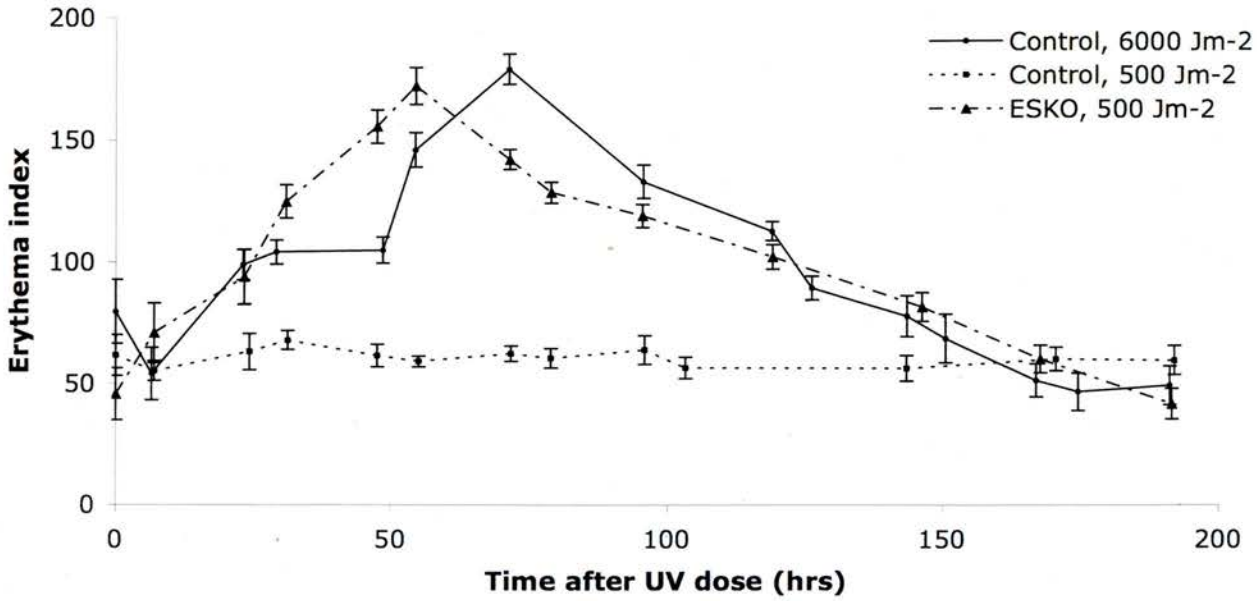

Figure 3.1 Epidermis specific knockout animals are much more sensitive to UVB irradiation induced erythema than controls.

In this experiment, the erythema index in ESKO animals was compared with controls after exposure to a single dose of UV. Erythema was measured once before exposure, to set a baseline level, and regularly thereafter, until erythema index had returned to pre-UV levels. Each group contained five animals. Values shown represent the mean erythema index ± SEM.

An erythema profile was established for *Ercc1* ESKO animals and control littermates and is shown in figure 3.1. A single dose of 500 Jm^{-2} UVB resulted in significant erythema in *Ercc1* ESKO animals, with a peak at around 48-60 hours after UV exposure. Erythema subsided in around a week. The same dose did not produce erythema in control littermates. A dose of 6000 Jm^{-2} UVB was required to elicit a response in controls that was comparable with the effect of 500 Jm^{-2} UVB on *Ercc1* ESKO animals. This translates to a twelve fold difference in UV sensitivity between the two groups.

Minimal erythemal doses (MEDs) were measured for *Ercc1* ESKO animals and for controls. Results are shown in figure 3.2. This was done by exposing mice to a variety of UV doses and comparing erythema index before UV, with the value measured 48 hours after exposure. This timepoint was chosen because erythema had been shown to peak at around this time after UV exposure, and therefore the smallest increase in erythema should be detectable. Any increase in erythema index was recorded, with an increase of greater than ten being considered significant. This was because measured erythema indices did vary by up to ten units from day to day in animals regardless of UV exposure.

Our control mice had an MED of 900 Jm^{-2}, while the *Ercc1* ESKO mice had an MED of 40 Jm^{-2}. This implies around a twenty fold increased sensitivity in the knockout mice.

Fig 3.2

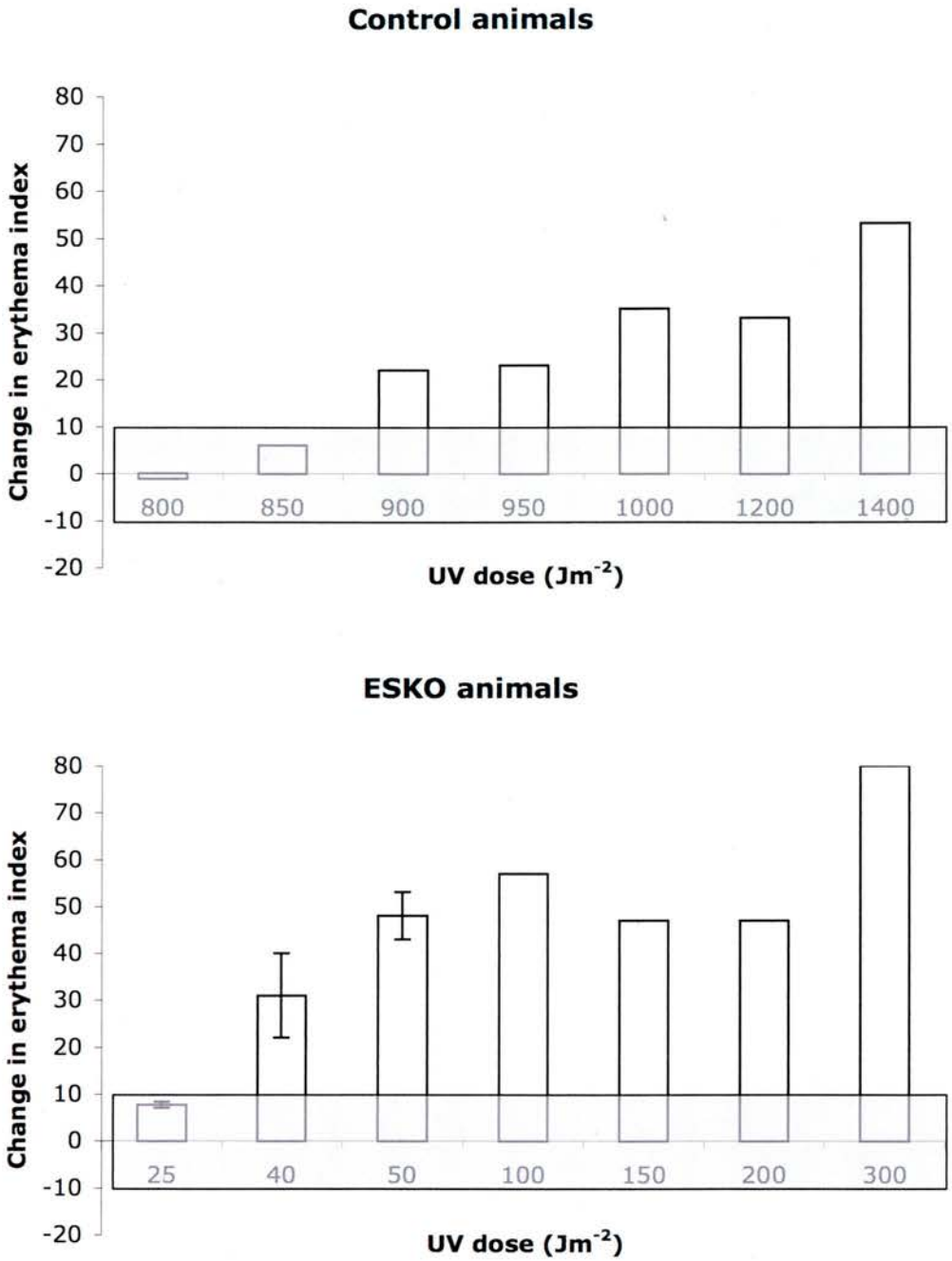

Figure 3.2 The minimal erythemal dose of UVB for the ESKO animals was much lower than control animals.

Erythema was measured before, and then 48 hours after UV exposure. Any change in the erythema index of more than ten units was considered significant. Each group consisted of one animal, apart from those with error bars which consisted of three animals.

3.3 Epidermal antigen presenting cells in *Ercc1* ESKO animals migrate more readily after UV exposure compared with controls

We hypothesised that UV induced LC migration is in fact due to DNA damage in both keratinocytes and LCs themselves. Therefore we expected to see some depletion of LCs in *Ercc1* ESKO animals, but not as much as would be seen in complete NER knockouts.

The number of LCs present in epidermal sheets was counted in *Ercc1* ESKO animals and controls one week after a single dose of UV, and the results are shown in figure 3.3. A single UV dose of 500 Jm^{-2}, which caused no erythema in controls but significant reddening in *Ercc1* ESKOs, resulted in a slight depletion in LCs in controls and 50% depletion in *Ercc1* ESKO animals. In order to induce 50% depletion in control animals, a dose of 6000 Jm^{-2} was required. This translates to a twelve fold increased sensitivity to the LC depleting effect of UV in *Ercc1* ESKO animals.

3.4 UV exposure causes suppression of the contact hypersensitivity response in control and *Ercc1* ESKO mice

A recognised test of the immune status of an animal is the contact hypersensitivity (CHS) assay (reviewed by Grabbe and Schwarz, 1998 and Norval, 2001). This assay assesses T cell function by examining the ability

Fig 3.3

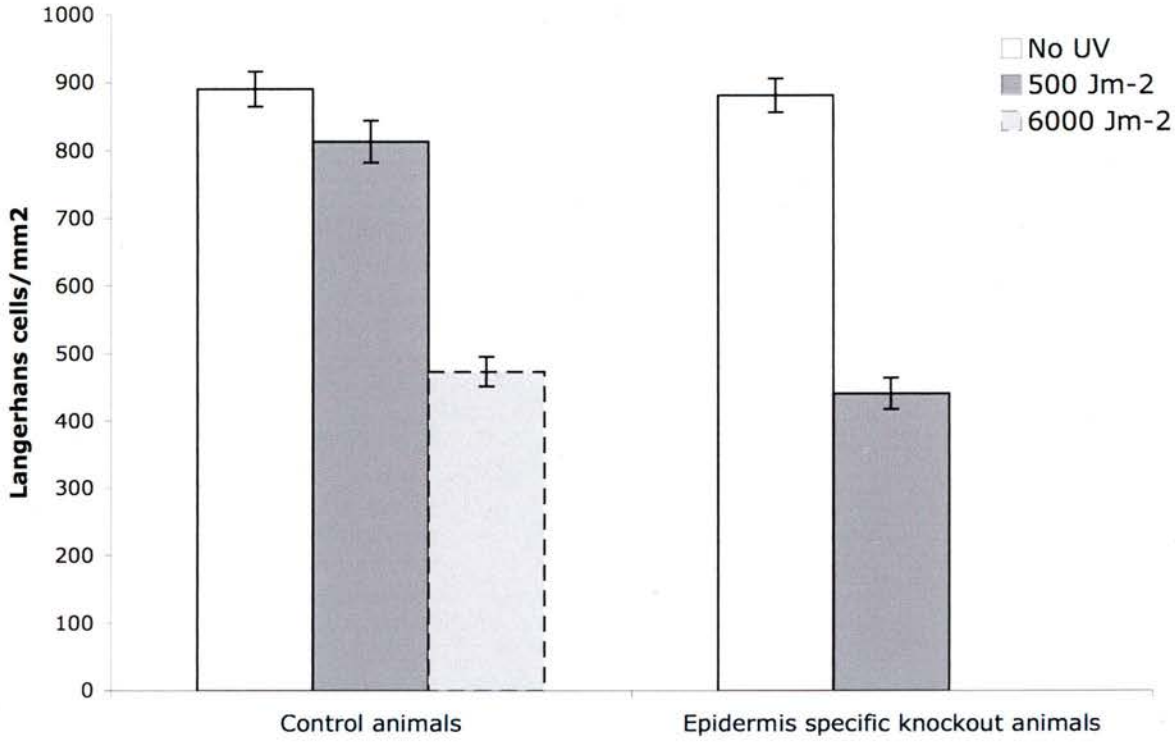

Figure 3.3 Epidermal Langerhans cells in epidermis specific knockout animals are more susceptible to the effects of cutaneous UVB exposure than control animals.

Epidermal Langerhans cells were counted one week after animals were exposed to a single UV dose. Each group consisted of five animals.

of the organism to mount an inflammatory response to a cutaneously applied sensitiser. Exposure of the skin to UV causes a suppression of this inflammatory response.

We have confirmed the local and systemic immunosuppressive effects of UV radiation in our control mice. When the mice were exposed to UV and sensitiser is applied dorsally, we were able to show that UV radiation caused local immunosuppression, as seen in figure 3.4a. When the mice were exposed to UV and sensitiser was applied ventrally, we confirmed that UV also caused systemic immunosuppression, shown in figure 3.4b. It should be noted that although the extent of suppression was similar in both experiments, in the absence of UV the contact hypersensitivity response was greater in dorsally sensitised animals than ventrally sensitised animals. This is possibly due to a larger number of antigen presenting cells present in dorsal skin compared with ventral skin.

We went on to assay the CHS response of our *Ercc1* ESKO animals, shown in figure 3.5. Although our *Ercc1* ESKO animals showed a suppression of the inflammatory response after UV exposure, we were unable to show a difference between controls and *Ercc1* ESKO animals. This may be due to the fact that with our UV lamp we were unable to give a low enough dose of UV. Figure 3.6 shows results obtained after a single UV dose of 500 Jm^{-2}, however this extent of immunosuppression was seen at doses as low as a single dose of 100 Jm^{-2}. Therefore, at all doses tested, the inflammatory

Fig 3.4

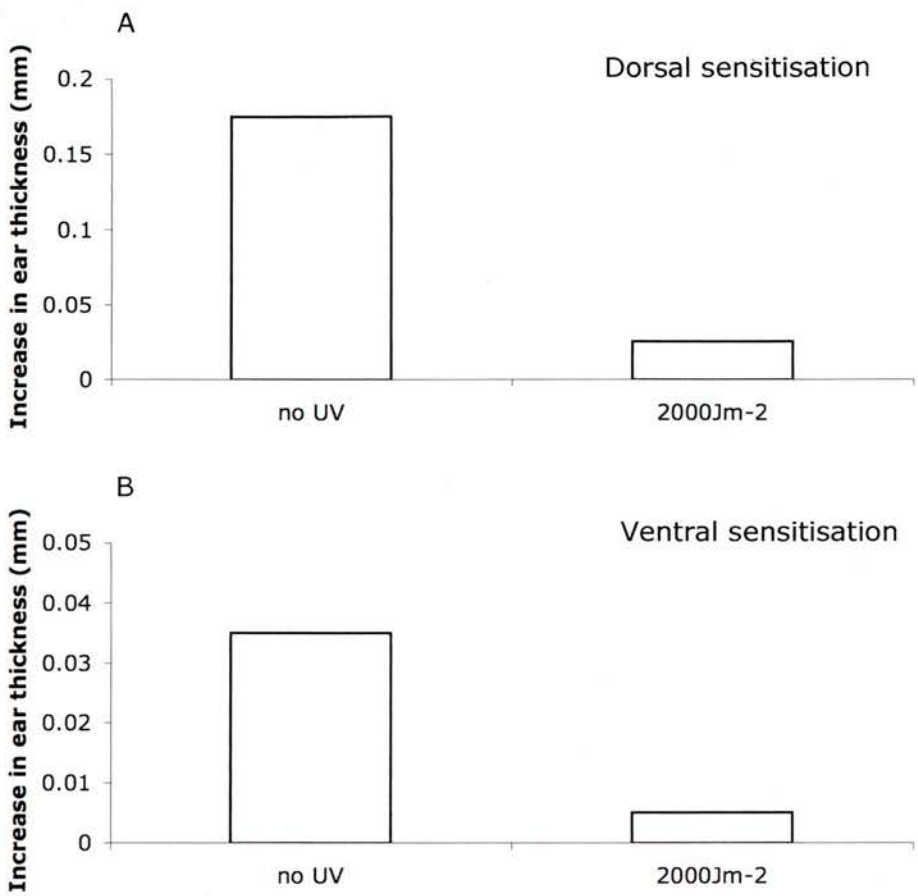

Figure 3.4 The contact hypersensitivity response is suppressed by UVB radiation in control animals after dorsal and ventral sensitisation with the irritant.

The contact hypersensitivity assay measures the ability of the organism to mount a secondary immune response to an irritant to which the organism has previously been exposed.

For A, the irritant was applied dorsally, two days after a single UV dose or a sham irradiation. After UV the response is suppressed, implying that UV exposure has acted locally to inhibit the primary immune response to the irritant.

For B, the irritant was applied ventrally, two days after a single UV dose or a sham irradiation. As after UV the response is suppresssed, we can conclude that UV exposure has acted systemically to inhibit the organism's primary response to the irritant.

Fig 3.5

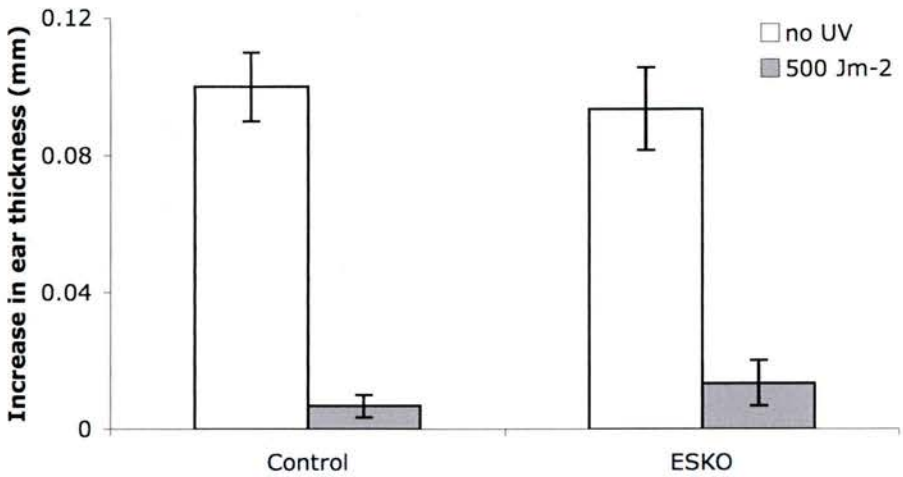

Figure 3.5 UVB irradiation causes suppression of the contact hypersensitivity response in control and epidermis specific knockout animals.

In this experiment the irritant was applied ventrally. Each group consisted of three animals.

response was almost completely abrogated in control animals as well as repair deficient animals.

3.5 UV irradiation causes altered cytokine profiles in *Ercc1* null keratinocytes compared with *Ercc1* wild type keratinocytes

Photoimmunosuppression is largely due to an altered cytokine environment caused by UV exposure. As mentioned previously, this relates to a Th2 bias in the immune response.

Data regarding cutaneous cytokine response to UV radiation in the literature are mixed. Whilst it is universally accepted that UV radiation causes immunosuppression, the exact mechanisms remain unclear. There is much evidence that cells present in the epidermis release anti-inflammatory mediators, with key cytokines including tumour necrosis factor-α and interleukin-10. However, there is also data suggesting that keratinocytes release pro-inflammatory mediators, causing inflammation and the influx of macrophages and neutrophils; which in turn release anti-inflammatory mediators and cause systemic immunosuppression (Kang et al, 1994 and Teunissen et al, 2002).

Keratinocytes themselves absorb the majority of the UV radiation insult and as such we wanted to determine whether the NER status of keratinocytes in culture affects the balance of cytokine release.

For these experiments we used spontaneously transformed keratinocytes isolated from our *Ercc1* wild type and null mice. We also used PAM 212 cells – a well characterised murine keratinocyte line to compare with our wild type cells.

In the series of figures illustrating cytokine levels, the in-house wild type cells and PAM 212 are shown on graphs together, where the *Ercc1* null cells are shown on separate graphs. This is because *Ercc1* null keratinocytes have a much lower survival rate after UV exposure, as they are considerably more sensitive to low doses than wild type keratinocytes (personal communication, Ann-Marie Ritchie). Due to this, a different range of UV doses had to be used for the repair proficient and deficient cells, although some of the same doses were used to enable direct comparison. It should also be noted that in each of the figures shown, the graph on the left shows the cytokine concentration in terms of picograms per millilitre of medium at the collection point forty eight hours after UV. The graph on the right shows the cytokine concentration in picograms per million cells at the collection point. Cells were plated at the same densities at the start of the experiment, but supernatants were collected forty eight hours after irradiation, which was seventy two hours after plating, so discrepancies in the number of cells in each dish were inevitable. UV slows growth and kills cells at higher doses,

and the *Ercc1* null cells are much more sensitive to these effects than the wild type cells. For this reason, the total number of cells in each dish was counted as soon as the supernatant was removed and the cell count at the end of the 48 hour period is expressed as percentage of the cells seeded in table 3.1.

Table 3.1. Percentage of adherent cells remaining after 48 hours

	Ercc1 +/+	PAM212	Ercc1 -/-
No UV	33%	8%	40%
12.5 Jm^{-2}	-	-	7%
50 Jm^{-2}	36%	5%	7%
150 Jm^{-2}	12%	4%	0.4%
500 Jm^{-2}	3%	0.8%	-

Ercc1 deficient keratinocytes were expected to show a similar cytokine profile to *Ercc1* proficient keratinocytes, although we expected higher levels of immunosuppressive cytokines to be released after lower UV doses. This would correlate with DNA damage being a trigger for photoimmunosuppression.

Data for the following inflammatory mediators will be discussed: tumour necrosis factor-alpha, interleukin-6, interleukin-12, interferon-gamma, interleukin-10 and macrophage chemotroattractant protein-1.

Tumour necrosis factor-alpha (TNF-α) is involved in local inflammation and is released by keratinocytes as well as other cell types. TNF-α has been shown to be present in greater quantities in repair deficient skin than control skin after UV exposure in vivo. We hypothesised that our cells would release increasing amounts of TNF-α in response to increasing UV doses, and that *Ercc1* null cells would produce more at lower doses. Figure 3.6 shows this is in fact the case. Both *Ercc1* wild type and null cells produced increasing amounts of TNF-α as the UV dose increased. After 50 Jm^{-2} UV, *Ercc1* null keratinocytes produced around six fold more TNF-α than the wild types,

Fig 3.6

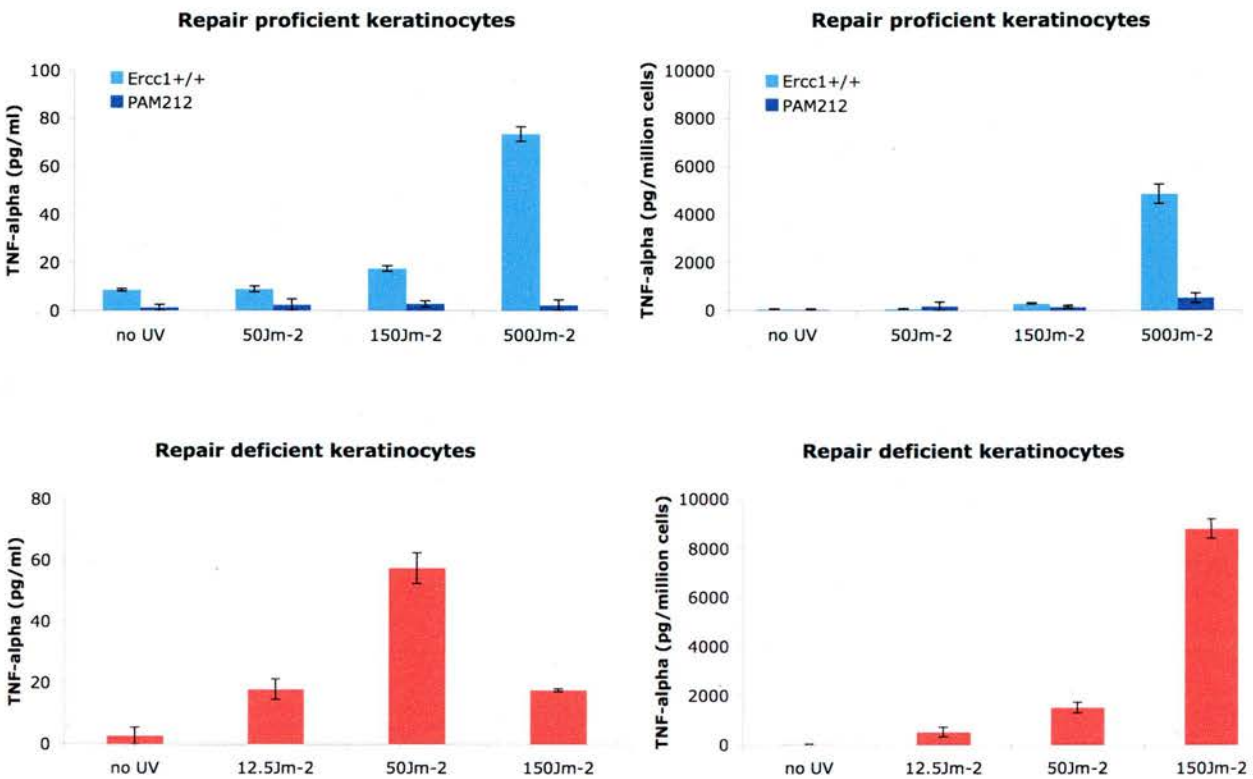

Figure 3.6 UVB irradiation causes increased release of TNF-alpha by repair deficient keratinocytes

Each value shown on the graphs is an average of two experiments. In each experiment, supernatants were collected 48 hours after UV or sham exposure and frozen immediately. These were then analysed in duplicate by cytometric bead array.

Error bars depict the range of the two experiments.

which translated to a twenty five fold increase in TNF-α after the correction for cell numbers. However, unlike previously published data, we did not see a large UV induced increase in TNF-α production in the PAM 212 cells, which was unexpected.

Whichever UV dose the cells are exposed to, the amount of damage caused is the same regardless of genotype. The difference between cell lines lies in the ability of the cells to repair this damage. Therefore, we concluded that TNF-α release after UVB exposure is triggered by the continued presence of damaged DNA in the keratinocyte nuclei.

Interleukin-6 (IL-6) is involved in the acute phase immune response. Its release by keratinocytes has been linked with UV exposure, however there is no data in the literature regarding IL-6 and NER deficient cells. With respect to the TNF-α data mentioned above, we expected our *Ercc1* deficient keratinocytes to produce more IL-6 than wild type keratinocytes after UV exposure due to the presence of unrepaired DNA damage in the nuclei.

Figure 3.7 shows that IL-6 production was significantly greater in *Ercc1* deficient keratinocytes than *Ercc1* proficient keratinocytes after UVB radiation. In both types of *Ercc1* wild type cells, we found IL-6 production to be negligible, and not affected by UV exposure.

Fig 3.7

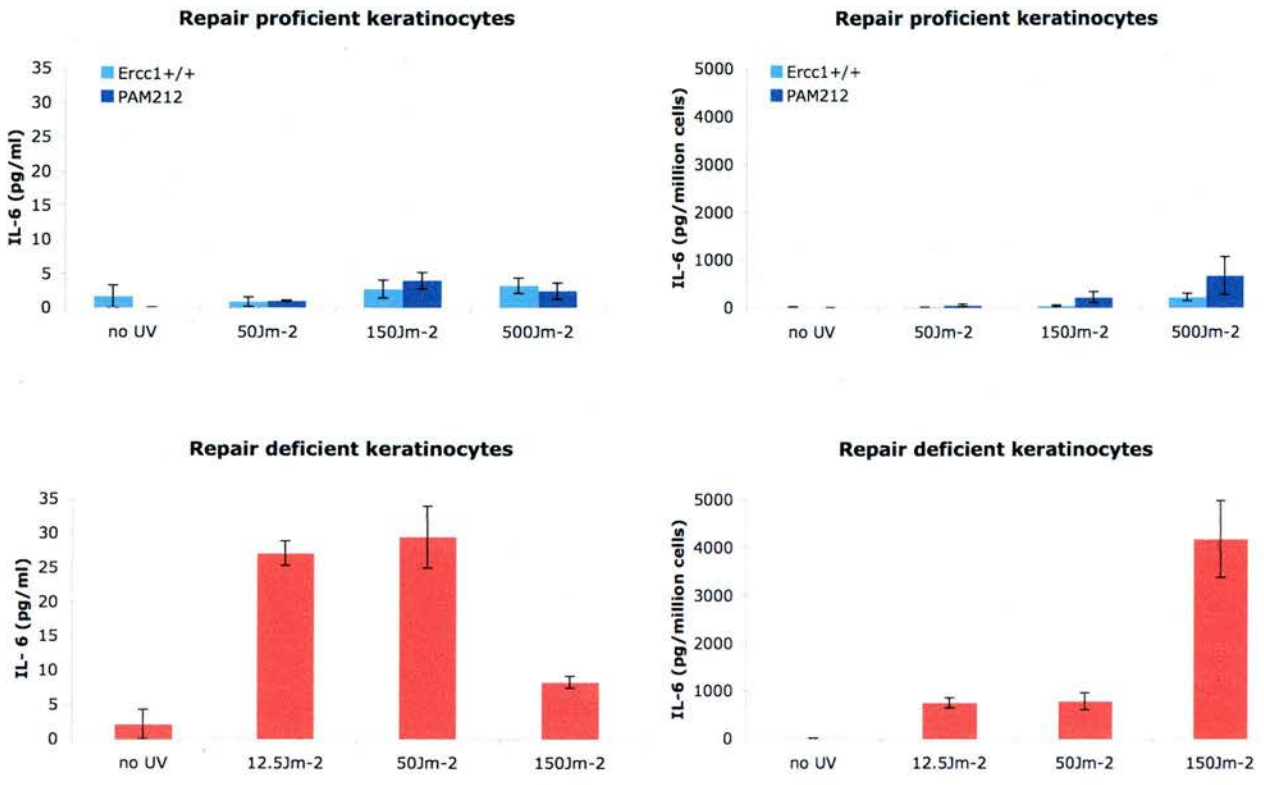

Figure 3.7 UVB irradiation causes increased release of IL-6 by repair deficient keratinocytes

Each value shown on the graphs is an average of two experiments. In each experiment, supernatants were collected 48 hours after UV or sham exposure and frozen immediately. These were then analysed in duplicate by cytometric bead array.

Error bars depict the range of the two experiments.

From this we can conclude that as predicted, IL-6 release by keratinocytes is triggered by the persistence of unrepaired CPDs.

We expected to see negligible production of interleukin-12 (IL-12) by all the keratinocytes in our experiments. This is because IL-12 is not a cytokine that has been linked with UV exposure, and is in fact noted for its ability to suppress the Th2 immune response, which UV is known to promote.

Figure 3.8 shows the results of the IL-12 experiments. The *Ercc1* wild type keratinocytes produced negligible IL-12 in response to UV, as expected. The *Ercc1* null keratinocytes appeared to produce some IL-12 in response to the higher dose of UV. This could have been caused by an unsuccessful attempt to upregulate NER in response to the presence of UV induced DNA damage – as previously mentioned, IL-12 has been shown to upregulate NER *in vitro* (Schwarz et al, 1996 and 2002). However, it is more likely that this result is an aberration – the peak only showed when IL-12 was measured in pg/million cells and not when it was measured in pg/ml, when in fact the amounts of IL-12 detected were extremely low. This means that the peak could have been due to a low number of surviving cells skewing the pg/million cells value.

In conclusion, wild type and *Ercc1* null keratinocytes produced negligible IL-12 in response to UVB radiation.

Fig 3.8

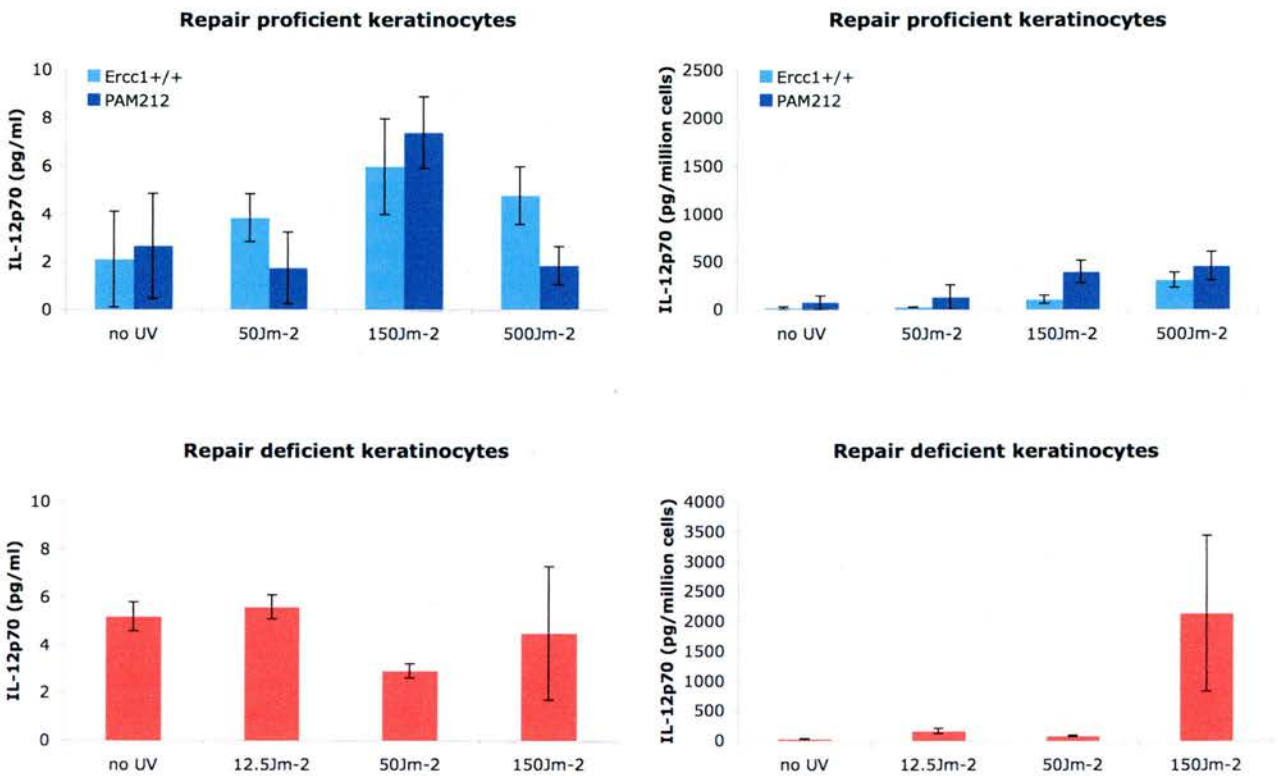

Figure 3.8 UVB irradiation causes negligible IL-12 production in wild type and Ercc1 null keratinocytes

Each value shown on the graphs is an average of two experiments. In each experiment, supernatants were collected 48 hours after UV or sham exposure and frozen immediately. These were then analysed in duplicate by cytometric bead array.

Error bars depict the range of the two experiments.

There is no evidence for interferon-gamma (IFN-γ) being released by keratinocytes in response to UV and as such we did not expect to see an increase in IFN-γ in our experiments.

Figure 3.9 shows the results of these experiments. As expected, UVB did not affect IFN-γ concentration in our cultures. However, as with IL-12 there appeared to be a peak in IFN-γ in the *Ercc1* null keratinocytes after high levels of UVB exposure, but again the overall concentration of cytokine was very low and this result is likely to have been affected by the low numbers of surviving cells present after *Ercc1* null cells had been exposed to such a relatively high UV dose.

Interleukin-10 (IL-10) is a Th2 cytokine and a suppressor of cellular immune responses. IL-10 release by keratinocytes has previously been linked with DNA damage. In light of this work, we expected our *Ercc1* null keratinocytes to produce more IL-10 at lower UV doses than *Ercc1* wild type keratinocytes.

The results of these experiments are shown in figure 3.10. *Ercc1* null cells produced IL-10 in a similar pattern to the wild types, but in greater quantities. After 150 Jm^{-2}, the amount of IL-10 in the supernatants from *Ercc1* nulls and wild types was similar, but when this was corrected for cell numbers, *Ercc1* nulls showed a twenty five fold increase in IL-10 concentration compared with wild types. However, PAM 212 cells released much more IL-10 overall than either of our own keratinocyte lines.

Fig 3.9

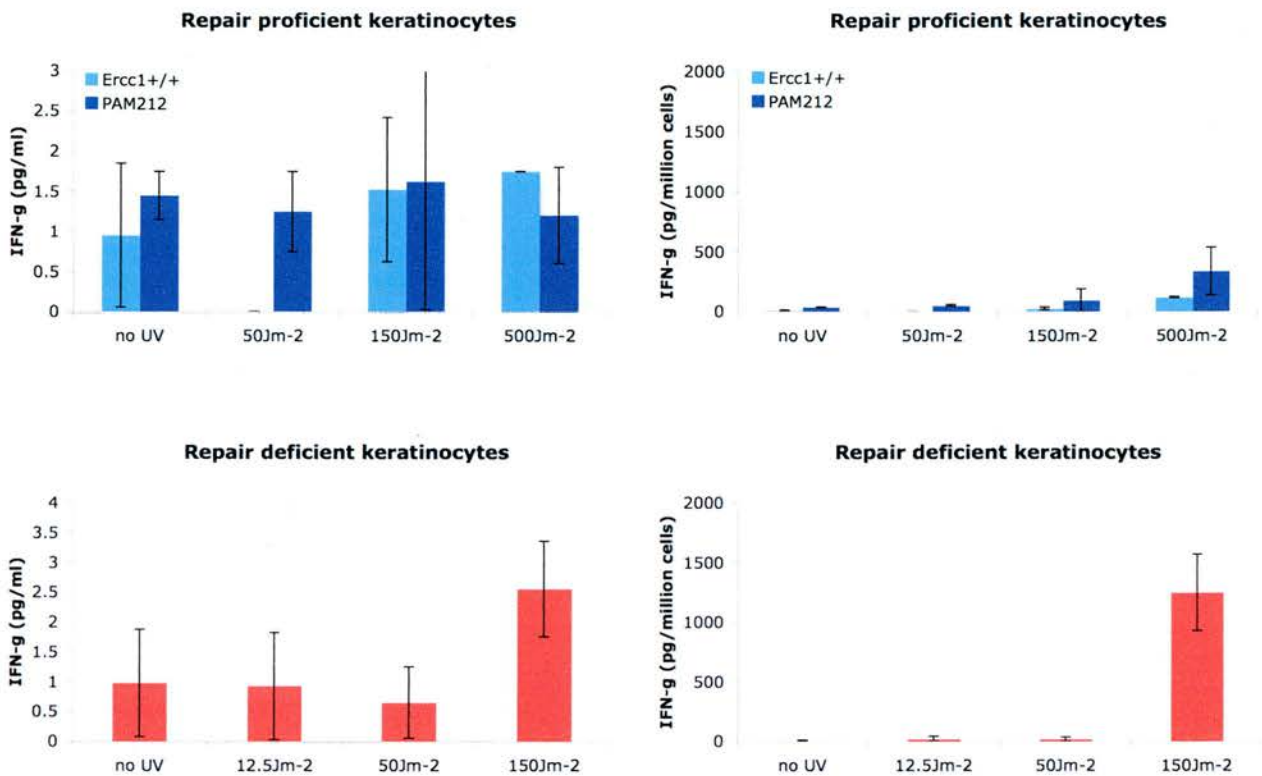

Figure 3.9 UVB irradiation does not affect IFN-g release by wild type or Ercc1 null keratinocytes

Each value shown on the graphs is an average of two experiments. In each experiment, supernatants were collected 48 hours after UV or sham exposure and frozen immediately. These were then analysed in duplicate by cytometric bead array.

Error bars depict the range of the two experiments.

Fig 3.10

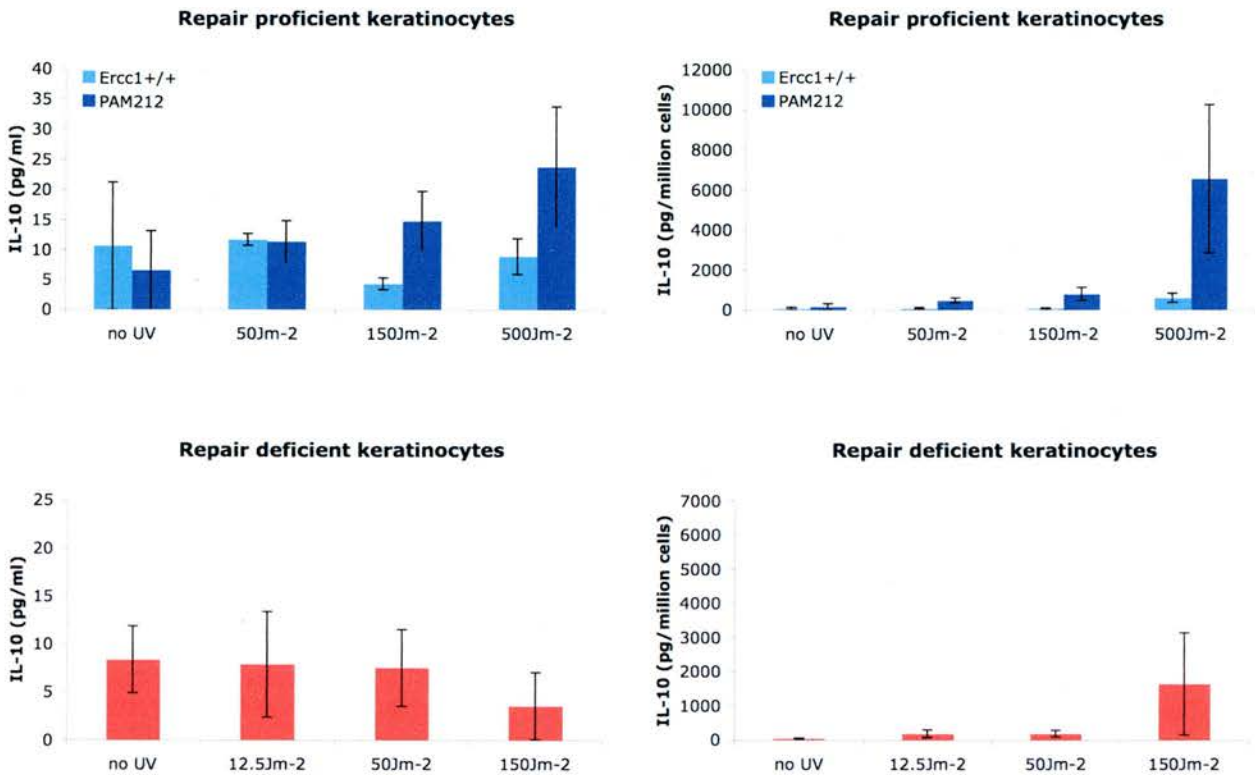

Figure 3.10 UVB irradiation results in an increased production of IL-10 by Ercc1 null and wild type keratinocytes

Each value shown on the graphs is an average of two experiments. In each experiment, supernatants were collected 48 hours after UV or sham exposure and frozen immediately. These were then analysed in duplicate by cytometric bead array.

Error bars depict the range of the two experiments.

Fig 3.11

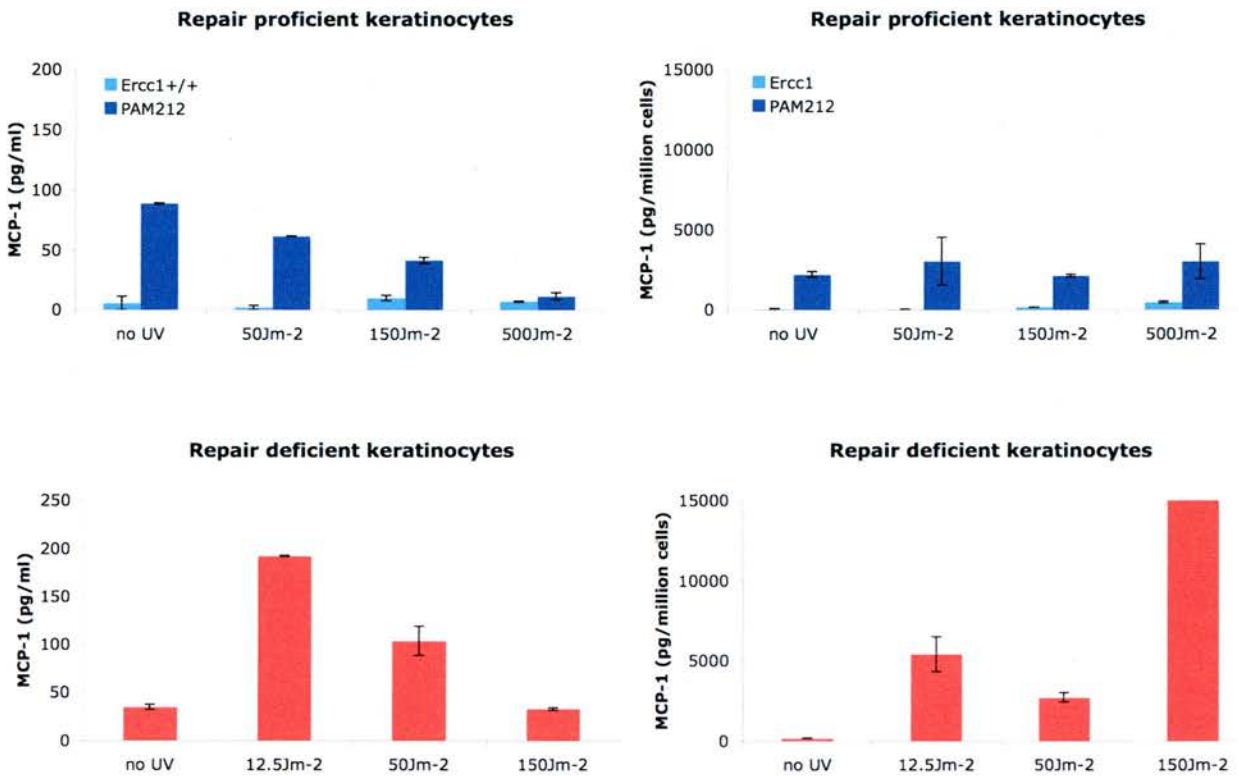

Figure 3.11 UVB irradiation causes increased release of MCP-1 by repair deficient keratinocytes but not wild type keratinocytes

Each value shown on the graphs is an average of two experiments. In each experiment, supernatants were collected 48 hours after UV or sham exposure and frozen immediately. These were then analysed in duplicate by cytometric bead array.

Error bars depict the range of the two experiments.

These results showed that IL-10 production in PAM212 cells was induced by UV irradiation. However we were not able to show significant induction of IL-10 in either of our *Ercc1* cell lines.

The effects of UVB radiation on keratinocyte macrophage chemoattractant protein-1 (MCP-1) expression have not been studied. With the knowledge that this chemokine suppressed the cellular immune response, we expected MCP-1 levels might be raised in response to UV.

The data obtained can be seen in figure 3.11. Although the PAM212 cells had a higher base level of MCP-1 production than our wild type cell line, both *Ercc1* wild type cell lines showed little alteration in MCP-1 production in response to UVB exposure. The *Ercc1* null keratinocytes showed a significant increase in MCP-1 production in response to UV.

From this result we can conclude that there is likely to be a link between persistence of damaged DNA in keratinocytes and induction of MCP-1 expression in these cells.

In summary, we found that neither of our wild type cell lines, nor our *Ercc1* deficient cell line, produced IL-12 or IFN-γ in response to UVB exposure and only the PAM212 cells produced IL-10 in response to UVB exposure. We found that TNF-α was produced in greater quantities at lower UV doses in the *Ercc1* deficient keratinocytes compared with the wild types. Finally, we

found that both IL-6 and MCP-1 were produced by *Ercc1* deficient keratinocytes in response to UVB, but were not produced by either of the wild type cell lines in response to the UVB doses used.

3.6 UVB exposure causes a tanning response in hairless, pigmented mice

Murine skin differs from human skin with respect to melanocyte distribution. In humans melanocytes are dispersed throughout the skin whereas in mice melanocytes are clustered around the hair follicles. Due to this, there has been some controversy over whether murine skin can in fact 'tan', and the guinea pig is accepted as having a more similar skin structure to humans.

We used pigmented, hairless mice and found, in accordance with Quevedo Jnr. et al, 2000, that following a chronic irradiation protocol involving three doses of 2000 Jm^{-2} for a week and 4000 Jm^{-2} thrice weekly thereafter, these mice did indeed develop a noticeable 'tan'. This started to appear after about four to six irradiations, becoming steadily more noticeable over three to four weeks, and is shown in figure 3.12. Furthermore, we found upon sectioning and staining for melanin, that much more melanin was visible in the skin of these animals, as seen in figure 3.13. This result meant that we were able to use the tanning process to investigate the mechanism of tanning further, using our repair deficient animals.

Fig 3.12

Figure 3.12 Hairless black mice become tanned after prolonged UVB treatment.

Long term thrice weekly irradiation of hairless, black mice results in 'tanning' of the skin. The animal on the left has not been exposed to UV, whereas the one on the right has been.

Fig 3.13

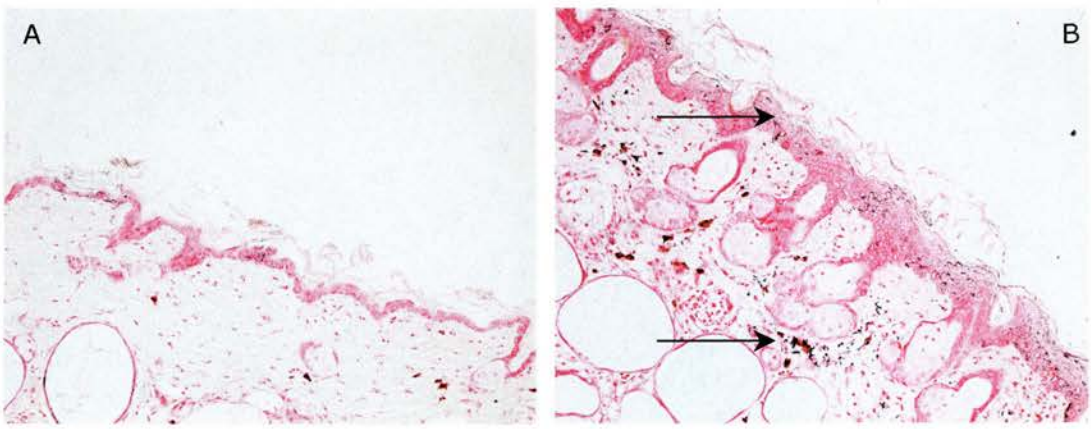

Figure 3.13 Melanin in the epidermis of hairless, black mice becomes more prolific after prolonged UVB exposure.

A shows a section taken from a hairless, black mouse with no UVB exposure and stained with the Masson-Fontana stain for melanin. Some melanocytes are visible in the dermis, although most will be congregated around hair follicles.

B shows a section taken from a chronically irradiated hairless, black mouse, stained as above. In this section the melanocytes are more numerous throughout the dermis. Melanin is also visible inside keratinocytes in the epidermal layers.

3.7 *Ercc1* ESKO animals tan more readily than wild type controls

As our *Ercc1* ESKO mice were so much more sensitive to UV induced erythema than controls, we expected that these mice, when crossed onto a pigmented hairless background, would also be more sensitive to UV induced tanning than controls.

We found that *Ercc1* ESKO mice were significantly more sensitive to the tanning effects of UVB than controls, as expected. An image of some of the animals in the experiment can be seen in figure 3.14. Not only were *Ercc1* ESKOs more tanned than control mice receiving the same UV doses, they were also more tanned than control mice receiving twelve-fold higher doses.

Figure 3.15 shows a graph of the melanin indices for each group of animals throughout the duration of the experiment. These values confirm the extreme sensitivity of the *Ercc1* ESKO animals to UV induced tanning.

Histological examination of sections from these animals confirmed these results. Sections were stained with Masson-Fontana stain for melanin and representative images are shown in figure 3.16.

In summary, *Ercc1* ESKO mice are significantly more sensitive to UV induced melanogenesis than wild type mice. From this we can conclude that

Fig 3.14

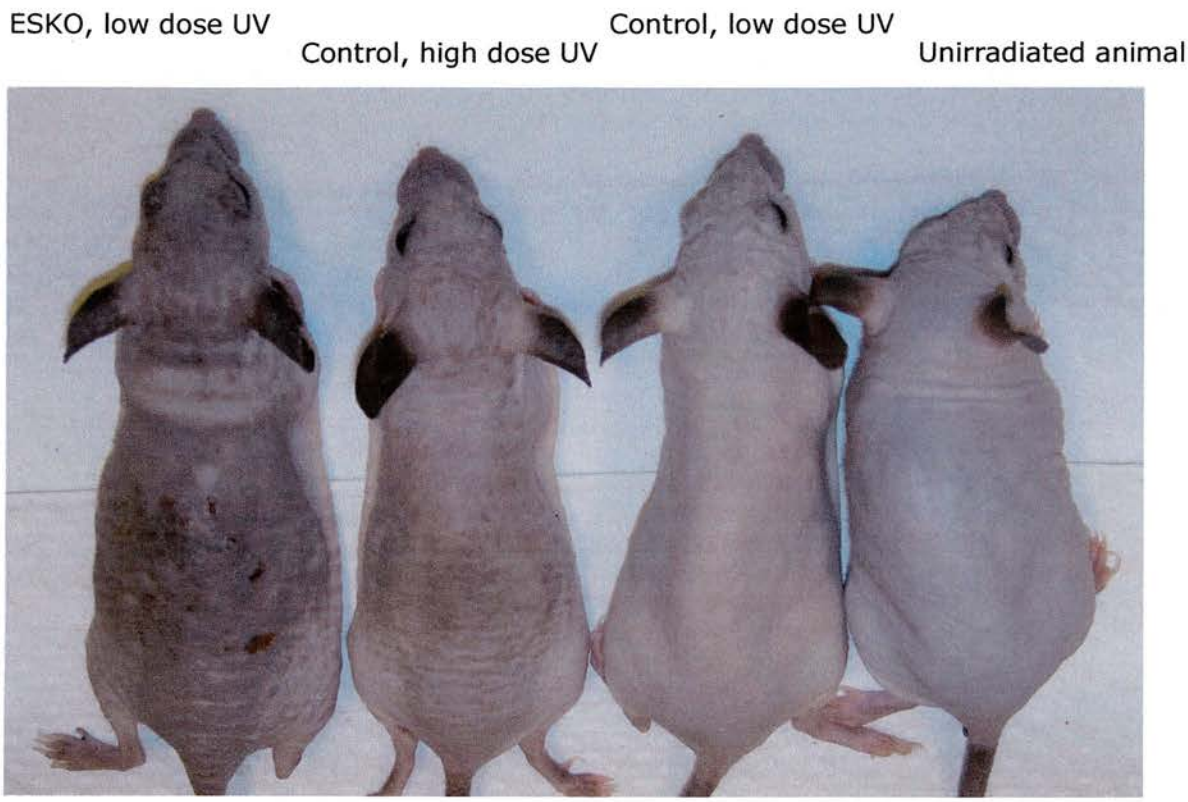

Figure 3.14 Epidermis specific knockout animals tan much more readily than control animals.

This figure shows the extent to which the animals tan. Animals receiving the low UV dose received 165Jm^{-2} three times for the first week, then 330Jm^{-2} three times a week for seven weeks. Animals receiving the high UV dose received 2000Jm^{-2} three times for the first week, then 4000Jm^{-2} three times a week for seven weeks.

Fig 3.15

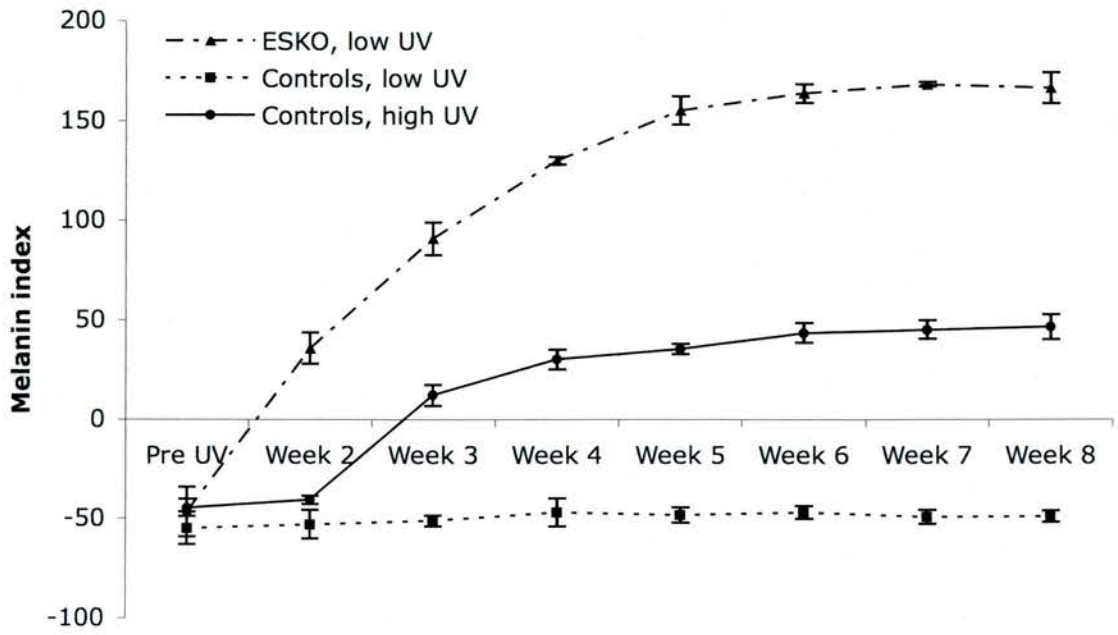

Figure 3.15 Epidermis specific knockout animals tan much more readily than control animals.

This figure shows the melanin indices of skin specific knockout animals receiving the low UV doses, control animals receiving low UV doses and control animals receiving high UV doses over an eight week period.

Fig 3.16

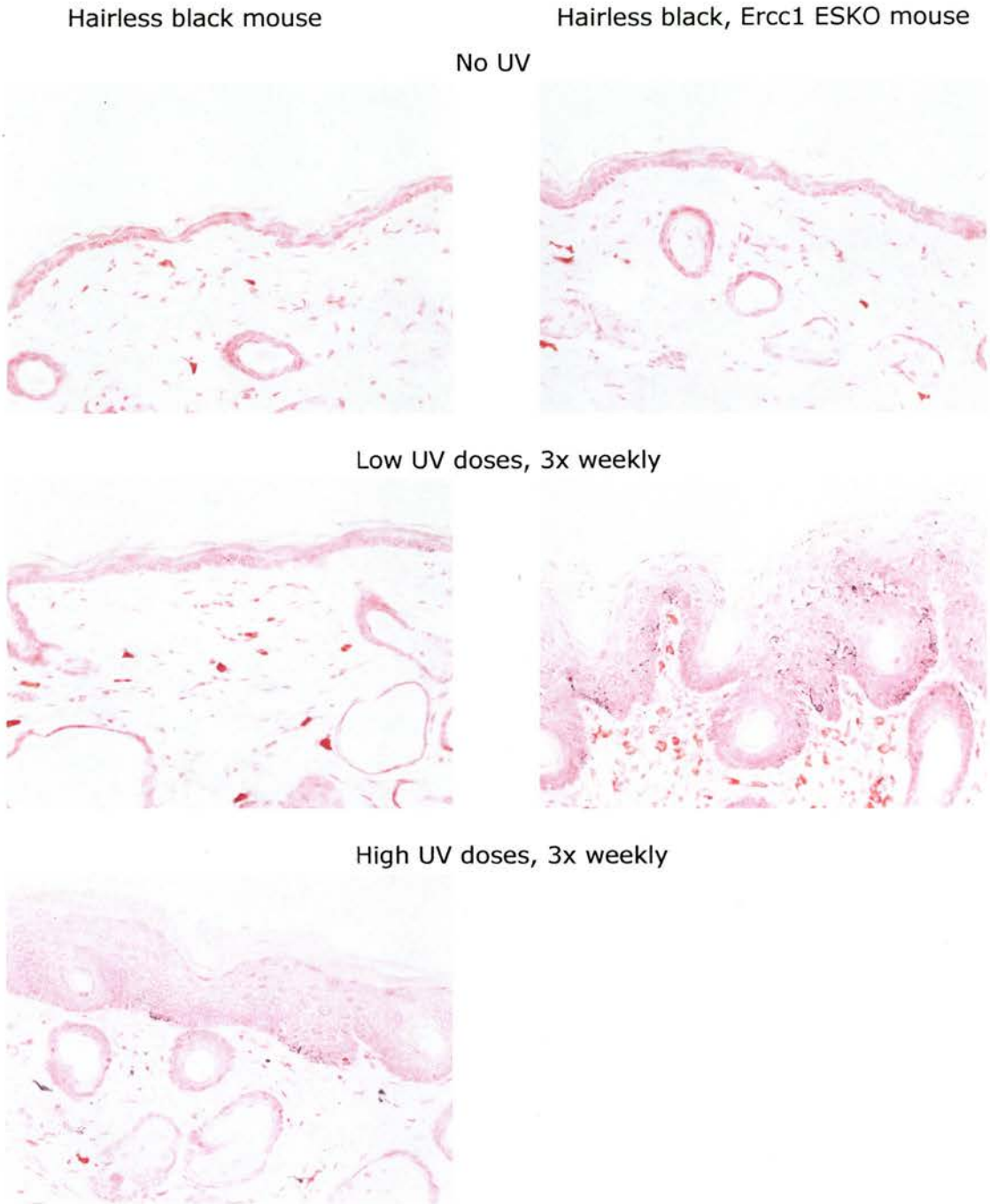

Figure 3.15 Epidermis specific knockout animals accumulate more melanin in the epidermis than controls

This figure shows accumulation of melanin in the epidermis during a chronic irradiation protocol. Animals receiving the low UV dose received 165 Jm^{-2} three times for the first week, then 330 Jm^{-2} three times a week for seven weeks. Animals receiving the high UV dose received 2000 Jm^{-2} three times for the first week, then 4000 Jm^{-2} three times a week for seven weeks.

DNA damage in keratinocytes plays a major role in the stimulation of melanocytes.

3.8 Discussion

The central role of *Ercc1* is its involvement in the nucleotide excision repair pathway, and it is this role that is most important when considering the downstream effects of UV induced DNA damage. However, *Ercc1* is also involved in other repair pathways, which may be relevant to the effects of cutaneous UV exposure. For these reasons, it was our aim to investigate the short term effects of UV exposure on our model mice. Our epidermis specific *Ercc1* knockout also enabled us to investigate the consequences of *Ercc1* deficiency in keratinocytes alone. Previous work on NER deficient models has addressed the effects of loss of NER in whole skin, which includes fibroblasts, Langerhans cells, mast cells, melanocytes and other cells of the immune system as well as keratinocytes themselves.

Mouse models deficient in transcription coupled repair have shown that erythema is linked with this form of NER (Berg et al, 1997 and 2000). UV induced DNA damage stalls RNA polymerases, initiating a cascade of events which result in erythema.

Our *Ercc1* ESKO mice were much more sensitive to UV induced erythema than controls. The minimal erythemal dose (MED) for our control mice was found to be 900 Jm^{-2}, which is comparable with other hairless, albino, repair proficient mice. The MED for our *Ercc1* ESKOs was found to be 40 Jm^{-2}, which is around twenty fold lower than controls, and also lower than MEDs reported for other NER knockout animals. *Xpa* and *Csb* knockouts have been reported to have MEDs approximately eight fold lower than their littermate controls (Berg et al, 2000).

This increased sensitivity in *Ercc1* knockout mice compared with other NER knockout mice implicates a role for the other types of damage that Ercc1 can repair in the process that causes erythema. However, as erythema subsided in a similar pattern and timescale in *Ercc1* ESKO mice and controls, we can conclude that the resolution of the local inflammation is controlled by systemic factors and is not influenced by the persistence of DNA damage in the keratinocytes.

UV radiation has been shown to induce the migration of LCs to the lymph nodes in the absence of antigen (Toews et al, 1980), and other full NER knockouts have been shown to be hypersensitive to UV induced LC migration (Miyauchi-Hashimoto et al, 1996 and Kolgen et al, 2003).

Previously in our lab, fully *Ercc1* deficient mice have been shown to have fewer LCs present in the skin than wild types, although these were depleted

normally following UV exposure. However, the LCs remaining in the epidermis of the knockout animals were severely morphologically affected (90% were damaged), compared with less extensive morphological damage in the wild types (20% of cells damaged). Analysis of the draining lymph node showed that the LCs did not accumulate there in the knockout after UV as would normally be expected. It was suggested that these unexpected results were due to the structural abnormalities of the skin that were seen in these mice: subcutaneous fat was missing, the thickness of the dermal layer was reduced and the nuclei of the epidermis appeared mis-shapen; and this abnormal environment would contribute to epidermal LCs behaving uncharacteristically (Jim Selfridge, PhD thesis, 1999).

This was the first study to use a conditional, epidermis specific knockout of a DNA repair gene to investigate UV induced Langerhans cell (LC) migration. We found *Ercc1* ESKO mice to be approximately twelve fold more sensitive to UV induced LC depletion compare with controls. This implies that the presence of DNA damage in keratinocytes is crucial, rather than the presence of DNA damage in LCs.

We can therefore conclude that factors produced by keratinocytes with DNA damage are playing a major part in the migration of LCs in the absence of antigen.

Other NER knockout mice have been shown to be more susceptible to UV induced suppression of the CHS response compared with control littermates. We had hoped to show an increased suppression of CHS response in our mice compared with controls, however we were not able to do this, due to the fact that as far as we were able to measure, the control mice were equally sensitive. The increased sensitivity of our controls compared with other studies may have been due to the fact our mice are hairless and albino, whereas most other such studies were carried out on mice with fur and pigment.

The studies carried out *in vitro* allowed us to concentrate on the effects of *Ercc1* deficiency in keratinocytes specifically, without the complicating factors of other cutaneous components. Spontaneously transformed *Ercc1* null keratinocytes were compared with *Ercc1* wild type keratinocytes, both of which were isolated from our mouse stocks. A further comparison involved PAM 212 cells, which are also *Ercc1* wild type, and a well characterised murine keratinocyte cell line (Shreedhar et al, 1998, Nishigori et al, 1996). *Ercc1* null keratinocytes could not be exposed to the highest doses used in the experiment, as these cells are much more sensitive to the effects of UV and show high levels of apoptosis at lower doses than the two wild type cell lines. However, it is important to note that any given UV dose causes the same amount of damage in all three cell lines. The differences in sensitivity are caused by the fact that the *Ercc1* nulls keratinocytes are unable to deal

with the damage, whereas the two wild type cell lines can repair the damage rapidly.

Firstly we found, as expected, that none of our cell lines produced IFN-γ, either constitutively or in response to UVB exposure. There has been no suggestion previously that IFN-γ, a potent suppressor of the Th2 immune response, is induced in keratinocytes after UV, and we have found nothing to challenge this.

IL-12 is also known to suppress the Th2 response and promote the Th1 response, and is in fact implicated in IFN-γ production. Furthermore, IL-12 has been shown to rescue UV exposed cells from photoimmunosuppression (Schwarz et al, 1996), presumably because of its ability to suppress Th2 and promote Th1 immune responses. In wild type mice, IL-12 injection into the skin reduces UV induced apoptosis; interestingly however, the same procedure does not reduce apoptosis in *Xpa* knockout mice (Schwarz et al, 2002). This implies that IL-12 may have a role in upregulating DNA repair pathways. We have concluded from our experiments that none of our cell lines expressed IL-12 constitutively, nor was it upregulated by UVB exposure. The *Ercc1* null cells did appear to show a peak in IL-12 concentration after the highest UV dose, when this was expressed in proportion to surviving cells. This is likely to be due to the low number of surviving cells in these cultures, as the absolute levels of IL-12 detected were very low. However this result was obtained both times the experiment was

carried out, and there is a possibility it could be a real result. To investigate this further, it would be necessary to carry out a more detailed set of experiments with a wider range of UV doses. From this, it would be possible to see whether there were a trend for increasing IL-12 release from the *Ercc1* null cells after UV.

In contrast to IL-12, IL-10 promotes the Th2 immune response. In mice, keratinocytes have been shown to produce IL-10 in response to UV, which contributes significantly to photoimmunosuppression. The addition of liposome encapsulated DNA repair enzyme to cultured keratinocytes has been shown to decrease IL-10 expression (Nishigori et al, 1996), implying a link between DNA damage and IL-10 release. *Xpa* and *Csb* deficient mice have been shown to upregulate IL-10 after UV exposure (Boonstra et al, 2001). This study was the first to investigate IL-10 production in NER deficient murine keratinocytes, however we did not find induction of IL-10 in either of our in-house keratinocyte lines. This was unexpected, however it could be explained by the fact that we only analysed IL-10 in the supernatant and did not consider any IL-10 that may be still within the cells. This could be assayed by lysing cells after the supernatant has been removed, then following a standard ELISA technique.

The release of TNF-α by UV exposed keratinocytes is well documented (reviewed by Schade et al, 2005). *Xpa* knockout mice have been shown to upregulate TNF-α production compared with controls after treatment with a

systemic immunosuppressive agent (Miyauchi-Hashimoto et al, 2001). As with our IL-10 experiment, this study was the first to investigate TNF-α production in *Ercc1* deficient murine keratinocytes, and our results correlated with work carried out using human primary keratinocytes isolated from XPA and XPD patients. These have been shown to release TNF-α at lower UV doses than keratinocytes isolated from normal human skin (Petit-Frere et al, 2000). In our study, we have found that *Ercc1* deficient mouse keratinocytes released TNF-α at lower UV doses than control keratinocytes.

IL-6 has been linked with UV induced DNA damage in normal keratinocytes (Kirnbauer et al, 1991 and Petit-Frere et al, 1998). However, a recent study showed that NER deficient primary human keratinocytes showed a lower degree of UV induction than controls (Petit-Frere et al, 2000). This would imply that IL-6 was in some way linked to the repair mechanism itself, rather than the presence of DNA photoproducts. However, the data presented in this paper showed cytokine release measured in supernatants twenty four hours after UV exposure, and failed to take into account high levels of cell death likely to be occurring in the NER deficient cultures. In taking this into account, we have shown that *Ercc1* deficient murine keratinocytes do in fact release more IL-6 after UV exposure than controls, and we therefore conclude that this is due to the presence of unrepaired DNA damage.

As far as we are aware, the effects of UV radiation on the expression of MCP-1 have not been addressed previously. This chemokine is involved in the maturation of monocytes and promotes a Th2 type immune response.

We have shown that our *Ercc1* deficient keratinocytes produced high levels of MCP-1 after UV exposure, which was not replicated in our repair proficient cells. It should also be noted that the levels of MCP-1 detected in this experiment were higher than the levels of any other inflammatory mediator assayed.

If the production of MCP-1 by *Ercc1* deficient keratinocytes was caused by the presence of damaged DNA, then we would expect to see some increase in MCP-1 produced by the wild type cells, particularly after higher UV doses. The fact that this does not occur implies that the release of MCP-1 in response to UV is a specific trait of this cell line, i.e. the production of MCP-1 is caused by the absence of DNA repair, rather than the presence of DNA damage. However, as these cell lines are spontaneously transformed, aberrant MCP-1 expression cannot be ruled out at this stage. To confirm the link between loss of NER and increased MCP-1 expression, the experiment would need to be repeated using the *Ercc1* null cell line containing an *Ercc1* replacement minigene. If restoring *Ercc1* levels in the cells resulted in lowered MCP-1 levels, we could conclude that loss of *Ercc1* increased MCP-1 production after UV exposure.

Finally, we wished to use our *Ercc1* epidermis specific knockout mice to address the tanning response. This was the first time a study investigating

the effects of DNA damage in keratinocytes on melanogenesis had been undertaken.

We found our mice to be extremely sensitive to UV induced melanogenesis. In order to address whether they are also sensitive to melanocyte proliferation, an assay requires to be developed which will allow the melanocytes themselves to be counted, something which cannot be done using the Masson-Fontana stain, as melanin in melanocytes and keratinocytes cannot be differentiated. Due to the extent of the hypersensitivity of our mice, we can infer that the majority of the sensitivity seen in the *Xpa* knockout mice (van Schanke et al, 2005) was due to loss of *Xpa* in the keratinocytes of these mice. Recent evidence suggests that the induction of expression of melanocyte stimulating hormone (MSH) by keratinocytes is crucial (D'Orazio et al, 2006), and this may be linked with DNA damage. This would correlate with the data we have obtained. To confirm this it would be necessary to compare our *Ercc1* keratinocyte specific knockouts with model with *Ercc1* deficient melanocytes. This work is currently being undertaken in our laboratory with a view to a future publication. Furthermore, it would be interesting to investigate levels of MSH expression in *Ercc1* deficient and proficient keratinocytes after UV exposure. This could be carried out using northern blotting techniques to measure MSH mRNA transcript.

In summary, the work in this chapter has addressed the consequences of loss of *Ercc1* in keratinocytes on the short term effects of UVB radiation.

The *Ercc1* gene has proved to be very important in the short term response to UV. Furthermore, our model has shown that unrepaired lesions in DNA trigger multiple events in keratinocytes. We have shown that induction of erythema is closely linked with DNA damage, although resolution follows a normal pattern despite persisting damage. We have confirmed that photoimmunosuppression is caused by DNA damage, and we have been able to show that it is DNA damage specifically in keratinocytes that causes LC depletion. We have also shown that factors released by keratinocytes with DNA damage are responsible for inducing melanogenesis.

It would be useful to carry out the same mouse model experiments; including erythema measurements, contact hypersensitivity and LC counts; detailed in this chapter using a complete *Ercc1* knockout mouse. This would allow a direct comparison between a model with *Ercc1* deficient keratinocytes only, and a model with *Ercc1* deficient keratinocytes, fibroblasts and dendritic cells. At present, the only suitable model would be the *Ercc1* liver corrected null mouse, which has a life expectancy of ten to twelve weeks. The intention was to carry out these experiments, but we were unable to obtain sufficient animals – this was due to unsatisfactory breeding of the stock on an albino and hairless background.

As mentioned previously, the melanogenesis experiments are being carried out using an *Ercc1* melanocyte specific knockout mouse model, to confirm the role of the keratinocyte in the melanogenesis process.

The results obtained and presented in this chapter have underlined the important roles that keratinocytes play. Keratinocytes absorb the majority of the UV insult, however, previously, the extent of their interactions with other cells in their local and systemic environment was less clear. The work detailed in this chapter has provided a unique view of the effects of UV induced DNA lesions on keratinocytes and the factors and mediators that these cells consequently release.

Chapter 4

Ercc1 epidermis specific knockout mice and the long term effects of UV irradiation

4.1 Introduction

This chapter will investigate the role of *Ercc1* in UV induced skin carcinogenesis. Nucleotide excision repair is crucial for the protection of the organism against skin cancer, with xeroderma pigmentosum patients having a one thousand fold increased risk of contracting skin cancer. Furthermore, these patients develop skin tumours at a considerably younger age than the general population (reviewed by Friedberg, 2001).

The NER pathway is essential for the removal of cyclobutane pyrimidine dimers (CPDs) and 6-4 photoproducts from the genome, without which cells are susceptible to malignant transformation. Furthermore, as mentioned in chapter three of this thesis, exposure to UV causes suppression of the immune system. Together with the mutagenic properties of UV, this increases the likelihood of tumour development, as the host immune system is compromised in its efforts to recognise and eliminate transformed cells.

To investigate the role of *Ercc1* in UV induced skin cancer, we used our epidermal specific *Ercc1* knockout (ESKO). This model has a normal life expectancy as *Ercc1* deficiency is restricted to the epidermis, and allowed us to carry out a long term UV irradiation protocol. It should be noted that by using this model we were able to investigate non-melanoma skin cancer (NMSC) specifically. Melanoma is a malignancy of melanocytes, and while our mice had NER deficient keratinocytes, their melanocytes were repair

proficient and therefore no more susceptible to transformation than the melanocytes in control mice. For the experiments reported in this chapter, we used the *Ercc1* ESKO mice and control mice on an albino, hairless background, so that there was no pigment or fur to interfere with the effects of UV irradiation on the two genotypes.

Previous mouse model knockouts of NER genes are highly susceptible to UV induced skin cancer, including *Xpa* knockouts (de Vries et al, 1995, Nakane, et al, 1995,) an *Xpc* knockout, (Sands et al, 1995) and a *Csb* knockout (van der Horst et al, 1997). Our hypothesis was that our *Ercc1* epidermal specific knockout mice would be much more susceptible to UV induced skin cancer than wild type controls, and due to the additional repair functions of *Ercc1*, possibly even more susceptible to UV induced skin cancer than other NER deficient model mice. At present *Ercc1* has been shown to have roles in the repair of inter-strand crosslinks (Chipchase and Melton, 2002 and Niedernhofer et al, 2004) as well as recombination in mouse embryonic stem cells (Niedernhofer et al, 2001) and haematopoiesis (Prasher et al, 2005); however it was unclear whether this would have any relevance for UV induced skin cancer.

The data in this chapter have been published recently (Doig et al, 2006) and the full paper is included in an appendix to this thesis.

4.2 Experimental design

To investigate the cancer susceptibility of our mice, we devised a chronic irradiation protocol. This involved the mice being exposed to the appropriate UV dose three times per week. To assess the susceptibility of the *Ercc1* ESKO mice compared with control mice, we compared a group of the *Ercc1* ESKO mice with two groups of control littermates. This was due to the vast difference in UV sensitivity between the two genotypes, described in chapter 3 of this thesis. We were aware that the doses the *Ercc1* ESKO mice were due to receive were extremely low, and likely to have no effect on the control mice. For this reason, we had a group of control mice receiving the same UV doses as the *Ercc1* ESKO mice, and also a second group of control mice receiving a higher UV dose. We hoped that this second group of control mice would develop tumours that would be comparable with the *Ercc1* ESKO mice.

For this experiment we used groups of animals that were age and sex matched. We had observed that despite all our animals being albino, there was a slight difference in colour between males and females in the stock, as females appeared slightly more pink, compared with the males which were whiter. We concluded after dissection that this was due to more subcutaneous fat in the males, however to avoid any possible discrepancies, we made sure all groups contained males and females.

Experimental groups (age and sex matched):

Group 1: *Ercc1* ESKO animals, n=6, receiving 125 Jm^{-2} three times weekly for the duration of the experiment.

Group 2: Control animals, n=4, receiving 125 Jm^{-2} three times weekly for the duration of the experiment.

Group 3: Control animals, n=3, receiving 1000 Jm^{-2} three times weekly for the duration of the experiment.

Animals were monitored weekly for any changes in skin condition, tumour development and tumour burden. Once tumours appeared, these were measured weekly and their appearance noted. Animals were killed once any single tumour measured over 10mm in diameter. Animals were also killed if any tumour appeared ulcerated or bleeding.

When an animal was killed, all tumours were excised and processed for histology, and sections of back skin with no obvious tumour development were also excised and fixed.

4.3 *Ercc1* ESKO mice develop tumours much more rapidly than control mice

During the experiment, weekly checks identified tumours early in their development. The first *Ercc1* ESKO animal to develop a tumour did so during week eight of the irradiation programme, and all the *Ercc1* ESKO animals had developed at least one tumour by sixteen weeks. Median tumour free survival time was ten weeks. By comparison, none of the control mice receiving the same UV dose as the *Ercc1* ESKO mice developed any tumours at all throughout the experiment, until we ended the protocol at fifty eight weeks, furthermore, none of these mice showed any adverse effects due to chronic UV exposure. These animals were culled as a result of age related deterioration rather than any adverse consequences of the prolonged UV exposure, indicating that this low dose is tolerated well by the mice. The other group of control mice, which were exposed to an eight fold higher dose, developed tumours from twenty nine weeks of irradiation; median tumour free survival for this group was thirty weeks. Tumour free survival data are shown in figure 4.1. These results implied around a twenty five fold increased sensitivity in the *Ercc1* ESKO mice compared with controls; calculated by multiplying the fold difference in median tumour free survival time (around three) by the fold difference in UV doses (around eight).

Fig 4.1

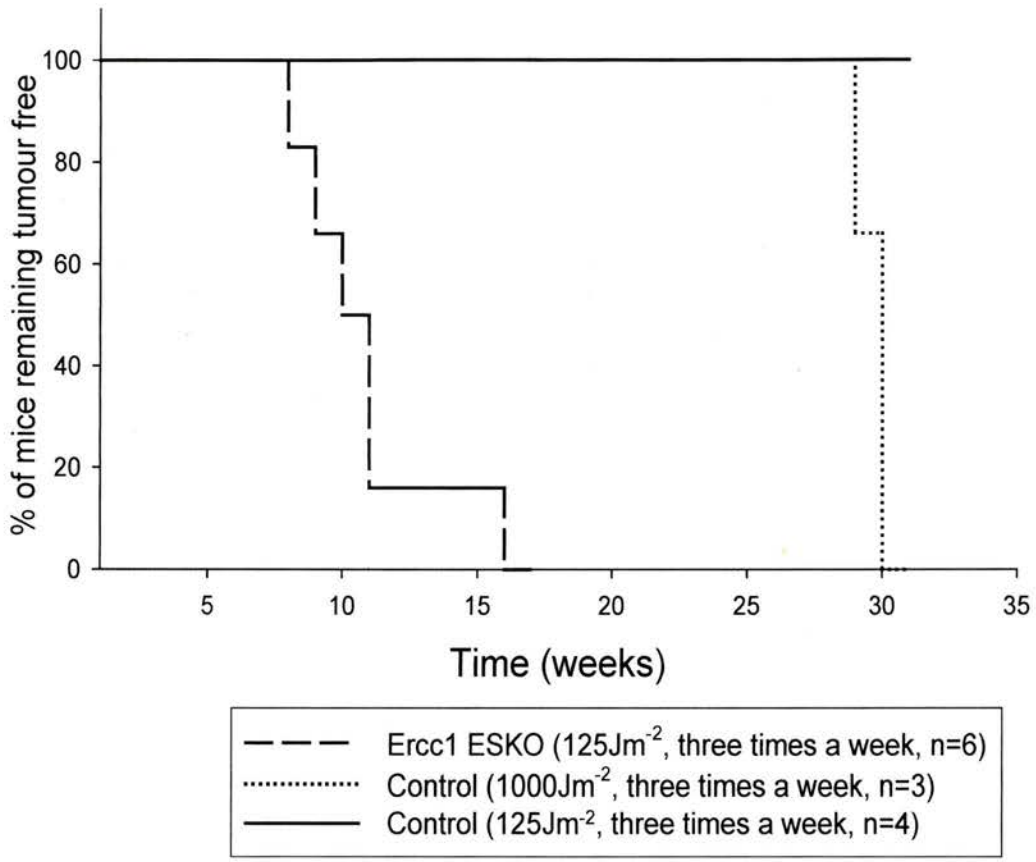

Figure 4.1 Ercc1 ESKO animals develop tumours much more rapidly than controls in a long term UV irradiation programme

The graph shows the percentage of mice remaining tumour free throughout the course of the experiment.

4.4 *Ercc1* ESKO mice developed more tumours per animal than controls

Animals were culled when they reached a pre-determined endpoint with relation to tumour burden, as mentioned earlier. If any tumour was more than 10mm in diameter or was ulcerated or bleeding, the animal was culled. At this point the total number of tumours on each animal was recorded. We found that at the experimental endpoint, *Ercc1* ESKO animals had slightly more tumours than controls in the higher dose group; p=0.09 by Mann-Whitney test – as mentioned previously, none of the controls in the lower dose group developed any tumours at all. Table 4.1 shows the average number of tumours per animal at the time of culling.

Table 4.1 Average number of tumours per animal

Group	Genotype	UV dose	Average tumours per animal
1	*Ercc1* ESKO	125 Jm^{-2}	5.2
2	Control	125 Jm^{-2}	0
3	Control	1000 Jm^{-2}	3

Examples of animals from groups 1 and 2 are shown in figure 4.2.

Fig 4.2

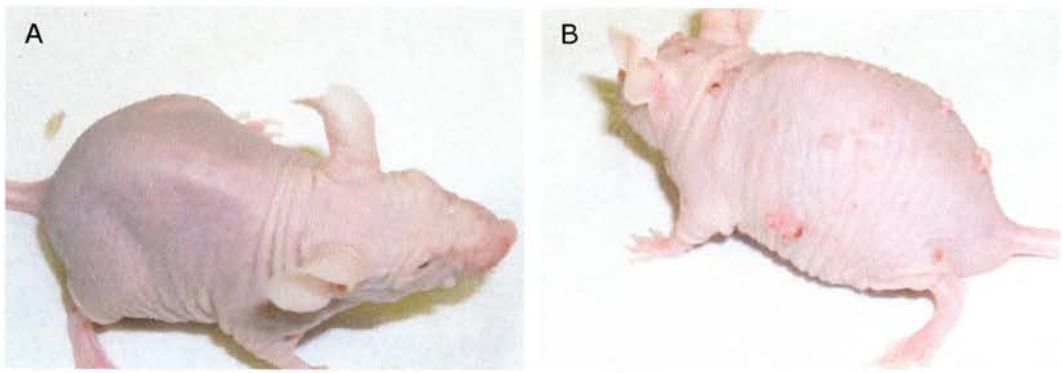

Control mouse

Ercc1 ESKO mouse

Figure 4.2 Ercc1 ESKO animals develop more tumours than controls

These images show mice from experimental groups 1 and 2. Panel A shows a control animal from the lower dose UV exposure group. None of the mice in this group developed tumours. Panel B shows an Ercc1 ESKO animal, also part of the lower UV dose protocol. This animal has multiple skin tumours, and furthermore, its skin is generally hyperkeratotic.

4.5 *Ercc1* ESKO mice developed tumours at a much lower cumulative UV dose than controls

In order to make a legitimate comparison of tumours between *Ercc1* ESKO mice and controls, we set up a second irradiation protocol using control mice only. The reason for this was that in the original experiment we obtained insufficient tumours in control mice to report any significant difference in tumour classification between genotypes, for which we required to harvest more tumours from control animals. This second experiment consisted of six control mice irradiated with 2000 Jm^{-2} three times weekly. Animals were monitored weekly as described previously and the same experimental parameters and endpoints were applied. Interestingly, we found that these animals did not develop tumours in half the time of those irradiated with 1000 Jm^{-2} three times weekly, however they did develop tumours somewhat earlier, starting at twenty one weeks. By thirty five weeks all the animals in this group had tumours.

This third group of control animals allowed us to analyse tumour free survival time between genotypes in terms of cumulative UV dose. The total amount of UV to which the animals had been exposed before developing any tumours was calculated and is shown graphically in figure 4.3. The cumulative UV dose at which 50% of *Ercc1* ESKO animals had developed tumours was 3.75 kJm^{-2}, whereas the cumulative UV dose at which 50% of control animals developed tumours was 140 kJm^{-2}. This implied

Fig 4.3

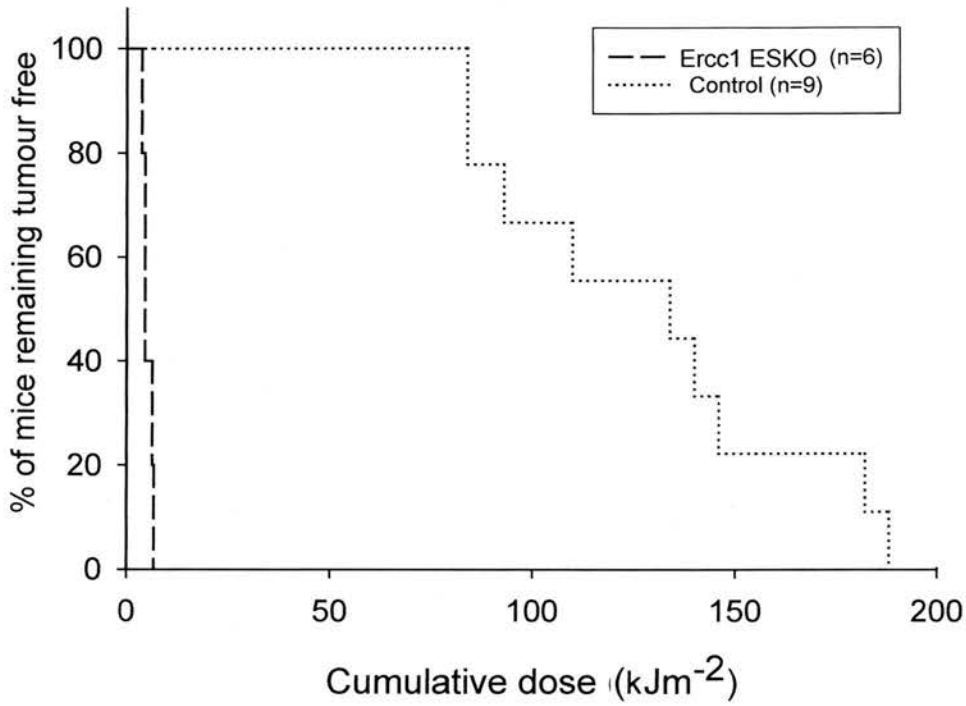

Figure 4.3 Tumour free survival with respect to cumulative UV dose

The individual UV doses to which the animals were exposed were added together to give values for cumulative dose and this is plotted against the percentage of mice remaining tumour free.

approximately forty fold increased sensitivity to UV induced carcinogenesis in *Ercc1* ESKO animals compared with controls.

From this point on, animals from the 1000 Jm^{-2} and 2000 Jm^{-2} groups, and their tumours, will be considered together as the controls.

4.6 Rates of tumour growth differed between *Ercc1* ESKO mice and control mice

During weekly monitoring of animals, growth of individual tumours was tracked. Figure 4.4 shows data recorded for tumour sizes, two, three and four weeks after those particular tumours were first identified. These graphs include tumours from control animals in both of the higher UV dose groups. It is also important to note that the data used to compile these graphs is by necessity selective: tumours used had to grow for at least four weeks before the animals were culled, while many of the tumours identified appeared less than four weeks before animals were culled. However, we found that tumours on *Ercc1* ESKO animals grew more rapidly than those on control animals, a conclusion we reached following the observation that a greater percentage of the tumours on *Ercc1* ESKO animals grew to larger sizes, compared with the controls, during the recorded period.

Fig 4.4

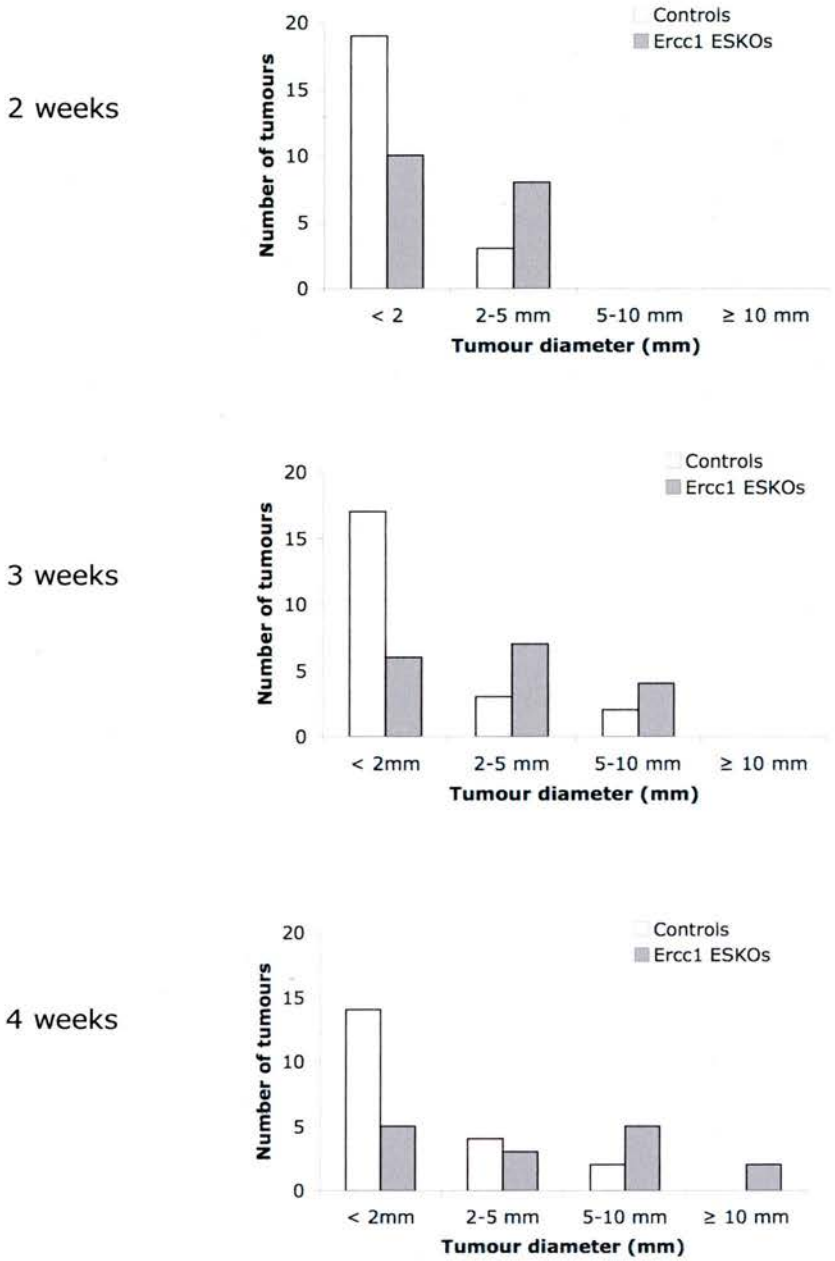

Figure 4.4 Tumours in *Ercc1* ESKO animals grow more rapidly than those in control animals

These three graphs show the sizes of tumours from each of the genotypes, showing their progression over a 4 week period from the point at which they were initially observed. These figures include tumours from control animals in 1000 Jm^{-2} and 2000 Jm^{-2} groups.

Fig 4.5

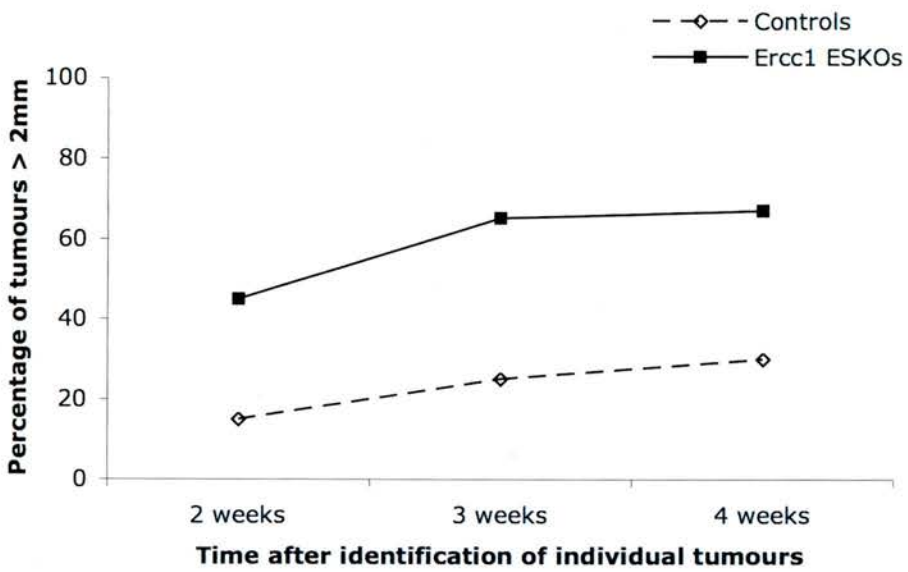

Figure 4.5 Ercc1 ESKO animals consistently have a greater number of tumours over 2mm in diameter

Tumours were recorded from the time they were first observed, for 4 weeks. This graph shows the same data as figure 4.4

Two weeks after the initial identification of tumours, 15% of those tumours on control mice exceeded 2mm in diameter, whereas 45% of tumours on *Ercc1* ESKO mice exceeded this threshold. At three weeks, these figures had developed to 25% of tumours over 2mm in diameter in control mice, compared with 65% in *Ercc1* ESKO mice. The percentage of tumours greater than 2mm in diameter over the time course for both genotypes is shown figure 4.5. Furthermore, at 4 weeks after the detection of tumours, 10% of tumours in control mice exceeded 5mm in diameter, compared with 45% in *Ercc1* ESKO mice. Tumour size distributions were significantly different between the two genotypes at all three time points: 2 weeks, χ^2_{1DF}, p=0.03; 3 weeks, χ^2_{2DF}, p=0.03; 4 weeks, χ^2_{2DF}, p=0.04.

4.7 *Ercc1* ESKO mice developed a different spectrum of tumour types compared with controls

All tumours were classified grossly and histopathologically. Grossly, tumours were classified as papules, or raised masses of less than 2mm diameter; exophytic lesions, or raised masses on stalks of 2mm or more in diameter; or endophytic lesions, or raised masses without stalk of 2mm or more in diameter. We found an equal distribution of papules, exophytic masses and endophytic masses between the two genotypes.

Tumours were classified histologically by Dr David Brownstein, Veterinary Pathologist. We found that in both genotypes most of the tumours classified grossly as endophytic masses were diagnosed histopathologically as squamous cell carcinomas (SCCs). We also found that in both genotypes most of the tumours grossly described as exophytic masses were diagnosed histopathologically as precancerous lesions acanthosis (hyperplasia) or actinic keratosis (isolated areas of dysplasia). However there was a significant difference between genotypes in the group of tumours that had been classified grossly as papules; $p<0.01$ by Fisher's exact test. In control mice, ten out of the seventeen papules were classified as carcinoma in situ, or full epidermal thickness dysplasia. However none of the fifteen papules from *Ercc1* ESKO animals were classified as carcinoma in situ. Eight of these were classified as actinic keratosis, with the other seven classified as SCCs. Furthermore, carcinoma in situ was diagnosed for only three of thirty one lesions in *Ercc1* ESKO mice, compared with fifteen of thirty four lesions from control mice; $p<0.002$ by Fisher's exact test.

The gross and histopathological classification of the tumours is shown in table 4.2.

Table 4.2

Histopathological diagnosis	Gross appearance					
	Papule (<2mm)		Endophytic (>2mm)		Exophytic (>2mm)	
	Control	*Ercc1* ESKO	Control	*Ercc1* ESKO	Control	*Ercc1* ESKO
Acanthosis	1	-	1	-	1	-
Actinic keratosis	3	8	1	2	1	4
Carcinoma *in situ* SCC**	10	-	-	1	5	2
GNS***	2	5	3	2	1	1
Grade 1	1	1	1	1	-	-
Grade 2	-	-	-	2	1	-
Grade 3	-	1	1	1	-	-
Keratoacanthoma	-	-	1	-	-	-
Total	17	15	8	9	9	7

** Squamous cell carcinoma
*** Grade not specified

Table 4.2 Comparison of tumour gross classification with respective histopathological diagnosis

Grossly, tumours were classified as papules, endophytic or exophytic. Upon sectioning, these were then classified histologically as actinic keratosis, carcinoma in situ, squamous cell carcinoma (grades 1-3) or keratoacanthoma.

This table includes all tumours identified from all animals, in particular both higher dose groups of control animals. There are more tumours <2mm in size in this figure compared with figure 4.4 because here we have included tumours that appeared less than 4 weeks before animals were culled.

Fig 4.6

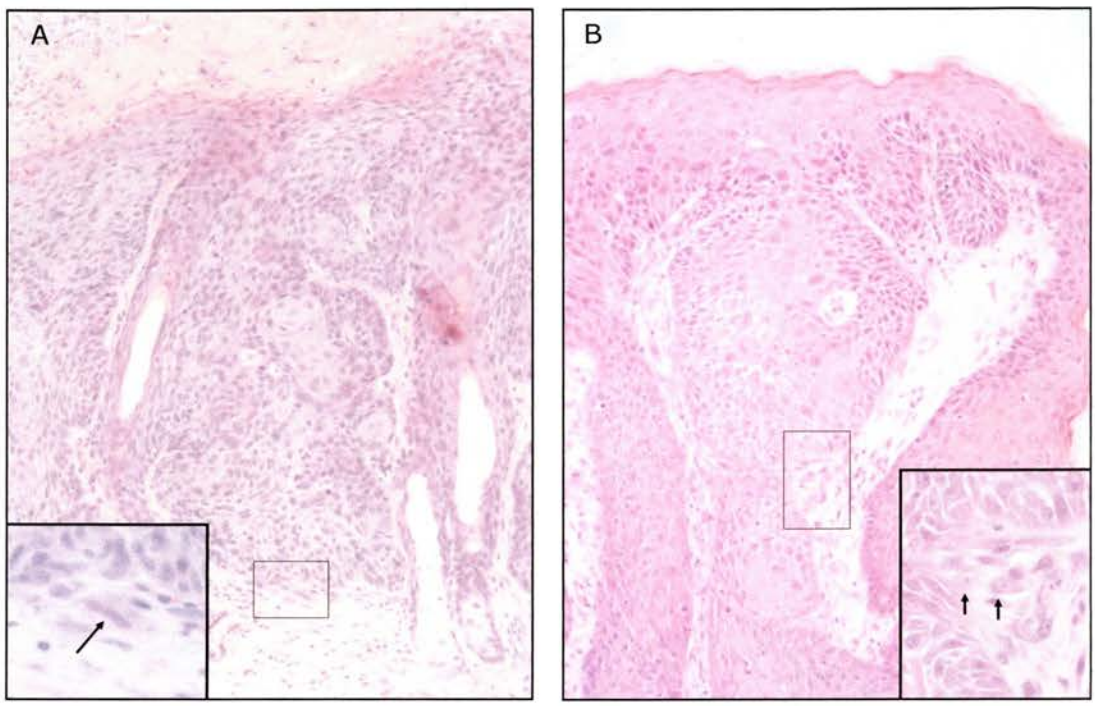

Figure 4.6 Tumours in *Ercc1* ESKO animals progress differently compared with tumours in controls

The image shown in panel A is taken from a control animal. This shows a squamous cell carcinoma GNS arising from an area of carcinoma *in situ*.

The image shown in panel B is taken from an *Ercc1* ESKO animal. This shows a squamous cell carcinoma GNS arising from an area of actinic keratosis.

The enlarged boxes show individual epithelial cells (arrows) that have invaded the dermis.

4.8 Invasive tumours arise from less dysplastic areas in *Ercc1* ESKO mice compared with controls

Tumours identified as SCC, type grade not specified (GNS), were described as cells or small groups of cells of the epidermis regarded to have invaded the basement membrane and penetrated the dermis. In control mice, all six SCC GNS that were described were found adjacent to areas of carcinoma in situ. In *Ercc1* ESKO mice, however, three of the eight SCC GNS arose from areas of carcinoma in situ, or full thickness dysplasia, but four arose from actinic keratoses, or partial thickness dysplasia. The other SCC GNS arose from a keratoacanthoma, a benign type of tumour.

Figure 4.6 shows examples of SCC GNS arising from carcinoma in situ, in a control mouse, and from actinic keratosis, in an *Ercc1* ESKO mouse.

4.9 *Ercc1* ESKO mice exhibit striking histological skin changes compared with control mice

Sections of skin that did not have any overt cancerous masses were also examined histopathologically, to compare epidermal hyperplasia between *Ercc1* ESKO and control groups.

Control mice that had been exposed to the higher doses of UV displayed mild, uniform epidermal hyperplasia, with no signs of dysplasia or hyperkeratosis. Cells of the stratum granulosum contained more keratohyalin granules than unirradiated mice and these were more dispersed and larger than normal.

In *Ercc1* ESKO mice, however, there were more striking changes as a result of the chronic irradiation protocol, despite the lower doses. We found epidermal hyperplasia was uneven although epidermal thickness reached three times that in the control mice that had been exposed to the highest doses. We observed diffuse hyperplastic actinic keratosis, as well as areas of hyperkeratosis and parakeratosis. The stratum granulosum was discontinuous with dispersed keratohyalin granules. In the cells of the basal layer we found hyperplasia and dysplasia, with cells displaying cytomegaly, karyomegaly and anisokaryosis. In the stratum spinosum cells were hypertrophied and occasionally apoptotic, with some dyskeratotic cells present. Furthermore, we observed dermal changes indicative of chronic inflammation and fibrosis, including infiltration of cells of the immune system. In summary, we found the entire dorsal skin of the *Ercc1* ESKO animals to be in a pre-cancerous state.

Images of skin sections showing the differences in epidermal hyperplasia between the two genotypes are shown in figure 4.7.

Fig 4.7

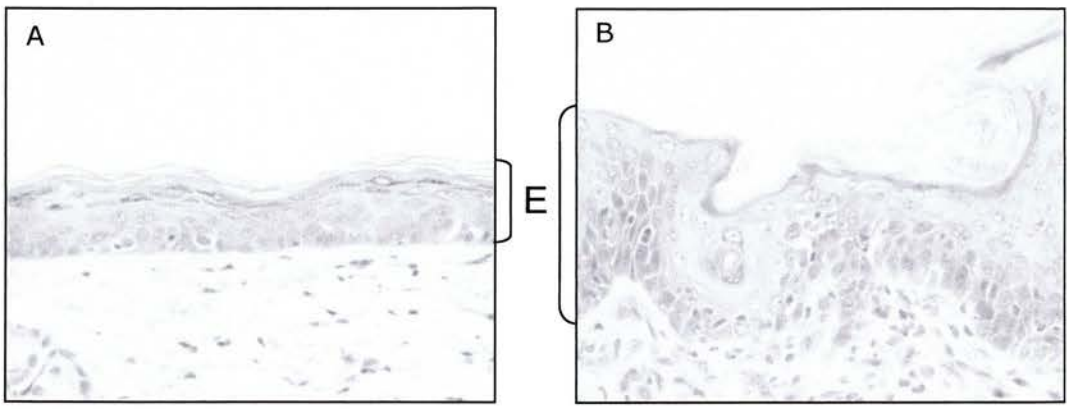

Figure 4.7 *Ercc1* ESKO animals have pronounced epidermal thickenening compared with controls after chronic UV exposure

The image in panel A is taken from a control animal that had been exposed to 2000 Jm^{-2} three times weekly for 25 weeks.

The image in panel B is taken from an *Ercc1* ESKO animal that had been exposed to 125 Jm^{-2} three times weekly for 12 weeks.

The epidermis is annotated 'E'.

4.10 Discussion

The essential role of *Ercc1* in NER was responsible for our hypothesis that our *Ercc1* epidermal specific knockout mice would be more susceptible to UV induced non melanoma skin cancer than controls; further to this we believed that the *Ercc1* knockout may be more susceptible to UV induced tumours than other NER knockout mice due to the role of *Ercc1* in other repair mechanisms. However, it was not fully clear whether the role of *Ercc1* in mechanisms other than NER would be important in protecting against UV induced skin cancer.

We have shown that the *Ercc1* ESKO mice are extremely sensitive to UV induced carcinogenesis, significantly more so than controls. Tumours were first detected on *Ercc1* ESKO mice after 8 weeks, and at this dose no tumours were detected on controls when the experiment was terminated after fifty eight weeks, implying that the *Ercc1* ESKO mice were at least seven fold more sensitive than controls. However this data may be skewed by the fact that this dose had no noticeable biological impact on the control mice at all.

A more reliable comparison for animals that have been exposed to different weekly doses can be made using the cumulative dose data. The cumulative dose required for 50% of *Ercc1* ESKO animals to develop tumours was 3.75

kJm^{-2}, compared with 140 kJm^{-2} required for 50% of control animals to develop tumours.

This is comparable with some of the published data for other NER knockouts, although it is important to take into account that results from animals with different genetic backgrounds and in different laboratories cannot be compared without a degree of caution. The cumulative dose required for 50% of *Xpa* knockout mice to develop tumours, when exposed to 32 Jm^{-2} daily, can be calculated from data published to be equal to 3.1 kJm^{-2} (extrapolated from Berg et al, 1997) or 3.7 kJm^{-2} (extrapolated from de Vries et al, 1998). However cumulative doses for control animals from this group calculates to around 25 kJm^{-2}, which is significantly lower than we found for our control animals. This difference between control animals must be due to differences in genetic background affecting UV induced tumour susceptibility. Furthermore, when the *Xpa* knockout animals were exposed to higher doses of UV, 80 Jm^{-2} daily, the cumulative dose required for 50% of these animals to develop tumours increased by around 40%. This demonstrates, as we found with our control animals, that UV carcinogenicity does not follow a linear scale with respect to dose. In other words, in a chronic irradiation protocol, doubling the dose to which the animals are exposed does not halve the time required for tumours to develop, and this fact makes it difficult to compare cumulative dose data from one experiment to the next. Certainly without data obtained by exposing groups of mice to different UV dose protocols, comparisons cannot be made reliably.

Other published data regarding UV induced skin cancer in NER mouse models is impossible to compare with our own as it was carried out on mice with fur (Sands et al, 1995, de Vries et al, 1995, Nakane et al 1995, van der Horst, 1997), and despite the fact that the mice may have been shaved prior to UV exposure, tolerance to UV is considerably higher than that observed in hairless albino mice. This is likely to be due to pigment in the skin as well as hair regrowth.

In summary, although our *Ercc1* ESKO knockout mice appear to display UV induced skin cancer sensitivity that is comparable with that of *Xpa* knockouts, when compared with controls in the respective experiments, the *Ercc1* ESKO animals prove to be more susceptible than the *Xpa* knockouts.

Consequently, the second part of our hypothesis; that *Ercc1* knockouts would be more susceptible to UV induced skin cancer than other NER models, due to the roles of *Ercc1* outwith NER; is difficult to address. It would be imprudent to make any conclusions about this without comparing our *Ercc1* mice directly with *Xpa* mice and other NER models directly in a single experiment, with the animals on the same genetic background. It may be that the genetic background is not relevant in the knockout animals but is relevant in the control animals; this could be because there is such a large difference in UV sensitivity brought about by NER deficiency and a relatively small difference caused by genetic background discrepancies. Nevertheless,

for any conclusions to be drawn it would be important to compare the different NER deficient models directly.

Histologically, we have made interesting observations in the *Ercc1* ESKO mice. We found that not only did these mice develop more skin tumours than controls, but we also found that the entire dorsal skin of these mice was in a pre-cancerous state. This only underlines the extreme susceptibility of these mice to skin cancers.

Furthermore, we found that the *Ercc1* ESKO mice showed accelerated tumour progression. Not only did tumours grow in size more rapidly on these mice than controls, we also report abnormally rapid progression through the normal tumour development steps, shown in figure 4.8. Specifically, we found that in *Ercc1* ESKO mice, malignant or invasive areas of tumour were developing from areas of actinic keratosis, rather than areas of carcinoma in situ. In control mice, we saw a normal pattern of tumour progression: squamous cell carcinomas were preceded by carcinoma in situ, or full thickness dysplasia, which was in turn preceded by actinic keratosis, or partial dysplasia. In *Ercc1* ESKO mice however, we saw squamous cell carcinomas arising from actinic keratosis, implying that partially dysplastic skin was giving rise to malignant development, effectively missing out the development of full thickness dysplasia. This was corroborated by the fact that we saw very few carcinomas in situ in *Ercc1* ESKO mice compared with controls.

Fig 4.8

Normal progression of UV induced
NMSC as seen in control animals:

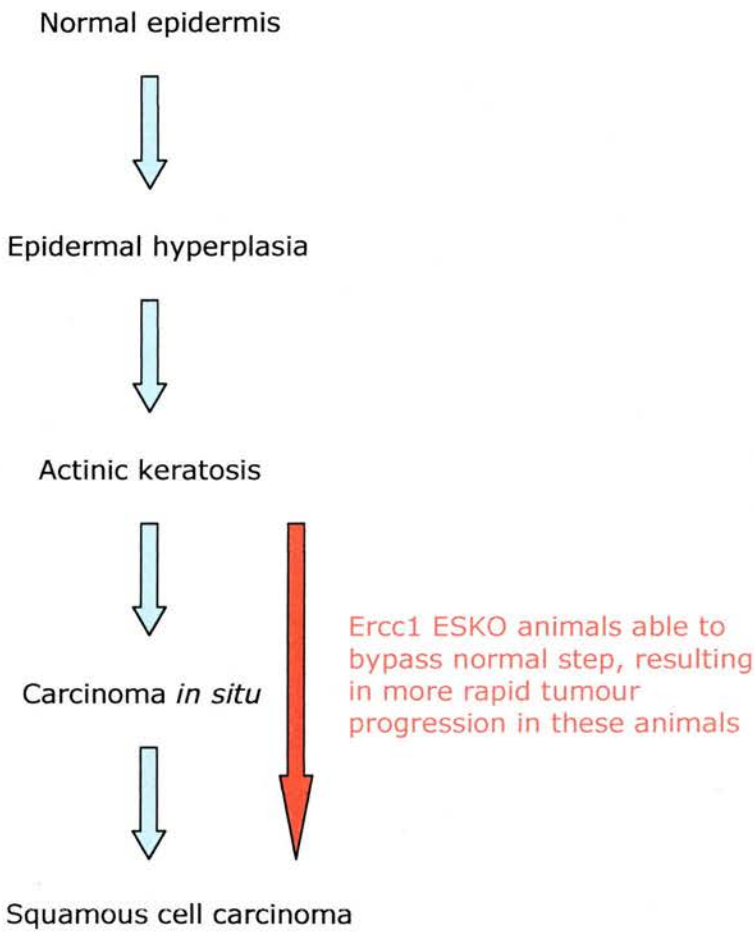

Figure 4.8 Model for tumour progression in *Ercc1* ESKO and control animals

Tumours in Ercc1 ESKO animals become invasive more rapidly than those in controls due to their ability to bypass normal steps in tumour progression.

With regards to the detailed histopathological analysis carried out for this experiment, we have reported phenomena previously unreported for other NER knockouts. However it is unclear whether this is the case because *Ercc1* mice have a different pattern of tumour progression than other NER knockouts, or whether this degree of detail simply has not been addressed by other groups working with NER mice.

Despite the fact we are unable to comment reliably on comparisons with other NER mice as yet, and therefore dissect the importance of the non-NER related roles of *Ercc1* in UV induced skin cancer, we have reported a novel model for UV induced non-melanoma skin cancer. We have provided a detailed histopathological analysis of tumour development in this model, furthering insights into the importance of the NER pathway in tumour initiation and progression. In addition, with its extreme susceptibility to skin cancer, the *Ercc1* ESKO mouse will be a useful model for investigating anti-cancer therapies.

Chapter 5

Investigation into the anti-cancer effect of topical thymidine dinucleotide application

5.1 Introduction

Topical thymidine dinucleotides (pTpT), when applied in combination with UV exposure, have been shown to provide some protection against the carcinogenic effect of UV. The mechanism of this protection is poorly understood. It has been attributed to upregulation of DNA repair mechanisms (Goukassian et al, 2004), and alternatively to increased apoptosis – perhaps due to the telomere homology of the sequence (Eller et al, 2002 and Puri et al, 2004).

Using our *Ercc1* epidermis specific knockout mice we hoped to provide some insight into the protective mechanism afforded by topical pTpT application. These mice are entirely defective in nucleotide excision repair, and as such, any level of protection conferred by pTpT against the carcinogenic effect of UVB cannot be due to upregulation of DNA repair.

5.2 Topical pTpT application suppresses the contact hypersensitivity response

As mentioned previously, topical pTpT has been shown to mimic some of the effects of UV radiation. In order to confirm one of the published short term effects of topical pTpT application and also to confirm a biological effect at the dose we intended to use on the mice in subsequent studies, we

Fig 5.1

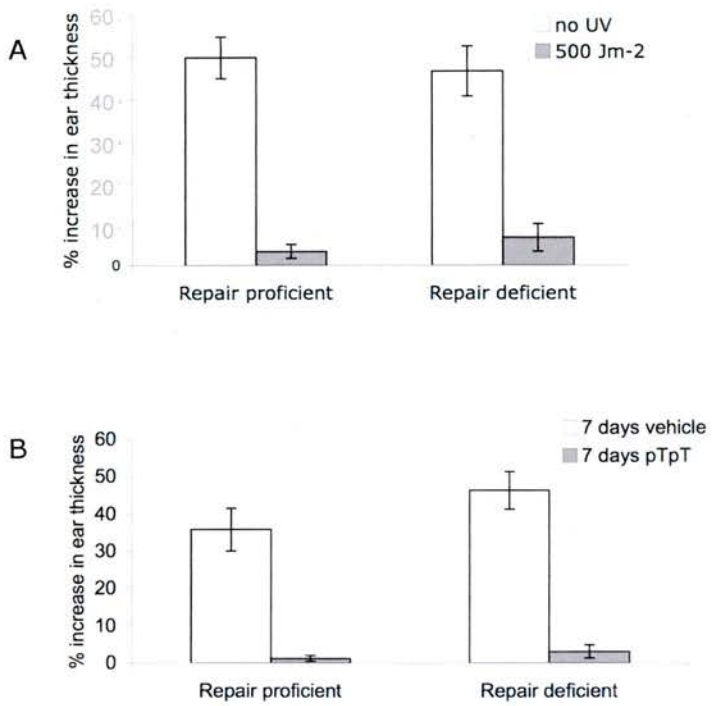

Figure 5.1 pTpT treatment alone suppresses the contact hypersensitivity response

The contact hypersensitivity response (CHS) quantifies the immune response by an elicitation step 5 days after sensitisation with an irritant. Ear thickness is measured before and 24 hours after elicitation and percentage increase calculated. A high percentage increase indicates a strong immune response.

(A) shows the effect of UV irradiation on the CHS response. Animals were either treated with a single 500 Jm^{-2} UVB dose 48 hours prior to sensitisation or sham-irradiated, with each group composed of 1 animal.

(B) shows the effect of pTpT on the CHS response. Animals were either treated with pTpT for seven days prior to sensitisation or treated similarly with vehicle alone, with each group containing 3 animals.

investigated the effect of pTpT on the contact hypersensitivity (CHS) response. In figure 5.1 we have shown that seven days of topical pTpT treatment prior to sensitisation with hapten suppressed the contact hypersensitivity response in a manner comparable with the suppression resulting from UV irradiation; we observed an almost total suppression of the CHS response in both cases. This result confirmed that application of the oligonucleotide at this concentration and in this vehicle on to mouse skin was having a biological effect.

5.3 The protective effect of pTpT is not caused by the oligonucleotide acting as a sunscreen

Initially it was important to confirm that the protective effect of pTpT against non-melanoma skin cancer (NMSC) was not caused by the dinucleotide itself acting as a chromophore. Genomic DNA acts as a chromophore which can lead to mutation, so there was precedent for the pTpT oligo being able to absorb UV radiation, thereby effectively shielding the cellular DNA. Nucleic acids absorb radiation in the UV spectrum under normal circumstances, and furthermore, we might expect pTpT to form pyrimidine dimers during UV exposure. It is unclear from the literature whether the pTpT oligonucleotide is able to absorb ultraviolet energy and dimerise in a similar manner to an adjacent pair of chromosomal thymidine bases. It is possible that for the dimerisation reaction to occur, the bases must be in a certain orientation

which is made possible by being part of a DNA double helix, and therefore dimerisation would not occur in a dinucleotide molecule.

Figure 5.2 shows that pTpT is not acting as a sunscreen. In this experiment, the erythema profile of *Ercc1* ESKO animals treated with pTpT for two days was compared with the erythema profile of *Ercc1* ESKO animals treated with vehicle alone, prior to a single 500 Jm^{-2} UVB dose. These in turn were compared with the erythema profile of untreated, control mice exposed to the same dose. The control mice showed no increase in erythema in response to this dose, which is well below the MED for these mice. Both groups of *Ercc1* ESKO animals showed a dramatic increase in erythema after this dose, which equates to around twelve MED, with comparable peak increases in erythema index and similar time courses for peak erythema and subsidence of the response. However there was no significant difference between groups, implying that pTpT is not acting as a sunscreen.

With this information we were able to proceed to a long term carcinogenicity experiment knowing that any protection we found to be conferred by topical pTpT was not due to the molecule absorbing UV radiation and acting as a sunscreen.

Fig 5.2

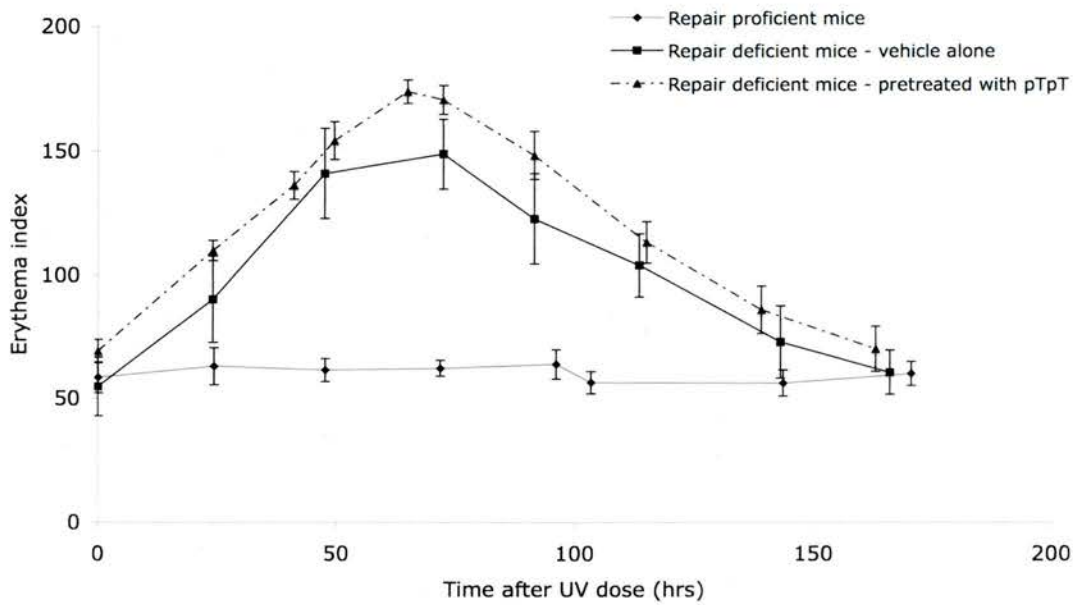

Figure 5.2 pTpT is not acting as a sunscreen

In this experiment, erythema index was measured after a single 500 Jm^{-2} UVB dose. Ercc1 ESKO mice treated with pTpT were compared with similar mice treated with vehicle alone, and with untreated control mice. Erythema was measured once before exposure, to set a baseline level, and regularly thereafter, until erythema index had returned to pre-UV levels. Each group contained five animals. Values shown here represent the mean erythema index for the group ± SEM.

5.4 Topical thymidine dinucleotide application affects UV induced carcinogenesis in *Ercc1* epidermis specific knockout animals

To determine whether pTpT application would protect *Ercc1* ESKO mice from UV induced carcinogenesis, the following experiment was set up:

Ercc1 ESKO animals were separated into two age and sex matched groups, with five animals in each group.

Group 1: *Ercc1* ESKO animals – one week of three treatments with pTpT vehicle only, then 125 Jm^{-2} UVB three times weekly, with pTpT vehicle applied after each UV dose.

Group 2: *Ercc1* ESKO animals – one week of three treatments with pTpT, then 125 Jm^{-2} UVB three times weekly, with pTpT applied after each UV dose.

Animals were monitored weekly for any changes in skin condition, tumour development and tumour burden. Once tumours appeared, these were measured weekly and their appearance noted. Animals were killed once any single tumour measured over 15mm in diameter. This new limit on tumour size was agreed with the veterinary staff in the animal house, after the experiment described in chapter 4 of this thesis, hence the difference in

endpoints between the two experiments. Animals were also killed if any tumour appeared ulcerated or bleeding.

When an animal was killed, all tumours were excised and fixed and processed for histology. Sections of back skin with no obvious tumour development were also excised and fixed.

5.5 pTpT treated animals remained tumour free for longer than untreated animals

Figure 5.3 depicts how long the animals in each group remained tumour free. The untreated group had a median tumour free survival of seven weeks compared with ten weeks for the pTpT treated group. Median tumour free survival was increased by three weeks in the pTpT treated group, equating to nearly 50% increase in tumour free survival. However the p-value for these groups is large, implying little statistical significance. This is mainly due to the small sample sizes, in combination with the only slightly longer tumour free survival of the UV plus pTpT group, compared with UV only controls. To increase the statistical significance of these results it would be necessary to repeat the experiment using greater numbers of animals.

Fig 5.3

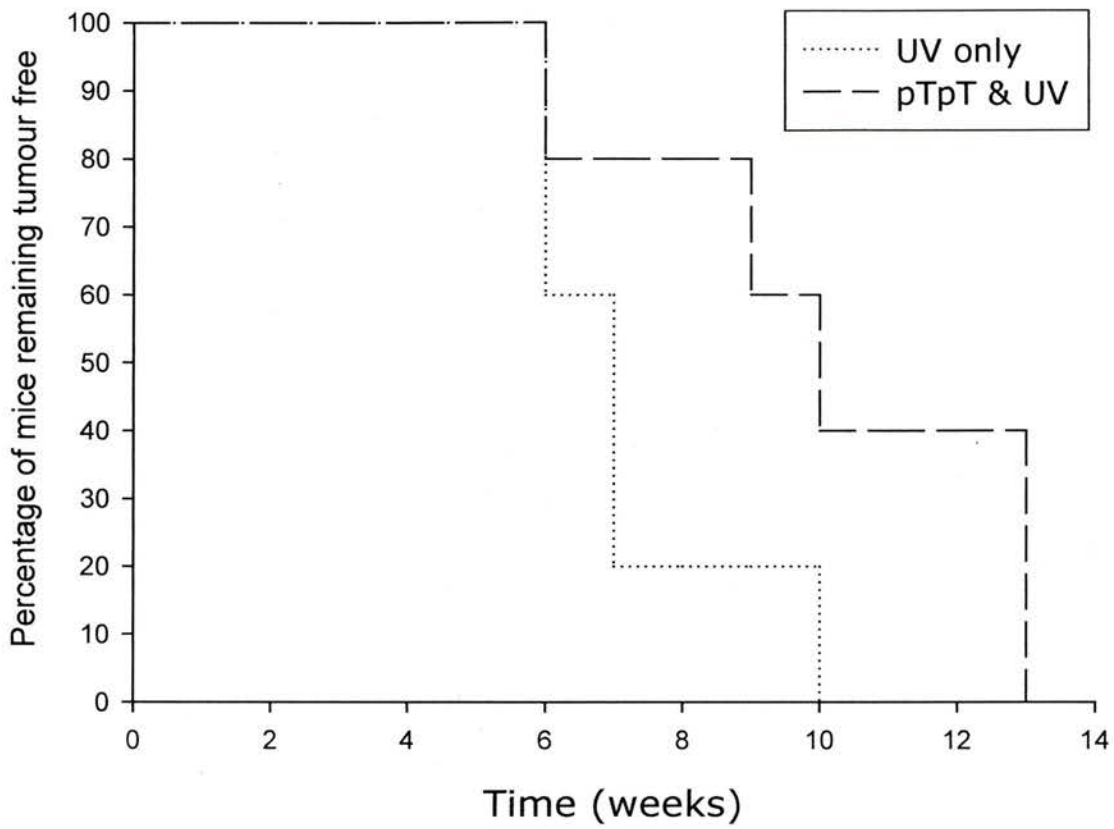

Figure 5.3 pTpT increases tumour free survival in chronically irradiated Ercc1 ESKO mice

This figure shows the percentage of mice remaining tumour free against the weeks of UV irradiation. We compared tumour free survival for Ercc1 ESKO mice treated with pTpT 3x weekly as well as undergoing 125Jm^{-2} UV doses 3x weekly, with animals undergoing the same UV regime without pTpT, treated with vehicle alone. Each group consisted of five animals.

5.6 pTpT treated animals had fewer tumours than untreated animals

The weekly total number of tumours per group was divided by the number of animals remaining in each group, to give an average number of tumours per animal, on a weekly basis, and these results are shown in figure 5.4.

At 15 weeks, the values for the UV only group appeared to dip. This aberration was caused by the fact that animals were culled when they reached certain welfare related endpoints, rather than at the end of a set period of time. Consequently, if an animal with an above average number of tumours were culled, the average for the group would drop. There was no 20-week value for the UV only group as all the animals in this group had been culled by this stage. In fact at 18 weeks only one animal in this group remained, explaining the lack of standard error data for this value.

The pTpT treated group had a lower average number of tumours per animal, particularly in the later stages of the experiment. At twelve weeks, $p=0.059$ by Mann-Whitney test for the null hypothesis that the average number of tumours in the UV only group was not greater that the average number of tumours in the UV plus pTpT group. At eighteen weeks, the same test gave $p=0.079$.

Fig 5.4

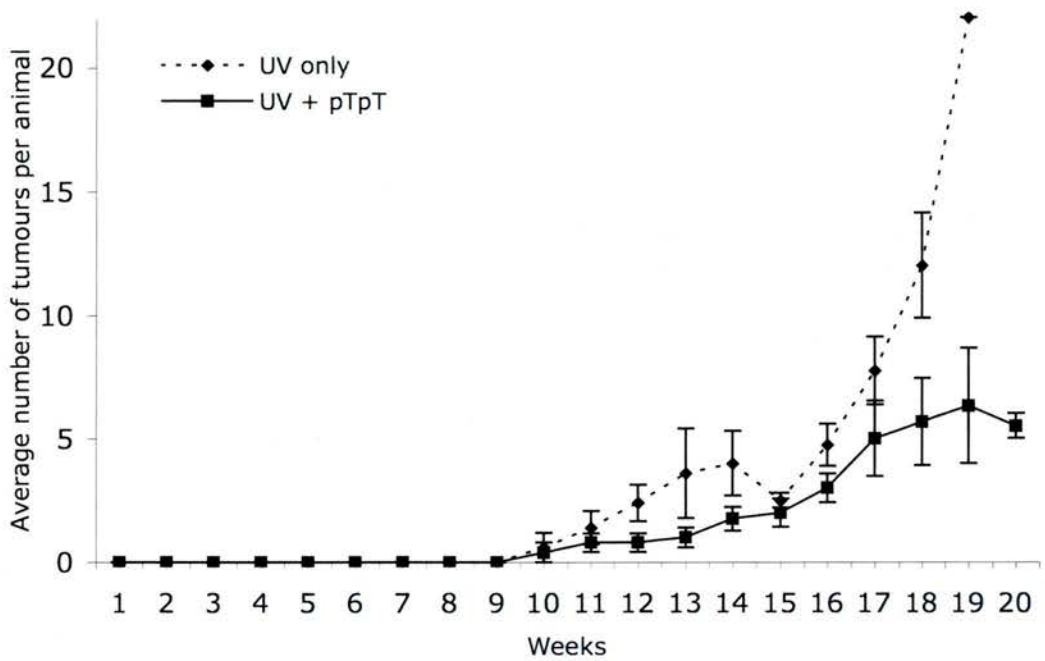

Figure 5.4 Ercc1 ESKO mice treated with pTpT developed fewer tumours during the chronic UV protocol than untreated mice

This figure shows average number of tumours per animal in both experimental groups. This figure was calculated using the total number of tumours per group, divided by the number of animals in the group.

5.7 pTpT treated animals develop a lower proportion of endophytic tumours compared with the UV only group

Gross tumour classification revealed a difference between the UV only and UV plus pTpT groups. Tumours that were 2mm or greater in diameter were classified as exophytic or endophytic depending on their macroscopic appearance. Tumours smaller than 2mm were recorded as macules or papules. Areas of discoloured skin were noted as macules, and raised areas were recorded as papules. Tumours with a 'stalk like' appearance, similar to papillomas, were classified as exophytic. Tumours that appeared simply as a raised mass within the skin, without a stalk, were classified as endophytic.

Figure 5.5 shows the types of tumours present in each group when animals were culled. The absolute number of exophytic tumours per animal was not significantly different in the UV only and UV plus pTpT groups, as $p=1$ using the Mann-Whitney test. However the absolute number of endophytic tumours per animal was much lower in the pTpT treated group and this difference was significant, as $p=0.016$ using the Mann-Whitney test. Thus, for the pTpT treated group, the proportion of exophytic tumours to endophytic tumours was significantly higher than in the UV only group, where proportionally, the number of exophytic tumours was much lower.

Fig 5.5

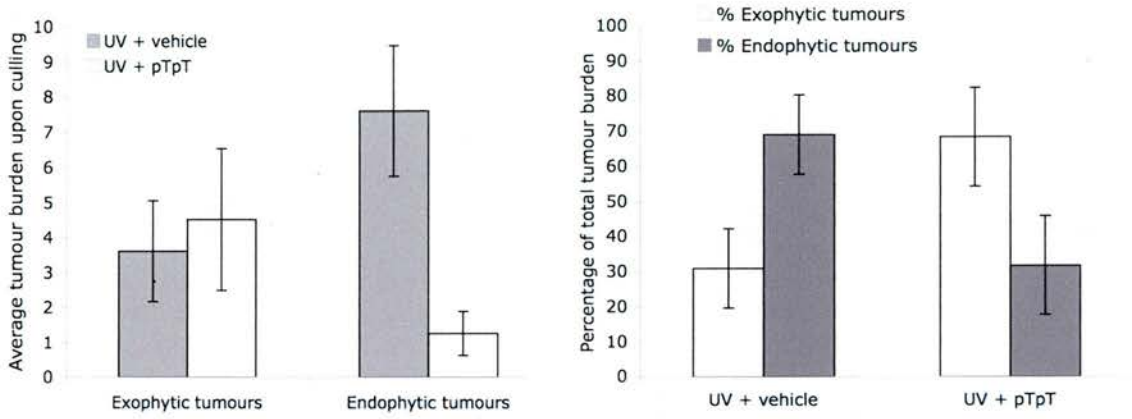

Figure 5.5 Ercc1 ESKO mice treated with pTpT developed a different spectrum of skin tumours compared with untreated mice

These graphs compare gross tumour classification according to experimental group. The graph on the left shows the average tumour burden upon culling, per mouse for both groups. The graph on the right shows the same data expressed as a percentage of the total tumour burden per mouse.

Fig 5.6

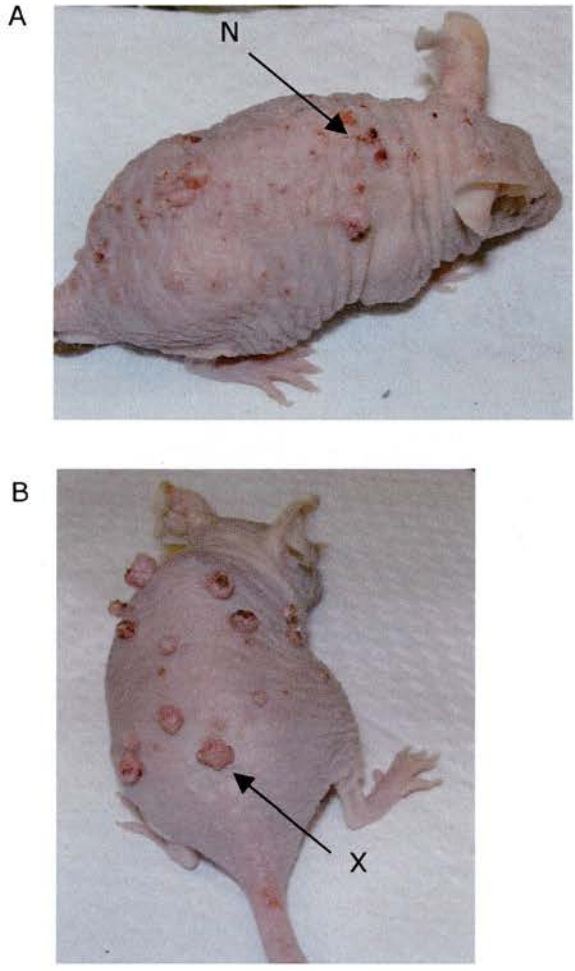

Figures 5.6 Gross appearance of tumours differ between UV only and UV + pTpT mice

Panel A shows a mouse treated with UV and vehicle. Panel B shows a mouse treated with UV and pTpT.

X shows an example of an exophytic tumour

N shows an example of an endophytic tumour

It should be noted that these photographs were not taken on the same day and as such are not intended as a comparison of tumour numbers, simply as a representation of the different types of tumours that were present in the two groups.

Figure 5.6 shows photographs of representative animals from the two experimental groups. The animal from the UV only group had a preponderance of endophytic lesions. The animal from the pTpT treated group had a much higher proportion of exophytic lesions. It should also be noted that there is a marked difference between the non-lesioned dorsal skin of these two animals. The skin of the animal from the UV only group had a very poor overall appearance, with almost no areas free from lesions. In comparison, the skin of the animal from the UV plus pTpT group had a much better macroscopic appearance, and grossly at least, appeared to be less affected by the chronic UV exposure. These observations were consistently noted for the other animals in the two groups.

5.8 Histopathological observations confirm a difference in the distribution of tumours between the two experimental groups

Tumours that had been classified as papules and exophytic or endophytic lesions on their gross appearance were classified histopathologically as actinic keratoses, carcinomas in situ, squamous cell carcinomas of grades 1 to 3, or keratoacanthomas. The tabulated data are shown in table 5.1.

A total of thirty six skin lesions from five UV only mice and twenty three lesions from four UV plus pTpT mice were classified histopathologically as

Table 5.1

Histopathological diagnosis	Gross appearance					
	Papule (<2mm)		Endophytic (>2mm)		Exophytic (>2mm)	
	UV only	UV+ pTpT	UV only	UV+ pTpT	UV only	UV+ pTpT
Actinic keratosis	0	4	3	0	4	4
Carcinoma *in situ*	6	3	10	0	0	3
SCC*	(2)	(3)	(7)	(6)	(3)	(0)
Grade 1	0	1	4	2	2	-
Grade 2	-	2	1	3	0	-
Grade 3	2	0	2	1	1	-
Keratoacanthoma	-	-	1	-	-	-
Total	8	10	21	6	7	7

* SCC: squamous cell carcinoma

Table 5.1 Comparison of tumour gross classification with respective histopathological diagnosis

Grossly, tumours were classified as papules, endophytic or exophytic. Upon sectioning, these were then classified histologically as actinic keratosis, carcinoma in situ, squamous cell carcinoma (grades 1-3) or keratoacanthoma.

well as grossly. The gross classification of lesions differed between UV only and UV plus pTpT mice (χ^2_{2df}=6.68, P<0.05).

There were 8/36 (22%) papules in UV only mice and 10/23 (43%) papules in UV plus pTpT mice. There were 21/36 (56%) endophytic lesions in UV only mice and 6/23 (26%) endophytic lesions in UV plus pTpT mice. There were 7/36 (19%) exophytic lesions in UV only mice and 7/23 (30%) exophytic lesions in UV plus pTpT mice. Thus, there were proportionately more papules and exophytic lesions and fewer endophytic lesions in UV plus pTpT mice than in UV only mice. From this we were able to conclude that treatment with pTpT inhibited conversion of papules to endophytic lesions and/or it encouraged exophytic versus endophytic growth.

Histopathological examination of the sections was carried out by Dr David Brownstein, veterinary pathologist. The histopathological classification of lesions (actinic keratosis (AK), keratoacanthoma, carcinoma *in situ* (CIS) or squamous cell carcinoma (SCC)) did not differ significantly between UV only and UV plus pTpT treated mice (χ^2_{3df}=2.64, P>0.10). Actinic keratosis comprised 7/36 lesions (19%) in UV only mice and 8/23 lesions (35%) in UV plus pTpT mice. CIS comprised 16/36 lesions (44%) in UV only mice and 6/23 lesions (26%) in UV plus pTpT mice. SCC comprised 12/36 lesions (33%) in UV only mice and 9/23 (39%) in UV plus pTpT mice. There was no difference in SCC grades between UV only and UV plus pTpT mice. Although these differences were not significant the higher prevalence of AK

and lower prevalence of CIS in UV plus pTpT mice compared with UV only mice suggests that pTpT may inhibit conversion of partial thickness dysplasia (AK) to full thickness dysplasia (CIS).

Actinic keratosis was classified as endophytic (3) or exophytic (4) in UV only mice and as papules (4) or exophytic (4) in UV plus pTpT mice. Therefore actinic keratosis lesions beyond the papule stage grew endophytically or exophytically in UV only mice and exophytically in UV plus pTpT mice.

Carcinoma *in situ* was classified as papules (6) or endophytic (10) in UV only mice and papules (3) and exophytic (3) in UV plus pTpT mice, which indicates a tendency of CIS to grow exophytically in UV plus pTpT mice and endophytically in UV only mice when greater than 2mm in diameter.

Squamous cell carcinomas were classified as papules, endophytic and exophytic in UV only and UV plus pTpT mice, with no significant difference between groups.

Taken together the results suggest that the reduced prevalence of endophytic lesions in UV plus pTpT mice compared to UV only mice resulted in part from a tendency of CIS and AK to grow exophytically rather than endophytically in pTpT treated mice.

5.9 Non lesional epidermis was more hyperplastic in UV only mice compared with UV plus pTpT mice

Epidermis of non-lesional irradiated skin was more hyperplastic in UV only mice than in UV plus pTpT mice, as shown in figure 5.7, although both groups displayed some degree of hyperplasia. Mean epidermal thickness in four UV only mice was found to be 119±31 μm compared with 58±19 μm in three UV+pTpT mice (P=0.032, t-test). These data are shown graphically in figure 5.8. Epidermal changes in UV only mice consisted of regions of hyperplastic actinic keratosis, regions of carcinoma *in situ* and in two mice, early Grade 1 squamous cell carcinomas. Epidermal changes in UV plus pTpT mice consisted of regions of epidermal hyperplasia, actinic keratosis, and carcinoma *in situ*. There were no squamous cell carcinomas. Epidermis in regions of actinic keratosis and carcinoma *in situ* were far less hyerplastic than similar regions in UV only mice. In the images in figures 5.6 it is possible to see that the non lesional skin of the UV only animal was in very poor condition, whereas the non lesional skin of the UV plus pTpT treated animal appeared much more normal. We were therefore able to infer that treatment with pTpT of UV irradiated skin effects reduces either epidermal proliferation or promotes apoptosis and also inhibits dysplasia.

Fig 5.7

Sections from UV only mice

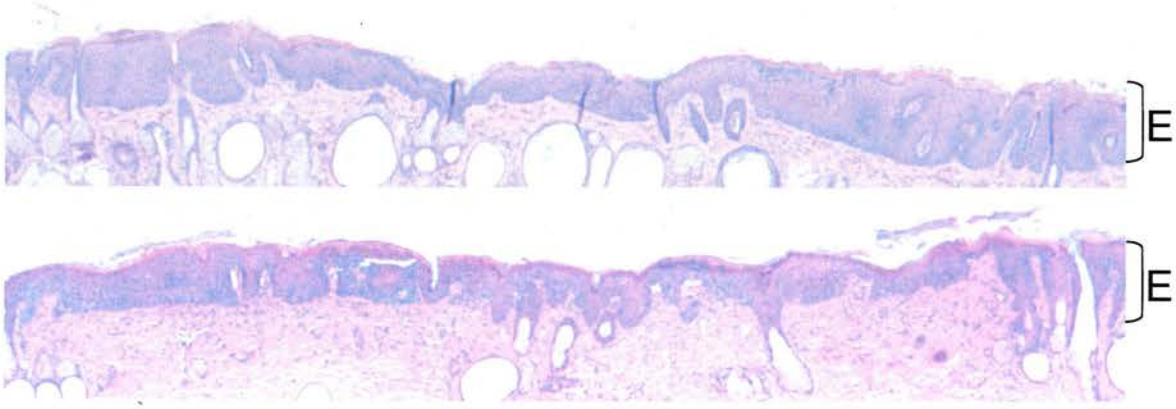

Sections from UV plus pTpT mice

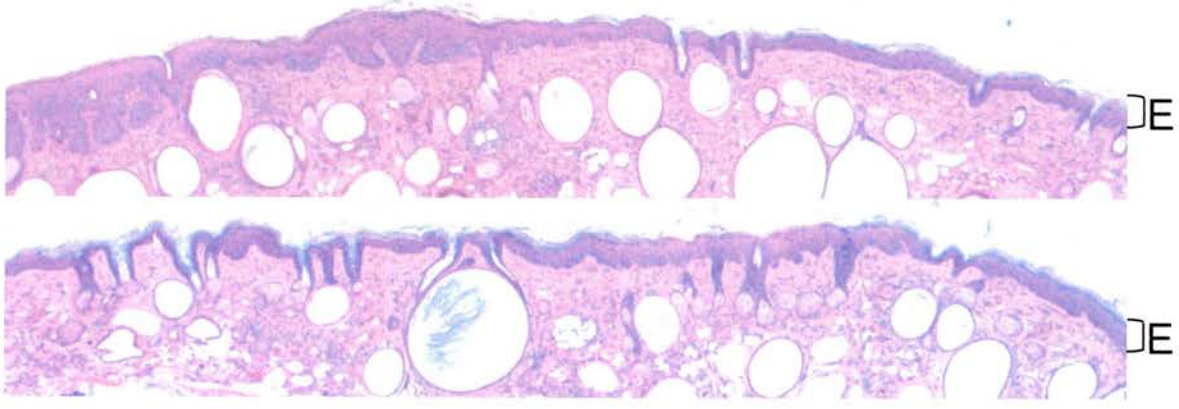

Figure 5.7 Mean epidermal thickness is greater in UV only mice than UV plus pTpT mice

The top two sections are taken from UV only animals, and the bottom two sections are taken from UV plus pTpT animals. Sections were stained with H&E. Images are representative of all animals in the groups.

E = epidermis

Fig 5.8

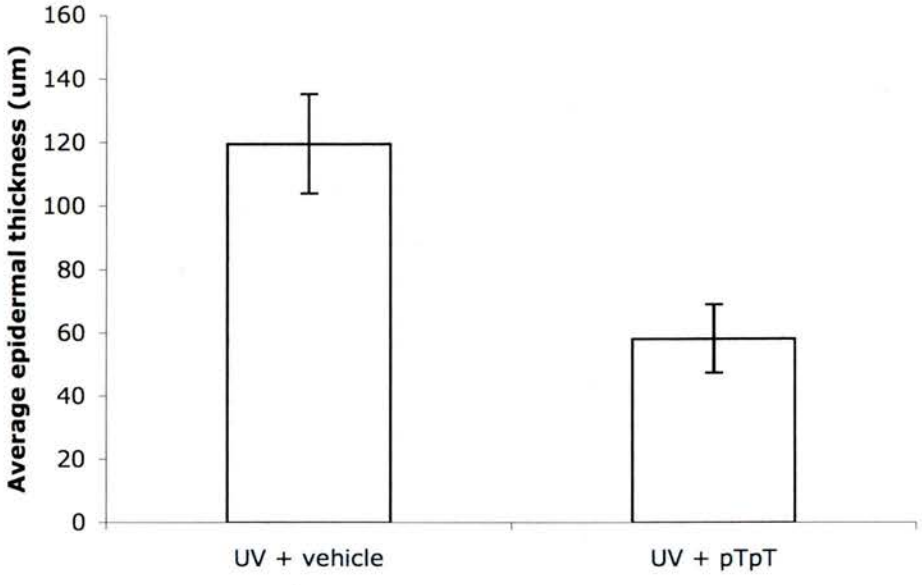

Figure 5.8 Average epidermal thickness was reduced in pTpT treated animals in carcinogenesis experiment

Mean epidermal thickness per animal was calculated by measuring a length of skin, measuring epidermal area over that length and dividing area by length to give an average thickness. The number of readings taken per animal varied depending on the amount of non-lesional skin available to measure, however around ten readings were calculated per animal. For these measurements, there were four animals in the UV only group and three in the UV plus pTpT group.

5.10 pTpT treatment does not appear to increase levels of apoptosis in the skin

Due to the fact that there was so little non lesional skin in the UV only animals, we were unable to do a full comparison of levels of apoptosis in normal skin using the skin biopsies taken. In the animals in the UV only group the majority of the skin was hyperplastic, so there were insufficient areas where numbers of apoptotic or sunburn cells could be counted. However we could not see an unusually high number of apoptotic cells in the UV plus pTpT group. It should also be noted that pTpT application alone does not induce erythema (data not shown), which implies that neither is it inducing apoptosis.

5.11 Analysis of skin by flow cytometry shows no increase in apoptosis in pTpT treated animals

In order to address the mechanism of pTpT conferred protection we investigated in which stage of cell cycle epidermal cells could be found. We saw no differences between UV only and UV plus pTpT groups, or between either of these groups and a group of age and sex matched animals that had had no treatment at all. This is shown in figure 5.9.

Fig 5.9

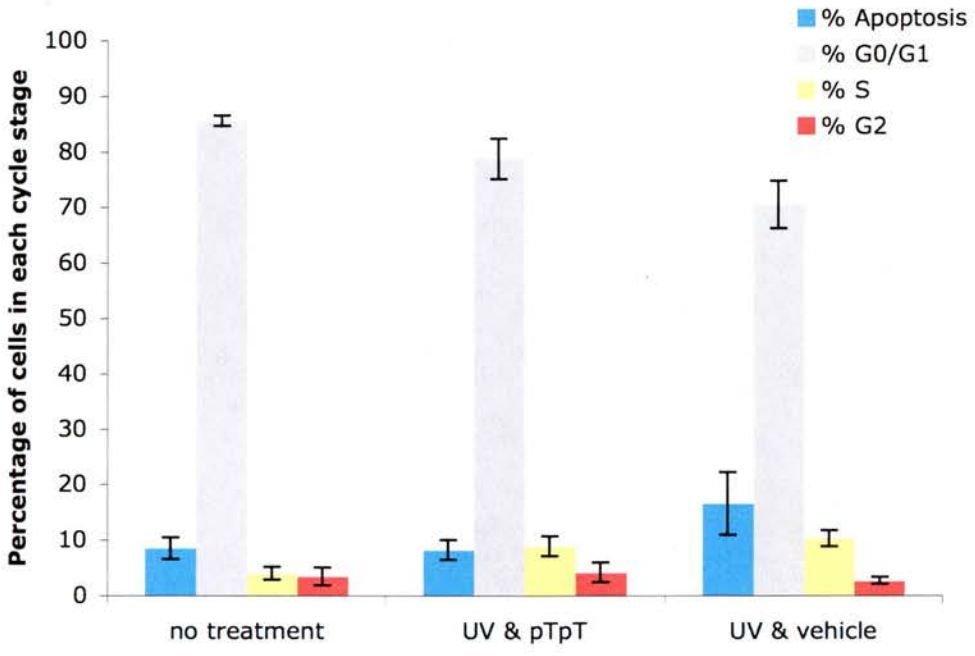

Figure 5.9 No increase in apoptosis levels in cells from back skin from animals treated with pTpT as well as UV

Epidermal cells were isolated and nuclei stained with propidium iodide. Nuclear DNA content was determined by flow cytometry. Each group contains at least three animals, and for each animal, ten thousand cells were scanned.

5.12 Discussion

In this chapter we have used our *Ercc1* epidemis specific knockout animals to investigate the mechanisms of pTpT induced UV protection.

We confirmed, firstly, that pTpT suppresses the contact hypersensitivity response (Cruz Jnr et al, 2000 and Curiel-Lewandrowski et al, 2003). This gave us confidence that the oligonucleotide was having a biological effect at the dose and in the vehicle used, and it initially backed up the assertion that pTpT mimics UV irradiation.

Importantly, we also showed that pTpT is not acting as a sunscreen. Without this result, or measuring DNA damage directly, and in the absence of a complex structural biochemical analysis into the action of UV on an adjacent pair of thymidine bases outwith a double helix, it would be impossible to conclude that the oligonucleotide is providing a protective effect by any other means.

We then went on to show that pTpT is protective against UV induced skin cancer in NER deficient skin, proving that the mechanism of pTpT protection is not solely attributable to the upregulation of NER.

Previously, work carried out investigating the action of pTpT on NER models used *Xpc* heterozygous mice (Goukassian et al, 2004). This study showed a

reduction in UV induced mutation rate as well as photocarcinogenesis in the *Xpc* heterozygotes as well as wild type mice. The study found a small increase in median tumour free survival time in pTpT treated *Xpc* heterozygotes compared with the untreated group, and the results found in the wild type mice were very similar. The writers concluded therefore that by mimicking UV exposure, pTpT enhanced DNA repair capacity in the absence of DNA damage. Our results do not support this conclusion. By using a model with a completely NER deficient epidermis, we have been able to show that pTpT confers protection that is not reliant on DNA repair mechanisms.

Furthermore, we have shown that the protection conferred by pTpT is not likely to be due to an increase in apoptosis. We have not seen increased apoptosis histologically nor have we seen erythema, a sensitive marker for cutaneous apoptosis. The effect of pTpT on apoptosis will be investigated further using a cell culture system. We plan to look at the effects of pTpT on the replicative cycle of spontaneously transformed Ercc1 null and wild type keratinocytes. We will also use these cells to assess the effects of pTpT on UV induced apoptosis. Preliminary data suggest that pTpT alone does not induce apoptosis.

The differentiation status of keratinocytes in culture is not easy to control. Primary keratinocytes initially proliferate, and cell cycle arrest can be induced by several mechanisms (Chaturvedi et al, 1999). Withdrawal of growth

supplements or addition of transforming growth factor-β (TGF-β) causes reversible growth arrest. Exposure to phorbol ester or interferon-γ, or addition of calcium ions to the medium, results in irreversible growth arrest. Lastly, primary keratinocytes may undergo irreversible replicative senescence. Immortalised keratinocytes may have varied states of differentiation. These cells by their very nature have disrupted cell cycle control machinery, and as such may behave in unexpected ways.

Characteristically, UV exposure leads to caspase dependent apoptosis in proliferating keratinocytes. A paper published giving a comprehensive insight into apoptosis and senescence in keratinocytes showed that cell cycle activity is crucial for susceptibility to apoptosis, as keratinocytes in cell cycle arrest are resistant to UV induced apoptosis (Chaturvedi et al, 1999). Furthermore, a study using a human melanoma cell line, MM-AN, in comparison with normal human melanocytes has suggested that t-oligo (oligonucleotides with telomere specific homology) induced apoptosis may preferentially affect transformed cells (Puri et al, 2004). It should be noted, that although MM-AN cells lack p53, the p53 homologue p73 induces apoptosis (Eller et al 2002). Therefore, if UV induced apoptosis and t-oligo induced apoptosis follow the same molecular pathways, this implies that cells that are cycling more rapidly are more susceptible to these types of programmed cell death.

Our hypothesis for the protective action of pTpT against UV induced carcinogenesis is that pTpT causes reduced proliferation in normal cells. The reduced epidermal thickness seen in the UV plus pTpT group compared with the UV only group backs this up, however it would be interesting to compare these results with epidermal thickness in completely untreated animals as well as animals treated with pTpT alone, with no UV exposure. This hypothesis is in agreement with several publications (Pedeux et al, 1998, Eller et al, 2003, Puri et al, 2004) and also correlates with what we have seen experimentally in our long term irradiation experiment: pTpT reduced UV induced epidermal hyperproliferation and hyperplasia, and encouraged hyperplastic areas to grow exophytically rather than endophytically; but had no effect on the severity of squamous cell carcinomas that were present in the two experimental groups. In other words, topical pTpT application was able to protect normal skin from neoplastic transformation to some degree; we found less dysplasia throughout the skin, together with an tendency of papules to develop into exophytic rather than endophytic tumours in pTpT treated mice; but once an SCC had formed, pTpT application did not modify the aggressive nature of the tumour. It should be noted that the *Ercc1* epidermal specific knockout mice used in these experiments are extremely sensitive to UV induced carcinogenesis (Doig et al, 2006 and chapter 4 of this thesis).

The reason that pTpT may be able to protect normal skin from malignant transformation is that keratinocytes in vivo form a complex structure known

as stratified epithelium (reviewed by Haake and Polakowska, 1993). Cells in the basal layer divide, but those that are pushed towards the outer layers of the skin become more differentiated as they reach the surface. Differentiating cells do not cycle, and become terminally differentiated before undergoing programmed cell death. The cells nearest to the surface of the skin, which absorb the majority of the UV insult, are therefore least likely to be cycling. By ensuring that these cells do not begin to divide uncontrollably, pTpT may prevent transformation. However, once an invasive tumour has formed, topical pTpT may not have much effect. This may be due partly to penetrance, because although it has been shown that pTpT in the vehicle used penetrates the stratum corneum effectively (Goukassian et al, 2004), it is conceivable that insufficient pTpT reaches the centre of a growing tumour to have an effect. That which does penetrate may induce some apoptosis, but from our results it would appear that this is insufficient to halt tumour growth.

From our experiments, as well as those carried out by other groups, it would appear that pTpT does provide some protection from UV induced carcinogenesis, and is worthy of further investigation. Further work could include immunohistochemical staining to investigate levels of proliferation in pTpT treated and untreated skin after chronic UV exposure.

It is worth noting that there are several other putative protective substances that may in future be used to protect us from UV induced skin cancer. These

include resveratrol, silibinin, caffeine, caffeine sodium benzoate, sodium salicylate, acetylsalicylic acid and dihydroxyacetone, which are outlined briefly below.

Resveratrol is a plant derived antioxidant substance found particularly in grapes and believed to have strong anti cancer properties. This substance has recently been shown to prevent UV induced skin carcinogenesis in hairless mice after topical application (Aziz et al, 2005). This study compared the effects of resveratrol treatment before and after UV exposure, and concluded that as the protective effect conferred when the substance was applied after UV exposure was at least as great as when the substance was applied before exposure, that the substance was not acting as a sunscreen. They concluded that its protective effect was due to the activation of a protective signalling cascade and propose the inhibition of *Survivin* phosphorylation as a putative mechanism. Tumour protection was quantified in terms of median tumour free survival time, which was significantly longer in resveratrol treated mice, and average tumour number per mouse, which was lower in resveratrol treated mice, however tumour spectrum was not addressed (Aziz et al, 2005).

Silibinin is another plant derived antioxidant that has been shown to protect against the effects of UV in hairless mice. Topical application of this substance reduces thymidine dimers in the skin and upregulates p53 activation (Dhanalakshmi et al, 2004). Furthermore, topical or oral

administration of silibinin has been shown to reduce UV induced carcinogenesis by inhibition of DNA synthesis and cell cycle progression (Mallikarjuna et al, 2004), and increased levels of UV induced apoptosis after silibinin treatment are purported to be due to DNA protein kinase dependent p53 activation (Dhanalakshmi et al, 2005). The authors report moderate increases in median tumour free survival time after topical and oral silibinin treatment during the UV protocol, but significant decreases in tumour multiplicity and volume (Mallikarjuna et al, 2004). The tumour spectrum was not addressed.

Oral administration of caffeine, either by itself or as a constituent of green tea has been shown to enhance the p53/p21 response to UV in mice, and increase the formation of sunburn or apoptotic cells (Lu et al, 2000). More recently, topically applied caffeine and caffeine sodium benzoate have been reported to have both a sunscreen effect and increase UV induced apoptosis in the skin, thereby reducing UV induced carcinogenesis. Tumour initiation and growth was slowed in UV irradiated mice (Lu et al, 2006). These substances are able to act as sunscreen agents because their molecular structure enables them to absorb UVB. The induction of apoptosis is reported to be p53 independent, and the proposed mechanism involves the induction of premature mitosis by the inactivation of the G2/M checkpoint (Lu et al, 2006).

Sodium salicylate (NAS) and acetylsalicylic acid (aspirin) have also been shown to protect against UV induced skin cancer in mice (Bair et al, 2004). NAS appeared to delay tumour formation as well as reduce tumour multiplicity, while aspirin delayed tumour formation but did not affect numbers of tumours formed. NAS absorbs UVB light and therefore appears to be acting as a conventional sunscreen. Aspirin, however, does not absorb UVB light yet still provides some protection against UV induced skin cancer, although not as effectively as NAS. The authors speculate that the protection conferred is due to the ability of aspirin to inhibit COX-2 and the oncogene AP-1. NAS, another non-steroidal anti-inflammatory drug with similar properties to aspirin, may therefore be protecting against skin cancer both by acting as a sunscreen, absorbing UVB rays, as well as acting at a molecular level to prevent tumour promotion (Bair et al, 2004). This makes it a particularly interesting prospective therapy for the prevention of skin cancer. It would be of interest to investigate the effects of these two substances on tumour spectrum, and our Ercc1 ESKO mouse would be an appropriate model with which to investigate any beneficial effects of these substances on the types of tumours induced by UV exposure.

Dihydroxyacetone (DHA) is a substance found in sunless tanning lotions. These products are not marketed as protective against skin cancer in any way, but a recent study has shown some degree of protection in mice (Petersen et al, 2003). DHA causes the Maillard reaction to occur in the skin, where amine groups are glycosylated and which results in the formation of a

brown colour. Although the complex formed absorbs visible light and some UVA, it appears that DHA itself may absorb in the UVB spectrum. It was shown that 20% DHA lotion (commercially available preparations contain 5% DHA) did provide protection against UV induced carcinogenesis when mice were exposed to moderate UV doses (Petersen et al, 2003). However, in vitro work suggests that DHA causes redox reactions which may result in DNA damage. In human keratinocytes, G2 arrest was reported, followed by apoptosis (Petersen et al 2004). Implications of long term use of this substance must be addressed, and whilst it is unlikely that commercially available preparations have sufficient DHA to cause carcinogenesis at present, if this substance is to be considered for long term use as a sunscreen, the molecular events must be thoroughly investigated.

Bacteriophage T4 endonuclease 5 (T4N5) has been shown to protect against UV induced immunosuppression (Kripke et al, 1992) and to repair CPDs in keratinocytes (Nishigori et al, 1996). The enzyme is encapsulated in specially formulated liposomes, and has recently been commercialised as Dimericine® by AGI Dermatics. This product has been shown to reduce the incidence of actinic keratosis and basal cell carcinoma in XP patients (Yarosh et al, 2001), and currently trials are underway testing the benefits of Dimericine® for renal transplant patients, as these have elevated risk of developing skin tumours due to the immunosuppressive medication they are required to take. The T4N5 enzyme recognises CPDs in the DNA and

creates nicks in the DNA adjacent to these, so it is likely that this enzyme functions by stimulating DNA repair mechanisms.

Of the above substances, DHA appears to have least potential, not least because of its potential mutagenic effects. It seems likely that the amount of the substance needed to create a protective effect is higher than that available on the market at present. It is questionable whether lotions with higher levels of DHA, and hence higher self-tanning properties, would be desirable or marketable. Furthermore, the protection offered by DHA appears to be solely a sunscreen effect, and therefore interest in this substance may be limited. Caffeine and caffeine compounds also appear to be acting mainly as sunscreens. There are many effective sunscreens available currently, and in future skin cancer protection is likely to be focused on substances that act at a cellular level, and therefore not only have a longer lasting effect, but may also be used as a post-exposure treatment.

Of the other substances; plant derived anti-oxidants reservatrol and silibinin, non-steroidal anti-inflammatories (NSAIDs) NSA and aspirin, T4N5 liposomes and pTpT; all may have future roles in skin cancer prevention. However, before this can be considered, it will be important to rule out any adverse effects from the long term application of these substances. The NSAIDs in particular, are a powerful group of drugs with many effects on the body. Aspirin is currently widely used as a blood thinning agent, and the effect of topically applied aspirin on blood clotting would need to be

addressed. T4N5 creates single strand DNA breaks, and although this substance has performed well in clinical trials to date, its long term effects remain to be seen. Use of this product may be clinically advantageous for patients with higher than normal risk of developing skin tumours, as is the case for XP sufferers and transplant patients; however before the product is available to the general population further assessment of long term risk will need to be addressed. All of the above agents seem to exert their effects by regulating the cell cycle, and investigation into the long term consequences of their use is a priority.

It is also important to consider the main benefit we derive from sun exposure, the stimulation of vitamin D_3 synthesis. The amount of UV to which we should be exposed is an area courting great controversy at present. This is because despite the undesirable effects of UV, chiefly the development of skin cancers, a certain amount of UV exposure is beneficial.

Exposure to UV has been linked with increased vitamin D levels, indeed members of the population that regularly use sun beds have been shown to have higher levels of vitamin D and increased bone mineral densities than other members of the population (Tangpricha et al, 2004), and although the validity of this study has been questioned (Weinstock and Lazowich, 2005, Holick and Tangpricha, 2005), there seems to be plenty of evidence that some exposure to sunlight is invaluable. People living far from the equator, especially those with heavily pigmented skin, may not be synthesising

sufficient vitamin D_3 on a chronic basis (Webb and Engelsen, 2006). Epidemiological studies have reported an increased risk of certain internal tumours allied with insufficient vitamin D levels (reviewed by Lucas et al, 2006). Finally, lack of sunlight has also been associated with seasonal depressive episodes.

The link between insufficient UV exposure and internal cancers, as well as other diseases, may in future drive preference towards a protective agent that doesn't act as a sunscreen. In this case, interest in pTpT and the other agents mentioned earlier may increase dramatically, as the basis for our sun protection shifts.

Chapter 6

Characterisation of a novel skin phenotype found in *Ercc1* liver corrected null mice

6.1 Introduction

This chapter will describe a novel fur phenotype reported in our TTR::*Ercc1* transgenic animals. As previously mentioned in the introduction to this thesis, these animals are *Ercc1* null but carry an *Ercc1* transgene controlled by the transthyretin (TTR) promoter. This transgene is highly expressed in the liver and restores NER function in this organ. These animals have a life expectancy of around three months, allowing us to study some of the consequences of *Ercc1* deficiency in organs apart from the liver.

It was noticed that some of the animals in the stock were suffering from varying degrees of alopecia. The stock was maintained as heterozygote crosses, and on closer inspection, it became obvious that all of the transgene containing *Ercc1* heterozygote and homozygous null animals in the stock were affected to a greater or lesser degree. *Ercc1* wild type animals were unaffected. The mildest phenotype was a subtle darkening of the coat, only visible in agouti animals. The agouti coat is composed of dark hairs, with a fair band near the tip – known as a sub-apical pheomelanin band – and in the affected animals it seemed that these fair bands were missing. In these animals the fur also had a greasy quality. In the moderately affected animals the greasiness and darkening of the coat was more visible, along with some thinning of the fur. In the more severely affected animals, hair was sparse on the body, although the hair on the head and around the tail was unaffected.

Mouse hair and follicle structure is similar to that of humans, and therefore there are many useful mouse models of human diseases of the skin and hair. Mouse hairs fall into several categories: truncal (pelage), vibrissae (also known as whiskers), cilia, tail hairs, feet hair, and genital/perianal hairs (reviewed by Sundberg and King, 2001). The hairs affected in these mice are the truncal or pelage hairs.

Pelage hairs are divided into four distinct sub-categories, first defined in 1926. These are guard, awl, auchene and zig-zag and microscopic images of these hairs are shown in figure 6.1. Guard hairs, also known as tylotrichs, are long and straight, with a graduated tip, and are scattered throughout the pelage. They differ from the other pelage hairs as they are a type of tactile hair, similar to vibrissae. In agouti mice these hairs lack the characteristic sub-apical pheomelanin band that causes the yellow appearance of the coat of these animals, this is only found in the other three types of pelage hairs. Awls are also straight, though shorter than guard hairs. Awls and guard hairs usually have three rows of medullary septae, as shown in the high magnification images in figure 6.1. Auchenes have a single constriction, or bend, and have two rows of medullary septae, shown in figure 6.1. Lastly, zig-zag hairs, which make up the majority of the pelage and are also known as underfur, have several constrictions or bends and only one row of medullary septae, again shown in figure 6.1. It should be noted that any hair follicle produces only one type of hair (Biology of the Laboratory Mouse, 1975).

Fig 6.1

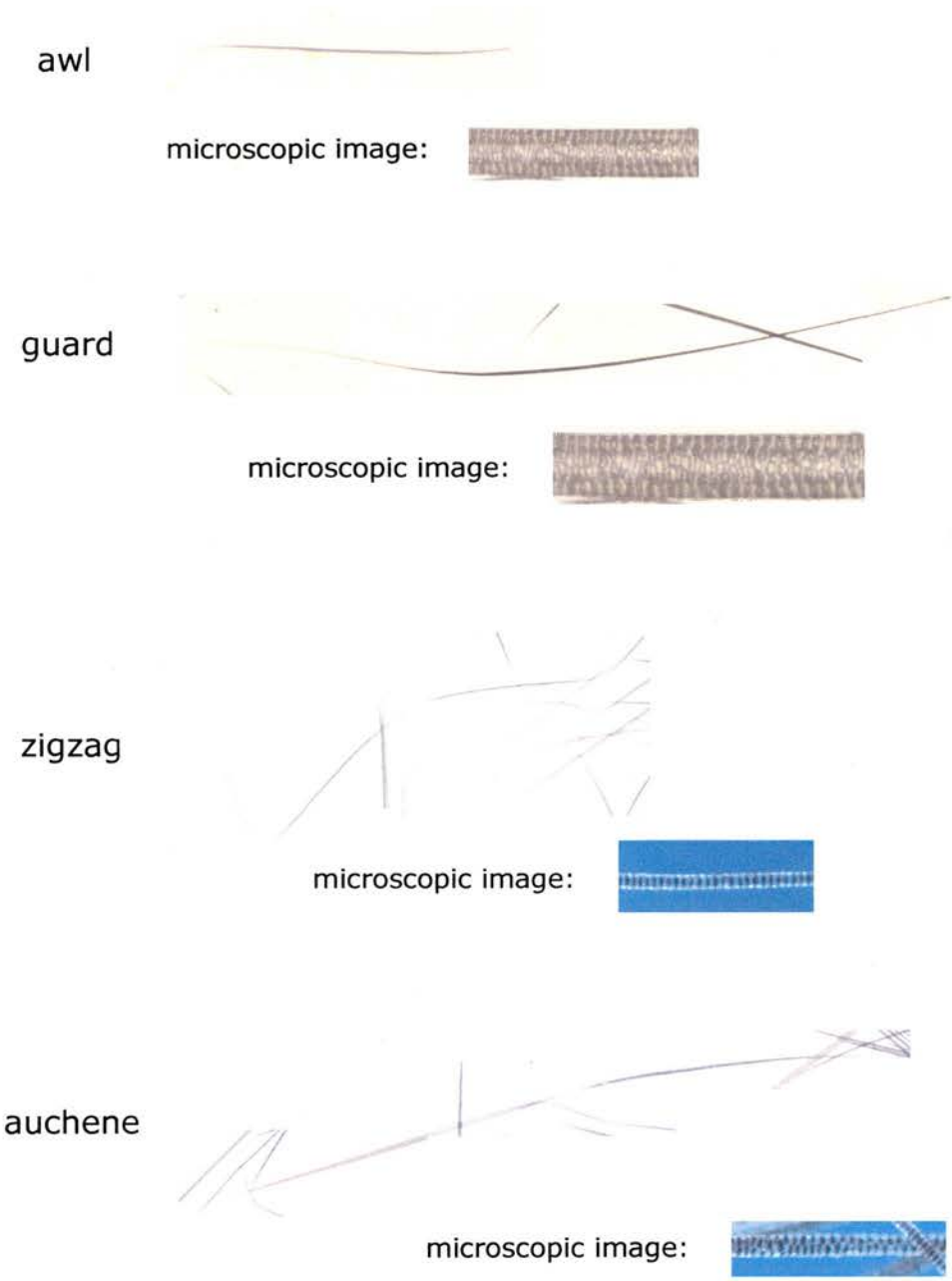

Figure 6.1 Hair types found in mouse pelage

Awl and guard hairs are straight hairs that are short and long respectively. Zig-zag and auchene hairs are constricted and therefore bend. Zig-zags normally make up 75% of the coat.

There is some precedent for proteins involved in NER to affect hair quality, which is why we decided to explore this phenotype. Trichothiodystrophy (TTD) is a syndrome characterised by brittle hair and nails (reviewed by Itin and Pittelkow, 1990), and has been attributed to various mutations in the *XPD* gene. Patients with TTD have ichthyosis and brittle hair due to a lack of cysteine rich matrix proteins, vital for creating the cross-linked structure necessary for normal hair development and growth. As mentioned previously, a mouse model exists for this disease, in which a point mutation has been mimicked from a human patient (de Boer et al, 1998). This *Xpd* mouse has brittle hair as shown by scanning electron micrograph, consistent with the human syndrome. Furthermore, hair from these mice has been reported to be deficient in sulphur, a key component of the cysteine rich cross-linking proteins present in normal hair. However, this disease is likely to be due to defects in the transcriptional role of the XPD protein rather than its role in NER. Keratinocytes from the TTD mouse model do not express normal levels of *Sprr2* mRNA; *Sprr2* is a gene associated with terminal differentiation of keratinocytes and as such is transcribed late compared with other genes (de Boer et al, 1998). The extremely low levels of *Sprr2* transcription in the TTD mouse model is purported by the authors to represent an exhaustion of the transcription machinery in the absence of XPD, and therefore they conclude that the TTD phenotype is caused by transcriptional insufficiency. No other NER deficient mice have been reported to show a TTD phenotype so it is unlikely that loss of NER is the causative factor in the disease.

Despite this, we were interested to investigate the hair phenotype in these mice further and perhaps uncover a novel role for *Ercc1*. As *Ercc1* heterozygotes and homozygous nulls were affected while wild types were not, we felt that there was a strong possibility that the *Ercc1* gene was involved in the phenotype.

6.2 Categorisation of the phenotype

When the phenotype was first recognised, a scoring system was developed with which to categorise the animals. The parameters used are described in table 6.1.

Table 6.1 TTR::Ercc1 stock fur phenotype

Category	Phenotype
0	Shiny, full coat – no abnormalities
1	Darkened coat, only visible in agouti animals
2	Coat dark and dull, some long straggly hairs
3	Coat dark, dull, greasy and thinning
4	Moderate hair loss, remaining hairs dark and greasy
5	Coat very sparse, few hairs remain on body

Photographic examples of animals in each category are shown in figure 6.2.

Fig 6.2

Category 0

Shiny full coat with no abnormalities

Category 1 (left)

Darkened coat only visible in agouti animals

(Category 0 animal on right)

Category 2

Coat dark and dull, some long straggly hairs

Category 3

Coat dark, dull, greasy and thinning

Category 4

Moderate hair loss, remaining hairs dark and greasy

Category 5

Coat very sparse, few hairs remaining on body

6.3 Animals were distributed throughout the five categories

Using the guidelines outlined above, animals were put into categories at around four to six weeks, when they were mature enough to have their first full adult coat. Figure 6.3 shows the distribution of *Ercc1* heterozygotes and homozygous null animals within these categories, for a cohort of 92 animals.

As a result of the mixed genetic background of this line, coat colour was segregating in the stock. It is important to note that this stock contained some black animals on which it was not possible to distinguish the mild phenotype. The more severe phenotypes were easily seen in either coat colour. As the category 1 phenotype was only visible in agouti animals, the few black animals have been omitted from the classification.

All *Ercc1* wild type animals seen in the stock were determined to be unaffected by the phenotype, and classified as category 0. None of the *Ercc1* heterozygous or null animals were classified as category 0, as all were affected by the phenotype to some degree. More than half of the *Ercc1* heterozygous animals were classified as category 1, as they had the mildest phenotype, which presented as a simple darkening of the coat. Around one tenth of heterozygous animals fell into each of the other categories, apart from category 4, which only contained one animal of the sixty in the cohort. Considering categories 3, 4 and 5 as 'severely phenotypic' resulted in one fifth of *Ercc1* heterozygous animals falling into this classification.

Fig 6.3

Distribution of animals in fur categories by genotype

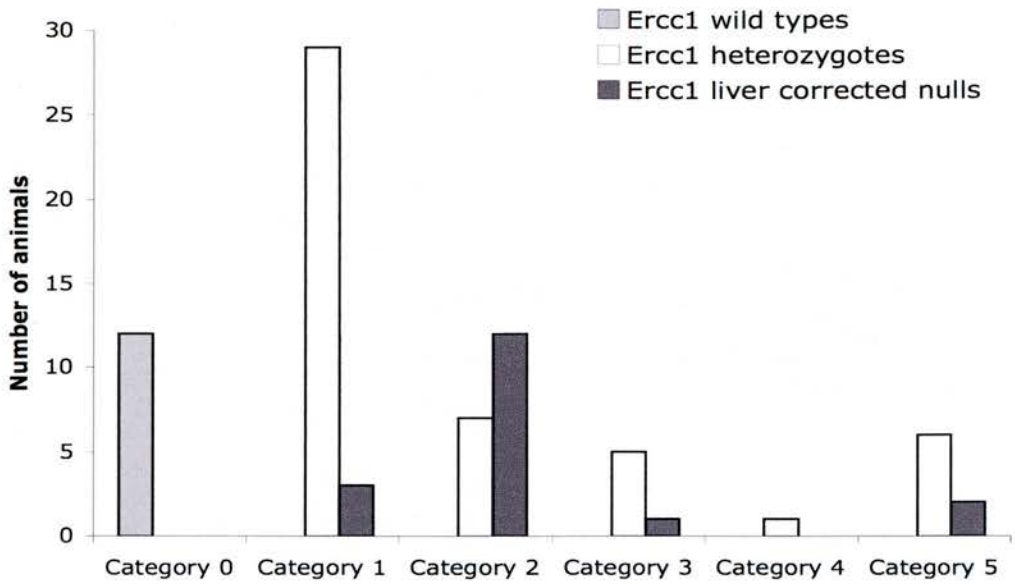

Fur category	Ercc1 wild types (n=12)	Ercc1 heterozygotes (n=60)	Ercc1 homozygous nulls (n=20)
0	12	0	0
1	0	29	3
2	0	7	12
3	0	5	1
4	0	1	0
5	0	6	2
Total:	12	60	20

Figure 6.3 Distribution of unusual fur phenotype in TTR::Ercc1 stock

Animals were put into categories according to the parameters shown in table 6.1 at 4-6 weeks of age. The graph and table above show the absolute numbers of animals in each group.

No *Ercc1* null animals were classified as category 0, as all were affected by the phenotype to some degree. More than half of the animals in the cohort were classified as category 2, with significant darkening of the coat presenting with some long hairs showing through. Approximately one tenth of animals fell into each of the other categories, apart from category 4, into which none of the *Ercc1* homozygous null animals were classified. Just under one fifth of the animals fell into the severely phenotypic categories.

6.4 Microscopic examination of hairs

Tufts of hairs were plucked from the dorsum of the animals and placed on a glass slide. These tufts were teased apart, then carefully fixed in place using clear nail polish. Once this had dried, the hairs could be examined microscopically. Zig-zag hairs could be identified by their characteristic constrictions.

In animals from categories 3 to 5, zig-zag hairs were found to be morphologically abnormal. They were found to be reduced in diameter, with irregular septae and disrupted cuticles. This can be seen in figure 6.4, where hairs from a category 0 animal are compared with hairs from a category 5 animal. Keratin appears white when viewed with polarised light, so images were also recorded using a polarised light source. These can be seen in figure 6.5, where hairs from a category 0 animal are compared again with

Fig 6.4

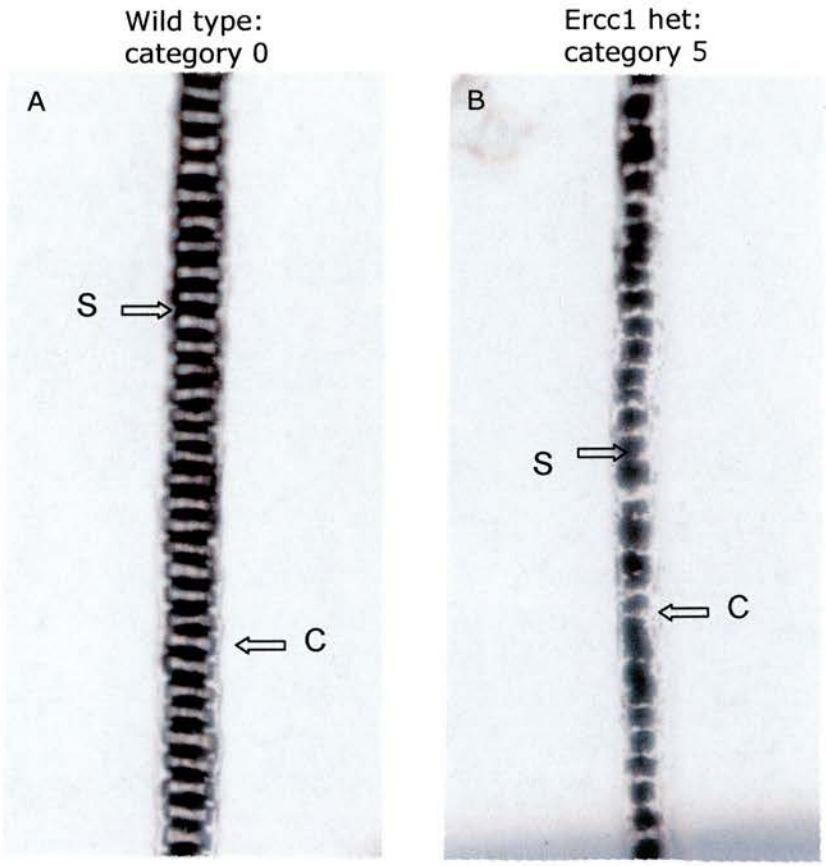

Figure 6.4 TTR::Ercc1 animals show narrowed zig-zag hairs

Panel A shows an image of a zig-zag hair from a wild type animal. The hair is thick, the septae are ordered (S) and the cuticle is intact (C). Panel B shows an image of a zig-zag hair from an animal with the unusual fur phenotype. The diameter of the hair is reduced, the septae are irregular and the cuticle is disrupted.

Fig 6.5

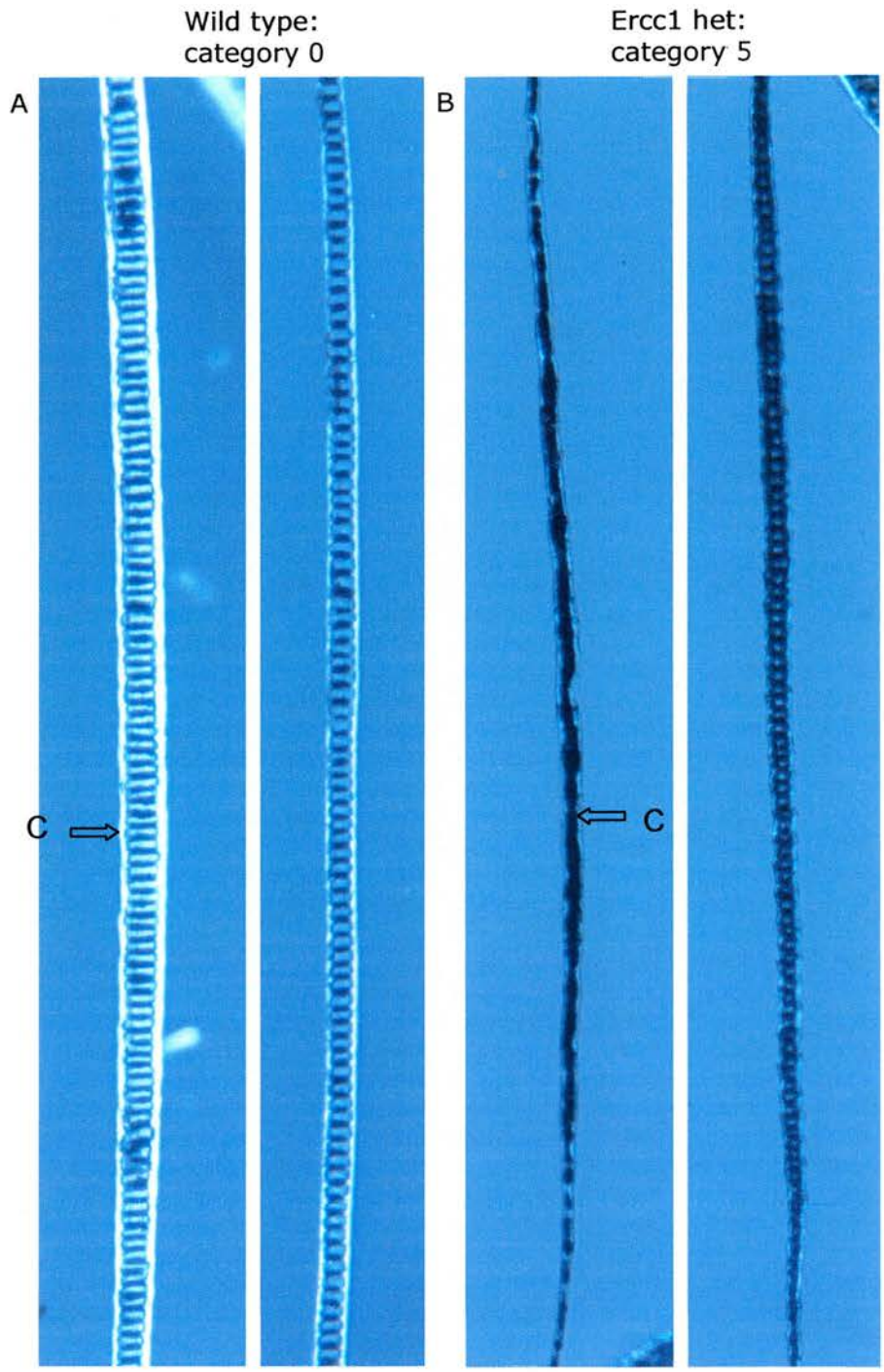

Figure 6.5 TTR::Ercc1 animals have visibly dystrophic zig-zag hairs when viewed using polarised light

Panel A shows two hairs from a wild type mouse. The septae are ordered and the keratin in the cuticles looks white in the polarised light (C). Panel B shows two hairs from a mouse with the abnormal hair phenotype. The septae are disordered and the cuticles have almost disappeared.

hairs from a category 5 animal. In these images, disruption of the septae and cuticles in the category animal is even more obvious.

6.5 Zig-zag hairs from phenotypic animals have a smaller diameter than those from non-phenotypic animals

From the microscopic images it was clear that zig-zag hairs from phenotypic animals were narrower than those from non-phenotypic animals. We quantified the difference by measuring the thickness of randomly selected hairs that were fixed onto glass slides using measurement tools in DP Soft image analysis software. As mentioned previously, zig-zag hairs have characteristic constrictions which cause them to bend by around 90°. In order to ensure a valid comparison, each hair was measured across the thickest point, equi-distant between constrictions.

The data obtained were analysed using analysis of variance (ANOVA) and are shown in figure 6.6. It is clear from this graph that the phenotype shows continuous variation throughout the stock. Animals in category 5 have significantly thinner zig-zag hairs on average than animals in category 0, with the average zig-zag hair thickness for the other categories lying between these two.

Fig 6.6

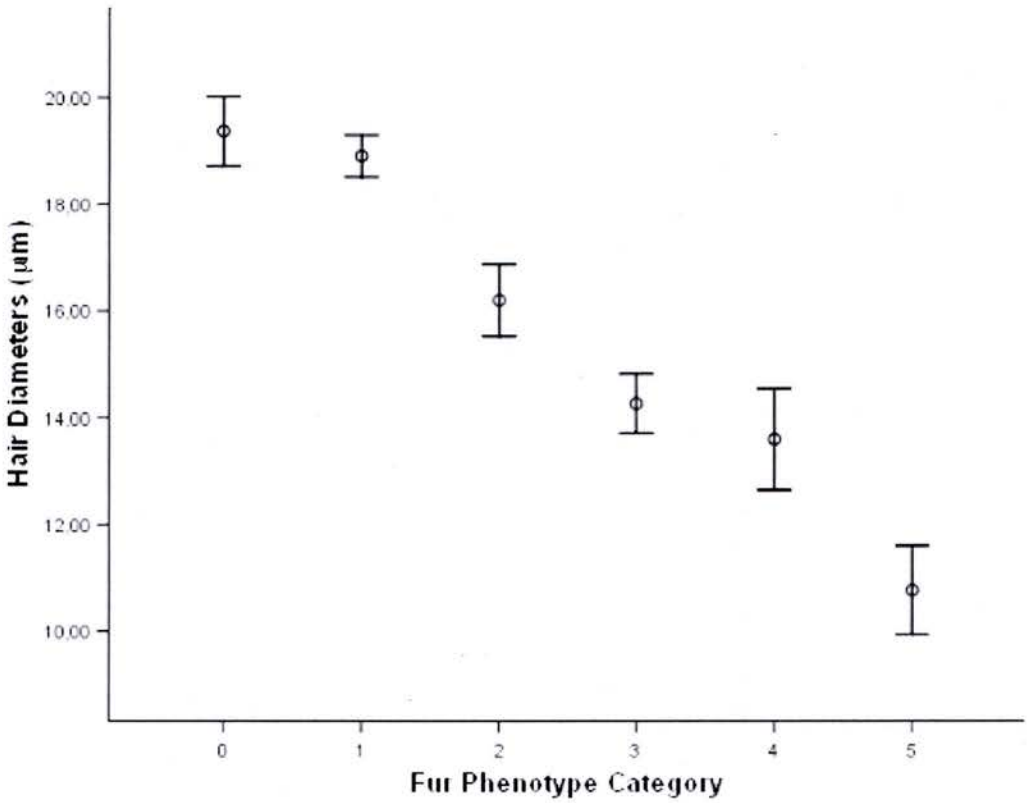

Figure 6.6 Animals with the abnormal fur phenotype have smaller diameter zig-zag hairs

This graph shows average hair diameters for each fur phenotype category. Each category contains at least five animals, and 20 measurements were taken from each animal.

Furthermore, auchene and guard hairs were also seen to be narrower and less regular in the phenotypic animals, compared with non-phenotypic animals. These were not analysed in as much detail as the zig-zag hairs because it was not possible to ensure measurement was taken in exactly the same way for every hair, as was possible for the zig-zag hairs, thanks to their structure.

6.6 Phenotypic animals have abnormal follicle and skin morphology

The tufts of hair that had been removed from the animals for analysis of the hairs also allowed us to examine the roots of the hairs. We found that hairs from the phenotypic animals had fewer roots attached, and those roots that were visible were shorter than those from non-phenotypic animals. The average length of roots in wild type animals was 292μm ±11μm, while the average root length in animals severely affected by the phenotype was 255μm ±8μm. Examples of these are shown in figure 6.7.

We also examined sections of skin from the animals, stained with haematoxylin and eosin. We found the phenotypic animals to have some abnormal skin features, shown in figure 6.8. Throughout the sections examined we found evidence of follicular keratosis and ectatic, or dilated, infundibuli (slides examined by Dr D Brownstein). This correlated with the extensive hair pathology we had seen.

Fig 6.7

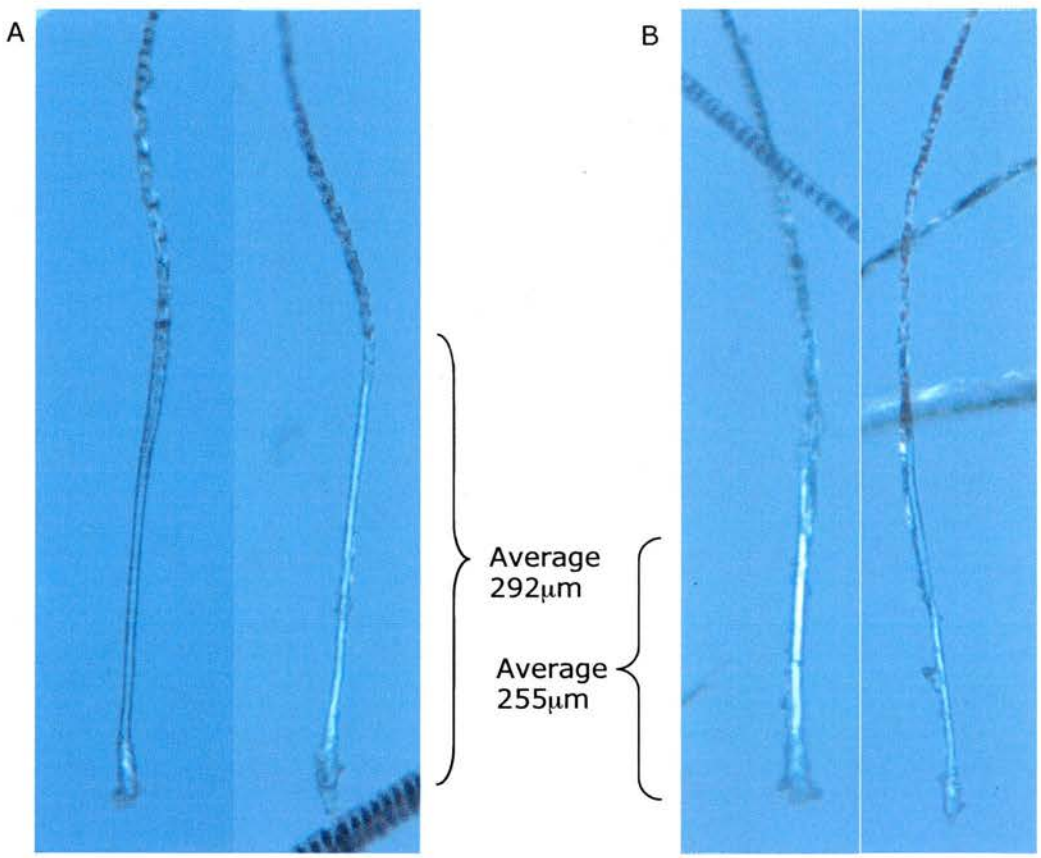

Figure 6.7 Animals with the abnormal fur phenotype have shortened roots compared with controls

The roots of zig-zag hairs were examined for differences. A shows images of roots from non-phenotypic animals, and B shows examples from phenotypic animals.

Fig 6.8

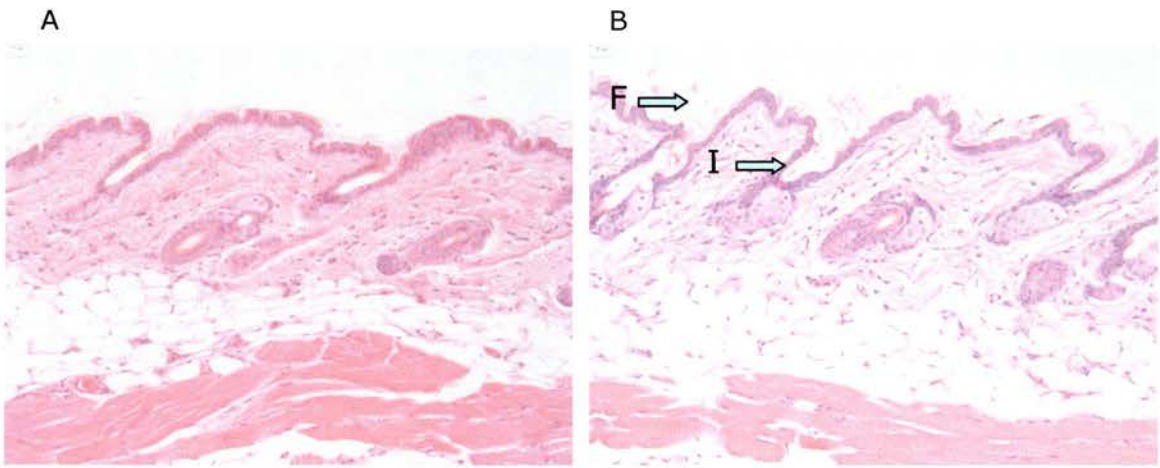

Figure 6.8 Animals with the abnormal fur phenotype show altered skin histology

Panel A shows an H&E stained section from an animal with normal fur. This animal has normal skin features. Panel B shows a similarly stained section from an animal with the abnormal fur phenotype. In this image we can see ectatic infundibuli (I) and evidence of follicular keratosis (F).

After characterising the phenotype itself, we began to search for a possible molecular explanation for the observations that had been made. The following sections of this chapter address this issue.

6.7 ERCC1 protein levels do not appear to correlate with phenotype

Firstly, we decided to investigate whether there was any correlation between levels of ERCC1 protein in the skin and the severity of the phenotype. To do this we used Western blotting techniques together with phospo-imagery to quantify protein levels, and the results of this analysis are shown in figure 6.9. We found no link between levels of ERCC1 in the skin with the severity of the phenotype.

6.8 Copy number of the TTR::*Ercc1* transgene does not appear to correlate with phenotype

In order to rule out the possibility that the TTR::*Ercc1* transgene had integrated into a site in the genome where it was disrupting a gene involved in skin or hair structure, we decided to investigate whether there was any correlation between the copy number of the transgene and the hair phenotype. Transgene copy number was estimated using a semi-quantitative PCR technique.

Fig 6.9

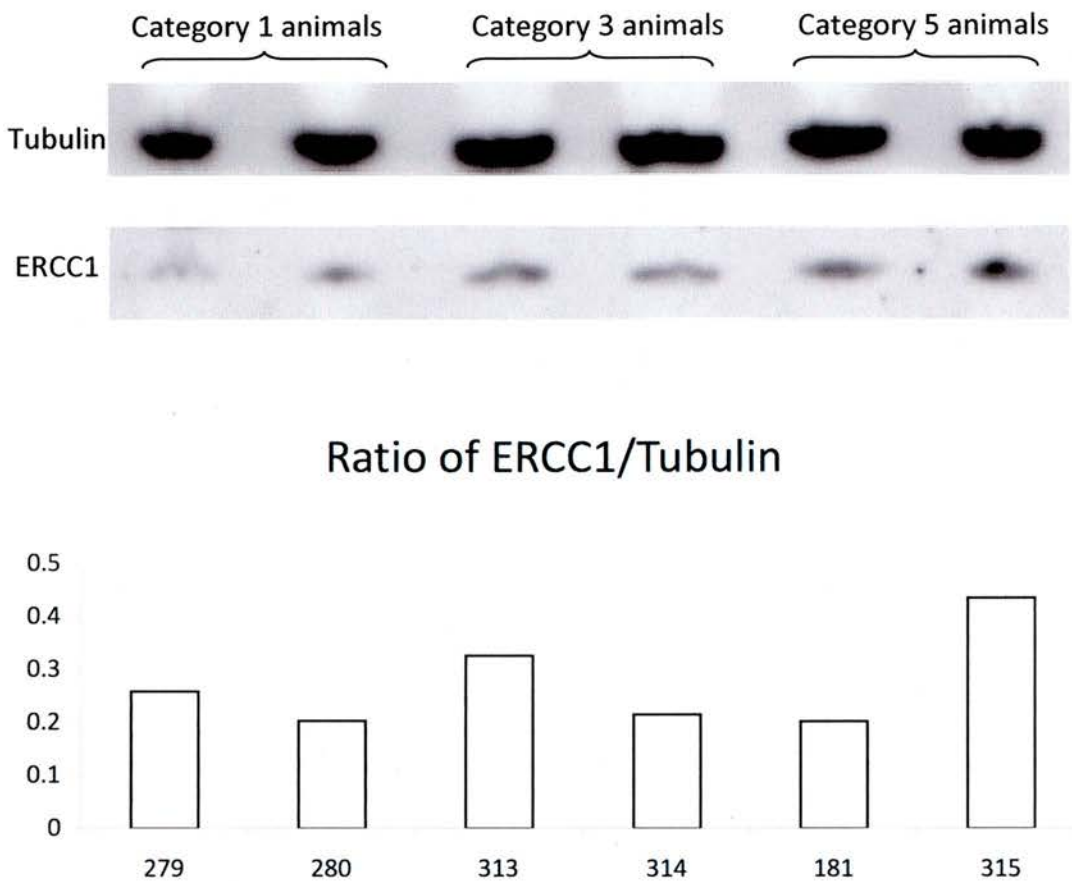

Figure 6.9 Western blot analysis of ERCC1 protein

We compared ERCC1 protein levels in the skin of Ercc1 heterozygous animals from different fur categories by Western blot. α-tubulin was used as a loading control, and the ratio of ERCC1 to tubulin calculated after signal intensities were measured using ImageQuant Controller and analysed using ImageQuant TL software.

We already had a reliable genotyping PCR for the TTR::*Ercc*1 transgene, and this was used to identify its presence in the animals. This PCR gives a 170bp band for the transgene, however if the wild type endogenous *Ercc1* gene is also present, the PCR gives a second, 600bp band. For this experiment, we used another PCR assay as an internal control. This was a PCR used in our laboratory to identify the DNA ligase I wild type allele, as we knew that our animals would all have the same number of copies of this allele, regardless of their *Ercc1* status. This PCR was ideal as an internal control, as the PCR product was a similar size, 300bp, and the primers used had a similar melting temperature to the ones used for the TTR::*Ercc*1 transgene.

Firstly, tests were carried out to determine the number of PCR cycles that were needed to give a quantitative estimate of DNA levels; normally, this PCR is run for 35 cycles. To do this, PCR assays were run using a DNA sample undiluted, and at a 1:2 dilution. These samples were run at 16, 18, 20, 22, 24, 26, 28 and 30 cycles to determine the point at which signals were detectable and the difference in band intensity or signal strength between the two samples was two-fold. Using this technique, we found that 24 cycles was the optimum, as shown in figure 6.10.

Using this information, we were able to set up a PCR using spectrophotometrically determined quantities of DNA from animals with the

Fig 6.10

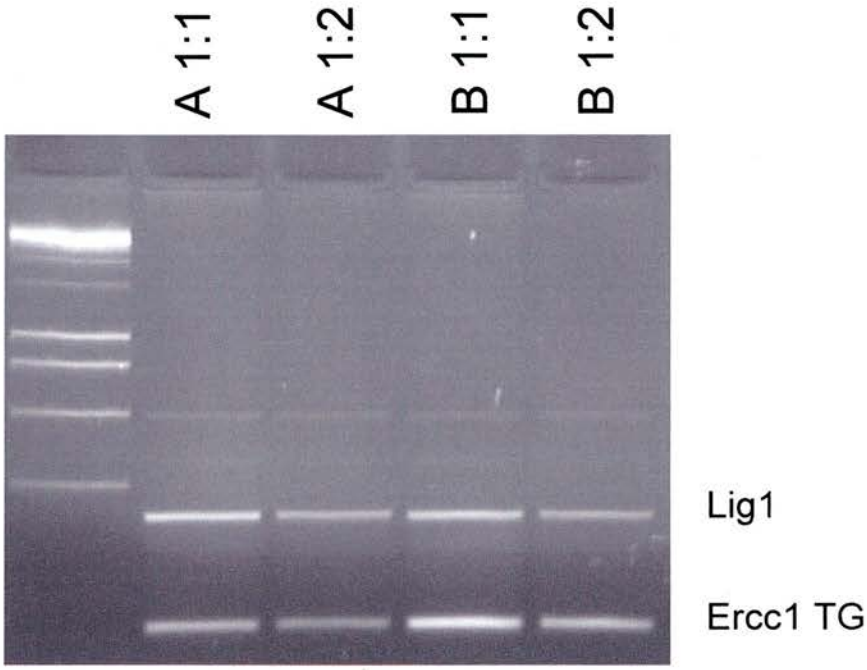

Band intensities (values measured using inverted figure):

	A 1:1	A 1:2	Ratio	B 1:1	B 1:2	Ratio
Lig I	0.14	0.27	1.93	0.15	0.29	1.93
Ercc1 TG	0.26	0.42	1.62	0.1	0.22	2.2

Figure 6.10 Quantitative analysis of Ercc1 transgene PCR band intensity is optimum at 24 cycles

We compared lig I and Ercc1 TG band intensities using samples A and B undiluted and diluted 1:2. Intensity ratios of the diluted and undiluted samples were calculated, and both the ratios obtained were very near 2.

mild phenotype and animals with the severe phenotype, to compare the signal for the *Ercc1* transgene.

The results of this experiment can be seen in figure 6.11. Ten *Ercc1* heterozygous, transgene positive animals were tested. Band intensities for the ligase I products and the *Ercc1* wild type products were found to be similar for all ten animals tested, indicating that the amount of DNA present was comparable for each sample. *Ercc1* transgene band intensities were similar for seven of the ten samples, and approximately doubled for the remaining three. It is likely that these three animals were homozygous and carried two arrays of the transgene insertion sequence, and the other seven were hemizygous, carrying one of the transgene insertion sequences. Of the three animals likely to be homozygous for the transgene, two were mildly phenotypic animals and one was a severely phenotypic animal, whilst of the seven animals likely to heterozygous for the transgene, three were mildly phenotypic and four were severely phenotypic. From these results, it appears that *Ercc1* transgene copy number bears no relation to the hair phenotype in these animals.

Fig 6.11

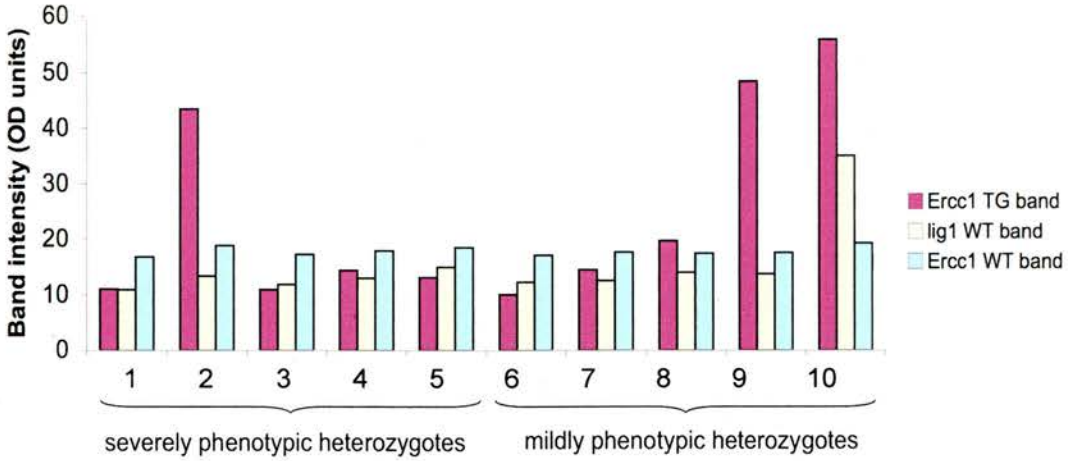

Band intensity ratios		Ercc1 TG ratio compared with lig1	Ercc1 TG ratio compared with Ercc1 WT
Severely phenotypic heterozygotes	1	1.0	0.66
	2	3.3	2.3
	3	0.92	0.63
	4	1.1	0.80
	5	0.87	0.71
Mildly phenotypic heterozygotes	6	0.82	0.59
	7	1.2	0.82
	8	1.4	1.1
	9	3.5	2.8
	10	1.6	2.9

Figure 6.11 Semi-quantitative PCR analysis of Ercc1 transgene reveals no correlation between transgene copy number and hair phenotype

The graph shows band intensity measured in optical density units using image analysis software after a 24 cycle PCR assay. The table shows the ratios of the Ercc1 transgene band compared with the two internal controls.

6.9 The origin of the *Ercc1* wild type allele in the animals does not appear to correlate with phenotype

As this stock has had genetic input from a number of different strains of mouse, including Balb/C, C57BL/6J and Ola129, we decided to investigate whether the origin of the *Ercc1* wild type allele the animals were carrying had any bearing on the phenotype. We were able to do this using previously identified polymorphisms in the promoter region of the endogenous *Ercc1* gene (David Melton, personal communication).

Figure 6.12 shows sequence upstream of and including *Ercc1* exon 1. The locations of two primers, Gen6 and Gen9-3′, are shown in burgundy. Between these two primers is a repeat sequence which varies slightly in size between species. Figure 6.13 shows PCR products from C57BL/6J, Balb/C and Ola129 animals run out on an agarose gel.

Using this PCR assay, we investigated some animals from the TTR::*Ercc1* stock, and the results can be seen in figure 6.14. Twelve animals were assayed, including two liver corrected null animals (with no copy of the *Ercc1* wild type allele), four severely phenotypic and four mildly phenotypic heterozygotes (with one copy of the *Ercc1* wild type allele each), and two *Ercc1* wild type animals (with two copies of the *Ercc1* wild type allele each). The *Ercc1* knockout allele in the stock was generated using cells from an Ola129 mouse, and as this PCR did not distinguish between *Ercc1* wild type

Fig 6.12

5'-CGTTGAATTGCTCATTTCGAAAAAATGGGCAAAGGATATGAGCCAATCTTTGTTAAAAGG

AATAGGCAAAGGAAATGAGCAAGAACAAAAAATATATAAGACCATTAAACTATTTCCTTA

GCAATCACAGAACTACAAGTTGGAACGGGGTGAAACTGTCCTTCCAGGAAATGAGTCATA

CTAAGTCATTCATGGGGCCCAGGTCTCGGAACACAGGTGTCCCTTCCTTCAGGAAGCCCG

TCCTCACACCCCAGCTGGGTCAGGTGCCCCCTAACACGGGCTCAATGTCCTCTGGGCTCT

CCCTTCCCGACCCTGCCCGCTCTGGGTTGTCCCTGTCTGACTGTCCCACTGGACTTTAAG

Gen6 →

CCACAGCTGTCGGTATCAGTCCCTGCTTGGGATGCAAGTGGGGAATGGCTTAGAAT**GAGT**

GAGTCAATGTCTGTGGGCTGAGTCCACCCACGCTTACAGGGAGGGCGTCCTCTGAAATCT

CACCTCCCTCCTCTCTCTCTCTCTCTCTCTCTCTCTGTCTCTCTCTCTCTTTGTCTCTGT

← Gen9-3'

CTCTCTCTCCTTTCCTCCTTTCCCTCCC**CCACCTCCTTTGATCATCACTGAGCC**GGATCT

GGAGTCTGGGAAGCGCTCAAGAGGGCCTTGGAACACAACTACTTGAAGTCAAAGTCTCCC

AGGTACCAAGATGCACAAGCTTCCATCCGCCCCAAACCACAGCGGTCCTCCAGGACCATA

GAGAGCAGCGCGAATAGAGTTCCCCGCTCTAACTCCTCCGGGGAGCAGCGAGACGAGCGA

AGGGCCAGAGCGGCC**GGAAGTGAGTCTAGCAGGAGTTGTGCTGGCTGTGCTGGCGTTGT G**

TCGCCTCTGTTTCCCCCCGTGGTATTTCCTTCTAGGCATCGGGAAAGACCAGGTGAGTTT-3'

Figure 6.12 Polymorphisms found in Ercc1 upstream sequence are mouse strain specific

In this sequence, taken from C57BL/6J, Ercc1 exon 1 is shown in blue, and the sequence used to determine mouse strain is upstream of this exon. The primers used are Gen6 and Gen9-3', and are shown in burgundy. The area of repeats shown in bold is the area where the strain specific differences occur. Using these primers, Ola129 mice give a 314bp product, C57BL/6J mice give a 294bp product and Balb/C mice give a ~400bp product.

Fig 6.13

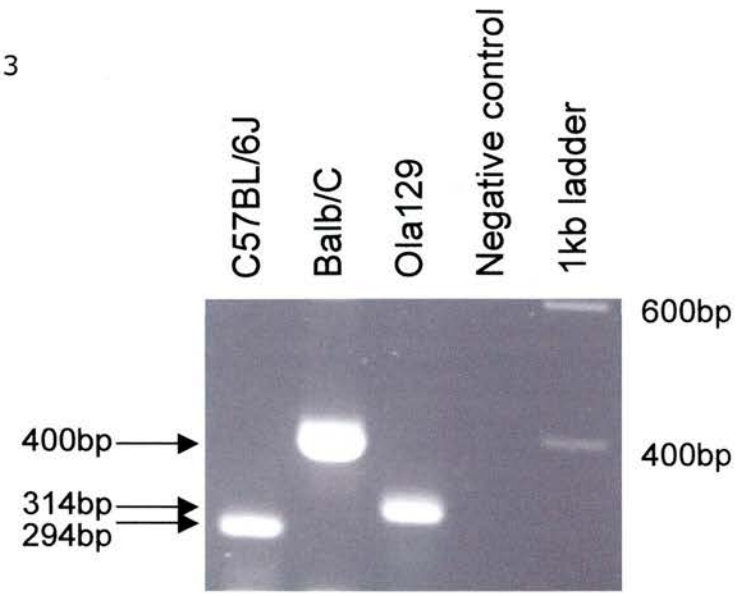

Figure 6.13 Primers Gen6 and Gen9-3' give different sized products in different mouse strains

The PCR assay was run on the following program:

94°C 5 mins, (94°C 1 min, 58°C 1 min, 72°C 1.5 mins) x 35, 72°C 10 mins

PCR products were visualised on a 2% agarose gel.

Fig 6.14

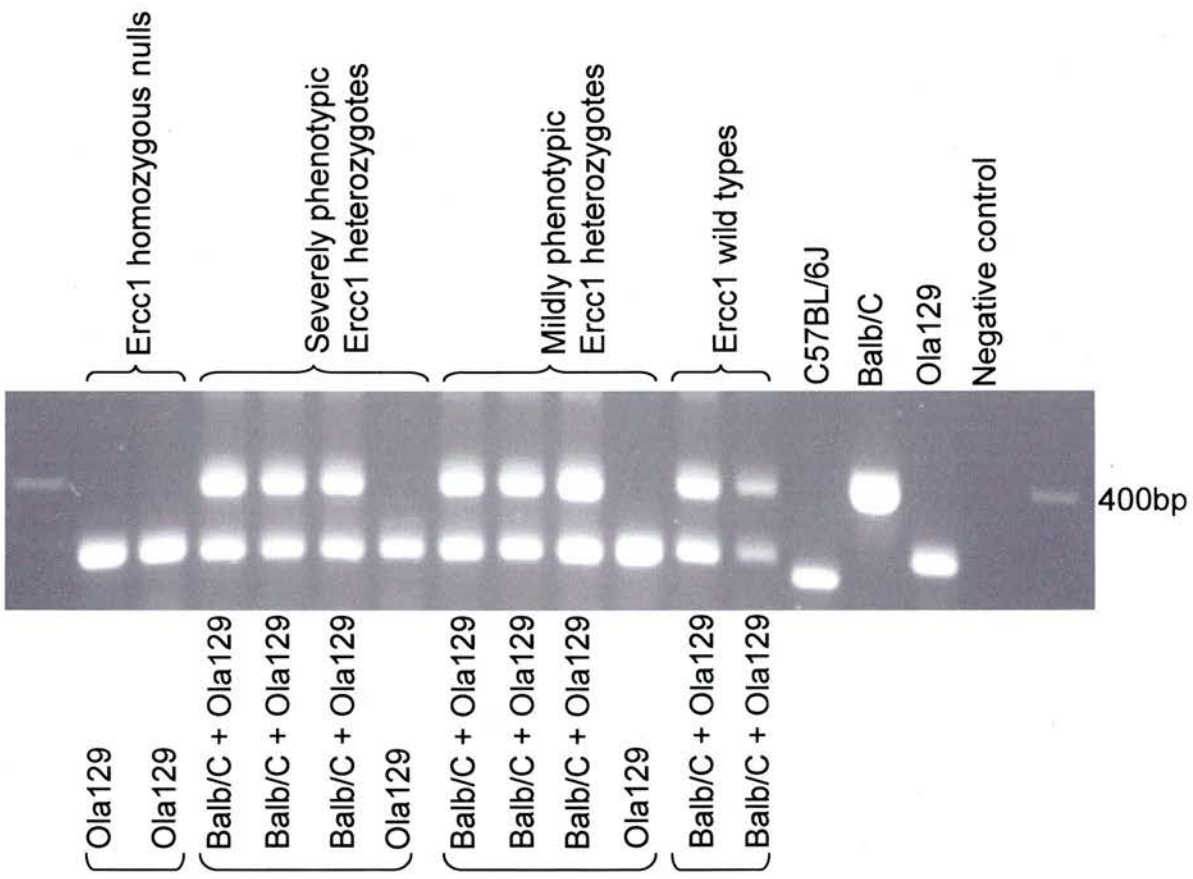

Figure 6.14 The strain of origin of the wild type Ercc1 allele does not correlate with severity of hair phenotype

Samples were assayed as described in figure 6.12.

and null alleles, the null allele was detected as an Ola129 allele in these results.

Both of the liver corrected null animals were positive for the Ola 129 allele, as expected. The two *Ercc1* wild type animals tested appeared to have one Ola129 derived wild type allele and one Balb/C derived allele each. Of the eight *Ercc1* heterozygous animals investigated, all had positive signals for Ola129, representing the one *Ercc1* null allele they carried. Six had a Balb/C derived wild type allele and two had an Ola129 derived allele. Furthermore, of the two with Ola129 derived wild type *Ercc1* alleles, one was severely phenotypic and one was mildly phenotypic. None of the animals carried a C57BL/6J derived *Ercc1* wild type allele.

These results showed that the origin of the wild type *Ercc1* allele the animals inherited bore no relevance to the status of their hair phenotype.

6.10 Discussion

It is of prime importance when considering the work presented in this chapter to know that although the TTR::*Ercc1* mouse stock has been in existence since the late 1990s, this phenotype has only been recognised relatively recently. The stock was being kept at a very low level, as the animals were not being used for any particular experiments, and animal numbers had

dropped drastically. Towards the end of 2004 we restarted a breeding program in order to produce more animals for use in experiments mentioned in the discussion of chapter 3 of this thesis, and to invigorate the meagre stock we crossed the remaining animals that were suitable for breeding with C57BL/6J stock mice. This meant that we had two breeding pairs with which to generate new stock.

It was in the following months that the hair phenotype described in the chapter was noticed. Prior to the bottleneck in the stock described above, no abnormal hair or skin features had been reported. It is highly unlikely that the severe features detailed here would have been missed. However, it is conceivable that the milder phenotype would not have been recognised, as the most striking feature of this is a darkening of the agouti coat. Unless the animals are seen next to an unaffected agouti animal, this change could go unrecognised. Furthermore, as mentioned earlier, this mild phenotype is not visible on a black coat, neither is it visible on chinchilla or other coat colours; and there may have been fewer agouti animals in previous generations.

There was a chance that *Ercc1* was involved directly with this phenotype; however the details underlying the mechanism, if in fact there was one, were far from straightforward. With this in mind, the characterisation of the phenotype in these mice has followed a system of elimination, where possible causes of the phenotype have been examined and discounted systematically.

One of the most obvious features of the mice, apart from the alopecia, were the long straggly hairs that were visible in the coats of the animals. The *Ragged* phenotype is caused by mutation in *Sox18* (Pennisi et al, 2000a) and is characterised by a sparse coat, which is abnormally dark with long guard hairs standing out from the rest of the coat (Carter and Phillips, 1954). The *Ragged* mouse was heterozygous for the *Ra* mutation, with the majority of homozygous mutants dying shortly after birth with a severe oedematous condition (Carter and Phillips, 1954). Those that survived were naked, with few hairs anywhere on their bodies. Although the phenotype of our mice seemed initially similar to the *Ragged* phenotype, we saw nothing that resembled the homozygous *Ragged* mutant described. This was despite paying particular attention to pups born to parents both of which were displaying the hair phenotype. Recent work has shown that despite the severity of the *Ra* mutation in *Sox18*, *Sox18*$^{-/-}$ mice are in fact viable and suffer only mild features of gene deficiency (Pennisi et al, 2000b). This indicated that the *Ra* phenotype is in fact caused by a dominant negative mutation, where the *Ra* mutated *Sox18* gene product causes a negative effect, with consequences more severe than complete absence of *Sox18* gene product. The hair phenotype in the *Sox18*$^{-/-}$ mice did bear some resemblance to that which we saw in our stock. These mice have a lower proportion of zig-zag hairs compared with wild types, but normal proportions of guard and awl hairs. They also lack the sub-apical pheomelanin band characteristic of the agouti coat colour, and therefore appear darker than wild

type littermates. However, morphologically the hairs are normal (aside from pigmentation differences) and there is no suggestion that the skin of these mice is adversely affected (Pennisi et al, 2000b). Taking all the evidence into account, it seems unlikely that our mice have a *Sox18* mutation, especially as *Sox18* is located on mouse chromosome 2 and is therefore not linked with *Ercc1*, so a mutation in this gene could not explain the *Ercc1* linked phenotype we have observed. However, it would be valuable to perform a western blot on skin samples from the mice from this stock, to investigate potential differences in SOX18 levels. It would also be interesting to sequence the *Sox18* gene in the mice to see if any mutation is present. Without this we cannot be sure that our phenotype is not caused by a *Sox18* mutation.

However, we have looked at hairs microscopically and concluded that the darkening of the fur seen in agouti animals is likely to be due to a loss of the tips of the hairs, rather than a pigment abnormality. We have not shown data that confirm this theory, as this difference is difficult to demonstrate, but we believe that hairs from severely affected animals often have blunt ends consistent with a brittle hair phenotype. This would result in shortening of hairs, particularly zig-zag hairs which seem to be most affected in our animals, and potential loss of the sub-apical pheomelanin band by breakage.

We considered the possibility that the animals with the more severe phenotype were expressing a lower level of ERCC1 protein than less

severely affected animals. However, after analysing protein extracted from skin samples, we found no correlation between levels of ERCC1 in skin and the severity of the phenotype.

The TTR::*Ercc1* mouse was generated by cloning *Ercc1* cDNA into a TTR vector. The construct generated was used for pronuclear injection, and mice expressing the transgene were used to create the stock (Selfridge et al, 2001). It was clear that the transgene had integrated into the genome as it was inherited through generations, however the integration site itself was unknown. For this reason we decided to investigate whether there was any correlation between the copy number of the transgene and the hair phenotype. It is important to note that a single integration site of the transgene is estimated to consist of four *Ercc1* cDNA sequences (Jim Selfridge, PhD thesis, 1999). Therefore, animals that are homozygous for the transgene, that is have received copies of the transgene from both parents, should have eight copies, and animals that are hemizygous should have four copies. However, using a semi-quantitative PCR technique, we found no correlation between transgene copy number and severity of the hair phenotype. The technique used can only be relied upon to give a rough estimate of sequence quantity and the result is far from authoritative. However, as we were looking for a doubling in the ratio of *Ercc1* transgene product compared with two internal control products, we felt that this was a simple assay worth trying. The results obtained indicated that we were able to use this technique to distinguish between homozygotes and hemizygotes, as there was a clear difference in transgene band intensity between two of

the animals and the other seven that we assayed, with only one animal giving an inconclusive result. To confirm these results there are two main options. Firstly, a real-time PCR assay could be developed to quantify *Ercc1* transgene DNA present in the samples. Secondly, an extensive breeding plan could be carried out to identify animals' transgene copy number by the genotypes of the offspring they produce, however this would be particularly consuming of time and resources.

In this chapter we have documented a phenotype that is present in *Ercc1* heterozygotes and *Ercc1* liver corrected null animals, but not in *Ercc1* wild types, and this was one of the main reasons that we suspected *Ercc1* involvement. However, the *Ercc1* liver corrected null animals certainly were not more severely affected than the heterozygous animals. Furthermore, the *Ercc1* liver corrected null animals are generally quite sick and die before reaching twelve weeks of age, so we were unsure whether the features noticed in these mice were indeed a real phenotype or were simply a consequence of general malaise and loss of condition, despite the narrowed, brittle hair phenotype characterised in these mice being unusual, and as far as we are aware, undocumented apart from in the TTD model mice (de Boer et al, 1998b).

This led us to query the integrity of the *Ercc1* wild type alleles present in the stock. Thanks to work carried out previously in the laboratory, we were aware of a repeat sequence in the promoter region of *Ercc1* that varied

slightly between mouse strains. As we knew that the stock contained a genetic mix from a number of different inbred mouse strains, we considered the possibility that a mutation in the wild type allele in combination with a renewed genetic background had given rise to the hair phenotype.

Our stock was carrying two *Ercc1* wild type alleles: an Ola129 derived allele and a Balb/C derived allele. There were distributed in the stock in a 1:2 ratio with no link to the severity of the phenotype.

During the course of the investigation, we came across an alarming trend. We found that the stock had ceased to produce *Ercc1* wild type animals. As *Ercc1* liver corrected null animals have limited viability and in any case, are in fact infertile (Hsia et al, 2003), breeding pairs are heterozygote crosses. Therefore, according to Mendelian ratios, we expected a quarter of all animals to be *Ercc1* wild types.

One possible explanation for this again revolved around the copy number of the liver replacement transgene. The transgene was originally designed to alleviate the severe liver phenotype seen in the absence of *Ercc1*, and in this respect it fulfilled its objective. However, overexpression of *Ercc1* has been notoriously difficult to achieve (Jim Selfridge, personal communication). We considered the possibility that the combination of two endogenous copies of *Ercc1* combined with two copies of the *Ercc1* liver replacement transgene may be incompatible with life. This could create a level of ERCC1 in the liver

that is simply not sustainable, and the animals die early in embryonic development. This would explain why when we first restarted the stock we saw wild type animals, but they subsequently disappeared - at the beginning, as we had crossed the stock out onto C57 mice, most animals that did have the transgene were hemizygous. However, as time went on we selected for the presence of the transgene, and it is likely that more and more animals in the stock were homozygous for the transgene. This could have coincided with the gradual loss of wild type animals from the stock. This idea was dismissed, however, when we revisited the levels of expression of *Ercc1* transcript from the transgene. Not only was there likely to be four copies of *Ercc1* cDNA in each transgene insertion site, but the mRNA levels produced by the transgene in the liver were several times greater than the levels produced by endogenous *Ercc1*. This meant that our hypothesis was extremely unlikely to be correct. To illustrate, we can compare an *Ercc1* wild type mouse that was hemizygous for the transgene with an *Ercc1* wild type mouse that had two copies of the transgene, under the two conditions: if the level of expression from the transgene were similar to that from the endogenous gene, we would be comparing expression levels of three times that of an endogenous gene with four times that of one endogenous gene. At these ratios, there is possible biological significance. However, if levels of expression from the transgene were around four times that of the endogenous gene, as is likely to be the case, we would be comparing expression levels of nine time that of an endogenous gene with expression levels of ten times that of an endogenous gene. As there is little difference

between these two levels of expression, we believe this hypothesis to be incorrect. Furthermore, northern blot analysis carried out when the mice were initially created found that levels of *Ercc1* mRNA transcribed by the transgene were in actual fact around ten times higher than endogenous liver *Ercc1* mRNA (Jim Selfridge, PhD thesis, 1999). This was because the TTR promoter that controls liver specific transgene expression is more active than the *Ercc1* liver promoter. In summary, although there could have been some silencing of transgene expression over time, we feel that the likely levels of expression preclude this explanation for the loss of *Ercc1* liver corrected wild type animals from the stock.

Another possible explanation for the phenomenon revolved around the relative proximity to *Ercc1* of the gene responsible for TTD: *Ercc2* or *Xpd*. *Xpd* null mice are embryonic lethals (de Boer et al, 1998a), however there is a mouse model for TTD which mimics a point mutation point in a TTD patient (de Boer et al, 1998b). Although it seemed extremely unlikely, we considered the possibility that our stock may have picked up an *Xpd* mutation that caused a TTD-like phenotype in one copy and was an embryonic lethal in two copies. If this were the case, the mutation would be closely linked to one of the *Ercc1* wild type alleles in our stock. *Ercc1* and *Ercc2/Xpd* are separated genetically by 25.5kb, and using this information we are able to calculate the chance of a recombination event occurring between these genes. One centimorgan distance equates to approximately 2000kb in the mouse (JAX Mouse Genome Informatics website; Genetics: Principles and

Analysis, 1998), meaning that on average one recombination even will occur in every 2000 kilobases of genetic code. Therefore, the recombination frequency between these two loci is approximately 1.3%.

For this hypothesis to be correct, the linked mutation in *Xpd* would have had to be a very specific type. Although the *Xpd* homozygous null mouse is an embryonic lethal, the heterozygous animals reported in the aforementioned publication are viable and do not shown symptoms of TTD. Our hypothesis required the *Xpd* mutation to be lethal in two copies and to cause a TTD phenotype in one copy, and such a mutation has not been reported. However, this would explain the absence of wild type animals in our stock, as well as the severity of the hair phenotype in the *Ercc1* heterozygotes, as these would also be heterozygous for the putative *Xpd* mutation. *Ercc1* liver corrected null animals would have two wild type *Xpd* alleles, so the hair phenotype seen in these animals would have to be attributed to the general lack of condition in these animals.

To test this hypothesis incontrovertibly required analysis of the *Xpd* sequence from the animals in this stock. However, as the only samples we had available were from animals that were heterozygous for the putative mutation, we decided first to expand the breeding scheme to analyse litters from a variety of different crosses. If this analysis correlated with our hypothesis, we planned to carry out the sequence analysis of *Xpd*.

We reasoned that if our hypothesis were correct, if we crossed a severely phenotypic, *Ercc1* heterozygous animal from our stock with wild type animals from other stock, we would see the following offspring: Firstly, we would see *Ercc1* wild types again. 50% of pups would be *Ercc1* heterozygotes and the other 50% would be *Ercc1* wild types. None of the *Ercc1* heterozygotes would show the hair phenotype, as these would have one functional *Xpd* allele that was linked with their *Ercc1* null allele, and a second functional *Xpd* allele linked to the *Ercc1* wild type allele from the parent from the new stock. All of the *Ercc1* wild types would have the hair phenotype, as these would have one defective *Xpd* allele linked to the wild type *Ercc1* allele from the TTR::ERCC1 stock, and a functional *Xpd* allele linked to the *Ercc1* wild type allele from the new stock, and effectively be heterozygous for the *Xpd* mutation as the *Ercc1* heterozygotes had been previously.

With this in mind, we set up pairs consisting of one *Ercc1* heterozygote from the stock and one animal that was either inbred C57BL/6J or Ola129, obtained from the animal house stock. We analysed the pups from the crosses for genotype as well as phenotype. We found, in short, that after crossing the stock out to either inbred strain, that the hair phenotype disappeared in all the progeny regardless of genotype. This result disproved the hypothesis that our stock harboured an *Xpd* mutant allele.

In summary, despite the fact that we identified a clear and consistent phenotype in this stock, we have been unable to find a molecular explanation

for the phenomenon. All the evidence points towards a 'background effect' – something characteristic of the stock in question relating to the overall genetic mix of the animals. In this case, although the phenotype may relate to *Ercc1* status, other unknown genes create a modulatory effect. It would be extremely difficult to identify candidate modulator genes. This explanation is particularly likely in this stock, where numbers of animals had dwindled and the current stock was expanded from a very small genetic pool.

Chapter 7

Characterisation of a novel neurological phenotype found in *Ercc1* liver corrected null mice

7.1 Introduction

NER deficiency has a strong association with neurological disease in human patients. All Cockayne syndrome patients, as well as many xeroderma pigmentosum and trichthiodystrophy patients, present with moderate to severe neurological symptoms (reviewed by de Boer and Hoeijmakers, 2000). The explanation for this revolves around the unique characteristics of cells that make up the central and peripheral nervous systems. These cells do not replicate as do cells in other tissues, and are extremely reliant on their repair systems. The cells of the nervous system are not exposed to UV induced DNA lesions in the same way as the skin, but they are susceptible to oxidative DNA lesions of endogenous metabolic source. Classically, base excision repair (BER) is considered to be of prime importance in the repair of such lesions, but it is likely that NER also plays an important role, as demonstrated by the neurological symptoms in XP patients. As neurons are terminally differentiated and no longer divide, they are able to dispense with global genome repair and rely on transcription coupled repair (reviewed by Nouspikel, 2006), although this differs from other terminally differentiated cell types, such as cardiac myocytes (van der Wees et al, 2006). It is unclear whether BER is able to act coupled with transcription (reviewed by Mellon, 2005), which may explain the importance of NER in neurons, as the existence of transcription coupled NER is well documented.

Due to the non-proliferative nature of neurons, un-repaired lesions in these cells are less likely to result in carcinogenesis, but instead lead to the blocking of transcription and programmed cell death. Aberrant loss of neurons is a factor in a number of serious human illnesses, including Alzheimer disease, Huntington disease and motor neuron disease (reviewed by Dickson, 2004 and Bursch and Ellinger, 2005). The mechanisms involved are extremely complex, and there are many stimuli that can lead to neurodegeneration, however there is an emerging body of work that implicates synaptic changes as early events in neurodegenerative processes, and it appears that loss of synaptic function may be an important initiator of neuron loss, as loss of synapses appears to be a very early pathogenic marker (reviewed by Wishart et al, 2006). Changes at the synapse are now considered a crucial early marker for neurodegeneration, and are a prime target for novel therapies aiming to prevent and treat the onset of these debilitating diseases.

A *Csb* mouse model for Cockayne syndrome appears to have mild neurological features (van der Horst et al, 1997), and a double *Xpa/Csb* knockout mouse has been reported to have severe neurological features, including tremors, clasping and abnormal gait, together with a life expectancy of less than three weeks (Murai et al, 2001). $Xpg^{-/-}$ mice have been reported to have significant atrophy of Purkinje cells (found in the cerebellum, an area of the brain involved in coordination and movement), with a life expectancy of around one month (Sun et al, 2001). Due to the short lifespan of these mice

it is not clear whether this is a neurodegenerative feature, or a failure in development.

With this information, we believed that our *Ercc1* liver corrected null mice would be a good model in which to further the study of the effects of NER deficiency on the central and peripheral nervous systems.

As reported earlier (Selfridge et al, 2001), *Ercc1* liver corrected null mice have normal hepatic appearance and function at the time of death. Kidney abnormalities were detected in the post mortem examination of these mice, specifically polyploidy, and plasma creatinine levels were slightly elevated, an indication of kidney malfunction. It appeared initially that these animals were dying at around three months of age from kidney failure. However, in unpublished work carried out in our laboratory, animals with the floxed *Ercc1* gene (as found in the epidermal specific *Ercc1* knockouts) were crossed with a Nestin-Cre expressing line. The nestin promoter is a neuronal specific promoter, and this line expresses Cre recombinase in neuronal cells. It was found that the nestin *Ercc1* mice died at around the same time as the liver corrected nulls, prompting speculation as to the neurological effects of loss of *Ercc1*. Due to a lack of neurobiology expertise in the laboratory and an absence of collaborators, the breeding scheme for these animals was not continued.

In 2005, we noticed that the *Ercc1* liver corrected null mice were displaying gait abnormalities indicative of ataxia, as well as the clasping reflex, an indicator of cerebellar abnormalities. This reawakened an interest in the possible neurological implications of defective nucleotide excision repair and loss of *Ercc1*, which led to the work described in this chapter.

7.2 *Ercc1* liver corrected null animals clasp when suspended by their tails

When mice are picked up by their tails the normal response is to hyper extend the rear limbs. We found that *Ercc1* liver corrected null mice do not do this, and instead they clasp their hind limbs together, as seen in figure 7.1. We found that this abnormal reaction progressively worsened with age, and by the time the animals were around ten weeks of age, the clasping was severe. The animals also showed signs of ataxia, displaying a lack of coordinated movement. This lack of coordination became so severe in the last month of the animals' three month lifespan that animals picked up by their tails and then lowered towards a surface were unable to stretch out their fore limbs and 'land' on the surface. Instead the animals clasped all four limbs together and when placed on a surface tended to remain on their back for a short time, before struggling to right themselves successfully. Furthermore, these animals displayed almost no self-initiated movement around their cage or when placed on an open surface.

Fig 7.1

a) b)

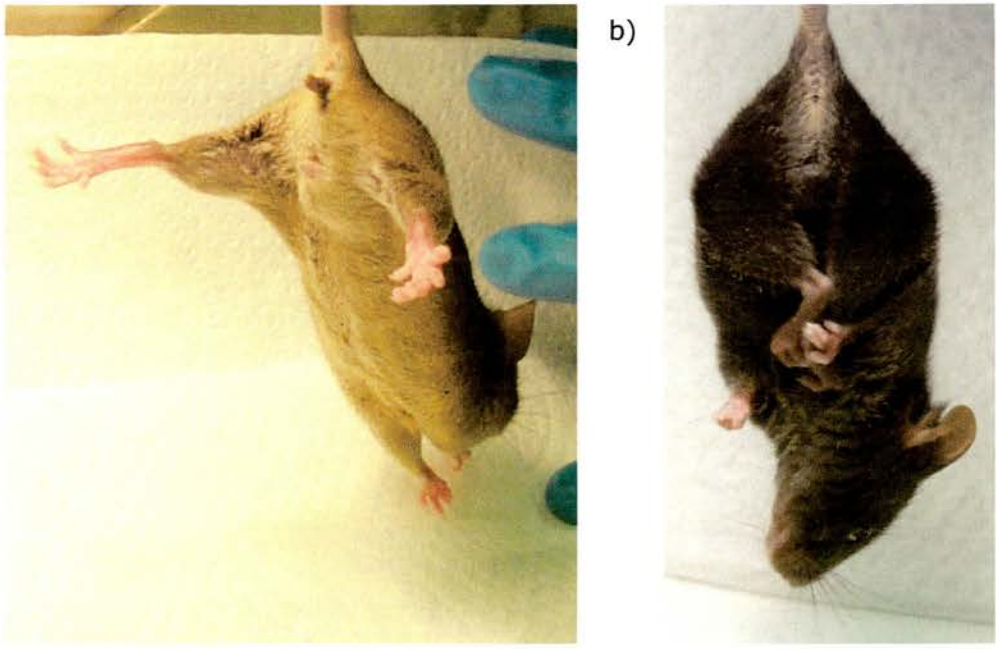

Figure 7.1 Clasping reflex seen in Ercc1 liver corrected null mice

When held by the tail and lowered towards a surface, Ercc1 liver corrected null mice clasped their hind limbs (b) rather than stretching them out as a control animal would (a). Clasping progressively worsened with age, often involving front limbs as well as hind limbs - this animal is around 10 weeks of age.

7.3 *Ercc1* liver corrected null animals perform poorly on the Roto-Rod

As we suspected that the *Ercc1* liver corrected null animals suffered from ataxia, we analysed their performance on the Roto-Rod. This is an apparatus which allows analysis of the animals' level of coordination and motor function. Animals were placed on a slowly rotating rod of around four centimetres in diameter, with the surface of the rod covered with ridged rubber to facilitate grip. The animals are therefore induced to walk forward continuously in order to maintain their balance on the rod, and the speed of rotation of the rod increases slowly but steadily. Measurements of time were recorded from the moment animals were placed on the rod until they were unable to maintain their forward motion and balance, and fell off onto the surface below the rod. The results of this experiment are shown in figure 7.2. *Ercc1* liver corrected null animals performed significantly worse than littermate controls at four and at eight weeks of age; $p<0.001$, t-test. At four weeks of age, *Ercc1* liver corrected null animals were able to stay on the Roto-Rod for approximately half the time that their littermate controls were able to manage. However at eight weeks of age, the performance of the *Ercc1* liver corrected nulls had declined further, whereas the performance of the controls had remained similar. At eight weeks, *Ercc1* liver corrected nulls were able to stay on the Roto-Rod for around a quarter of the time that the control littermates recorded. From these data, we concluded that *Ercc1* liver corrected null animals have defective coordination and a potential cerebellar defect.

Fig 7.2

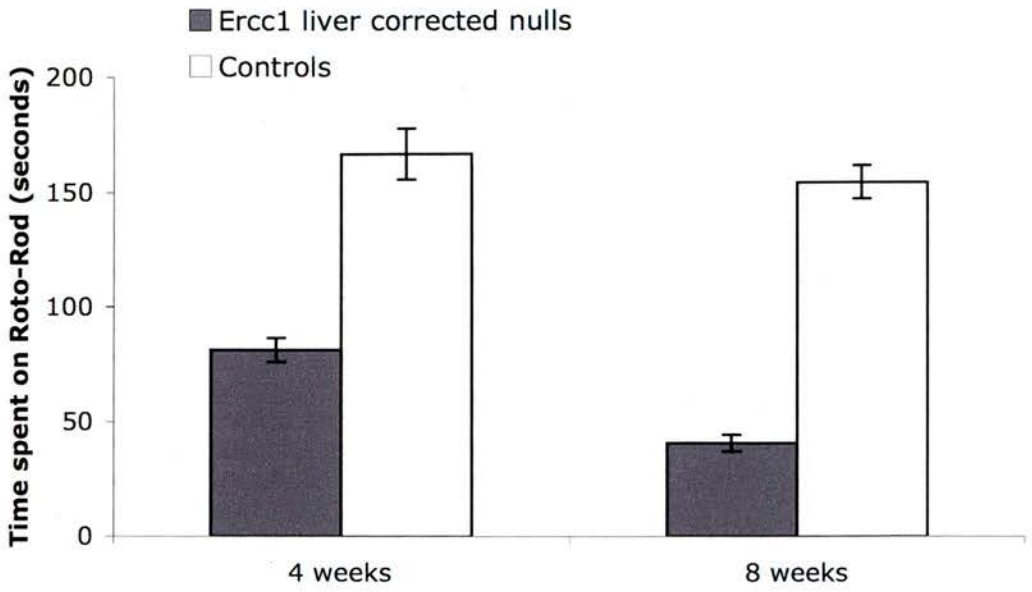

Figure 7.2 Ercc1 liver corrected null mice perform poorly on the Roto-Rod compared with wild type littermates

Animals were tested on the Roto-Rod at 4 weeks and 8 weeks of age. There were ten animals in each group, and readings for each animal were averaged over three consecutive days.

7.4 *Ercc1* liver corrected null animals have a proportionately smaller cerebellum than littermate controls

Roto-Rod performance is generally recognised to be an indicator of cerebellar function, and as such we decided to investigate gross size of the cerebellum in *Ercc1* liver corrected null and control animals. Measurements were taken after whole brains were dissected and fixed. Images of the brains were taken from above for analysis, with readings obtained as two-dimensional measurements of surface area. Using this method of analysis, we were able to show that *Ercc1* liver corrected nulls appear, on average, to have a slightly smaller cerebellum in proportion to total brain size, compared with control littermates, as shown in figure 7.3; $p<0.0001$. It was imperative to make the comparison of cerebellar size as a percentage of the total brain size: as the *Ercc1* liver corrected null animals have somewhat retarded growth, the gross size of their brains is significantly smaller than that of wild type littermates.

7.5 *Ercc1* liver corrected null animals perform poorly in the opto-kinetic response (OKR) test compared with wild type littermates

We felt that the *Ercc1* liver corrected null animals did not respond to visual stimuli in the same way as controls, so we assayed the visual acuity of the mice using the opto-kinetic response (OKR) test. This test uses a striped,

Fig 7.3

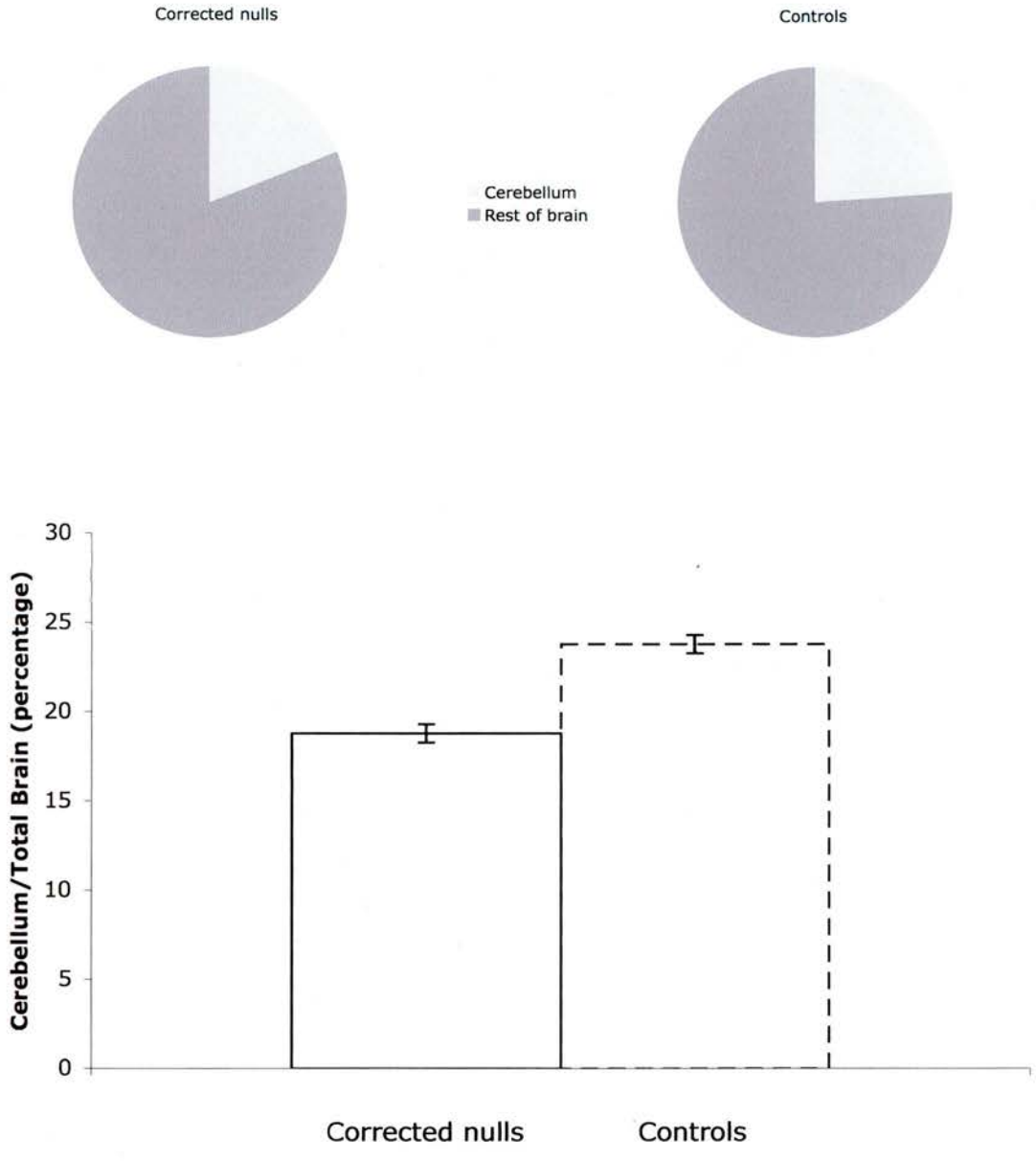

Figure 7.3 Ercc1 liver corrected null mice have a smaller cerebellum relative to total brain compared with wild type littermates

Measurements were taken using a two dimensional image capture system and surface area values compared. There were 12 animals in each group.

rotating drum to ascertain whether the mice are able to follow, or 'track' the movement of the stripes (first described by Thaung et al, 2002, used as an indicator of phenotype by Hart et al, 2005). We tested animals at four and eight weeks of age, and we used three different categories of stripe size: these different stripe sizes form stripes subtending angles of 2°, 4° and 8° on the retina of the animals, with 8° stripes the easiest for the animals to focus on and 2° the hardest. We found that the *Ercc1* liver corrected null animals performed extremely poorly in all the tests we carried out compared with littermate controls. The results obtained are shown in figure 7.4. At four weeks of age, both the *Ercc1* liver corrected null animals performed slightly better with 4° stripes than the other two sizes, although in all categories *Ercc1* liver corrected null animals recorded about a quarter of the number of tracks of their littermate controls. At eight weeks of age, the littermate controls performed similarly across all categories, and similarly to how they had at four weeks of age. The *Ercc1* liver corrected nulls performed extremely poorly at this age, with none of the animals recording any tracks at the 2° stripe category, and very few tracks at 4° or 8° either. In the 4° stripe category, *Ercc1* liver corrected null animals performed significantly worse than controls at 4 weeks of age; $p=0.0049$ by Mann-Whitney test, as well as at 8 weeks of age; $p=0.0043$ by Mann-Whitney test. From these data, we were able to conclude that *Ercc1* liver corrected null animals experience defects in visual acuity from an early age.

Fig 7.4

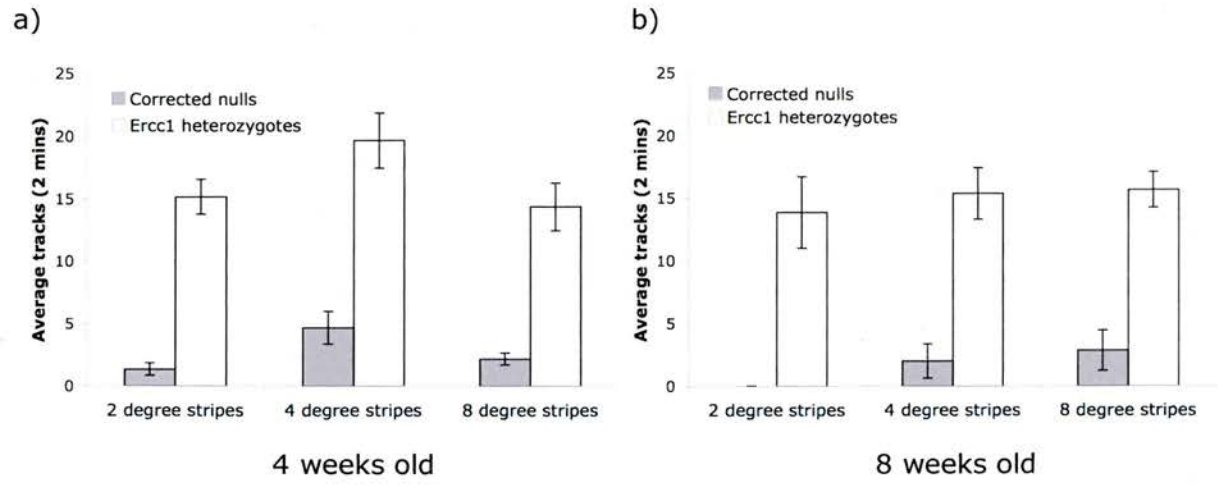

Figure 7.4 Ercc1 liver corrected null mice perform poorly in the optokinetic response (OKR) test compared with wild type littermates

Animals were tested in the optokinetic response (OKR) drum at 4 weeks (a) and 8 weeks of age (b). There were six animals in each group. Each animal was tested using three different stripe sizes (narrower stripes are more difficult for the animals to see), and 'tracks' or head movements following the stripes were counted over a two minute period. The stripes were rotated for one minute clockwise followed by one minute anti-clockwise. Animals were monitored using video equipment and counts were carried out later whilst watching the footage on a television.

7.6 *Ercc1* liver corrected null animals have normal anterior compartments of the eye

In order to investigate the cause of the apparent loss of visual acuity in the *Ercc1* liver corrected nulls, we used a slit lens camera to assess the anterior compartment of the eye. The mice were held in front of a magnifying lens and a small light source was moved close to the eye. This allowed us to assess the constrictory capacity of the pupil, and once the light was shining onto the eye, we were able to look for any evidence of cataract. Images taken of the eyes of some of the animals can be seen in figure 7.5, and these appear normal in both controls and *Ercc1* liver corrected nulls. We found no evidence of cataracts or loss of dilatory or constrictory capacity of the iris, and concluded that loss of visual acuity in these animals is not due to a defect in the anterior compartment of the eye.

7.7 The retinas of *Ercc1* liver corrected null animals appear grossly and microscopically normal

We analysed the retinas of the *Ercc1* liver corrected null animals macroscopically as well as microscopically. Images of retinas in live mice were taken using an ophthalmoscope, and no evidence of degeneration was noted in any of the mice investigated. We then went on to analyse the retina of these animals microscopically. Eye orbits were dissected and

Fig 7.5

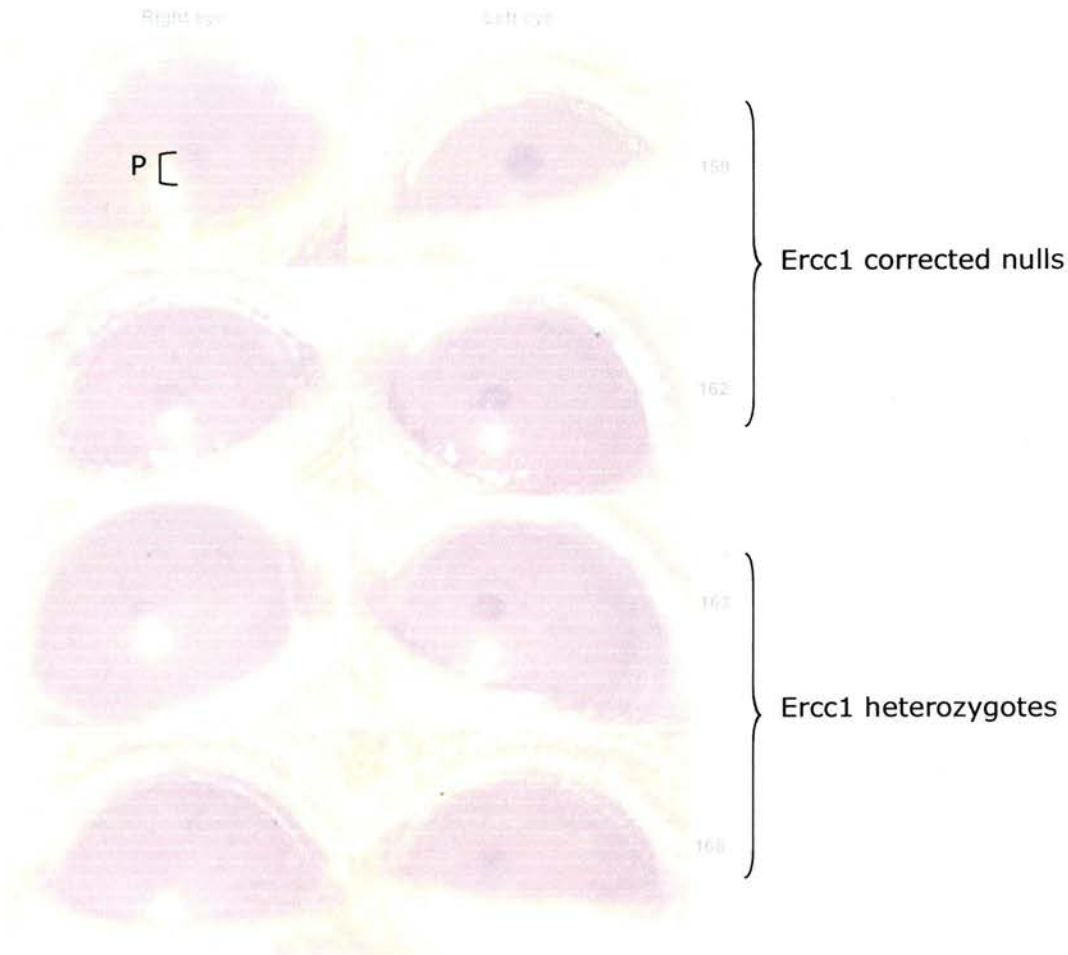

Figure 7.5 Ercc1 liver corrected null mice have normal dilation and constriction of the pupils of the eyes

Animals were photographed using a slit lens camera and a movable light source to assess constriction of the pupil in response to light. All these images show constricted pupils (P).

Fig 7.6

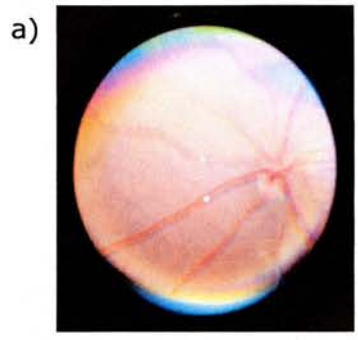

Image of retina taken using ophthalmoscope

(Courtesy of Dr A. Hart)

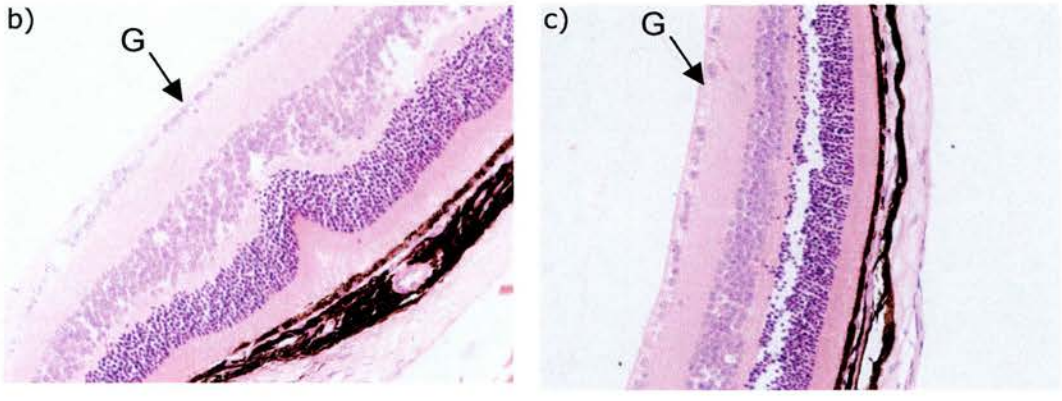

Figure 7.6 Ercc1 liver corrected null mice have normal retinal structure

Firstly, retinas were imaged *in vivo* using an ophthalmoscope, and were found to be normal in Ercc1 liver corrected nulls and controls, similar to that shown in (a). Secondly, eye orbits were fixed, embedded and serially sectioned before staining with H&E. These images were taken at the level of the optical nerve. (b) is an image taken from an Ercc1 heterozygote, and (c) is an image from a liver corrected Ercc1 null. The liver corrected Ercc1 null does appear to have a slight loss of cells in the ganglion cell layer (shown as G) although this difference is unlikely to be significant. Retinas were examined in animals of approximately eight weeks of age.

fixed from some animals, and serially sectioned to provide a view of the entire retina, particularly that around the optic nerve, shown in figure 7.6. We found no evidence of retinal degeneration microscopically either. We did find evidence of some cell loss in the ganglion cell layer of the *Ercc1* liver corrected null animals, although on further inspection this was determined to be insignificant. From this investigation we were able to conclude that loss of visual acuity in the *Ercc1* liver corrected null animals is not due to degeneration of the retina.

7.8 No evidence of degeneration of neuromuscular junctions (NMJs) in *Ercc1* liver corrected null mice

We considered the possibility that the neurological phenotype seen in the *Ercc1* liver corrected null mice, was due to degeneration of the neuromuscular junctions (NMJs), as this is implicated as an early event in many neurodegenerative disorders (reviewed by Gllingwater and Ribchester, 2003). We examined neuromuscular innervation of the transversus abdominis (TA) muscle, from the abdomen, and the deep lumbrical muscle, from the hind paw, in animals of ten weeks of age, when the neurological phenotype was advanced. Using immunofluorescence techniques we were able to visualise muscular endplates together with incoming axons (carried out by Dr Tom Gillingwater). Firstly, we found axonal bundles to be intact and non-fragmented, as shown in figure 7.7.

Fig 7.7

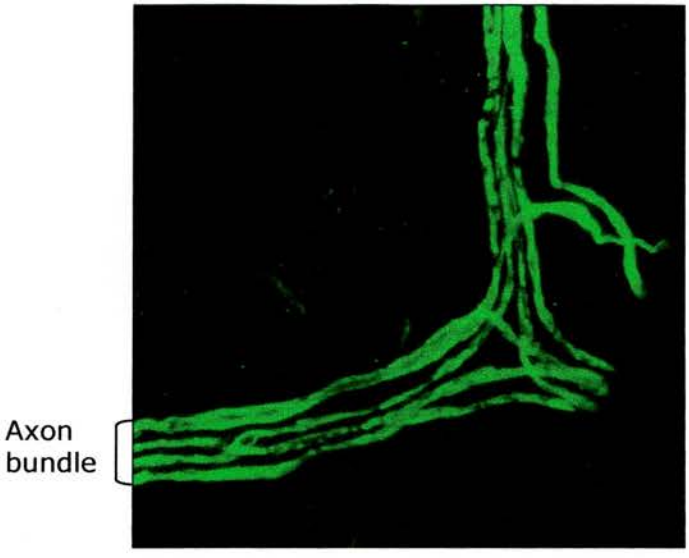

Figure 7.7 Ercc1 liver corrected null mice have normal axonal bundles

Animals were culled at 10 weeks of age, when severely atactic. Axon bundles were detected using α-bungarotoxin.

Fig 7.8

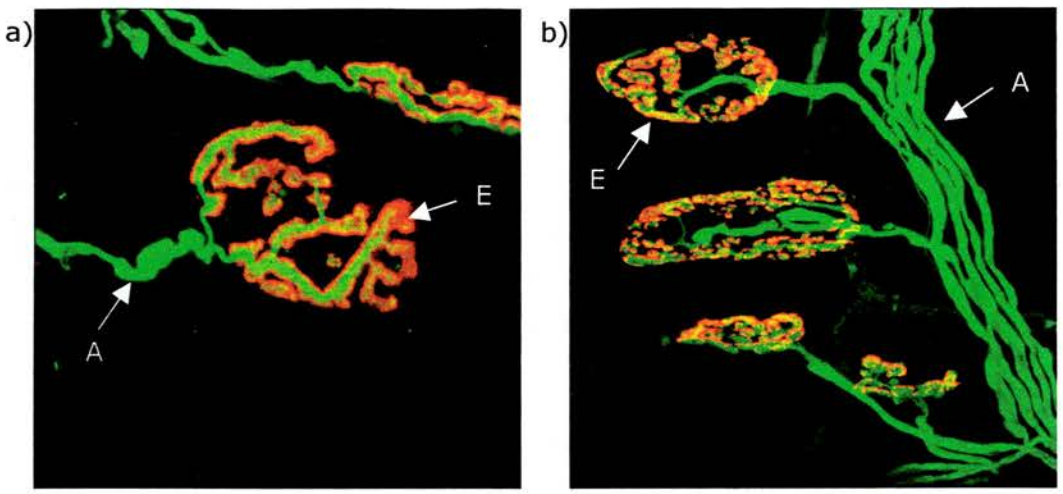

Ercc1 liver corrected null
TA muscle

Ercc1 liver corrected null
Lum muscle

Figure 7.8 Ercc1 liver corrected null mice do not show degeneration of neuromuscular junctions

Animals were culled at 10 weeks of age, when severely atactic, and transversus abdominis (TA) and deep lumbrical (Lum) muscles were dissected and stained. Acetylcholine receptors appear red and axons green. Both these images show normal synapses, as all the endplate receptors, stained red (E), are covered by incoming axons, stained green (A).

Furthermore, we found that NMJs in these animals were normal, shown in figure 7.8. In normal NMJs, the incoming neuron branches and covers an entire muscular endplate; whereas in abnormal NMJs the axons start to retract, failing to cover the endplates (c.f Gillingwater and Ribchester, 2003). We saw no evidence of this in any of the *Ercc1* liver corrected nulls analysed, despite the advanced ataxia observed in these animals.

7.9 Slight differences found in timing of synapse elimination between *Ercc1* liver corrected nulls and *Ercc1* heterozygotes

Using the same immunofluorescence techniques mentioned above, we were able to investigate the process of developmental synapse elimination at the neuromuscular junction in post-natal *Ercc1* liver corrected null mice. Synapse elimination occurs in the days after birth in all mammals, where synapses which are initially innervated by more than one motor neuron are progressively pruned until they become mono-innervated. In mice this process is completed by around 15 days post partum. We compared *Ercc1* liver corrected null animals with *Ercc1* heterozygotes at five and ten days after birth, and found differences between the genotypes. At five days, we found that in the *Ercc1* liver corrected null animals, more NMJs were mono-innervated than in the *Ercc1* heterozygous animals, implying slightly accelerated synapse elimination in the *Ercc1* liver corrected nulls. This is shown in figure 7.9. However, at ten days, we found the reverse to be the

Fig 7.9

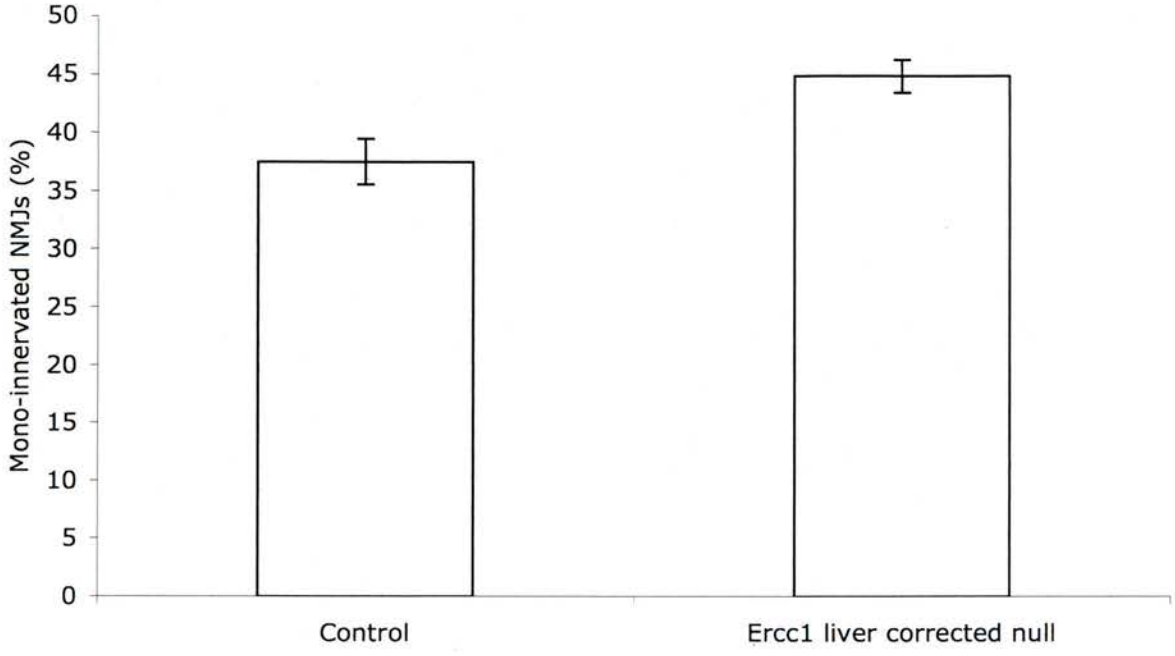

Figure 7.9 Synapse elimination is slightly accelerated in a Ercc1 liver corrected null mouse compared with a control at 5 days of age

Around 100 synapses were counted for each mouse and categorised as mono-innervated or multiply-innervated. Two mice of each genotype were assayed.

Fig 7.10

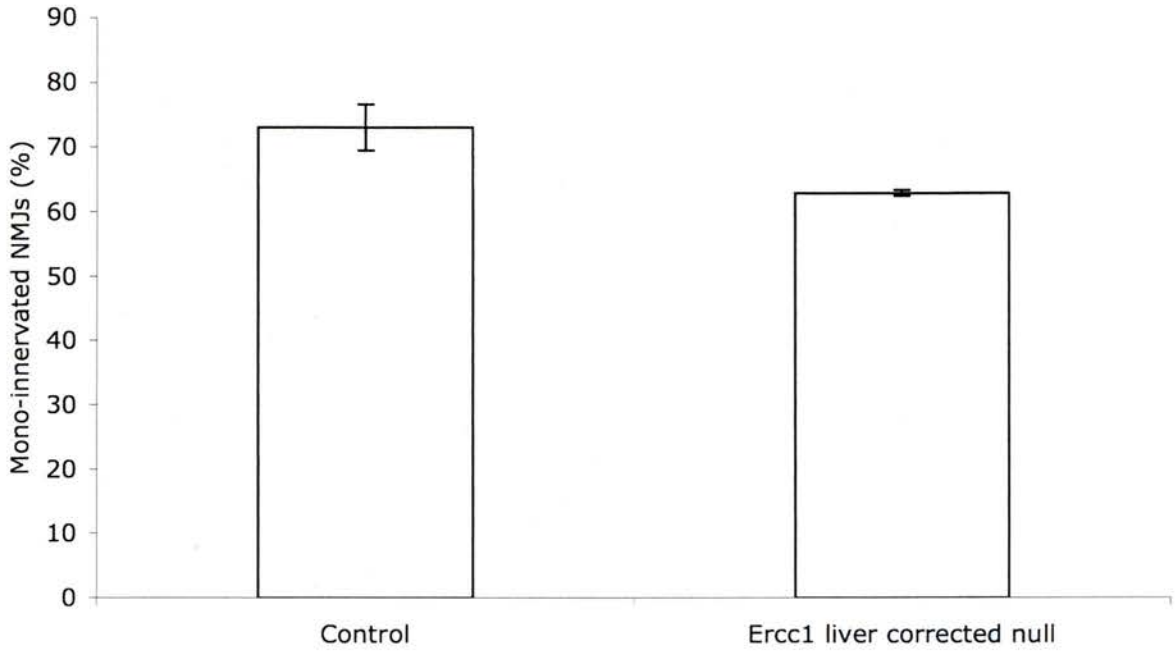

Figure 7.10 Synapse elimination is delayed in a Ercc1 liver corrected null mouse compared with a control at 10 days of age

Around 100 synapses were counted for each mouse and categorised as mono-innervated or multiply-innervated. Two mice of each genotype were assayed.

case. As can be seen in figure 7.10, we found fewer mono-innervated NMJs in the *Ercc1* liver corrected null animals compared with the *Ercc1* heterozygous animals. At fifteen days we found no difference between the genotypes.

7.10 Our *Ercc1* liver corrected null mouse stock does not carry the C57BL/6J linked *α-synuclein* mutation

It has been reported that C57BL/6J animals from a specific UK source carry a mutation in *α-synuclein* (observed by Specht and Schoepfer, 2001), a gene linked with Parkinson's disease and cerebellar abnormalities. In order to rule out the possibility of our stock carrying this mutation and it thereby affecting their neurological characteristics, we checked seven animals from the stock, of differing genotypes, for the presence of the mutated *α-synuclein* allele. We used PCR to amplify two genetic markers in the *α-synuclein* sequence, D6Mit122 and D6Mit357, which are separated by approximately 1cM genetic distance. D6Mit357 had been found to be deleted in the mutated allele, while D6Mit122 was not deleted and therefore served as a positive control for the *α-synuclein* gene. In all the animals tested we obtained positive results for both markers, as shown in figure 7.11. From this we concluded that our stock did not carry the reported mutated *α-synuclein* allele.

Fig 7.11

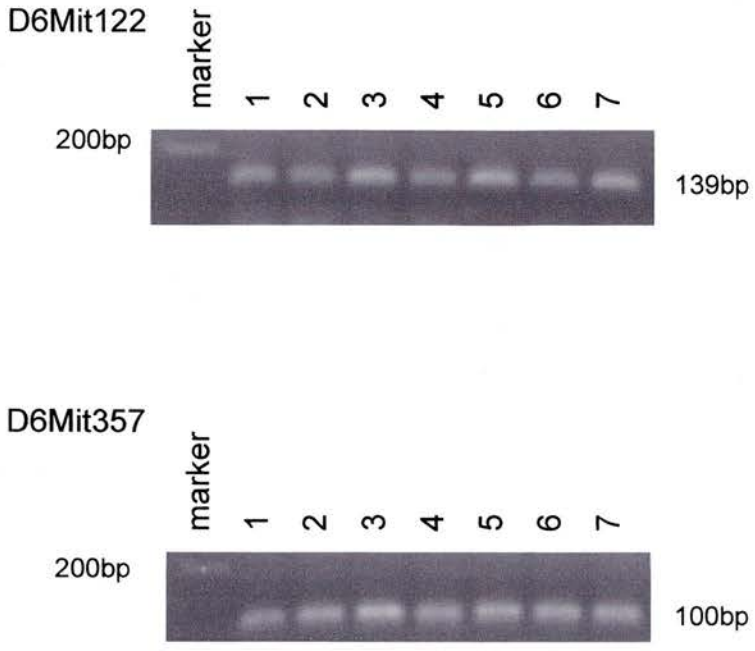

Figure 7.11 Our stock does not carry the α-synuclein mutation carried by some C57BL/6J mice

DNA from 7 animals from the stock, including 3 Ercc1 liver corrected nulls, were tested for the presence of the α-synuclein mutation reported in some C57BL/6J animals. Two genetic markers were amplified by PCR; D6Mit122 which falls outwith the reported deletion, and D6Mit357 which falls within the deletion. Therefore, all animals should be positive for D6Mit122, but only those which don't carry the mutation will be positive for D6Mit357.

Primers used:

D6Mit122a and D6Mit122b, 139bp product

D6Mit357a and D6Mit357b, 100bp product

PCR program:

94°C 5mins, (94°C 30secs, 55°C 30secs, 72°C 30secs)x30, 72°C 10mins

7.11 *Ercc1* liver corrected null mice have swollen brains consistent with uraemic disease

Post-mortem analysis carried out by Dr David Brownstein revealed brain swelling in the *Ercc1* liver corrected null mice. We found evidence of oedema throughout the brain, as indicated by areas appearing as gaps in the tissue, particularly around capillaries. Gaps seen in brain tissue upon histological examination are not uncommon, often caused by the processing of the tissue, particularly when brains are immersion fixed rather than perfused with fixative, however we felt we saw evidence of lesions aside from those which may have occurred through processing. In any case, all brains analysed were fixed concurrently and in the same manner. It should be noted that during this post-mortem analysis, no cerebellar abnormalities were observed.

Figure 7.12 shows images taken from the hippocampus, an area of grey matter. In the brains from the *Ercc1* liver corrected nulls we observed a spongey, moth eaten appearance, which was not seen in controls despite similar processing. This appearance is characteristic of an accumulation of fluid in the brain. In figure 7.13 similar features can be seen in the periaqueductal grey matter, an area deep in the centre of the brain. Figure 7.14 shows images of white matter from controls and *Ercc1* liver corrected nulls. White matter not only contains neurons, but also glial cells including astrocytes and oligodendrocytes. In *Ercc1* liver corrected nulls we

Fig 7.12

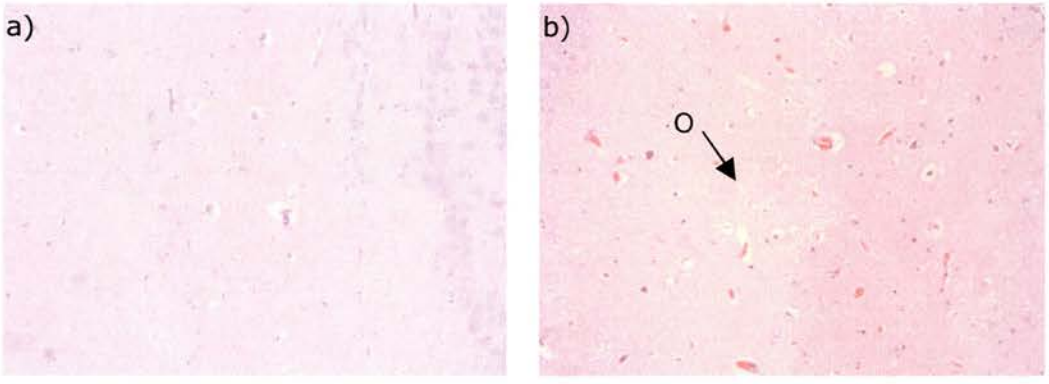

Figure 7.12 Evidence of oedema in hippocampus of Ercc1 liver corrected null brains

These images are taken of sections from the hippocampus, part of the grey matter of the brain after staining with H&E.

(a) is a section from a control brain. Gaps can be seen in the images as white spaces, however these are an artefact of the dehydration process.

(b) is a section from an Ercc1 liver corrected null brain. Gaps can also be seen that are probably artefacts of processing, however there are more gaps and areas with a moth-eaten, spongey appearance, characteristic of oedema and marked with (O).

Fig 7.13

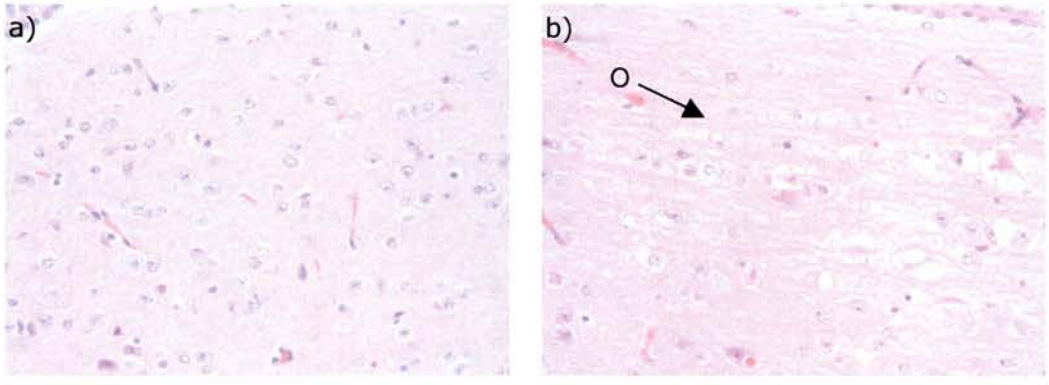

Figure 7.13 Evidence of oedema in the periaqueductal grey matter of Ercc1 liver corrected null brains

These images are taken of sections from the periaqueductal grey matter after staining with H&E.

(a) is a section from a control brain. Gaps can be seen in the images as white spaces, however these are an artefact of the dehydration process.

(b) is a section from an Ercc1 liver corrected null brain. Gaps can also be seen that are probably artefacts of processing, however there are more gaps and areas with a moth-eaten, spongey appearance, characteristic of oedema and marked with (O).

Fig 7.14

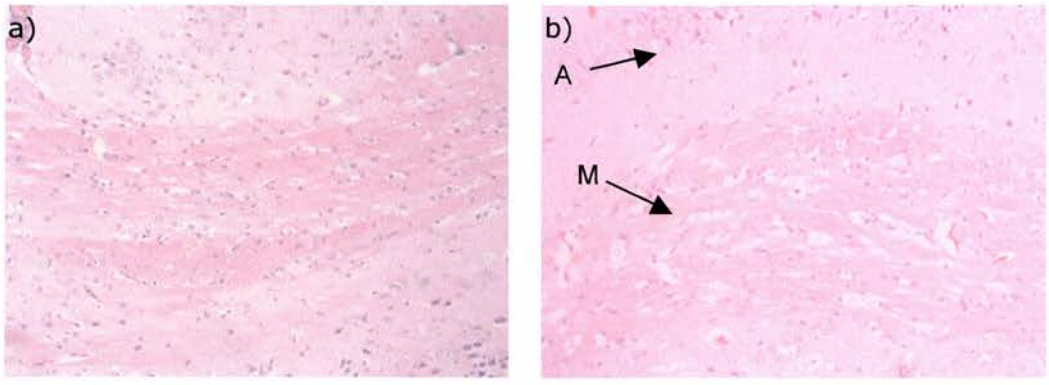

Figure 7.14 Evidence of oedema in white matter of Ercc1 liver corrected null brains

These images are taken of sections from the corpus callosum, part of the white matter of the brain, after staining with cresyl violet.

(a) is a section from a control brain. Some gaps can be seen in the images as white spaces, however these are an artefact of the dehydration process.

(b) is a section from an Ercc1 liver corrected null brain. Astrocyte swelling (A) is visible as well as separation of myelin fibres (M).

Fig 7.14

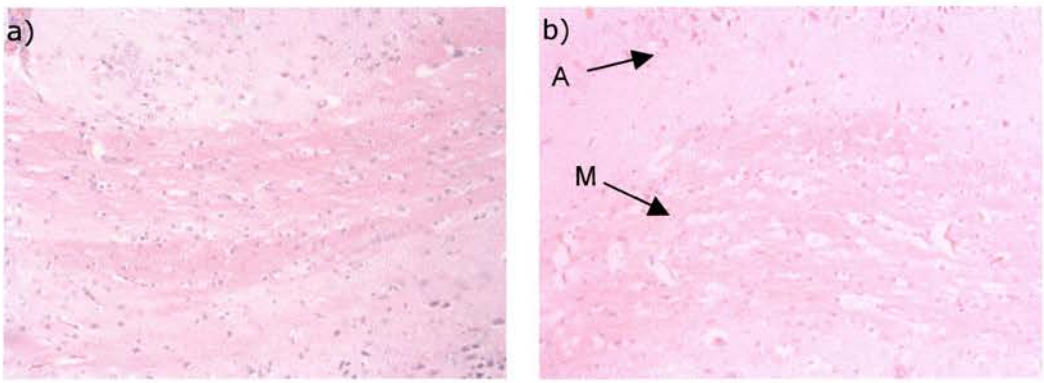

Figure 7.14 Evidence of oedema in white matter of Ercc1 liver corrected null brains

These images are taken of sections from the corpus callosum, part of the white matter of the brain, after staining with cresyl violet.

(a) is a section from a control brain. Some gaps can be seen in the images as white spaces, however these are an artefact of the dehydration process.

(b) is a section from an Ercc1 liver corrected null brain. Astrocyte swelling (A) is visible as well as separation of myelin fibres (M).

observed swelling of astrocytes, characterised by expansion of the cytoplasm and swollen nuclei with visible vesicles in these cells; astrocytes affected in this way are commonly known as Alzheimer type 2 cells, named after the man who first described them and not linked with Alzheimer disease. In these images we also observed separation of myelin fibres, a further characteristic of oedema.

7.12 *Ercc1* liver corrected null mice suffer from proteinuria from a young age

In order to confirm the diagnosis of uraemia in these mice, we measured levels of protein in urine samples collected. Colorimetric strips were used which identified protein urine concentrations as 0mg/ml, 0.3mg/ml, 1mg/ml or 5mg/ml. Animals were tested at 3-4 weeks of age and 8-10 weeks of age and results are shown in figure 7.15. We found that *Ercc1* heterozygotes had protein urine concentrations of 0.3mg/ml at both time points, in accordance with evidence suggesting a baseline protein urine concentration in mice higher than humans (Lorraine Rose, personal communication). At 3-4 weeks two of the ten *Ercc1* liver corrected nulls had protein urine concentrations of 1mg/ml and the other eight animals in the group had protein urine concentrations of 5mg/ml. At 8-10 weeks of age all ten *Ercc1* liver corrected null animals had protein urine concentrations of 5mg/ml. When analysed using the χ^2_{2df} test, these data gave p=0. The

Fig 7.15

	3-4 weeks of age		8-10 weeks of age	
Urine [Protein] (mg/ml)	Liver corrected Ercc1 nulls	Ercc1 heterozygotes	Liver corrected Ercc1 nulls	Ercc1 heterozygotes
0	0	0	0	0
0.3	0	10	0	10
1	2	0	0	0
5	8	0	10	0

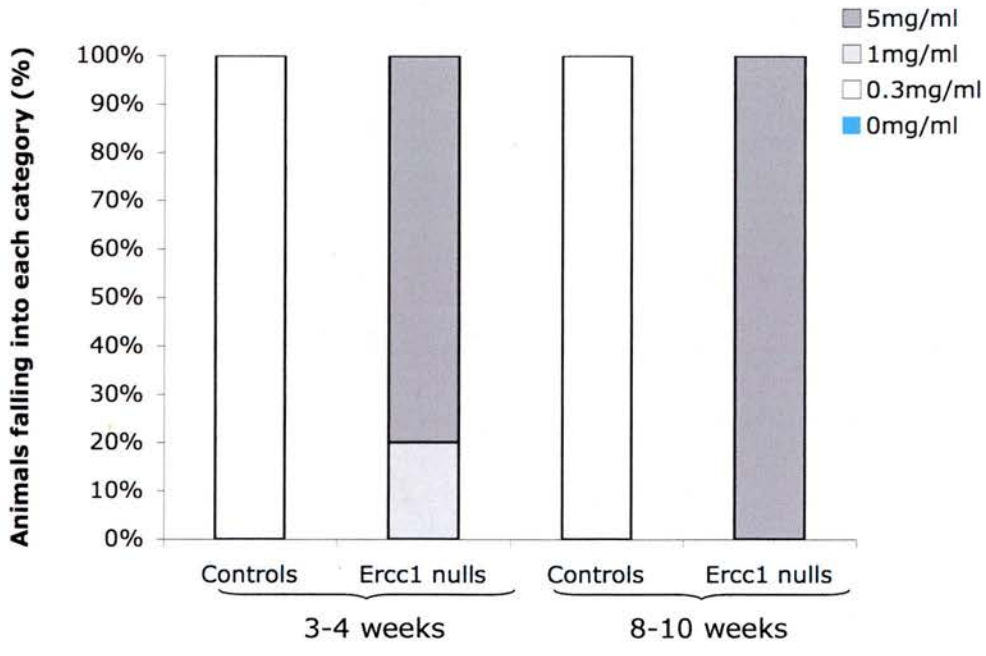

Figure 7.15 Ercc1 liver corrected null mice have high concentrations of protein in the urine compared with control mice

Protein in the urine was tested using Combur strips which change colour according to protein concentration. Results fall into one of four categories. Ten animals were tested in each group, at each timepoint.

high levels of proteinuria we found in these animals are consistent with impaired kidney function and systemic uraemia.

7.14 Discussion

The inability of *Ercc1* liver corrected null mice to remove bulky DNA lesions from the cells of the central and peripheral nervous systems has made them an interesting model with which to investigate the neurological system. We had observed certain features that were indicative of neurological abnormalities, and these features seemed to worsen with age. This chapter has addressed the characterisation of these features.

The neurological abnormalities in the mice were first noted when we observed the clasping reflex. Although this reflex has been used as an indicator of neurological dysfunction (recently in Komatsu et al, 2006 and Pang et al, 2006), this is controversial, because other transgenic mouse lines have been reported to clasp without showing other neurological symptoms (Tom Gillingwater, personal communication). However, it was this feature of the mice that persuaded us to look at the performance of the mice in more rigorous neurological assays.

Firstly, we addressed the motor abilities of the *Ercc1* liver corrected null animals, and found, as expected, that they performed extremely poorly on

the Roto-Rod from the time they were first tested, shortly after weaning, and that their performance deteriorated further with increased age. These data appeared to correlate with a relatively small cerebellar size in the *Ercc1* liver corrected null animals compared with controls, although this analysis was carried out by a fairly crude method; an improvement on this would be to section the entire brains of the mice and use specialised computer software to create a virtual three-dimensional model of the brain. This would enable an accurate volumetric measurement of appropriate brain compartments to be made.

We found that *Ercc1* liver corrected null mice appear to have impaired visual function, as assayed using the opto-kinetic response test, however, we found no evidence of cataract formation, retinal degeneration or any other structural abnormalities in the eyes. The opto-kinetic response test requires the mice to 'track', or move their heads as they follow the moving stripes, and we considered the possibility that the *Ercc1* liver corrected nulls lacked sufficient mobility to comply. Certainly as the mice approach three months of age their mobility is extremely compromised, and for this reason the results obtained for the older group of mice may be unreliable. However, at four weeks of age, when we first tested the mice, we still found that the *Ercc1* liver corrected null mice performed very poorly compared with control littermates, and at this age their mobility does not differ noticeably from their littermates. Taking this into account, together with the absence of structural pathology in the eyes, would suggest that the visual

impairment in the *Ercc1* liver corrected null mice is due to a functional abnormality. This could be assayed by measuring neuron firing in the optic centre of the brain, although to do this would require specialist expertise.

Loss of neurological synapses plays a part in several neurodegenerative disorders, including Alzheimer disease, Huntington disease, motor neuron disease and prion disease, as well as cerebral ischaemia, and for this reason we decided to investigate neuromuscular junction (NMJ) structure in the *Ercc1* liver corrected null mice. As far as we are aware, this type of assay has not been carried out in other NER knockout mice. Initially we looked at older mice, with severe neurological features, and we found no evidence of synapse loss or degeneration in these animals; furthermore, axons and axon bundles appeared normal. This has implications for the weight loss seen in these animals, as this is therefore not due to lack of innervation of the muscles leading to wasting.

We went on to use the same immunocytochemical techniques to investigate the process known as synapse elimination in the *Ercc1* liver corrected null mice. Initially in development, muscular endplates are multi-innervated by several axons. In the days after birth, axonal inputs are lost in a carefully regulated process known as synapse elimination, leaving all muscular endplates mono-innervated (reviewed by Gllingwater and Ribchester, 2003). The regulation of this process is poorly understood, although a limited supply of neutrotrophic factors has been implicated

(Nguyen et al, 1998) and there is evidence that disruption of the carefully coordinated elimination process can result in pathology. It has been suggested that adult neuropathies may be caused by aberrant synapse elimination processes (Gillingwater and Ribchester, 2003); consequently there is a great interest in dissecting the synapse elimination mechanism.

We found some differences in synapse elimination timing between *Ercc1* liver corrected null mice and controls. At five days post-partum, *Ercc1* liver corrected nulls appeared to have slightly accelerated synapse elimination compared with controls, however when we looked at mice ten days post-partum, we found that *Ercc1* liver corrected nulls had significantly delayed synapse elimination. At fifteen days post-partum, we found no differences between *Ercc1* liver corrected null mice and controls. Although we counted at least one hundred synapses in each mouse, and categorised these as multiply- or mono-innervated, we looked at only two mice of each genotype at each timepoint, and to improve this experiment it would would be vital to look at a greater number of mice, ideally at a range of timepoints post-partum. From the experiments carried out thus far, we have found an indication that the synapse elimination process is altered in the *Ercc1* liver corrected null mice, so to consider a greater cohort of mice would now be both useful and interesting.

Post-mortem investigation revealed unusual brain features in the *Ercc1* liver corrected null animals. We saw no evidence of neuronal loss, which

we had expected to see due to apoptosis of neurons with DNA damage. Furthermore, we saw no cerebellar abnormalities, which we had expected to see due to the ataxia we had observed in the animals. Instead we found evidence of encephalopathy, or non-inflammatory brain disease. Encephalopathy is due to organ failure, usually hepatic, and is a relatively common side effect of liver cirrhosis or cancer in human patients. Less commonly, encephalopathy can be caused by kidney failure, or systemic uraemia. This is rarely reported in humans as kidney failure is usually treated before it is sufficiently severe to cause uraemia (reviewed by Burn and Bates, 1998). Uraemic encephalopathy is therefore more common in animals, and has been described mainly in the rat, however mild behavioural defects have been reported in partially nephrectomised mice and linked with uraemic encephalopathy (Al Banchaabouchi et al, 1999).

In the brains of *Ercc1* liver corrected null mice we observed features of oedema. In grey matter we saw spaces in the neuropil, or extracellular matter, characteristic of fluid accumulation. In white matter we also saw spaces between cells and separation of myelin fibres, as well as astrocyte swelling. Astrocytes are a class of glial cell that are particularly susceptible to the effects of metabolic encephalopathy, primarily because they form an important part of the blood-brain barrier. We did not observe any necrosis of the cerebral cortex, another characteristic of metabolic encephalopathy, although as this is due to prolonged swelling of the brain pressing the

extremities of the cortex against the skull, it may be that the mice do not live long enough for us to observe this feature.

We believe the *Ercc1* liver corrected null mice suffer from uraemic encephalopathy as a result of deteriorating kidney function. Previously, our laboratory has reported a kidney phenotype in these mice (Selfridge et al, 2001) consisting of generalised nuclear polyploidy, particularly in the proximal tubules; which was reported to be due to an accumulation of endogenous damage similar to that which had caused liver polyploidy in the simple *Ercc1* knockouts. These data, along with evidence for raised levels of plasma creatinine in these mice (Selfridge et al, 2001) and the increased proteinuria reported here, strengthen this model.

In order to confirm oedematous brain swelling, precise measurement of animal weight and brain weight could be taken at the time of post-mortem. This would enable calculation of the ratio of brain weight to body weight, and we would expect to see an increased brain weight compared with body weight in the *Ercc1* liver corrected nulls, which would correlate with fluid accumulation in the brain. However, this would require extremely precise weighing apparatus. Another possible procedure involves injecting fluoresceinated albumin intravenously shortly before culling the mice, and looking for evidence of fluorescence in the brain; normally the fluoresceinated albumin should not enter the brain, but in oedema, the passage of fluid into the brain results in fluorescence appearing there.

Levels of blood urea nitrogen could also be assayed in the mice, as this constitutes the most accurate test of uraemia. Proteinuria is likely to be raised before the onset of uraemia, and as such is a less accurate indicator.

The time course of the neurological symptoms observed in the *Ercc1* liver corrected null mice requires careful consideration. We have documented behavioural abnormalities in the mice from four weeks of age, and although we know that brain oedema is significant by ten weeks of age, it is unclear at what point in time this becomes the case. Diagnosis of brain oedema is not straightforward, as processing artefacts complicate matters, and due to this, diagnosis can only be made reliably when the symptoms are fairly advanced. Therefore it is unclear whether the animals have uraemia when the behavioural abnormalities were first reported; if they do not, the case for alternative consequences of *Ercc1* deficiency in the central nervous system is strengthened. Measurement of blood urea nitrogen in animals of a range of ages would prove invaluable in pin-pointing the onset of uraemia. A previous experiment showed that the *Ercc1* liver corrected null animals had elevated plasma creatinine at 7 weeks of age but not at 3 weeks of age (Selfridge et al, 2001), and this is an area which warrants further investigation.

The logic behind looking for an explanation for the neurological phenotype observed in these mice was largely rooted in the anecdotal results

obtained from the *Ercc1* Nes::Cre mice mentioned at the start of this chapter. These mice died at the same time as the *Ercc1* liver corrected nulls and had *Ercc1* knocked out specifically in the central nervous system; or so we believed. Recently, evidence of nestin expression has been reported in adult podocytes as well as at certain developmental stages of the kidney and heart (Wagner et al, 2006), a fact which undermines our hypothesis that *Ercc1* deficiency has consequences for the neurological system itself, apart from indirectly. The breeding scheme for the *Ercc1* nestin mice was discontinued some time ago, and unfortunately we have no access to these mice or samples from them. Had we access to kidneys and brains from these mice, it would be extremely useful to look at the kidneys for evidence of polyploidy and enlarged nuclei, as well as the brains for evidence of oedema. Such evidence would resolve the mystery of why the *Ercc1* nestin mice died at the same age as the *Ercc1* liver corrected nulls, in the absence of any clear indication that *Ercc1* deficiency in the central nervous system was solely and directly to blame.

We have documented a clear neurological phenotype in *Ercc1* liver corrected null mice, with reference to behavioural as well as histopathological abnormalities. We have concluded that the mice die with secondary effects of kidney failure, namely uraemic encephalopathy. We have been unable to show conclusively any direct effects of *Ercc1* deficiency on the central nervous system itself; and although this by no means proves that there are no effects, it does suggest that this may be the

case. The ability of NER to function in a transcription coupled manner, where stalled RNA polymerases initiate the repair process, may underline its importance in the repair of DNA damage in neurons and other terminally differentiated tissues. It is plausible that *Ercc1* deficiency has dual effects on the central nervous system, with direct and indirect influences. As detailed above, there are further experiments that could be carried out to clarify the issues raised, and these issues must be addressed before we are able to understand the role of *Ercc1* in the central nervous system.

Chapter 8

Summary

Nucleotide excision repair (NER) deficiency has many consequences on the organism, as shown by the range of symptoms displayed by xeroderma pigmentosum, trichothiodystrophy and Cockayne syndrome patients. Over the past fifteen years, proteins involved in the NER pathway have been assigned to seven xeroderma pigmentosum complementation groups, however, despite the essential role of *Ercc1* in NER, this has not been assigned an XP group. This is because until very recently, *Ercc1* deficiency had not been recognised in humans, and was suspected to cause early embryonic lethality. A single human patient has been identified with *Ercc1* deficiency in the Netherlands, and this patient displayed very severe developmental abnormalities and died shortly after birth. Analysis on the genetic and phenotypic features of this patient is ongoing (personal communication, Dr Nicolaas Jaspers); although it is clear that *Ercc1* deficiency in humans results in severe pathology.

Ercc1 was the first NER protein to be knocked out in the mouse, and was found to cause severe runting and a very short life expectancy, with mice dying from liver failure (McWhir et al, 1993). Other groups have created knockouts and mutated forms of other NER proteins (as detailed in the introduction to this thesis), whilst our group has concentrated on creating *Ercc1* models with a longer life expectancy on which to study the effects of *Ercc1* deficiency in tissues other than the liver.

This thesis has addressed the consequences of *Ercc1* deficiency in the mouse by further characterising two particular mouse models created in our laboratory: the *Ercc1* liver corrected null and the *Ercc1* epidermis specific knockout. Briefly, the *Ercc1* liver corrected null uses an *Ercc1* transgene controlled by liver specific promoter transthyretin to alleviate liver pathology on an otherwise *Ercc1* null background; while the *Ercc1* epidermis specific knockout uses the *Cre*-lox*P* system with epidermal specific promoter K5 and a floxed *Ercc1* to create a mouse with *Ercc1* deficiency solely in the epidermal layers of the skin.

Chapter 3 addressed the differences in the short term responses of the *Ercc1* ESKO mouse, compared with controls, to UV irradiation. We found that *Ercc1* ESKO mice were extremely sensitive to UV induced erythema, photoimmunosuppression and tanning, compared with *Ercc1* proficient controls. These results confirmed the importance of DNA damage in the development of these responses, and underlined the role of the keratinocyte as an initiator of a cascade of events involving cytokine release and activation of various other cell types. Previous work carried out has shown NER deficient mice to be more susceptible to UV induced erythema (Berg et al, 1997 and 2000), photoimmunosuppression (Miyauchi-Hashimoto et al, 1996, Boonstra et al, 2001, Kolgen et al, 2003) and tanning (van Schanke et al, 2005) than control mice. However, the mice used in these studies were NER deficient throughout their organ systems, and as such the roles of the different compartments of the skin could not be addressed. We have shown

that persistent, UV induced DNA damage in keratinocytes is responsible for erythema, Langerhans cell migration, suppression of the contact hypersensitivity response and melanocyte activation.

Perhaps the most striking feature of NER deficiency is the cancer susceptibility of a large proportion of patients, and chapter 4 utilised the UV sensitivity of the *Ercc1* ESKO mice to address their susceptibility to UV induced skin tumours. The results presented in this chapter were published earlier this year as part of a paper describing the creation and phenotype of the mice (Doig et al, 2006). We found that the *Ercc1* ESKO mice were extremely sensitive to UV induced skin cancer compared with controls, and when compared with other NER knockouts, at least as sensitive if not more so. This supported our hypothesis, which was that not only would *Ercc1* ESKO mice be more susceptible to UV induced skin cancer than controls, but also that due to roles of ERCC1 in other repair processes, they would be more susceptible than simple NER knockouts such as *Xpa* null mice (Berg et al, 1997 and de Vries et al, 1998). ERCC1 is involved in the repair of inter-strand crosslinks (Bessho et al, 1997) and homologous recombination repair (Sargent et al, 2000), however it is unclear how important these roles are in the context of UV exposure. Not only did we find that *Ercc1* ESKO mice were more sensitive to UV induced carcinogenicity than controls in terms of median tumour free survival time; we also found accelerated tumour progression in the *Ercc1* ESKO mice. This has not been reported for other NER knockouts, although it may be simply that a histopathological study of

the depth that we have reported has not been undertaken with the other NER mice.

In chapter 5 we have used the proven skin cancer sensitivity of the *Ercc1* ESKO mice to consider the protective mechanism of action of topical thymidine dinucleotide (pTpT) application. As we have shown that *Ercc1* ESKO animals are protected to some degree from UV induced skin cancer, we have concluded that pTpT does not exert its protective action through the upregulation of NER. We have not been able to identify increased apoptosis in response to pTpT in the skin of animals exposed to UV; nor have we identified increased apoptosis in keratinocytes *in vitro* after pTpT treatment, with or without UV (personal communication, Anne-Marie Ritchie). Therefore, we hypothesise that pTpT exerts its protective effect by decreasing cellular proliferation. This correlates with results obtained in our long term UV carcinogenicity experiment where we saw reduced epidermal hyperproliferation in pTpT treated mice compared with mice treated with vehicle alone, as well as with a report that pTpT induces S phase arrest (Pedeux et al, 1998). There is speculation that this could be due to the telomere homology of pTpT (Eller et al, 2002, Puri et al, 2004), however both of these reports suggest increased apoptosis rather than cell cycle arrest as the outcome. Regardless of its mechanism of action, pTpT appears to be an effective protective agent against UV induced skin cancer, and with further investigation may in future prove an important therapy, in particular for individuals with elevated skin cancer risk.

In chapter 6 we addressed a novel phenotype identified in the *Ercc1* liver corrected null mice, which concerned an abnormal appearance of the fur of the animals in the stock. This phenotype occurred in *Ercc1* heterozygous animals as well as *Ercc1* nulls, but not in wild types; and bore similarities to the brittle hair phenotype observed in human trichothiodystrophy patients that carry mutations in *XPD*, as well as the *Xpd* mouse model for trichothiodystrophy (de Boer et al, 1998b). Despite this, we were unable to link the phenotype with *Ercc1* deficiency, and when we out-crossed the animals in the stock, we did not observe the phenotype in the offspring in a predictable manner. For these reasons, we concluded that the phenotype we had observed was due to a background effect, caused by the mix of mouse strains that have contributed to the *Ercc1* liver corrected null stock over the years.

Chapter 7 concerned the abnormal neurological features observed in the *Ercc1* liver corrected null mice. We found that these mice displayed features including clasping, poor motor ability and impaired vision, and these symptoms appeared to worsen with age. We concluded after extensive post-mortem examination that these mice suffered from uraemic encephalopathy, resulting from kidney pathology. Kidney pathology has been reported previously in these mice (Selfridge et al, 2001), and we now conclude that this is having secondary effects on the neurological system. Uraemic encephalopathy causes brain oedema and swelling and results when a

failing renal system is unable to filter toxins from the blood, which effectively poison the brain. Although we have been unable to identify neuropathology caused directly by *Ercc1* deficiency in the nervous system, we cannot rule out functional disorders, furthermore, there are more analyses that could be carried out on younger animals, as detailed in chapter 7 itself.

In summary, the work detailed in this thesis has used tissue specific *Ercc1* knockout mouse models to characterise further the consequences of nucleotide excision repair deficiency, adding to a large body of work from laboratories around the world which should enable us to help not only those patients suffering from repair deficiency syndromes, but also to deepen our understanding of cancer - one of the most common and devastating diseases in the developed world.

Al Banchaabouchi, M., D'Hooge, R., Marescau, B., De Deyn, P.P. Behavioural deficits during the acute phase of mild renal failure in mice. *Metab Brain Dis* **14**, 173-87 (1999).

Alberts, B., Bray, D., Lewis, J., Raff, M., Roberts, K. and Watson, J.D. *Molecular Biology of the Cell*, (Garland Publishing, 1994).

Aziz, M.H., Reagan-Shaw, S., Wu, J., Longley, B.J. and Ahmad, N. Chemoprevention of skin cancer by grape constituent resveratrol: relevance to human disease? *FASEB J* **19**, 1193-5 (2005).

Bair, W.B.3rd., Hart, N., Einspahr, J., Liu, G., Dong, Z., Alberts, D. and Bowden, G.T. Inhibitory effects of sodium salicylate and acetylsalicylic acid on UVB-induced mouse skin carcinogenesis. *Cancer Epidemiol Biomarkers Prev* **11**, 1645-52 (2002).

Barber, L.A., Spandau, D.F., Rathman, S.C., Murphy, R.C., Johnson, C.A., Kelley, S.W., Hurwitz, S.A. and Travers, J.B. Expression of the platelet-activating factor receptor results in enhanced ultraviolet B radiation induced apoptosis in a human epidermal cell line. *J Biol Chem* **273**, 18891-7 (1998).

Berg, R.J., de Vries, A., van Steeg, H. and de Gruijl, F.R. Relative susceptibilities of XPA knockout mice and their heterozygous and wild type littermates to UVB induced skin cancer. *Cancer Res* **57**, 581-4 (1997).

Berg, R.J., Rebel, H., van der Horst, G. T., van Kranen, H. J., Mullenders, L.H., van Vloten, W. A. and de Gruijl, F. R.. Impact of global genome repair versus transcription-coupled repair on ultraviolet carcinogenesis in hairless mice. *Cancer Res* **60**, 2858-63 (2000).

Bessho, T., Mu, D. and Sancar, A. Initiation of DNA interstrand cross-link repair in humans: the nucleotide excision repair system makes dual incisions 5' to the cross-linked base and removes a 22- to 28-nucleotide-long damage-free strand. *Mol Cell Biol* **17**, 6822-30 (1997).

Bessho, T. Nucleotide excision repair 3' endonuclease XPG stimulates the activity of base excision repair enzyme thymine glycol DNA glycosylase. *Nucleic Acids Res* **27**, 979-83 (1999).

Biesterfeld, S., Gerres, K., Fischer-Wein, G. and Bocking, A. Polyploidy in non-neoplastic tissues. *J Clin Pathol* **47**, 38-42 (1994).

Boonstra, A., van Oudenaren, A., Baert, M., van Steeg, H., Leenen, P.J., van der Horst, G.T., Hoeijmakers, J.H., Savelkoul, H. F. and Garssen, J.. Differential ultraviolet-B-induced immunomodulation in XPA, XPC, and CSB DNA repair-deficient mice. *J Invest Dermatol* **117**, 141-6 (2001).

Bootsma, D., Kraemer, K.H., Cleaver, J.E. and Hoeijmakers, J.H.J. *The Genetic Basis of Human Cancer*, 245-74 (McGraw-Hill, New York, 1998).

Braun, M.C., Lahey, E. and Kelsall, B.L. Selective suppression of IL-12 production by chemokines. *J Immunol* **164**, 3009-17 (2000).

Burn, D.J. and Bates, D. Neurology and the kidney. *J Neurol Neurosurg Psychiatry* **65**, 810-21 (1998).

Bursch, W. and Ellinger, A. Autophagy--a basic mechanism and a potential role for neurodegeneration. *Folia Neuropathol* **43**, 297-310 (2005).

Carter, T.C. and Phillips, R.J.S. Ragged, a semidominant coat texture mutant: In the house mouse. *J Hered* **45**, 151-4 (1954).

Chaker, M.B., Tharp, M.D. and Bergstresser, P.R. Rodent epidermal Langerhans cells demonstrate a greater histochemical specificity for ADP than ATP and AMP. *J Invest Dermatol* **82**, 496-500 (1984).

Chaturvedi, V., Qin, J.Z., Denning, M.F., Choubey, D., Diaz, M.O. and Nickoloff, B.J. Apoptosis in proliferating, senescent, and immortalised keratinocytes. *J Biol Chem* **274**, 23358-67 (1999).

Chipchase, M.D. and Melton, D.W. The formation of UV-induced chromosome aberrations involves ERCC1 and XPF but not other nucleotide excision repair genes. *DNA Repair* **29**, 335-40 (2002).

Chung, H.-J. and Levens, D. c-myc expression: keep the noise down! *Mol Cells* **20**, 157-66 (2005).

Clydesdale, G.J., Dandie, G.W. and Muller, H.K. Ultraviolet light induced injury: Immunological and inflammatory effects. *Immunology and Cell Biology* **79**, 547-568 (2001).

Colella, S., Nardo, T., Botta, E., Lehmann, A.R. and Stefanini. Identical mutations in the CSB gene associated with either Cockayne syndrome of the DeSanctis-Cacchione variant of xeroderma pigmentosum. *Hum Mol Genet* **9**, 1171-5 (2000).

Coleman, D.L., Dagg, C.P., Fuller, J.L., Green, M.C., Kaliss, N., Russell, E.S. and Staats, J. *Biology of the Laboratory Mouse*, (Dover Publications, Inc., New York, 1975).

Cotran, R.S., Kumar, V. and Collins, T. *Robbins Pathologic Basis of Disease*, (W.B.Saunders Co., 1999).

Coverly, D., Kenny, M.K., Lane, D.P. and Wood, R.D. Requirement for the replication protein SSB in human DNA excision repair. *Nature* **349**, 538-41 (1991).

Cozzarelli, N.R. Editorial expression of concern (re. Proc Natl Acad Sci USA (1993) 90(22):10499-503). *Proc Natl Acad Sci USA* **100**, 11816 (2003).

Cruz Jnr, P.D., Leverkus, M., Dougherty, I., Gleason, M.J., Eller, M.S., Yaar, M. and Gilchrest, B.A. Thymidine dinucleotides inhibit contact hypersensitivity and activate the gene for tumour necrosis factor alpha. *J Invest Dermatol* **114**, 253-8 (2000).

Curiel-Lewandrowski, C., Venna, S.S., Eller, M.S., Cruikshank, W., Dougherty, I., Cruz Jnr, P.D. and Gilchrest, B.A. Inhibition of the elicitation phase of contact hypersensitivity by thymidine dinucleotides is in part mediated by increased expression of interleukin-10 in human keratinocytes. *Exp Dermatol* **12**, 145-52 (2003).

D'Orazio, J.A., Nobuhisa, T., Cui, R., Arya, M., Spry, M., Wakamatsu, K., Igras, V., Kunisada, T., Granter, S.R., Nishimura, E.K., Ito, S. and Fisher, D.E. Topical drug rescue strategy and skin protection based on the role of Mc1r in UV-induced tanning. *Nature* **443**, 340-4 (2006).

Dandie, G.W., Clydesdale, G.J., Jacobs, I. & Muller, H.K. Effects of UV on the migration and function of epidermal antigen presenting cells. *Mutat Res* **422**, 147-54 (1998).

de Boer, J., Donker, I., de Wit, J., Hoeijmakers, J.H. and Weeda, G. Disruption of the mouse xeroderma pigmentosum group D DNA repair/basal transcription gene results in preimplantation lethality. *Cancer Res* **58**, 89-94 (1998a).

de Boer, J., de Wit, J., van Steeg, H., Berg, R.J.W., Morreau, H., Visser, P., Lehmann, A.R., Duran, M., Hoeijmakers, J.H. and Weeda, G. A mouse model for the basal transcription/DNA repair syndrome trichothiodystrophy. *Mol Cell* **1**, 981-90 (1998b).

de Boer, J., van Steeg, H., Berg, R.J.W., Garssen, J., de Wit, J., van Oostrum, C.T.M., Beems, R.B., van der Horst, G.T.J., van Kreijl, C.F., de Gruijl, F.R., Bootsma, D., Hoeijmakers, J.H.J. and Weeda, G. Mouse model for the DNA repair/basal transcription disorder trichothiodystrophy reveals cancer predisposition. *Cancer Res* **59**, 3489-94 (1999).

de Boer, J., Andressoo, J.O., de Wit, J., Huijmans, J., Beems, R.B., van Steeg, H., Weeda, G., van der Horst, G.T.J., van Leeuwen, W., Themmen, A.P.N., Meradji, M. and Hoeijmakers, J.H.J. Premature aging in mice deficient in DNA repair and transcription. *Science* **296**, 1276-9 (2002).

de Boer, J. & Hoeijmakers, J.H. Nucleotide excision repair and human syndromes. *Carcinogenesis* **21**, 453-60 (2000).

de la Chapelle, A. Genetic predisposition to colorectal cancer. *Nat Rev* **4**, 769-80 (2004).

de Laat, W.L., Appeldoorn, E., Jaspers, N.G. and Hoeijmakers, J.H. DNA structural elements required for ERCC1-XPF endonuclease activity. *J Biol Chem* **273**, 7835-42 (1998).

de Laat, W.L., Jaspers, N.G.J. and Hoeijmakers, J.H.J. Molecular mechanism of nucleotide excision repair. *Genes and Dev* **13**, 768-85 (1999).

de Lange, T., Shiue, L., Myers, R.M., Cox, D.R., Naylor, S.L., Killery, A.M. and Varmus, H.E. Structure and variability of human chromosome ends. *Mol Cell Biol* **10**, 518-27 (1990).

de Lange, T. Protection of mammalian telomeres. *Oncogene* **21**, 532-40 (2002).

de Vries, A., van Oostrom, C.T., Hofhuis, F.M. Dortant, P.M., Berg, R.J., de Gruijl, F.R., Wester, P.W., van Kreijl, C.F., Capel, P.J., van Steeg, H. and Verbeek, S.J. Increased susceptibility to ultraviolet-B and carcinogens of mice lacking the DNA excision repair gene XPA. *Nature* **377**, 169-73 (1995).

de Vries, A., Berg, R.J., Wijnhoven, S., Westerman, A., Wester, P.W., van Kreijl, C.F.,Capel, P.J., de Gruijl, F.R., van Kranen, H.J. and van Steeg, H. XPA-deficiency in hairless mice causes a shift in skin tumor types and mutational target genes after exposure to low doses of U.V.B. *Oncogene* **16**, 2205-12 (1998).

Deliconstantinos, G., Villiotou, V. & Stravrides, J.C. Release by ultraviolet B (u.v.B) radiation of nitric oxide (NO) from human keratinocytes: a potential role for nitric oxide in erythema production. *Br J Pharmacol* **114**, 1257-65 (1995).

Dhanalakshmi, S., Mallikarjuna, G.U., Singh, R.P. and Agarwal, R. Silibinin prevents ultraviolet radiation-caused skin damages in SKH-1 hairless mice via a decrease in thymine dimer positive cells and an up-regulation of p53-p21/Cip1 in epidermis. *Carcinogenesis* **25**, 1459-65 (2004).

Dhanalakshmi, S., Agarwal, C., Singh, R.P. and Agarwal, R. Silibinin up-regulates DNA-protein kinase-dependent p53 activation to enhance UVB-induced apoptosis in mouse epithelial JB6 cells. *J Biol Chem* **280**, 20375-83 (2005).

Dickson, D.W. Apoptotic mechanisms in Alzheimer neurofibrillary degeneration: cause or effect? *J Clin Invest* **114**, 23-7 (2004).

Doig, J., Anderson, C., Lawrence, N.J., Selfridge, J., Brownstein, D.G., Melton, D.W. Mice with skin-specific DNA repair gene (Ercc1) inactivation are hypersensitive to ultraviolet irradiation-induced skin cancer and show more rapid actinic progression. *Oncogene* **25**, 6229-38 (2006).

Donahue, B.A., Yin, S., Taylor, J-S., Reines, D. and Hanawalt, P.C. Transcript cleavage by RNA polymerase II arrested by a cyclobutane pyrimidine dimer in the DNA template. *Proc Natl Acad Sci USA* **91**, 8502-6 (1994).

El-Ghorr, A.A. and Norval, M. The UV waveband dependencies in mice differ for the suppression of contact hypersensitivity, delayed-type hypersensitivity and cis-urocanic acid formation. *J Invest Dermatol* **112**, 757-62 (1999).

Eller, M.S., Yaar, M. and Gilchrest, B.A. DNA damage and melanogenesis. *Nature* **372**, 413-4 (1994).

Eller, M.S., Oostrom, K. and Gilchrest, B.A. DNA damage enhances melanogenesis. *Proc Natl Acad Sci USA* **93**, 1087-92 (1996).

Eller, M.S., Maeda, T., Magnoni, C., Atwal, D. and Gilchrest, B.A. Enhancement of DNA repair in human skin cells by thymidine dinucleotides: Evidence for a p53 mediated mammalian SOS response. *Proc Natl Acad Sci USA* **94**, 12627-32 (1997).

Eller, M.S., Puri, N., Hadshiew, I.M., Venna, S.S. and Gilchrest, B.A. Induction of apoptosis by telomere 3' overhang specific DNA. *Exp Cell Res* **276**, 185-93 (2002).

Eller, M.S., Li, G.Z., Firoozabadi, R., Puri, N. and Gilchrest, B.A. Induction of a p95/Nbs1 mediated S phase checkpoint by telomere 3' overhang specific DNA. *FASEB J* **17**, 152-62 (2003).

Eller, M.S., Liao, X., Liu, S-Y., Hanna, K., Backvall, H., Opresko, P.L., Bohr, V.A. and Gilchrest, B.A. A role for WRN in telomere based DNA damage responses. *Proc Natl Acad Sci USA* **103**, 15073-8 (2006).

Enk, C.D., Mahanty, S., Blauvelt, A. and Katz, S.I. UVB induces IL-12 transcription in human keratinocytes in vivo and in vitro. *Photochem Photobiol* **63**, 854-9 (1996).

Farr, P. and Diffey, B.L. Quantitative studies on cutaneous erythema induced by ultraviolet radiation. *Br. J. Dermatol.* **111**, 673-82 (1984).

Fiorentino, D.F., Zlotnik, A., Mosmann, T.R., Howard, M. and O'Garra, A. IL-10 inhibits cytokine production by activated macrophages. *J Immunol* **147**, 3815-22 (1991).

Fisher, M.S. & Kripke, M.L. Systemic alteration induced in mice by ultraviolet light irradiation and its relationship to ultraviolet carcinogenesis. *Proc Natl Acad Sci U S A* **74**, 1688-92 (1977).

Friedberg, E.C. How nucleotide excision repair protects against cancer. *Nature Reviews Cancer* **1**, 22-33 (2001).

Friedberg, E.C and Meira, L.B. Database of mouse strains carrying targeted mutations in genes affecting biological responses to DNA damage version 7. *DNA Repair* **5**, 189-209 (2006).

Friedmann, P.S. and Gilchrest, B.A. Ultraviolet radiation directly induces pigment production by cultured human melanocytes. *J Cell Physiol* **133**, 88-94 (1987).

Garssen, J., Vandebriel, R.J., de Gruijl, F.R., Wolvers, D.A.W., van Dijk, M., Fluitman, A. and van Loveren, H. UVB exposure-induced systemic modulation of Th1- and Th2- mediated immune responses. *Immunology* **97**, 506-14 (1999).

Garssen, J., van Steeg, H., de Gruijl, F., de Boer, J., van der Horst, G.T., van Kranen, H., van Loveren, H., van Dijk, M., Fluitman, A., Weeda, G. and Hoeijmakers, J. H. Transcription-coupled and global genome repair differentially influence UV-B-induced acute skin effects and systemic immunosuppression. *J Immunol* **164**, 6199-205 (2000).

Gervais, V., Lamour, V., Jawhari, A., Frindel, F., Wasielewski, E., Dubaele, S., Egly, J-M.,Thierry, J.C., Kieffer, B. and Poterszman, A. TFIIH contains a PH domain involved in DNA nucleotide excision repair. *Nat Struct Mol Biol* **11**, 616-22 (2004).

Giglia-Mari, G., Coin, F., Ranish, J.A., Hoogstraten, D., Theil, A., Wijgers, N., Jaspers, N.G., Raams, A., Argentini, M., van der Spek, P.J., Botta, E., Stefanini, M., Egly, J.M., Aebersold, R., Hoeijmakers, J.H. and Vermeulen, W. A new, tenth subunit of TFIIH is responsible for the DNA repair syndrome trichothiodystrophy group A. *Nat Genet* **36**, 714-9 (2004).

Giglia-Mari, G., Miquel, C., Theil, A.F., Mari, P.O., Hoogstraten, D., Ng, J.M., Dinant, C., Hoeijmakers, J.H. and Vermeulen, W. Dynamic interaction of TTDA with TFIIH is stabilised by nucleotide excision repair in living cells. *PLoS Biol* **4**, e106 (2006).

Gilchrest, B.A. and Eller, M.S. The tale of the telomere: Implications for prevention and treatment of skin cancers. *J Invest Dermatol Symp Proc* **10**, 124-30 (2005).

Gillespie, J. and Marshall, R. A comparison of the proteins of normal and trichothiodystrophic human hair. *J Invest Dermatol* **80**, 195-202 (1983).

Gillingwater, T.H. and Ribchester, R.R. The relationship of neuromuscular synapse elimination to synaptic degeneration and pathology: insights from WldS and other mutant mice. *J Neurocytol* **32**, 863-81 (2003).

Goukassian, D.A., Eller, M.S., Yaar, M. and Gilchrest, B.A. Thymidine dinucleotide mimics the effect of solar simulated irradiation of p53 and p53 regulated proteins. *J Invest Dermatol* **112**, 25-31 (1999).

Goukassian, D.A., Bagheri, S., El-Keeb, L., Eller, M.S., and Gilchrest, B.A. DNA oligonucleotide treatment corrects the age associated decline in DNA repair activity. *FASEB J* **16**, 754-6 (2002).

Goukassian, D.A., Helms, E., van Steeg, H., van Oostrom, C., Bhawan, J. and Gilchrest, B.A. Topical DNA oligonucleotide therapy reduces UV induced mutations and photocarcinogenesis in hairless mice. *Proc Natl Acad Sci USA* **101**, 3933-8 (2004).

Grabbe, S. and Schwarz, T. Immunoregulatory mechanisms involved in elicitation of allergic contact hypersensitivity. *Immunology Today* **19**, 37-44 (1998).

Griffith, J.D., Comeau, L., Rosenfield, S., Stansel, R.M., Bianchi, A., Moss, H. and de Lange, T. Mammalian telomeres end in a large duplex loop. *Cell* **97**, 503-4 (1999).

Gupta, S. Hepatic polyploidy and liver growth control. *Semin Cancer Biol* **10**, 161-71 (2000).

Haake, A.R. and Polakowska, R.R. Cell death by apoptosis in epidermal biology. *J Invest Dermatol* **101**, 107-12 (1993).

Halliday, G.M. Inflammation, gene mutation and photoimmunosuppression in response to UVR-induced oxidative damage contributes to photocarcinogenesis. *Mutat Res* **571**, 107-20 (2005).

Halliwell, B. Oxidative stress and neurodegeneration: where are we now? *J Neurochem* **97**, 1634-58 (2006).

Harada, Y.N., Shiomi, N., Koike, M., Ikawa, M., Okabe, M., Hirota, S., Kitamura, Y.,Kitagawa, M., Matsunaga, T., Nikaido, O. and Shiomi, T. Postnatal growth failure, short life span, and early onset of cellular senescence and subsequent immortalisation in mice lacking the xeroderma pigmentosum group G gene. *Mol Cell Biol* **19**, 2366-72 (1999).

Harper, J.W., Adami, G.R., Wei, N., Keyomarsi, K. and Elledge, S.J. The p21 Cdk-interacting protein Cip1 is a potent inhibitor of G1 cyclin-dependent kinases. *Cell* **75**, 805-16 (1993).

Hart, A.W., McKie, L., Morgan, J.E., Gautier, P., West, K., Jackson, I.J. and Cross, S.H. Genotype–Phenotype Correlation of Mouse Pde6b Mutations. *Invest Ophthalmol Vis Sci* **46**, 3443-50 (2005).

Hartl, D.L. and Jones, E.W. *Genetics: Principles and Analysis*, (Jones and Bartlett, Toronto, 1998).

Hefferin, M.L. and Tomkinson, A.E. Mechanism of DNA double-strand break repair by non-homologous end joining. *DNA Repair* **4**, 639-48 (2005).

Hoeijmakers, J.H.J. Genome maintenance mechanisms for preventing cancer. *Nature* **411**, 366-74 (2001).

Holick, M.F. and Tangpricha, V. Reply to MA Weinstock and D Lazowich. *Am J Clin Nutr* **82**, 707-8 (2005).

Hollander, M.C., Philburn, R.T., Patterson, A.D., Velasco-Miguel, S., Friedberg, E.C.,Linnoila, R.I. and Fornace, A.J. Jr. Deletion of XPC leads to lung tumors in mice and is associated with early events in human lung carcinogenesis. *Proc Natl Acad Sci USA* **102**, 13200-5 (2005).

Hsia, K.T., Millar, M.R., King, S., Selfridge, J., Redhead, N.J., Melton, D.W. and Saunders, P.T. DNA repair gene Ercc1 is essential for normal spermatogenesis and oogenesis and for functional integrity of germ cell DNA in the mouse. *Development* **130**, 369-78 (2003).

Inoue, K., Hosoi, J., Ideta, R., Ohta, R., Ifuku, O. and Tsuchiya, T. Stress augmented ultraviolet irradiation induced pigmentation. *J Invest Dermatol* **121**, 165-71 (2003).

Itin, P.H. and Pittelkow, M.R. Trichothiodystrophy: Review of sulphur deficient brittle hair syndromes and association with the ectodermal dysplasias. *J Am Acad Dermatol* **20**, 705-15 (1990).

Janeway, C.A., Travers, P., Walport, M. and Schlomchik, M. *Immunobiology*, (2001).

Jawhari, A., Laine, J.P., Dubaele, S., Lamour, V., Poterszman, A., Coin, F., Moras, D. and Egly, J.M. p52 mediates XPB function within the transcription/repair factor TFIIH. *J Biol Chem* **277**, 31761-7 (2002).

JAX, T.J.L. Mouse Genome Informatics. (2006).

Jimbo, T., Ichihashi, M., Mishima, Y. & Fujiwara, Y. Role of excision repair in UVB-induced depletion and recovery of human epidermal Langerhans cells. *Arch Dermatol* **128**, 61-7 (1992).

Jiricny, J. The multifaceted mismatch repair system. *Nat Rev Mol Cell Biol* **7**, 335-46 (2006).

Jun, S.H., Kim, T.G. and Ban, C. DNA mismatch repair system. Classical and fresh roles. *FEBS J* **273**, 1609-19 (2006).

Kang, K., Hammerberg, L., Meunier, K. and Cooper, D. CD11b+ macrophages that infiltrate human epidermis after in vivo ultraviolet exposure potently produce IL-10 and represent the major secretory source of epidermal IL-10 protein. *J Immunol* **153**, 5256-64 (1994).

Kapetanaki, M.G., Guerrero-Santoro, J., Bisi, D.C., Hsieh, C.L., Rapic-Otrin, V., Levine, A.S. The DDB1-CUL4ADDB2 ubiquitin ligase is deficient in xeroderma pigmentosum group E and targets histone H2A at UV-damaged DNA sites. *Proc Natl Acad Sci USA* **103**, 2588-93 (2006).

Kirnbauer, R., Kock, A., Neuner, P., Forster, E., Krutmann, J., Urbanski, A., Schauer, E, Ansel, J.C., Schwarz, T. and Luger, T.A. Regulation of epidermal cell interleukin-6 production by UV light and corticosteroids. *J Invest Dermatol* **96**, 484-9 (1991).

Kock, A., Schwarz, T., Kirnbauer, R., Urbanski, A., Perry, P., Ansel, J.C. and Luger, T.A. Human keratinocytes are a source for tumour necrosis factor alpha: evidence for synthesis and release upon stimulation with endotoxin or ultraviolet light. *J Exp Med* **172**, 1609-14 (1990).

Kolgen, W., van Steeg, H., van der Horst, G.T., Hoeijmakers, J.H., van Vloten, W.A., de Gruijl, F.R. and Garssen, J. Association of transcription-coupled repair but not global genome repair with ultraviolet-B-induced Langerhans cell depletion and local immunosuppression. *J Invest Dermatol* **121**, 751-6 (2003).

Komatsu, M., Waguri, S., Chiba, T., Murata, S., Iwata, J., Tanida, I., Ueno, T.,Koike, M., Uchiyama, Y., Kominami, E. and Tanaka K. Loss of autophagy in the central nervous system causes neurodegeneration in mice. *Nature* **441**, 880-4 (2006).

Komura, K., Hasegawa, M., Hamaguchi, Y., Saito, E., Kaburagi, Y., Yanaba, K., Kawara, S., Takehara, K., Seki, M., Steeber, D.A., Tedder, T.F. and Sato, S. Ultraviolet light exposure suppresses contact hypersensitivity by abrogating endothelial intercellular adhesion molecule-1 up-regulation at the elicitation site. *J Immunol* **171**, 2855-62 (2003).

Kraemer, K.H. Sunlight and skin cancer: another link revealed. *Proc Natl Acad Sci USA* **94**, 11-4 (1997).

Kripke, M.L., Cox, P.A., Alas, L.G. and Yarosh, D.B. Pyrimidine dimers in DNA initiate systemic immunosuppression in UV-irradiated mice. *Proc Natl Acad Sci USA* **89**, 7516-20 (1992).

Kuchel, J.M., Barnetson, R.S. and Halliday, G.M. Nitric oxide appears to be a mediator of solar-simulated ultraviolet radiation-induced immunosuppression in humans. *J Invest Dermatol* **121**, 587-93 (2003).

Kuerbitz, S.J., Plunkett, B.S., Walsh, W.V. and Kastan, M.B. Wild-type p53 is a cell cycle checkpoint determinant following irradiation. *Proc Natl Acad Sci USA* **89**, 7491-5 (1992).

Kulaksiz, G., Reardon, J.T. and Sancar, A. Xeroderma pigmentosum complementation group E protein (XPE/DDB2): purification of various complexes of XPE and analyses of their damaged DNA binding and putative DNA repair properties. *Mol Cell Biol* **25**, 9784-92 (2005).

Lane, D.P. p53, guardian of the genome. *Nature* **358**, 15-6 (1992).

Leadon, S.A. and Cooper, P.K. Preferential repair of ionising radiation-induced damage in the transcribed strand of an active human gene is defective in Cockayne syndrome. *Proc Natl Acad Sci USA* **90**, 10499-503 (1993).

Lehmann, A.R. The xeroderma pigmentosum group D (XPD) gene: one gene, two functions, three diseases. *Genes and Dev* **15**, 15-23 (2001).

Lehmann, A.R. Translesion synthesis in mammalian cells. *Exp Cell Res* **312**, 2673-6 (2006).

Li, J., Farthing, P.M. and Thornhill, M.H. Oral and skin keratinocytes are stimulated to secrete monocyte chemoattractant protein-1 by tumour necrosis factor alpha and interferon gamma. *J Oral Pathol Med* **29**, 438-44 (2000).

Li, R., Waga, S., Hannon, G.J., Beach, D. and Stillman, B. Differential effects by the p21 CDK inhibitor on PCNA-dependent DNA replication and repair. *Nature* **371**, 534-7 (1994).

Lin, Q., Clark, A.B., McCulloch, S.D., Yuan, T., Bronson, R.T., Kunkel, T.A. and Kucherlapati, R. Increased susceptibility to UV-induced skin carcinogenesis in polymerase eta-deficient mice. *Cancer Res* **66**, 87-94 (2006).

Lingner, J., Hughes, T.R., Shevchenko, A., Mann, M., Lundblad, V. and Cech, T.R. Reverse transcriptase motifs in the catalytic subunit of telomerase. *Science* **276**, 561-7 (1997).

Lu, Y.P., Lou, Y.R., Li, X.H., Xie, J.G., Brash, D., Huang, M.T. and Conney, A.H. Stimulatory effect of oral administration of green tea or caffeine on ultraviolet light-induced increases in epidermal wild-type p53, p21(WAF1/CIP1), and apoptotic sunburn cells in SKH-1 mice. *Cancer Res* **60**, 4785-91 (2000).

Lu, Y.P., Lou, Y.R., Xie, J.G., Peng, Q.Y., Zhou, S., Lin, Y., Shih, W.J. and Conney, A.H. Caffeine and caffeine sodium benzoate have a sunscreen effect, enhance UVB-induced apoptosis, and inhibit UVB-induced skin carcinogenesis in SKH-1 mice. *Carcinogenesis* **Ahead of print**(2006).

Lucas, R.M., Repacholi, M.H. and McMichael, A.J. Is the current public health message on UV exposure correct? *Bull World Health Organ* **84**, 485-91 (2006).

Ma, L., Siemssen, E.D., Noteborn, H.M. and van der Eb, A.J. The xeroderma pigmentosum group B protein ERCC3 produced in the baculovirus system exhibits DNA helicase activity. *Nucleic Acids Res* **22**, 4095-102 (1994).

Mallikarjuna, G., Dhanalakshmi, S., Singh, R.P., Agarwal, C. and Agarwal, R. Silibinin protects against photocarcinogenesis via modulation of cell cycle regulators, mitogen-activated protein kinases, and Akt signaling. *Cancer Res* **64**, 6349-56 (2004).

Masutani, C., Araki, M., Sugasawa, K., van der Spek, P., Yamada, A., Uchida, A., Maekawa, T., Bootsma, D., Hoeijmakers, J.H.J. and Hanaoka, F. Identification and characterisation of XPC-binding domain of hHR23B. *Mol Cell Biol* **17**, 6915-23 (1997).

Masutani, C., Kusumoto, R., Yamada, A., Dohmae, M., Yokoi, M., Yuasa, M., Araki, M., Iwai, S., Takio, K. and Hanaoka, F. The XPV (seroderma pigmentosum variant) gene encodes human DNA polymerase eta. *Nature* **399**, 700-4 (1999).

McLoone, P., Woods, G.M. and Norval, M. Decrease in Langerhans cell and increase in lymph node dendritic cells following chronic exposure of mice to suberythemal doses of solar simulated radiation. *Photochem Photobiol* **81**, 1186-73 (2005).

McWhir, J., Selfridge, J., Harrison, D.J., Squires, S. and Melton, D.W. Mice with DNA repair gene (ERCC-1) deficiency have elevated levels of p53, liver nuclear abnormalities and die before weaning. *Nature Genetics* **5**, 217-24 (1993).

Mellon, I. Transcription-coupled repair: a complex affair. *Mutat Res* **577**, 155-61 (2005).

Mirchandani, K.D. and D'Andrea, A.D. The Fanconi anaemia/BRCA pathway: A coordinator of cross-link repair. *Exp Cell Res* **312**, 2647-53 (2006).

Miyauchi-Hashimoto, H., Tanaka, K. and Horio, T. Enhanced inflammation and immunosuppression by ultraviolet radiation in xeroderma pigmentosum group A (XPA) model mice. *J Invest Dermatol* **107**, 343-8 (1996).

Miyauchi-Hashimoto, H., Kuwamoto, K., Urade, Y., Tanaka, K. and Horio, T. Carcinogen induced inflammation and immunosuppression are enhanced in xeroderma pigmentosum group A model mice associated with hyperproduction of prostaglandin E2. *Journal of Immunology* **166**, 5783-91 (2001).

Mizuno, K., Okamoto, H. and Horio, T. Ultraviolet B radiation suppresses endocytosis, subsequent maturation, and migration activity of Langerhans cell-like dendritic cells. *J Invest Dermatol* **122**, 300-6 (2004).

Molenda, M., Mukkamala, L. and Blumenberg, M. Interleukin IL-12 blocks a specific subset of the transcriptional profile responsive to UVB in epidermal keratinocytes. *Mol Immunol* **43**, 1933-40 (2006).

Moloney, F.J., Comber. H., O'Lorcain, P., O'Kelly, P., Conlon, P.J. and Murphy, G.M. A population based study of skin cancer incidence and prevalence in renal transplant recipients. *Br J Dermatology* **154**, 498-504 (2006).

Moodycliffe, A.M., Kimber, I. and Norval, M. Role of tumour necrosis factor alpha in ultraviolet B light induced dendritic cell migration and suppression of contact hypersensitivity. *Immunology* **81**, 79-84 (1994).

Moodycliffe, A.M., Ngiem, D., Clydesdale, G. and Ullrich, S.E. Immune suppression and skin cancer development: regulation by NKT cells. *Nature Immunology* **1**, 521-5 (2000).

Mu, D., Hsu, D.S. and Sancar, A. Reaction mechanism of human DNA repair excision nuclease. *J Biol Chem* **271**, 8285-94 (1996).

Murai, M., Enokido, Y., Inamura, N., Yoshino, M., Nakatsu, Y., van der Horst, G.T.,Hoeijmakers, J.H., Tanaka, K. and Hatanaka, H. Early postnatal ataxia and abnormal cerebellar development in mice lacking Xeroderma pigmentosum Group A and Cockayne syndrome Group B DNA repair genes. *Proc Natl Acad Sci USA* **98**, 13379-84 (2001).

Nagy, A. Cre recombinase: the universal reagent for genome tailoring. *Genesis* **26**, 99-109 (2000).

Nakamura, M., Sundberg, J.P. and Paus, R. Mutant laboratory mice with abnormalities in hair follicle morphogenesis, cycling, and/or structure: annotated tables. *Exp Dermatol* **10**, 369-90 (2001).

Nakane, H., Takeuchi, S., Yuba, S., Saijo, M., Nakatsu, Y., Murai, H., Nakatsuru, Y., Ishikawa, T., Hirota, S., Kitamura, Y., Kato, Y., Tsunoda, Y., Miyauchi, H., Horio, T., Tokunaga, T., Matsunaga, T., Nikaido, O., Nishimune, Y., Okada, Y. and Tanaka, K. High incidence of ultraviolet B or chemical carcinogen induced skin tumours in mice lacking the xeroderma pigmentosum group A gene. *Nature* **377**, 165-8 (1995).

Newbery, H.J., Gillingwater, T.H., Dharmasaroja, P., Peters, J., Wharton, S.B., Thomson, D., Ribchester, R.R. and Abbott, C.M. Progressive loss of motor neuron function in wasted mice: Effects of a spontaneous null mutation in the gene for the eEF1A2 translation factor. *J Neuropathol Exp Neurol* **64**, 295-303 (2005).

Ng, J.M., Vrieling, H., Sugasawa, K., Ooms, M.P., Grootegoed, J.A., Vreeburg, J.T., Visser, P., Beems, R.B., Gorgels, T.G., Hanaoka, F., Hoeijmakers, J.H. and van der Horst, G.T. Developmental defects and male sterility in mice lacking the ubiquitin-like DNA repair gene mHR23B. *Mol Cell Biol* **22**, 1233-45 (2002).

Ng, J.M., Vermeulen, W., van der Horst, G.T., Bergink, S., Sugasawa, K., Vrieling, H. and Hoeijmakers, J.H. A novel regulation mechanism of DNA repair by damage-induced and RAD23-dependent stabilisation of xeroderma pigmentosum group C protein. *Genes and Dev* **17**, 1630-45 (2003).

Nguyen, Q.T., Parsadanian, A.S., Snider, W.D. and Lichtman, J.W. Hyperinnervation of neuromuscular junctions caused by GDNF overexpression in muscle. *Science* **279**, 1725-9 (1998).

Nichols, A.F., Itoh, T., Graham, J.A., Liu, W., Yamaizumi, M. and Linn, S. Human damage-specific DNA-binding protein p48. Characterisation of XPE mutations and regulation following UV irradiation. *J Biol Chem* **275**, 21422-8 (2000).

Niedernhofer, L.J., Essers, J., Weeda, G., Beverloo, B., de Wit, J., Muijtjens, M., Odijk, H., Hoeijmakers, J.H. and Kanaar, R. The structure-specific endonuclease Ercc1-Xpf is required for targeted gene replacement in embryonic stem cells. *EMBO J* **20**, 6540-9 (2001).

Niedernhofer, L.J., Lalai, A.S. and Hoeijmakers, J.H.J. Fanconi Anaemia (Cross)linked to DNA repair. *Cell* **123**, 1191-8 (2005).

Niedernhofer, L.J., Odijk, H., Budzowska, M., van Drunen, E., Maas, A., Theil, A.F., de Wit, J., Jaspers, N.G., Beverloo, H.B., Hoeijmakers, J.H. and Kanaar, R.The structure-specific endonuclease Ercc1-Xpf is required to resolve DNA interstrand cross-link-induced double-strand breaks. *Mol Cell Biol* **24**, 5776-87 (2004).

Nishigori, C., Yarosh, D.B., Ullrich, S.E., Vink, A.A., Bucana, C.D., Roza, L. Kripke, M.L. Evidence that DNA damage triggers interleukin-10 cytokine production in UV-irradiated murine keratinocytes. *Proc Natl Acad Sci U S A* **93**, 10354-9 (1996).

Norval, M. Effects of solar radiation on the human immune system. *J Photochem Photobiol B* **63**, 28-40 (2001).

Norval, M. Immunosuppression induced by ultraviolet radiation: relevance to public health. *Bull World Health Organ* **80**, 906-7 (2002).

Norval, M. The mechanisms and consequences of ultraviolet induced immunosuppression. *Prog Biophys Mol Biol* **92**, 108-18 (2006).

Nouspikel, T. DNA repair in differentiated cells: Some new answers to old questions. *Neuroscience* **Epub ahead of print**(2006).

O'Donovan, A., Davies, A.A., Moggs, J.G., West, S.C. and Woods, R.D. XPG endonuclease makes the 3' incision in human DNA nucleotide excision repair. *Nature* **371**, 432-5 (1994).

Obata, M. and Tagami, H. Alteration in murine epidermal Langerhans cell population by various UV irradiations: quantitative and morphologic studies on the effects of various wavelengths of monochromatic radiation on Ia-bearing cells. *J Invest Dermatol* **84**, 139-45 (1985).

Pang, T.Y., Stam, N.C., Nithianantharajah, J., Howard, M.L. and Hannan, A.J. Differential effects of voluntary physical exercise on behavioral and brain-derived neurotrophic factor expression deficits in Huntington's disease transgenic mice. *Neuroscience* **141**, 569-84 (2006).

Pedeux, R., Al-Irani, N., Marteau, C., Pellicier, F., Branche, R., Ozturk, M., Franchi, J. and Dore, J-F. Thymidine dinucleotides induce S phase cell cycle arrest in addition to increased melanogenesis in human melanocytes. *J Invest Dermatol* **111**, 472-7 (1998).

Pennisi, D., Gardner, J., Chambers, D., Hosking, B., Peters, J., Muscat, G., Abbott, C. and Koopman, P. Mutations in Sox18 underlie cardiovascular and hair follicle defects in ragged mice. *Nat Genet* **24**, 434-7 (2000a).

Pennisi, D., Bowles, J., Nagy, A., Muscat, G. and Koopman, P. Mice null for Sox18 are viable and display a mild coat defect. *Mol Cell Biol* **20**, 9331-6 (2000b).

Petersen, A.B., Na, R. and Wulf, H.C. Sunless skin tanning with dihydroxyacetone delays broad-spectrum ultraviolet photocarcinogenesis in hairless mice. *Mutat Res* **542**, 129-38 (2003).

Petersen, A.B., Wulf, H.C., Gniadecki, R. and Gajkowska, B. Dihydroxyacetone, the active browning ingredient in sunless tanning lotions, induces DNA damage, cell-cycle block and apoptosis in cultured HaCaT keratinocytes. *Mutat Res* **560**, 173-86 (2004).

Petit-Frere, C., Clingen, P.H., Grewe, M., Krutmann, J., Roza, L., Arlett, C.F. and Green, M.H. Induction of interleukin-6 production by ultraviolet radiation in normal human epidermal keratinocytes and in a human keratinocyte cell line is mediated by DNA damage. *J Invest Dermatol* **111**, 354-9 (1998).

Petit-Frere, C., Capulas, E., Lowe, J.E., Koulu, L., Marttila, R.J., Jaspers, N.G., Clingen, P.H., Green, M.H. and Arlett, C.F. Ultraviolet B induced apoptosis and cytokine release in xeroderma pigmentosum keratinocytes. *J Invest Dermatol* **115**, 687-93 (2000).

Prasher, J.M.L., A.S., Heijmans-Antonissen, C., Ploemacher, R.E., Hoeijmakers, J.H.J., Touw, I.P. and Niedernhofer, L.J. Reduced haematopoietic reserves in DNA interstrand crosslink repair-deficient Ercc1-/- mice. *EMBO J* **24**, 861-71 (2005).

Puri, N., Eller, M.S., Byers, H.R., Dykstra, S., Kubera, J. and Gilchrest, B.A. Telomere based DNA damage responses: a new approach to melanoma. *FASEB J* **18**, 1373-81 (2004).

Quevedo Jnr, W.C., Holstein, T.J., Dyckman, J., McDonald, C.J. and Isaacson, E.L. Inhibition of UVR induced tanning and immunosuppression by topical applications of vitamins C and E to the skin of hairless (hr/hr) mice. *Pigment Cell Res* **13**, 89-98 (2000).

Ramirez, A., Page, A., Gandarillas, A., Zanet, J., Pibre, S., Vidal, M., Tusell, L., Genesca, A., Whitaker, D.A., Melton, D.W. and Jorcano, J.L. A keratin K5Cre transgenic line appropriate for tissue specific or generalised Cre mediated recombination. *Genesis* **39**, 52-7 (2004).

Rapic-Otrin, V., Navazza, V., Nardo, T., Botta, E., McLenigan, M., Bisi, D.C., Levine, A.S. and Stefanini, M. True XP group E patients have a defective UV-damaged DNA binding protein complex and mutations in DDB2 which reveal the functional domains of its p48 product. *Hum Mol Genet* **12**, 1507-22 (2003).

Reardon, J.T., Bessho, T., Kung, H.C., Bolton, P.H. and Sancar, A. In vitro repair of oxidative DNA damage by human nucleotide excision repair system: possible explanation for neurodegeneration in xeroderma pigmentosum patients. *Proc Natl Acad Sci USA* **94**, 9463-8 (1997).

Rivas, J.M. and Ullrich, S.E. Systemic suppression of delayed type hypersensitivity by supernatants from UV irradiated keratinocytes. An essential role for IL-10. *J Immunol* **149**, 3865-71 (1992).

Russo, P.A.J. and Halliday, G.M. Inhibition of nitric oxide and reactive oxygen species production improves the ability of a sunscreen to protect from sunburn, immunosuppression and photocarcinogenesis. *Br J Dermatol* **155**, 408-15 (2006).

Sancar, A. Excision repair in mammalian cells. *J Biol Chem* **270**, 15915-8 (1995).

Sancar, A. DNA excision repair. *Annu Rev Biochem* **65**, 43-81 (1996).

Sands, A.T., Abuin, A., Sanchez, A., Conti, C.J. and Bradley, A. High susceptibility to ultraviolet induced carcinogenesis in mice lacking XPC. *Nature* **377**, 162-5 (1995).

Sargent, R.G., Meservy, J.L., Perkins, B.D., Kilburn, A.E., Intody, Z., Adair, G.M., Nairn, R.S. and Wilson, J.H. Role of the nucleotide excision repair gene ERCC1 in formation of recombination-dependent rearrangements in mammalian cells. *Nucleic Acids Res* **28**, 3771-8 (2000).

Schade, N., Esser, C. and Krutmann, J. Ultraviolet B radiation induced immunosuppression: molecular mechanisms and cellular alterations. *Photochem Photobiol* **4**, 699-708 (2005).

Schwarz, A., Stander, S., Berneburg, M., Bohm, M., Kulms, D., van Steeg, H., Grosse-Heitmeyer, K., Krutmann, J. and Schwarz, T. Interleukin-12 suppresses ultraviolet radiation induced apoptosis by inducing DNA repair. *Nature Cell Biology* **4**, 26-31 (2002).

Schwarz, A., Maeda, A., Wild, M.K., Kernbeck, K., Gross, N., Arangane, Y., Beissert, S., Vestweber, D. and Schwarz, T. Ultraviolet radiation induced regulatory T cells not only inhibit the induction but can suppress the effectro phase of contact hypersensitivity. *J Immunol* **172**(2004).

Schwarz, T. Ultraviolet radiation-induced tolerance. *Allergy* **54**, 1252-61 (1999).

Selfridge, J., Pow, A.M., McWhir, J., Magin, T.M. and Melton, D.W. Gene targeting using a mouse HPRT minigene/HPRT-deficient embryonic stem cell system: inactivation of the mouse ERCC-1 gene. *Somat Cell Mol Genet* **18**, 325-36 (1992).

Selfridge, J. PhD thesis, University of Edinburgh (1999).

Selfridge, J., Hsia, K.T., Redhead, N.J. & Melton, D.W. Correction of liver dysfunction in DNA repair-deficient mice with an ERCC1 transgene. *Nucleic Acids Res* **29**, 4541-50 (2001).

Seroz, T., Perez, C., Bergmann, E., Bradsher, J. and Egly, J-M. p44/SSL1, the regulatory subunit of the XPD/RAD3 helicase, plays a crucial role in the transcriptional activity of TFIIH. *J Biol Chem* **275**, 33260-6 (2000).

Shay, J.W. and Wright, W.E. Telomerase therapeutics for cancer: challenges and new directions. *Nat Rev Drug Discov* **5**, 577-84 (2006).

Shreedhar, V., Giese, T., Sung, V.W. and Ullrich, S.E. A cytokine cascade including prostaglandin E2, IL-4 and IL-10 is responsible for UV induced systemic immune suppression. *J Immunol* **160**, 3783-9 (1998).

Sijbers, A.M., de Laat, W.L., Ariza, R.R., Biggerstaff, M., Wei, Y.F., Moggs, J.G., Carter, K.C., Shell, B.K., Evans, E., de Jong, M.C., Rademakers, S., de Rooij, J., Jaspers, N.G., Hoeijmakers, J.H. and Wood, R.D. Xeroderma pigmentosum group F caused by a defect in a structure-specific DNA repair endonuclease. *Cell* **86**, 811-22 (1996).

Simon, J.C., Cruz Jnr, P.D., Bergstresser, P.R. and Tigelaar, R.E. Low dose ultraviolet B irradiated Langerhans cells preferentially activate CD4+ cells of the T helper 2 subset. *J Immunol* **145**, 2087-91 (1990).

Smogorzewska, A. and de Lange, T. Different telomere damage signaling pathways in human and mouse cells. *EMBO J* **21**, 4338-48 (2002).

Snellman, E., Strozyk, M., Segerback, D., Klimenko, T. and Hemminki, K. Effect of the spectral range of a UV lamp on the production of cyclobutane dimers in human skin in situ. *Photoderm Photoimmunol Photomed* **19**, 281-6 (2003).

Specht, C.G. and Schoepfer, R. Deletion of the alpha-synuclein locus in a subpopulation of C57BL/6J inbred mice. *BMC Neurosci* **2**, Epub (2001).

Sun, X.Z., Harada, Y.N., Takahashi, S., Shiomi, N. and Shiomi, T. Purkinje cell degeneration in mice lacking the xeroderma pigmentosum group G gene. *J Neurosci Res* **64**, 348-54 (2001).

Sundberg, J.P. and King, L.E. Jnr. Morphology of hair in normal and mutant laboratory mice. *Eur J Dermatol* **11**, 357-61 (2001).

Sung, P., Bailly, V., Weber, C., Thompson, L.H., Prakash, L. and Prakash, S. Human xeroderma pigmentosum group D gene encodes a DNA helicase. *Nature* **365**, 852-5 (1993).

Tanaka, K., Miura, N., Satokata, I., Miyamoto, I., Yoshida, M.C., Satoh, Y., Kondo, S., Yasui, A., Okayama, H. and Okada, Y. Analysis of a human DNA excision repair gene involved in group A xeroderma pigmentosum and containing a zinc finger domain. *Nature* **348**, 73-6 (1990).

Tangpricha, V., Turner, A., Spina, C., Decastro, S., Chen, T.C. and Holick, M.F. Tanning is associated with optimal vitamin D status (serum 25-hydroxyvitamin D concentration) and higher bone mineral density. *Am J Clin Nutr* **80**, 1645-9 (2004).

Teunissen, M.B.M., Piskin, G., di Nuzzo, S., Sylva-Steenland, R.M.R., de Rie, M.A. and Bos, J.D. Ultraviolet B radiation induces a transient appearance of IL-4+ neutrophils, which support the development of Th2 responses. *J Immunol* **168**, 3732-9 (2002).

Thaung, C., Arnold, K., Jackson, I.J. and Coffey, P.J. Presence of visual head tracking differentiates normal sighted from retinal degenerate mice. *Neurosci Lett* **325**, 21-4 (2002).

Thompson, L.H. and Schild, D. Recombinational repair and human disease. *Mutat Res* **509**, 49-78 (2002).

Thorel, F., Constantinou, A., Dunand-Sauthier, I., Nouspikel, T., Lalle, P., Raams, A., Jaspers, N.G., Vermeulen, W., Shivji, M.K., Wood, R.D. and Clarkson, S.G. Definition of a short region of XPG necessary for TFIIH interaction and stable recruitment to sites of UV damage. *Mol Cell Biol* **24**, 10670-80 (2004).

Tian, M., Shinkura, R., Shinkura, N. and Alt, F.W. Growth retardation, early death, and DNA repair defects in mice deficient for the nucleotide excision repair enzyme XPF. *Mol Cell Biol* **24**, 1200-5 (2004).

Toews, G.B., Bergstresser, P.R. and Streilein, J.W. Epidermal Langerhans cell density determines whether contact hypersensitivity or unresponsiveness follows skin painting with DNFB. *J Immunol* **124**, 445-57 (1980).

Tremeau-Bravard, A., Perez, C. and Egly, J-M. A role of the c-terminal part of p44 in the promoter escape activity of transcription factor IIH. *J Biol Chem* **276**, 27693-7 (2001).

Tripsianes, K., Folkers, G., Eiso, A.B., Das, D., Odijk, H., Jaspers, N.G.J., Hoeijmakers, J.H.J., Kaptein, R. and Beiens, R. The structure of the human ERCC1/XPF interaction domains reveals a complimentary role for the two proteins in nucleotide excision repair. *Structure* **13**, 1849-58 (2005).

van der Horst, G.T., van Steeg, H., Berg, R.J., van Gool, A.J., de Wit, J., Weeda, G., Morreau, H., Beems, R.B., van Kreijl, C.F., de Gruijl, F.R., Bootsma, D. and Hoeijmakers, J.H. Defective transcription coupled repair in Cockayne syndrome B mice is associated with skin cancer predisposition. *Cell* **89**, 425-35 (1997).

van der Horst, G.T., Meira, L., Gorgels, T.G., de Wit, J., Velasco-Miguel, S., Richardson, J.A., Kamp, Y., Vreeswijk, M.P., Smit, B., Bootsma, D., Hoeijmakers, J.H. and Friedberg, E.C. UVB radiation-induced cancer predisposition in Cockayne syndrome group A (Csa) mutant mice. *DNA Repair* **1**, 143-57 (2002).

van der Wees, C., Jansen, J., Vrieling, H., van der Laarse, A., Van Zeeland, A. and Mullenders, L. Nucleotide excision repair in differentiated cells. *Mutat Res* **Epub ahead of print**(2006).

van Gool, A.J., Citterio, E., Rademakers, S., van Os, R., Vermeulen, W., Constantinou, A., Egly, J.M., Bootsma, D. and Hoeijmakers, J.H.J. The Cockayne syndrome B protein, involved in transcription-coupled DNA repair, resides in an RNA polymerase II containing complex. *EMBO J* **16**, 5955-65 (1997).

van Schanke, A., Jongsma, M.J. Bisschop, R., van Venrooij, G.M., Rebel, H. and de Gruijl, F.R. Single UVB overexposure stimulates melanocyte proliferation in murine skin, in contrast to fractionated or UVA-1 exposure. *J Invest Dermatol* **124**, 241-7 (2005).

Venema, J., van Hoffen, A., Natarajan, A.T., van Zeeland, A.A. and Mullenders, L.H.F. The residual repair capacity of xeroderma pigmentosum complementation group C fibroblasts is highly specific for transcriptionally active DNA. *Nucleic Acids Res* **18**, 443-8 (1990a).

Venema, J., Mullenders, L.H.F., Natarajan, A.T., van Zeeland, A.A. and Mayne, L.V. The genetic defect in Cockayne syndrome is associated with a defect in repair of UV induced DNA damage in transcriptionally active DNA. *Proc Natl Acad Sci USA* **87**, 4707-11 (1990b).

Vink, A.A., Strickland, F.M., Bucana, C., Cox, P.A., Roza, L., Yarosh, D.B. and Kripke, M.L. Localisation of DNA damage and its role in altered antigen-presenting cell function in ultraviolet-irradiated mice. *J Exp Med* **183**, 1491-500 (1996).

Virador, V.M., Muller, J., Wu, X., Abdel-Malek, Z.A., Yu, Z.X., Ferrans, V.J., Kobayashi, N., Wakamatsu, K., Ito, S., Hammer, J.A. and Hearing, V.J. Influence of alpha-melanocyte-stimulating hormone and ultraviolet radiation on the transfer of melanosomes to keratinocytes. *FASEB J* **16**, 105-7 (2002).

Vogelstein, B. and Kinzler, K.W. *The genetic basis of human cancer*, (McGraw-Hill, 1998).

Volker, M., Mone, M.J., Karmakar, P., van Hoffen, A., Schul, W., Vermeulen, W.,Hoeijmakers, J.H., van Driel, R., van Zeeland, A.A. and Mullenders, L.H. Sequential assembly of the nucleotide excision repair factors in vivo. *Mol Cell* **8**, 213-24 (2001).

Wagner, N., Wagner, K.D., Scholz, H., Kirschner, K.M. and Schedl, A. Intermediate filament protein nestin is expressed in developing kidney and heart and might be regulated by the Wilms' tumor suppressor Wt1. *Am J Physiol Regul Integr Comp Physiol* **291**, R779-87 (2006).

Webb, A.R. and Engelsen, O. Calculated ultraviolet exposure levels for a healthy vitamin D status. *Photochem Photobiol* **Sept Epub ahead of print**(2006).

Weeda, G., Donker, I., de Wit, J., Morreau, H., Janssens, R., Vissers, C.J., Nigg, A., van Steeg, H., Bootsma, D. and Hoeijmakers, J.H.J. Disruption of mouse ERCC1 results in a novel repair syndrome with growth failure, nuclear abnormalities and senescence. *Curr Biol* **7**, 427-39 (1997).

Weeda, G., Broekhof, J.L.M., de Wit, J. and Hoeijmakers, J.H.J. Lethal and viable targeted mutations in the basal transcription/DNA repair helicase Xpb: a mouse model for the human repair disorder xeroderma pigmentosum. *In preparation* (2006).

Weinstock, M.A. and Lazowich, D. Tanning and vitamin D status. *Am J Clin Nutr* **82**, 707 (2005).

Wijnhoven, S.W., Beems, R.B., Roodbergen, M., van den Berg, J., Lohman, P.H., Diderich, K., van der Horst, G.T., Vijg, J., Hoeijmakers, J.H. and van Steeg, H. Accelerated aging pathology in ad libitum fed Xpd(TTD) mice is accompanied by features suggestive of caloric restriction. *DNA Repair* **4**, 1314-24 (2005).

Wijnhoven, S.W.P., Hoogervorst, E.M., de Waard, H., van der Horst, G.T.J. and van Steeg, H. Tissue specific mutagenic and carcinogenic responses in NER defective mouse models. *Mutat Res* **Currently in print**(2006).

Wishart, T.M., Parson, S.H. and Gillingwater, T.H. Synaptic vulnerability in neurodegenerative diseases. *J Neuropathol Exp Neurol* **65**, 733-9 (2006).

Wold, M.S. and Kelly, T. Purification and characterisation of replication protein A, a cellular protein required for in vitro replication of simian virus 40 DNA. *Proc Natl Acad Sci USA* **85**, 2523-7 (1988).

Yaar, M. and Gilchrest, B. Melanocyte biology: before, during, and after the Fitzpatrick era. *J Invest Dermatol* **122**, xxvii-xxix (2004).

Yarosh, D., Klein, J., O'Connor, A., Hawk, J., Rafal, E. and Wolf, P. Effect of topically applied T4 endonuclease V in liposomes on skin cancer in xeroderma pigmentosum: a randomised study. *The Lancet* **357**, 926-9 (2001).

Yoon, T., Chakrabortty, A., Franks, R., Valli, T., Kiyokawa, H. and Raychaudhuri, P. Tumor-prone phenotype of the DDB2-deficient mice. *Oncogene* **24**, 469-78 (2005).

Yuen, K.S., Nearn, M.R. and Halliday, G.M. Nitric Oxide mediated depletion of Langerhans cells from the epidermis may be involved in UVA radiation induced immunosuppression. *Nitric Oxide: Biology and Chemistry* **6**, 313-8 (2002).

Oncogene (2006), 1–10

www.nature.com/onc

ORIGINAL ARTICLE

Mice with skin-specific DNA repair gene (*Ercc1*) inactivation are hypersensitive to ultraviolet irradiation-induced skin cancer and show more rapid actinic progression

J Doig[1], C Anderson[2], NJ Lawrence[1], J Selfridge[1], DG Brownstein[3] and DW Melton[1]

[1]*Sir Alastair Currie Cancer Research UK Laboratories, Molecular Medicine Centre, University of Edinburgh, Western General Hospital, Edinburgh, UK;* [2]*Department of Pathology, Royal Infirmary of Edinburgh, 51 Little France Crescent, Edinburgh, UK and* [3]*Research Animal Pathology Core Laboratory, Queen's Medical Research Institute, University of Edinburgh, Edinburgh, UK*

***Ercc1* has an essential role in the nucleotide excision repair (NER) pathway that protects against ultraviolet (UV)-induced DNA damage and is also involved in additional repair pathways. The premature death of simple *Ercc1* mouse knockouts meant that we were unable to study the role of *Ercc1* in the skin. To do this, we have used the Cre–lox system to generate a skin-specific *Ercc1* knockout. With a Cre transgene under control of the bovine keratin 5 promoter we achieved 100% recombination of the *Ercc1* gene in the epidermis. Hairless mice with *Ercc1*-deficient skin were hypersensitive to the short-term effects of UV irradiation, showing a very low minimal erythemal dose and a dramatic hyperproliferative response. Ultraviolet-irradiated mice with *Ercc1*-deficient skin developed epidermal skin tumours much more rapidly than controls. These tumours appeared to arise earlier in actinic progression and grew more rapidly than tumours on control mice. These responses are more pronounced than have been reported for other NER-deficient mice, demonstrating that *Ercc1* has a key role in protecting against UV-induced skin cancer.**

Oncogene advance online publication, 08 May 2006; doi:10.1038/sj.onc.1209642

Keywords: Ercc1; nucleotide; excision repair; skin cancer; ultraviolet irradiation

Introduction

The nucleotide excision repair (NER) pathway has evolved to deal primarily with ultraviolet (UV)-induced DNA damage. In man, the lack of a functional NER pathway has severe consequences, principally a 1000-fold increased incidence of skin cancer. This, among other features, is a characteristic of the human inherited NER deficiency disease, xeroderma pigmentosum (reviewed by Friedberg, 2001). ERCC1 plays an essential role in the NER pathway, acting as an endonuclease, in conjunction with XPF, to make the 5′ incision at the lesion site. *Ercc1* is essential for NER, but is also involved in homologous recombination, double-strand break repair and the repair of interstrand crosslinks (discussed by Chipchase and Melton, 2002). Elevated levels of the commonest oxidized base, 8-oxoguanine, in *Ercc1*-deficient tissues also implicate *Ercc1* in the repair of oxidative DNA damage (Selfridge *et al.*, 2001; Hsia *et al.*, 2003). Unlike the situation for many of the NER genes, there are no known cases of ERCC1 deficiency in man, suggesting that this mutation may be an embryonic lethal, perhaps because of the additional repair functions of the gene. To investigate the role of *Ercc1* in mice, we targeted the gene and found that *Ercc1*-deficient animals were born severely runted and died by 3 weeks of age with liver failure (McWhir *et al.*, 1993). We found a novel phenotype, with the development of premature hepatocyte polyploidy, that was more reminiscent of a premature ageing disorder than an NER deficiency disease (Nunez *et al.*, 2000). The liver phenotype was corrected by an *Ercc1* transgene controlled by a liver-specific gene promoter, but liver-corrected nulls now died by 12 weeks of age with kidney and additional abnormalities (Selfridge *et al.*, 2001).

The premature death of *Ercc1* knockouts meant that we were unable to study the role of *Ercc1* in the skin. To do this, we have utilized the Cre–lox system (reviewed by Kuhn and Torres, 2002) to produce a skin-specific *Ercc1* knockout mouse. We have generated a mouse line that has *loxP* sites inserted into its *Ercc1* gene (floxed *Ercc1*) to mark it for subsequent inactivation. To achieve *Ercc1* gene inactivation, we used a transgenic line where Cre recombinase is under the control of the promoter from the bovine keratin 5 (K5) gene (Ramirez *et al.*, 2004). Expression from this promoter is largely restricted to the basal layer of stratified epithelia (Ramirez *et al.*, 1994).

Simple knockout mice for the NER genes *Xpa*, *Xpc* and *Csb* have been produced (de Vries *et al.*, 1995; Nakane *et al.*, 1995; Sands *et al.*, 1995; van der Horst *et al.*, 1997). These mice are viable and, although the

Correspondence: Professor DW Melton, Sir Alastair Currie Cancer Research UK Laboratories, Molecular Medicine Centre, University of Edinburgh, Western General Hospital, Crewe Road, Edinburgh EH4 2XU, UK.
E-mail: David.Melton@ed.ac.uk
Received 6 January 2006; revised 7 March 2006; accepted 20 March 2006

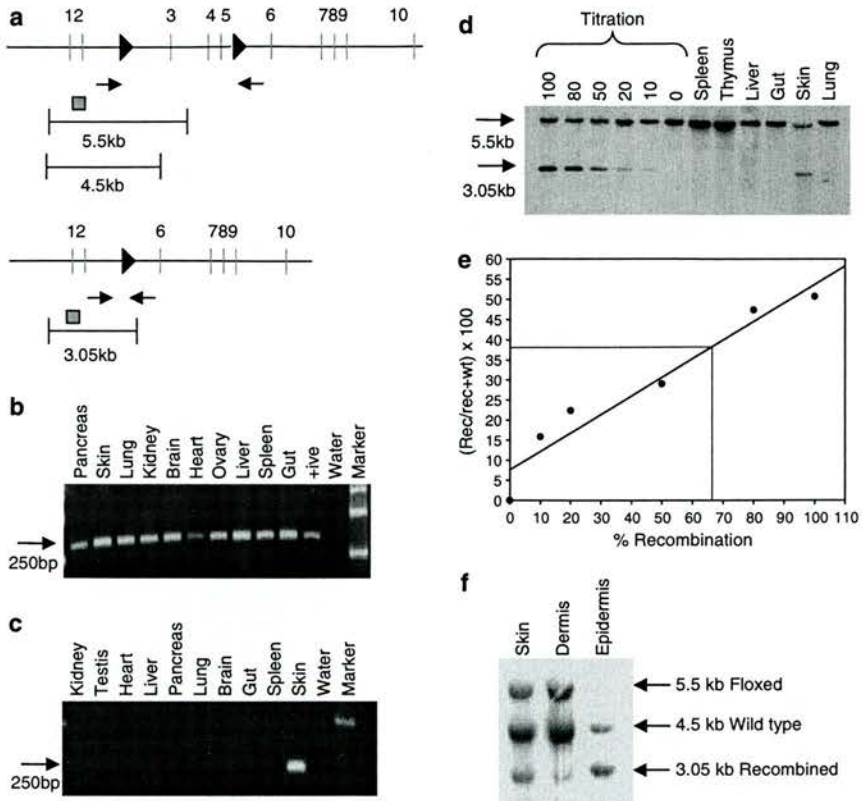

Figure 1 Skin-specific and constitutive recombination of the *Ercc1* floxed allele. (**a**) Schematic representation of floxed and recombined *Ercc1* alleles. *Ercc1* exons are numbered. The grey squares represent the probe used in Southern blots to distinguish the floxed (5.5 kb *EcoRI* fragment) and wild-type alleles (5.5 or 4.5 kb fragment depending on the presence of a polymorphic *EcoRI* site in intron 2 in the wild-type allele of our mice) from the recombined allele (3.05 kb fragment). See Supplementary Information Figure 1 for the location of this *EcoRI* polymorphism. Small arrows represent the positions of the polymerase chain reaction (PCR) primers used to detect the recombined allele. Large arrowheads represent *loxP* sites. (**b**) Constitutive recombination in $Ercc1^{flox/+}$ with $K5Cre^{M}$ mice detected by PCR analysis. DNA from the tissues indicated, showing the 250 bp PCR product, diagnostic for recombination of the floxed allele, in all tissues. (**c**) Skin-specific recombination in $Ercc1^{flox/+}$ mice with K5Cre fathers detected by PCR analysis. (**d**) Skin-specific recombination in $Ercc1^{flox/+}$ with $K5Cre^{P}$ mice detected by quantitative Southern analysis. DNA (10 μg) from the tissues indicated was digested with *EcoRI* alongside a titration curve with the indicated levels of recombination. The probe used is indicated above. The 5.5 kb band is from the wild-type (and floxed) alleles, and the 3.05 kb band is from the recombined allele. (**e**) Estimate of skin-specific recombination in $Ercc1^{flox/+}$ with $K5Cre^{P}$ mice. The intensity of the bands from the wild-type (and floxed) and recombined alleles was determined by phosphorimagery and the (recombined/recombined and wild-type bands) $\times 100$ was plotted against the percent recombination. Simple regression analysis was used to draw the line for the recombination standards, from which the level of recombination (67% in this skin sample) was estimated. (**f**) Epidermis-specific recombination in $Ercc1^{flox/+}$ with $K5Cre^{P}$ mice detected by quantitative Southern analysis. Southern analysis was carried out as in (**d**). The 5.5 kb band is from the floxed allele, the 4.5 kb band is from a wild-type allele with a polymorphic *EcoRI* site in intron 2 and the 3.05 kb band is from the recombined allele. Note the complete absence of the floxed allele in the epidermis, indicating 100% recombination.

degree of sensitivity differs, are generally highly sensitive to UV irradiation. Our hypothesis is that, because of the additional repair functions, the consequences of *Ercc1* deficiency in UV-irradiated mouse skin will be more severe than for simple NER deficiency alone. Here, we report the production of viable mice with high levels of *Ercc1* inactivation in their epidermis. The *Ercc1* skin-specific knockout mice are hypersensitive to the short-term effects of UV irradiation. The mice develop UV-induced epidermal skin tumours much more rapidly than controls. The tumours arose earlier in actinic progression and grew more rapidly than tumours on control mice.

Results

Generation of Ercc1 *skin-specific knockout mice*

The *Ercc1* gene was floxed using the double replacement gene targeting strategy, devised for use with the *Hprt*-deficient embryonic stem (ES) cell line, HM-1, and *Hprt* minigenes (Stacey *et al.*, 1994; Moore *et al.*, 1995; Selbert *et al.*, 1998). In the first step, the exon 3–5 region of the *Ercc1* gene was replaced with an *Hprt* minigene to inactivate the *Ercc1* allele (see Supplementary Information, Figure 1). Although a new line of *Ercc1* knockout mice was generated from these cells, the original knockout line with a *neo* gene insertion (McWhir

et al., 1993) was used for the matings described below to generate skin-specific *Ercc1* gene inactivation. In the second round of gene targeting, the *Hprt* marker in the knockout clone was replaced with the *Ercc1* exon 3–5 region, flanked by *loxP* sites, and a new strain homozygous for the *Ercc1* floxed allele was established (Figure 1a).

To obtain skin-specific *Ercc1* inactivation, we used a line containing a Cre transgene under the control of the bovine keratin 5 promoter (K5Cre transgene; kindly provided by Dr José Jorcano, CIEMAT, Madrid, Spain). $Ercc1^{flox/-}$ with K5Cre mice served as our experimental animals in the UV irradiation experiments described below, $Ercc1^{flox/+}$ with K5Cre littermates served as controls. To facilitate our irradiation studies mice were produced on a hairless (*hr*) and albino background.

Ercc1$^{flox/-}$ *mice with K5Cre mothers show runting and early death and recombination of the floxed allele in all tissues*

We have demonstrated previously that progeny from K5Cre-containing mothers show constitutive recombination of a floxed allele as a result of Cre expression in oocytes (Ramirez *et al.*, 2004). As expected, all $Ercc1^{flox/-}$ progeny of mothers with the K5Cre transgene were born severely runted and died before weaning with identical premature polyploidy in hepatocytes to that seen in simple *Ercc1* knockouts (see Supplementary Information, Figure 2; McWhir *et al.*, 1993).

Polymerase chain reaction (PCR) analysis on DNA extracted from $Ercc1^{flox/+}$ K5Cre^{M} (transgene inherited from mother) littermates, which are perfectly viable, revealed recombination in all tissues sampled (Figure 1b). The extent of recombination was quantified by Southern blotting. Varying amounts of DNA from an ES cell line heterozygous for a recombined floxed allele ($Ercc1^{rec/+}$) were added to wild-type tissue DNA to provide a titration curve for the level of recombination. Phosphorimagery was used to determine the ratio of recombined/recombined and non-recombined alleles. Recombination levels ranged from 80 to 100% in all the tissues examined (data not shown), demonstrating widespread recombination in $Ercc1^{flox/-}$ K5Cre^{M} mice.

Ercc1$^{flox/-}$ *mice with K5Cre fathers show skin-specific recombination of the floxed allele*

All $Ercc1^{flox/-}$ progeny with K5Cre derived from their fathers (K5Cre^{P}) developed normally into adulthood and showed normal viability. Polymerase chain reaction analysis on tissues from these animals revealed skin-specific recombination of the floxed allele and only very low levels of recombination in other tissues (Figure 1c). Although not visible in this figure, faint bands were sometimes detected in the lung, pancreas and brain from some animals. Southern blotting indicated that the level of recombination in the skin of these animals was 50–70% (Figure 1d and e) and $<5\%$ in any internal tissue. Skin consists of epidermis and dermis and K5Cre is expressed only in the basal layer of the epidermis. The efficiency of Cre-mediated recombination was more accurately estimated after separation of the epidermis from the dermis (Figure 1f). This determination was facilitated by the exploitation of a polymorphism in intron 2 of the wild-type *Ercc1* gene segregating in our stock that allowed recombined, floxed and wild-type alleles to be distinguished. In the absence of this polymorphism (see Figure 1a and Supplementary Information Figure 1), the wild-type and floxed alleles are indistinguishable by Southern analysis. In the separated epidermis, the floxed band was undetectable, indicating 100% recombination. The low level of recombination detected in the dermis sample probably reflects the presence of epidermally derived hair follicles.

$Ercc1^{flox/-}$ mice with paternally inherited K5Cre will now be described as *Ercc1* skin-specific knockout, or experimental animals and $Ercc1^{flox/+}$ K5Cre^{P} littermates will be described as controls.

Ercc1 *skin-specific knockout mice show an extreme short-term response to UVB irradiation*

The minimal erythemal dose (MED) for control mice was 900 J m^{-2}, within the range reported previously for repair-proficient animals. However, the MED for *Ercc1* skin-specific knockouts was only 40 J m^{-2}, a 20-fold difference and lower than values reported previously for NER knockout mice.

Ercc1 skin-specific knockout and control mice were UVB-irradiated (500 J m^{-2}) and the epidermal thickness on the outer surface of the ear was determined at varying times thereafter (Figure 2). As expected, there was a minimal response to this dose in control animals, but there was pronounced epidermal hyperplasia in the mutants, peaking 7 days after irradiation with a sevenfold increase in epidermal thickness. Proliferation within the epidermis was also measured using 5-bromo-2′-deoxyuridine (BrdU) incorporation (Figure 2). Again proliferation in the *Ercc1* skin-specific knockouts peaked at day 7, with a 20-fold increase in the positively stained nuclei over controls.

Unirradiated skin from the back and upper surface of the ear were indistinguishable histologically between experimental and control mice (Figure 3a and b). Epidermis from the ear of UVB-irradiated (500 J m^{-2}) control mice showed mild, uniform hyperplasia on day 7; by day 10 epidermis was indistinguishable from unirradiated controls. Epidermis from irradiated *Ercc1* skin-specific knockouts showed the expected undulation of the basal layer and was irregularly hyperplastic on day 7, far in excess of that seen in controls. Basal cells and spinous cells were hypertrophied and nuclei were larger than those of control mice at day 7, but flow cytometry on isolated propidium iodide-stained nuclei provided no evidence of increased ploidy as seen in *Ercc1*-deficient liver and kidney (Selfridge *et al.*, 2001). There was prominent hypergranulosis in the stratum granulosum and prominent hyperkeratosis. On day 10,

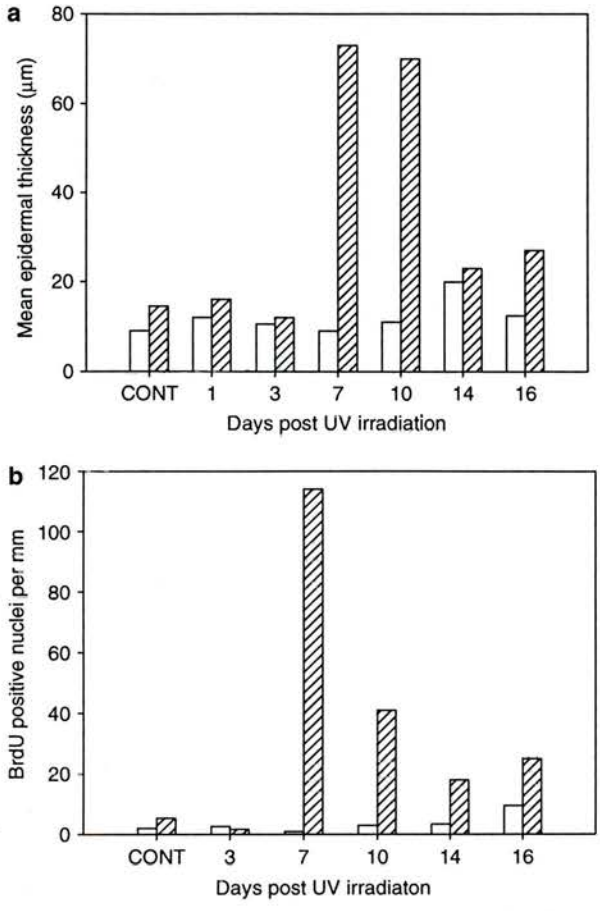

Figure 2 *Ercc1* skin-specific knockouts show an extreme short-term response to UVB. *Ercc1* skin-specific knockout and control mice were UVB irradiated (500 Jm^{-2}) and the mean epidermal thickness on the upper surface of the ears (panel a) and the number of 5-bromo-2′-deoxyuridine-positive nuclei per mm of epidermis (panel b) was determined at varying times thereafter. Unshaded bars, control; shaded bars, *Ercc1* skin-specific knockout. Each point is the mean from two ears. CONT, non-irradiated sample.

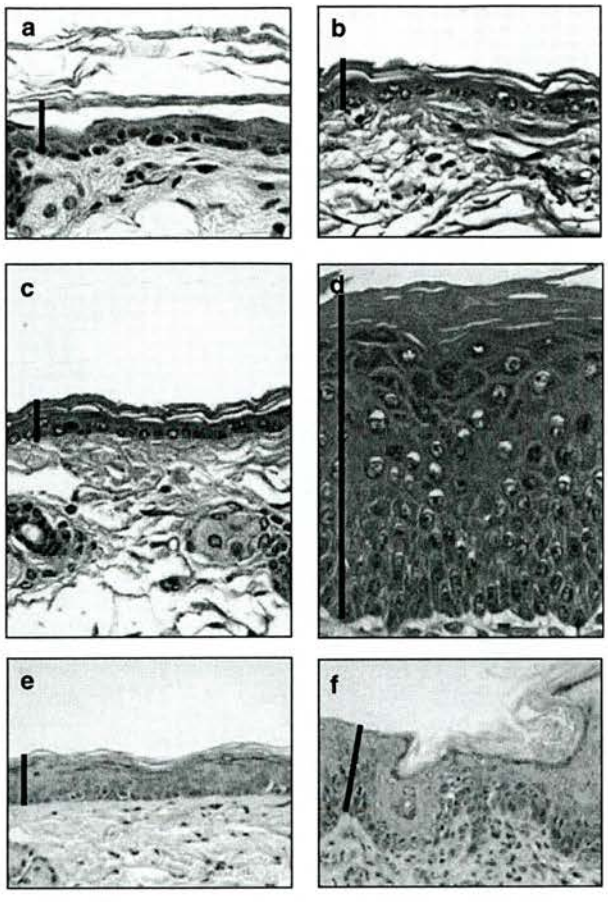

Figure 3 Acute and chronic UVB-induced skin changes in *Ercc1* skin-specific knockout mice. (**a**) Control and (**b**) *Ercc1* skin-specific knockout, haematoxylin and eosin (H&E)-stained sections through the upper surface of the ear of non-irradiated mice. (**c**) Control and (**d**) *Ercc1* skin-specific knockout, ear sections on day 10 following a single dose (2000 Jm^{-2}) of UVB irradiation. (**e**) Control and (**f**) *Ercc1* skin-specific knockout, H&E-stained sections through back skin of chronically UVB-irradiated mice (control, 25 weeks, 2000 Jm^{-2}, three times a week; experimental, 12 weeks, 125 Jm^{-2}, three times a week). For all images the original magnification was × 190. The bar indicates the extent of the epidermis in each figure.

epidermis from experimental mice had continued hypertrophy and hyperplasia of basal/spinous cells and hypergranulosis and hyperkeratosis was more exaggerated than on day 7.

Ear epidermis from control mice responded in the same way to a higher dose of UVB (2000 $J\,m^{-2}$). There was transient mild acanthosis which had returned to normal on day 10 (Figure 3c). Epidermis from *Ercc1* skin-specific knockouts responded similarly to that of mice that received the lower dose with the following differences: The hyperplasia was even more pronounced and there were multiple intracorneal pustules and diffuse intercellular epidermal oedema on day 7 and less hypergranulosis on days 7 and 10 (Figure 3d). The increase in epidermal thickness in *Ercc1* skin-specific knockouts was more pronounced than that reported for other NER gene knockouts.

Ercc1 *skin-specific knockouts are hypersensitive to ultraviolet-induced skin cancer*

To investigate the longer term effects of UVB irradiation *Ercc1* skin-specific knockouts were irradiated with 125 $J\,m^{-2}$ three times a week. Higher, or more frequent, doses produced a level of erythema that was too severe for a chronic irradiation protocol. All ($n=6$) *Ercc1* skin-specific knockouts contracted multiple skin tumours. The earliest tumour was seen at 8 weeks and all animals had tumours at 17 weeks (Figure 4a). Control mice ($n=2$) receiving the same dose remained tumour free until they were finally killed owing to age-related deterioration after 58 weeks of continuous irradiation. Control mice ($n=6$) receiving a 16-fold higher dose (2000 $J\,m^{-2}$) started to develop tumours at 21 weeks and all had tumours at 35 weeks. The cumulative UVB dose

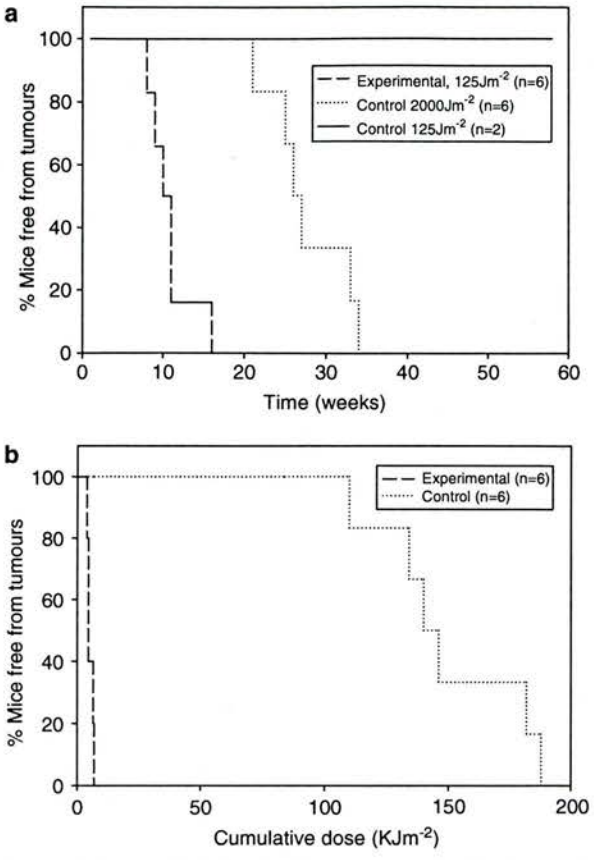

Figure 4 Ultraviolet-induced skin tumour production in *Ercc1* skin-specific knockout mice. Mice were UVB irradiated three times a week and the time to appearance of the first skin tumour on each animal was recorded. (**a**) Tumour-free incidence against elapsed time from start of irradiation protocol. (**b**) Tumour-free incidence against cumulative UVB dose.

for 50% of the *Ercc1* skin-specific knockout mice to develop tumours was 3.75 kJ m^{-2}. The equivalent dose for control mice was 140 kJ m^{-2} (Figure 4b). The average number of tumours/animal was 5.2 for *Ercc1* skin-specific knockouts and 3.7 for controls. This value for controls was calculated from the six mice in this experiment and three additional mice from an earlier experiment.

Skin tumours grow more quickly in Ercc1 *skin-specific knockout mice*

Throughout the chronic irradiation experiments, tumours were measured weekly, consequently we were able to compare tumour growth in the two genotypes (Figure 5). Two weeks after first detection, only 15% of tumours from control mice exceeded 2 mm in diameter, compared to 45% from *Ercc1* skin-specific knockouts. Three weeks after first detection, 25% of tumours from control mice exceeded 2 mm, compared to 65% for experimental mice. The size difference was still present 4 weeks after first detection, where only 10% of tumours from control mice exceeded 5 mm, compared to 45% from experimental mice. These tumour size distributions were significantly different between genotypes at all three time points (2 weeks, χ^2_{1DF}, $P=0.03$; 3 weeks, χ^2_{2DF}, $P=0.03$; 4 weeks, χ^2_{2DF}, $P=0.04$). It was not possible to monitor tumour growth for more than 4 weeks as the presence of tumours exceeding 10 mm in diameter on *Ercc1* skin-specific knockouts necessitated termination of the protocol.

Chronic irradiation-induced skin changes in Ercc1 *skin-specific knockout mice*

The back skin of chronically irradiated control mice (25 weeks, 2000 Jm^{-2} UVB, three times a week) showed mild, uniform hyperplasia to a maximum thickness of 32 μm (Figure 3e). Two or three layers of cells now formed the stratum granulosum and these were flattened to polygonal and had more keratohyalin granules, which were more dispersed and larger, than unirradiated mice. There was no dysplasia or hyperkeratosis. In chronically irradiated *Ercc1* skin-specific knockouts (12 weeks, 125 Jm^{-2} UVB, three times week) more pronounced changes were present in both the epidermis and dermis (Figure 3f). There was diffuse hyperplastic actinic keratosis. Epidermal hyperplasia was uneven resulting in surface irregularity with epidermal pegs extending into the dermis, and epidermal thickness was increased to a maximum of 97 μm. There was patchy hyperkeratosis and parakeratosis. The stratum granulosum was highly variable. Although discontinuous, in areas where it occurred it was two or three cells thick. Cells containing keratohyalin granules varied from flattened to polygonal. In polygonal cells of the stratum granulosum, keratohyalin granules were dispersed and variable in size. The most striking epidermal changes were in the stratum basale where basal cells were hyperplastic and dysplastic. The stratum basale ranged from one to four cells thick. Basal cells were polygonal with prominent intercellular spaces traversed by intercellular bridges. Polygonal basal cells exhibited cytomegaly, karyomegaly and anisokaryosis. Cells of the stratum spinosum were hypertrophied and occasionally apoptotic. Rare dyskeratotic cells were also present. Changes in the dermis consisted of fibrosis and chronic inflammation.

A different skin tumour spectrum in Ercc1 *skin-specific knockout mice*

Proliferative UV-induced skin lesions were classified based on their gross and histopathological appearance (Table 1). All tumours scored in the experiment described in Figure 4 appear in Table 1. There was an equal distribution of papules, endophytic masses and exophytic masses between genotypes. In both groups the majority of endophytic masses (>2 mm) were squamous cell carcinomas (SCC). Similarly, in both groups, most exophytic masses were precancerous lesions (acanthosis or actinic keratosis), or carcinoma *in situ*. However, among the smallest tumour class, papules (<2 mm), there was a striking difference in the prevalence of carcinoma *in situ*. Whereas 10 of 17 papules were

Table 1 Histopathological classification of actinic and neoplastic lesions in *Ercc1* skin-specific knockout and control mice

Histopathological diagnosis	*Gross appearance*					
	Papule (<2 mm)		*Endophytic (>2 mm)*		*Exophytic (>2 mm)*	
	Control	*Ercc1*[a]	*Control*	*Ercc1*	*Control*	*Ercc1*
Acanthosis	1	—	1	—	1	—
Actinic keratosis	3	8	1	2	1	4
Carcinoma *in situ*	10	—	—	1	5	2
SCC						
GNS	2	5	3	2	1	1
Grade 1	1	1	1	1	—	—
Grade 2	—	—	—	2	1	—
Grade 3	—	1	1	1	—	—
Keratoacanthoma	—	—	1	—	—	—
Total	17	15	8	9	9	7

Abbreviations: GNS, grade not specified; SCC, squamous cell carcinoma. [a]*Ercc1* skin-specific knockout.

carcinoma *in situ* in control mice (Figure 6a), none of the 15 papules were carcinoma *in situ* in *Ercc1* skin-specific knockout mice (Figure 6b) ($P<0.01$, z-test). Combining results for all the gross categories, carcinoma *in situ* was only diagnosed in three of 31 lesions in *Ercc1* skin-specific knockout mice, versus 15 of 34 lesions in controls ($P<0.002$, z-test). In the eight tumours identified as SCC grade not specified (GNS) in *Ercc1* skin-specific knockout mice, four appeared to arise from areas of adjacent actinic keratosis (partial thickness dysplasia) (Figure 6d) and three appeared to arise from adjacent carcinoma *in situ* (the remaining tumour arose from a keratoacanthoma). By contrast, all six SCC GNS identified in control mice were adjacent to carcinoma *in situ* (Figure 6c).

Discussion

Ercc1 is essential for NER, but is also involved in other repair pathways relevant to the repair of UV-induced DNA damage in the skin. This led to our hypothesis that the consequences of *Ercc1* deficiency in the skin will be more severe than those reported for other NER gene knockouts. Until now the early lethality in both simple and liver-corrected *Ercc1* knockouts (McWhir *et al.*, 1993; Selfridge *et al.*, 2001) has prevented investigation of this hypothesis. Here we have used the Cre–lox system to generate mice with *Ercc1*-deficient skin. The Cre transgene used was under the control of the bovine K5 gene promoter, which is expressed in the basal layer of the epidermis (Ramirez *et al.*, 2004). Southern analysis on epidermis from $Ercc1^{flox/-}$ mice, where the K5Cre transgene was inherited from the male parent, indicated 100% recombination with only low levels (<5%) detected in other tissues.

We have previously shown that *Ercc1* is essential for normal liver (McWhir *et al.*, 1993) and kidney function (Selfridge *et al.*, 2001) and for gametogenesis (Hsia *et al.*, 2003). The *Ercc1* skin-specific knockouts have normal viability and, in the absence of UV irradiation, their skin was indistinguishable from controls, so we conclude that *Ercc1* is not a skin-essential gene. However, *Ercc1* skin-specific mice were hypersensitive to both the short- and long-term effects of UVB irradiation. Hypersensitivity to UV has been reported previously for NER knockout mice, most notably for *Xpa, Xpc* and *Csb* (Nakane *et al.*, 1995; Sands *et al.*, 1995; de Vries *et al.*, 1995; van der Horst *et al.*, 1997).

Erythema is triggered by cytokines in response to stalled RNA polymerases at sites of UV-induced DNA damage in keratinocytes. This conclusion was reached from the low MEDs shown by *Xpa* (complete NER knockout) and *Csb* (defective transcription coupled repair only) knockout mice and the higher MED reported for *Xpc* knockouts (defective global genome repair only) (Berg *et al.*, 1997, 2000). The MED for our *Ercc1* skin-specific knockouts was lower and the 20-fold difference from our control mice, which are themselves heterozygous for *Ercc1* deficiency, was also greater than reported for other NER knockouts. The MED of *Xpa* and *Csb* mutants was between 135 and 270 $J\,m^{-2}$ and the MED of *Xpc* knockouts and control mice was between 1080 and 2160 $J\,m^{-2}$ (Berg *et al.*, 2000). A lower MED for *Xpa* mice (62.5 Jm^{-2}) was reported by van Schanke *et al.* (2005), but the MED for control mice was also lower (500 Jm^{-2}).

Another acute effect of UVB is to elicit epidermal hyperplasia. The resulting skin thickening reduces UV penetration to the basal layer of the epidermis and underlying dermis. At the peak of the response to 500 Jm^{-2} UVB, the epidermis was sevenfold thicker in *Ercc1* skin-specific knockouts than controls. Epidermal thickening (10-fold more than controls) and cellular abnormalities were even more pronounced at 2000 Jm^{-2}. Acute UV-induced epidermal thickening has not been studied so thoroughly in other NER knockouts. Examination of irradiated skin sections in reports for other NER knockouts shows the strongest response in *Xpa* knockouts following 1200 Jm^{-2} (de Vries *et al.*, 1995), where the thickening was only around half the

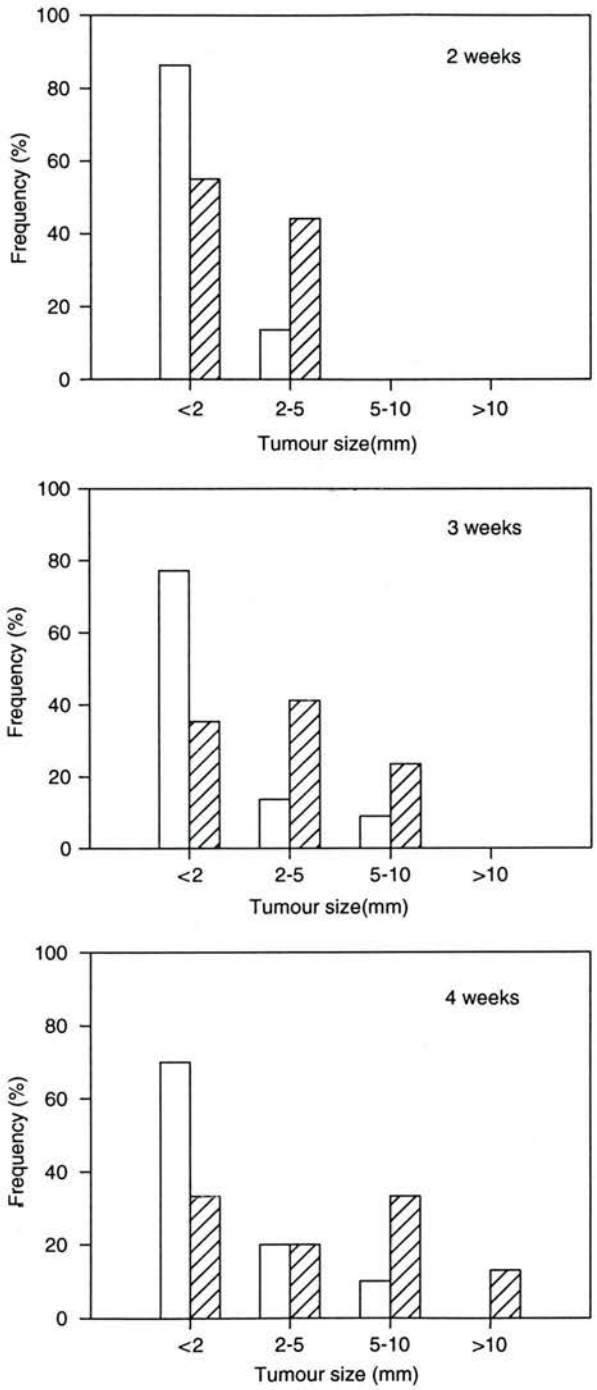

Figure 5 Skin tumour growth in *Ercc1* skin-specific knockout mice. Tumour diameter (mm) was determined 2, 3 and 4 weeks after each tumour was initially detected. The frequency (%) of tumours in the different size categories is indicated. Unshaded bars, control; shaded bars, *Ercc1* skin-specific knockout. Two-week measurements: control, $n=22$ tumours; *Ercc1* skin-specific knockout, $n=18$. Three-week measurements: control, $n=22$; experimental, $n=17$. Four-week measurements: control, $n=20$; experimental, $n=15$.

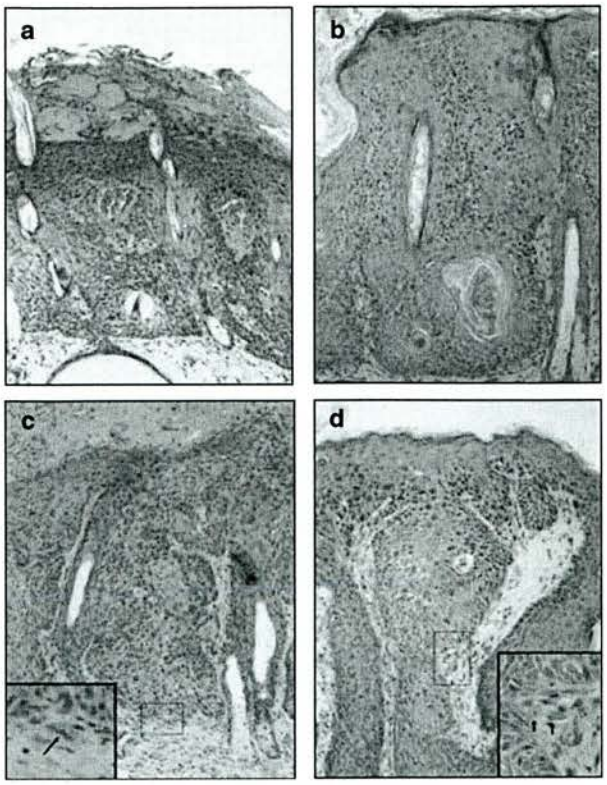

Figure 6 Rapid actiic progression in skin tumours from *Ercc1* skin-specific knockout mice. (**a**) Typical papule from control mouse showing carcinoma *in situ*. (**b**) Typical papule from *Ercc1* skin-specific knockout mouse showing actinic keratosis. (**c**) Squamous cell carcinoma (SCC) grade not specified (GNS) from control mouse with adjacent carcinoma *in situ*. (**d**) Squamous cell carcinoma GNS from *Ercc1* skin-specific knockout mouse with adjacent actinic keratosis. In (**c**) and (**d**) high-power insets of the regions indicated by the boxes show individual epithelial cells (arrows) invading the dermis, upon which the diagnosis of SCC GNS was based. For all images the original magnification was $\times 100$ (insets $\times 400$).

maximum level reported here for *Ercc1* skin-specific knockouts. Thus, the epidermal thickening and cellular abnormalities in our *Ercc1* skin-specific knockouts are more pronounced than reported for other NER knockouts.

Ercc1 skin-specific knockout mice were also hypersensitive to UV-induced skin cancer. The simple comparison of tumour yield understates the difference between *Ercc1* skin-specific knockout and control mice because the more rapid growth of tumours on mutant mice meant that the maximum tumour size end point was reached far earlier after the first tumour was detected on mutant compared to control animals. As the carcinogenic effect of UVB is not directly proportional to dose, the most rigorous comparisons of sensitivity require equivalent doses. At the lowest dose ($125\,Jm^{-2}$, three times a week) tumours were first detected on *Ercc1* skin-specific knockouts after 8 weeks. At the same dose no tumours were detected on control mice up to 58 weeks when the protocol was terminated,

indicating that *Ercc1* skin-specific knockouts were >sevenfold more sensitive than controls. Based on the ratio of median tumour induction times at the same dose, *Xpa* mice were only fourfold, *Xpc* mice threefold and *Csb* mice were twofold more sensitive than controls (Berg *et al.*, 1997, 2000). A much higher dose (2000 J m^{-2}) was required to generate a comparable number of skin tumours in our control mice. The cumulative UVB dose for 50% of *Ercc1* skin-specific knockout mice to develop skin tumours (3.75 k J m^{-2}) was 37-fold lower than for controls. This sensitivity is comparable to that reported for *Xpa* knockouts where, at 32 J m^{-2} day^{-1}, 50% of mice developed tumours at a cumulative dose of 3.1 k J m^{-2} (Berg *et al.*, 1997), or 3.7 k J m^{-2} (de Vries *et al.*, 1998). At the higher dose of 80 J m^{-2}day^{-1} the corresponding cumulative doses were 5.5 k J m^{-2} (Berg *et al.*, 1997) and 7.7 k J m^{-2} (de Vries *et al.*, 1998). Many of the other skin carcinogenesis protocols have used much higher UVB doses, or shaven as opposed to *hr* mice, or different UV sources with possible discrepancies in dosimetry, making comparison with our data difficult. Cumulative UVB doses under these high daily dose conditions for 50% of mice to develop tumours (or for a high frequency of tumour production) were: *Xpc* 300 k J m^{-2} (Sands *et al.*, 1995); *Ddb2* 210 k J m^{-2} (Itoh *et al.*, 2004); TTD (*Xpd* point mutation modelling trichothiodystrophy) 103 k J m^{-2} (de Boer *et al.* 1999); *Xpa* 84 k J m^{-2} (Nakane *et al.*, 1995) and 22 k J m^{-2} (de Vries *et al.*, 1995); *Csb* 45 KJm^{-2} (van der Horst *et al.*, 1997). Thus, in a similar protocol and not withstanding that the genetic backgrounds are different, sensitivity to UV-induced skin cancer in *Ercc1* skin-specific knockouts is comparable to that seen in *Xpa* knockouts and exceeds that reported for other NER knockouts. In addition to an increased frequency, tumours on *Ercc1* skin-specific knockout mice were larger and grew more quickly than on control littermates. This has not been reported for other NER knockouts.

One explanation for the decreased frequency of carcinoma *in situ* in *Ercc1* skin-specific knockout mice is that SCCs arise earlier in actinic progression in these animals, before full-thickness actinic dysplasia, which was our criterion for a diagnosis of carcinoma *in situ*. Support for this hypothesis comes from comparing the histological environment in which SCC GNS occurred in *Ercc1* skin-specific knockout and control mice. Squamous cell carcinoma GNS was the classification given to tumours in which individual epidermal cells or small nests of epidermal cells had clearly penetrated the basement membrane and invaded the dermis. Half the tumours identified as SCCs GNS in *Ercc1* skin-specific knockout mice appeared to arise from areas of adjacent actinic keratosis, whereas all SCCs GNS identified in control mice were adjacent to carcinoma *in situ*. Further evidence for earlier progression to SCC in *Ercc1* skin-specific knockout mice was the trend towards a higher prevalence of SCC among papules: 7/15 for *Ercc1* skin-specific knockouts and 3/17 for controls. Larger cohorts will be necessary to confirm this trend.

In *Ercc1* skin-specific knockout mice, half (12/24) of all raised epidermal masses (papules and exophytic masses) were hyperplastic actinic keratosis (actinic papillomas). By contrast, only four of 26 raised epidermal masses were diagnosed as actinic keratosis in control mice. This difference in the prevalence of hyperplastic actinic keratosis could have resulted from a greater tendency for focal hyperplasia to occur in actinic lesions of experimental versus control mice. Alternatively, or in addition, the diffuse background of actinic keratosis in *Ercc1* skin-specific knockout mice, revealed in samples from non-gross lesional skin, provided a far greater opportunity for superimposition of focal exuberant hyperplasia than in control mice in which the background skin histopathology was non-dysplastic acanthosis.

Thus, in addition to the expected increased frequency of UV-induced epidermal skin tumours in *Ercc1* skin-specific knockout mice, the tumours are also larger, grow more quickly and show more rapid actinic progression to SCC than in control mice. Increased skin tumour frequency in NER knockout mice has been reported previously, but the more rapid actinic progression has not. We do not know whether this is specific to *Ercc1* deficiency, or is a previously undetected general feature of NER-deficient epidermis, that could result from increased UV-induced mutagenesis and the pronounced proliferative response. This could be a direct effect of *Ercc1* deficiency on progression, or an indirect effect of the increased tumour growth rate.

We have shown that *Ercc1* has an essential role in protecting the skin against the short- and long-term effects of UVB irradiation. The combined erythemal, hyperproliferative and skin tumour responses in *Ercc1* skin-specific knockout mice are stronger than reported for other NER gene knockouts. In addition, we have demonstrated more rapid actinic progression in *Ercc1*-deficient skin. Molecular analysis of mutations arising in these tumours will be necessary to confirm our hypothesis that the consequences of *Ercc1* deficiency in skin are more severe than for other NER genes.

Materials and methods

Generation of hairless Ercc1 *skin-specific knockout mice*

Hairless (*hr*) mice on an MF-1 background were obtained from Harlan UK Ltd, Bicester, Oxan, UK. These were crossed separately with our K5Cre (Ramirez *et al.*, 2004), *Ercc1* floxed and original *Ercc1* knockout lines (McWhir *et al.*, 1993) and albino progeny were intercrossed to produce albino hairless K5Cre, *Ercc1* floxed and *Ercc1* knockout lines. K5Cre containing *Ercc1*$^{+/-}$ males from a cross between albino hairless K5Cre and *Ercc1* knockout lines were mated with albino hairless *Ercc1*$^{flox/flox}$ females to produce experimental (*Ercc1*$^{flox/-}$ with K5Cre) and control (*Ercc1*$^{flox/+}$ with K5Cre) littermates on a segregating background.

Mouse genotyping

Ercc1. The *Ercc1* null (*Ercc1*$^{-}$) allele was the original knockout allele with a *neo* gene insertion (McWhir *et al.*, 1993), rather than the new knockout allele described here, which was generated as an intermediate in the production of the floxed allele. A triplex PCR (Selfridge *et al.*, 2001) distinguished

Ercc1^{+} and *Ercc1*^{flox} alleles from the *Ercc1*$^{-}$ allele. Primers 033 M for exon 4 (5′-CCCGTGTTGAAGTTTGTGCG, mouse *Ercc1* cDNA sequence 429–448, GenBank Accession no X07414) and 035 M for exon 5 (5′-CGAAGGGCGAAGTT CTTCCC, mouse *Ercc1* cDNA sequence 598–579) gave a 0.6 kb product for the wild-type and floxed alleles. The null allele was detected as a 0.8 kb product from the exon 5 primer and a primer for the *neo* cassette (5′-GGTTCGAAATGACCG ACCAAGCG, 958–980 GenBank Accession no V00618). A PCR reaction with primers 432E and 159 M distinguished between the wild-type (1.8 kb product) and floxed (1.4 kb) alleles (see Supplementary Information, Figure 1). 432E (5′-TGCAGAGCCTGGGGAAGAACTTCGC; mouse *Ercc1* cDNA sequence exon 5; positions 568–592, GenBank Accession no. X07414) and 159 M (5′-TAGCCAGCTCCTTGAGA GCC; mouse *Ercc1* cDNA sequence exon 6, positions 657–638) with cycle conditions: 94°C 1 min, 66°C 1 min and 72°C 1.5 min for 35 cycles.

Keratin 5 Cre Genotyping for the K5Cre transgene was performed using primers G13586 (5′-ACCTGCCATGAAGA-CAGCGTTTGCAC, B. taurus gene for keratin 5, promoter region, positions 1115–1140, GenBank Accession no. Z32746) and G13587 (5′-TGCACGTTCACCGGCATCAACG, Bacteriophage P1 Cre recombinase gene, coding region, positions 877–856, GenBank Accession no. X03453). A 1.4 kb product specific for the transgene was obtained with conditions: 94°C 1 min, 66°C 1 min and 72°C 1.5 min for 30 cycles.

Recombination of the Ercc1 *floxed allele*
Recombination of the *Ercc1* floxed allele was detected with primers F25731 (5′-TGTCTCCCTGGCTCTGGATCTGAC) and F25732 (5′-TCAAAGTATGGTAGCCAAGGCAGC), which lie immediately 5′ of the first *loxP* site and 3′ of the second *loxP* site, respectively (see Figure 1 and Supplementary Information, Figure 1). A 0.25 kb product specific for the recombined allele was obtained with conditions: 94°C 1 min, 68°C 1 min and 72°C 1.5 min for 25 cycles. Under these conditions, the distance between the primers on the non-recombined floxed allele is too great to give a PCR product.

Southern analysis
Separation of the epidermis from the dermis of mouse tails has been described previously (Remenyik *et al.*, 2003). DNA was extracted from mouse tissues and subjected to Southern analysis as described (Thompson *et al.*, 1989). The probe used was a 600-bp PCR product spanning exons 1 and 2 (Figure 1). This product was obtained with primers F29600 (5′-GAGTCT AGCAGGAGTTGTGCTGGC, mouse *Ercc1* cDNA sequence 1–24, GenBank Accession no. X07414) and F29601 (5′-CTTCCTCCTGGTGGGTGGTCCTGAGG, mouse *Ercc1* cDNA sequence 161–136) with conditions: 94°C 1 min, 64°C 1 min and 72°C 1 min for 35 cycles.

Ultraviolet irradiation experiments
Animals were irradiated with a UVB light source (Phillips TL20W/12RS tube, emitting 2.4 J m^{-2} s^{-1} and calibrated to national standards). To study short-term responses, animals were killed at varying times after irradiation and ears were removed and fixed in Methacarn (methanol:chloroform:acetic acid, 3:2:1). Five micron transverse sections were cut and stained with haematoxylin and eosin (H&E). Epidermal area was measured along the length of the irradiated (upper) surface, and the mean epidermal thickness was calculated by dividing the area by the length. This was done to correct for local variations in epidermal thickness along the length of the ear. Immunohistochemistry for BrdU incorporation was carried out by a modification (see Supplementary Information) of a method described previously (Nunez *et al.*, 2000).

For long-term irradiations, animals were monitored weekly and changes in skin condition, tumour onset and tumour size were recorded. An animal was killed when its largest tumour exceeded 10 mm in diameter. Tumours and apparently unaffected areas of back skin were removed, fixed in buffered formalin and processed for histology with H&E staining as described above.

Gross and histologic classification of tumours
Ultraviolet irradiation-induced skin tumours were classified based on their gross and histologic appearance using a modification of the scheme proposed by Gallagher *et al.* (1984) and Canfield *et al.* (1988). Briefly, skin lesions were classified according to their gross appearance as papules (raised epidermal mass less than 2 mm in diameter), exophytic masses (growth projecting from surface greater than 2 mm in diameter), and endophytic masses (inward growing mass greater than 2 mm in diameter).

Histologic classification consisted of non-neoplastic appendage cysts, acanthosis (epidermal hyperplasia without dysplasia), and actinic keratosis (epidermal hyperplasia with dysplasia of basal cell layer, or basal and spinous cell layer, but retention of external granular cell layer). Epithelial neoplasms consisted of carcinoma *in situ* (full-thickness dysplasia, absent stratum granulosum, intact basement membrane) and SCC (penetration of basement membrane and dermal invasion). Grade 1 SCC had prominent keratin pearls with obvious granular cell layer; Grade 2 SCC had fewer keratin pearls with few or absent granular cells often associated with parakeratosis; Grade 3 SCC had no keratin pearls, but keratinized groups of cells or individual cells. Squamous cell carcinomas with GNS were those carcinomas consisting of individual cells or small nests of cells which were judged to have penetrated the basement membrane and invaded the superficial dermis.

Acknowledgements

Ultraviolet dosimetry was carried out by Dr Stephen Pye (Lothian University Hospitals NHS Trust). The *Ercc1* gene targeting was carried out by Kan-Tai Hsia. *Ercc1* skin-specific knockout mice were produced with the support of a programme Grant (SP2095/0301) from Cancer Research UK to DWM. The UV irradiation work on these mice was supported by a project grant from the Association for International Cancer Research to DWM. NJL was supported by a PhD scholarship from the Raven Trust.

References

Berg RJ, de Vries A, van Steeg H, de Gruijl FR. (1997). *Cancer Res* **57**: 581–584.

Berg RJ, Rebel H, van der Horst GTJ, van Kranen HJ, Mullenders LH, van Vloten WA *et al.* (2000). *Cancer Res* **60**: 2858–2863.

Canfield PJ, Greenoak GE, Macasaet EN, Reeve VE, Gallagher CH. (1988). *Pathology* **20**: 109–117.

Chipchase MD, Melton DW. (2002). *DNA Repair* **1**: 335–340.

de Boer J, van Steeg H, Berg RJ, Garssen J, de Wit J, van Oostrom CT *et al.* (1999). *Cancer Res* **59**: 3489–3494.

de Vries A, Berg RJ, Wijnhoven S, Westerman A, Wester PW, van Kreijl CF *et al.* (1998). *Oncogene* **16**: 2205–2212.
de Vries A, van Oostrom CT, Hofhuis FM, Dortant PM, Berg RJ, de Gruijl FR *et al.* (1995). *Nature* **377**: 169–173.
Friedberg EC. (2001). *Nat Rev Cancer* **1**: 22–33.
Gallagher CH, Canfield PJ, Greenoak GE, Reeve VE. (1984). *J Invest Dermatol* **83**: 169–174.
Hsia K-T, Millar MR, King S, Selfridge J, Redhead NJ, Melton DW *et al.* (2003). *Development* **130**: 369–378.
Itoh T, Cado D, Kamide R, Linn S. (2004). *Proc Natl Acad Sci USA* **101**: 2052–2057.
Kuhn R, Torres RM. (2002). *Methods Mol Biol* **180**: 175–204.
Magin TM, McEwan C, Milne M, Pow AM, Selfridge J, Melton DW. (1992). *Gene* **122**: 289–296.
Mansour SL, Thomas KR, Capecchi MR. (1988). *Nature* **336**: 348–352.
McWhir J, Selfridge J, Harrison DJ, Squires S, Melton DW. (1993). *Nat Genet* **5**: 217–224.
Moore RC, Redhead NJ, Selfridge J, Hope J, Manson JC, Melton DW. (1995). *Bio/Technology* **13**: 999–1004.
Nakane H, Takeuchi S, Yuba S, Saijo M, Nakatsu Y, Murai H *et al.* (1995). *Nature* **377**: 165–168.
Nunez F, Chipchase MD, Clarke AR, Melton DW. (2000). *FASEB J* **14**: 1073–1082.
Ramirez A, Bravo A, Jorcano JL, Vidal M. (1994). *Differentiation* **58**: 53–64.
Ramirez A, Page A, Gandarillas A, Zanet J, Pibre S, Vidal M *et al.* (2004). *Genesis* **39**: 52–57.
Remenyik E, Wikonkal NM, Zhang W, Paliwal V, Brash DE. (2003). *Oncogene* **22**: 6369–6376.
Sands AT, Abuin A, Sanchez A, Conti CJ, Bradley A. (1995). *Nature* **377**: 162–165.
Selbert S, Bentley DJ, Melton DW, Rannie D, Lourenco P, Watson CJ *et al.* (1998). *Transgenic Res* **7**: 387–396.
Selfridge J, Hsia K-T, Redhead NJ, Melton DW. (2001). *Nucleic Acids Res* **29**: 4541–4550.
Selfridge J, Pow AM, McWhir J, Magin TM, Melton DW. (1992). *Somat Cell Mol Genet* **18**: 325–336.
Stacey A, Schnieke A, McWhir J, Cooper J, Colman A, Melton DW. (1994). *Mol Cell Biol* **14**: 1009–1016.
Thompson S, Clarke AR, Pow AM, Hooper ML, Melton DW. (1989). *Cell* **56**: 313–321.
van der Horst GT, van Steeg H, Berg RJ, van Gool AJ, de Wit J, Weeda G *et al.* (1997). *Cell* **89**: 425–435.
van Schanke A, Jongsma MJ, Bisschop R, van Venrooij GM, Rebel H, de Gruijl FR. (2005). *J Invest Dermatol* **124**: 241–247.

Supplementary Information accompanies the paper on the Oncogene website (http://www.nature.com/onc).